

UNIVERSITÉ DU QUÉBEC À MONTREAL

THE LITHOSPHERIC FLEXURE OF SOUTH AMERICA INDUCED BY
SEDIMENT ACCUMULATION ON THE PASSIVE MARGIN DURING THE
CENOZOIC ERA

THESIS
PRESENTED
AS PARTIAL REQUIREMENT
OF THE MASTERS OF EARTH SCIENCES

BY
ERIKA ZARAY CALDERON GOYENECHÉ

OCTOBER 2014

UNIVERSITÉ DU QUÉBEC À MONTRÉAL
Service des bibliothèques

Avertissement

La diffusion de ce mémoire se fait dans le respect des droits de son auteur, qui a signé le formulaire *Autorisation de reproduire et de diffuser un travail de recherche de cycles supérieurs* (SDU-522 – Rév.01-2006). Cette autorisation stipule que «conformément à l'article 11 du Règlement no 8 des études de cycles supérieurs, [l'auteur] concède à l'Université du Québec à Montréal une licence non exclusive d'utilisation et de publication de la totalité ou d'une partie importante de [son] travail de recherche pour des fins pédagogiques et non commerciales. Plus précisément, [l'auteur] autorise l'Université du Québec à Montréal à reproduire, diffuser, prêter, distribuer ou vendre des copies de [son] travail de recherche à des fins non commerciales sur quelque support que ce soit, y compris l'Internet. Cette licence et cette autorisation n'entraînent pas une renonciation de [la] part [de l'auteur] à [ses] droits moraux ni à [ses] droits de propriété intellectuelle. Sauf entente contraire, [l'auteur] conserve la liberté de diffuser et de commercialiser ou non ce travail dont [il] possède un exemplaire.»

UNIVERSITÉ DU QUÉBEC À MONTREAL

FLEXURE LITHOSPHERIQUE DU CONTINENT SUD-AMÉRICAIN INDUITE
PAR L'ACCUMULATION DE SÉDIMENTS SUR LES MARGES PASSIVES AU
COURS DU CÉNOZOÏQUE.

MÉMOIRE
PRÉSENTÉ
COMME EXIGENCE PARTIELLE
DE LA MAÎTRISE EN SCIENCE DE LA TERRE

PAR
ERIKA ZARAY CALDERON GOYENECHÉ

OCTOBRE 2014

ACKNOWLEDGMENTS

I would like to express my most sincere appreciation to my Thesis Director, Doctor Alessandro Forte for providing me with the opportunity of accomplishing this project of research, for his direction, his approachability, for the financial support and for his valuable academic guidance, which allowed me to have a vast learning experience during the course of the development of this project.

I would like to express my profound gratitude to my family. My parents, Clara and Gabriel, my sisters: Sandra, Maria and Katherine for their motivation and unconditional support throughout my Master Program

To my colleague, Catherine Phaneuf, for her friendship and collaboration all through the development of my Masters.

To all my friends, specially, Kelly, Wendy, Ladys, Clara, Alexa and Christian for their continuous stimulus.

For his exceptional support, his constant motivation and the living moments. I would like to express my gratitude to Salus F.

Thank you, to those who contributed to the realization of this project in one way or another.

TABLE OF CONTENTS

LIST OF FIGURES	vii
LIST OF TABLES	xvi
LIST OF SYMBOLS AND ABBREVIATIONS	xvii
ABSTRACT	xviii
RÉSUMÉ	xx
CHAPTER I	
INTRODUCTION	1
CHAPTER II	
METHODOLOGY	6
2.1 Database Construction	6
2.2 Development of Histograms	6
2.3 Use of FORTRAN	7
2.3.1 Numerical algorithm to find sediment densities	7
2.3.2 Algorithm to Find Sediment Load using the thickness from high spatial resolution Global sediment Database (Divins,2003).....	8
2.3.3 Numerical Algorithm to Determine Flexure	8
2.3.4 Use of Generic Mapping Tool GMT	9
CHAPTER III	
ISOSTASY AND LITHOSPHERIC FLEXURE	10
3.1 Isostasy	10
3.1.1 Local Isostasy	11
3.1.2 Regional Flexural Isostasy	12
3.1.3 2-D Lithospheric Flexure on a Sphere	15
3.1.4 Spherical Harmonic Solutions of the 2-D Flexure	18

CHAPTER IV

RESULTS	22
4.1 Database.....	22
4.2 Histograms.....	24
4.2.1 Zone I: The Caribbean	25
4.2.2 Zone II: The Amazon	30
4.2.3 Zone III: Argentina-Brazil	34
4.2.4 Zone IV: Scotia	40
4.3 Lithospheric Flexure.....	46
4.3.1 Numerical calculation of Lithospheric Flexure.....	46
4.4 Cumulative Flexural Response as a Function of Time.....	48
4.4.1 Flexural Response of the Lithosphere during the Quaternary (0-2.588 million years)	48
4.4.2 Flexural Response of the Lithosphere from the Paleocene to the Present.....	61
4.4.3 Uplift of the Continent of South America since the Pliocene, the Miocene, the Oligocene, the Eocene and the Paleocene	88
4.5 Flexural Response by Age Intervals.....	97
Cenozoic Flexural Response of the Lithosphere	97
4.5.1 Pliocene-Quaternary flexural response of the Lithosphere.....	98
4.5.2 Flexural Response of the Lithosphere during the Pliocene-Quaternary, Miocene-Pliocene, Oligocene-Miocene, Eocene-Oligocene and Paleocene-Eocene interval ages.	103
4.5.3 Cenozoic Uplift of the Continent of South America.....	128
4.6 Where does the sediment come from?.....	134
4.6.1 The Magdalena River	134
4.6.2 The Orinoco River.....	137
4.6.3 The Amazon River	139
4.6.4 La Plata River System	142
4.7 South American Ocean Currents	145

CHAPTER V

DISCUSSION.....	158
-----------------	-----

CHAPTER VI

CONCLUSIONS.....	161
APPENDIX A	
SPHERICAL HARMONIC FUNCTIONS.....	170
APPENDIX B	
DATABASE OF CENOZOIC SEDIMENT THICKNESS.....	178
APPENDIX C	
FORTRAN ALGORITHM TO CALCULATE LITHOSPHERIC FLEXURE	188
APPENDIX D	
FLEXURAL TOPOGRAPHY OF SOUTH AMERICA CONTINENT CUMULATIVE SINCE THE PALEOCENE.....	191
APPENDIX E	
FLEXURAL TOPOGRAPHY DURING THE CENOZOIC EPOCH	194
REFERENCES.....	198

LIST OF FIGURES

Figure	Page
3.1 Local Compensation Models. (Taken from Gupta H. K. 2011).....	11
3.2 Lithospheric flexure caused by surface loads. (Taken from Gupta H. K. 2011).....	12
3.3 Models for calculating the hydrostatic restoring force on lithospheric plates deflected by an applied load q_a . (a) Oceanic Case. (b) Continental case. (Taken from Turcotte & Schubert, 2002).	13
4.1 Location of four sediments deposition zones (I to IV) and the sites of wells utilized in different campaigns of the Ocean Drilling Program (ODP) and Deep Sea Drilling Project (DSDP).....	23
4.2 Histogram of the percent sediment thickness in the Quaternary. Zone I.....	26
4.3 Histogram of the percent sediment thickness in the Pliocene. Zone I.....	26
4.4 Histogram of the percent sediment thickness in the Miocene. Zone I.....	27
4.5 Histogram of the percent sediment thickness in the Oligocene. Zone I.....	28
4.6 Histogram of the percent sediment thickness in the Eocene. Zone I.....	28
4.7 Histogram of the percent sediment thickness in the Paleocene. Zone I.....	29
4.8 Histogram of the percent sediment percentage in the Quaternary. Zone II.....	30
4.9 Histogram of the percent sediment thickness in the Pliocene. Zone II.....	31
4.10 Histogram of the percent sediment thickness in the Miocene. Zone II.....	32
4.11 Histogram of the percent sediment thickness in the Oligocene. Zone II.....	32
4.12 Histogram of the percent sediment thickness in the Eocene. Zone II.....	33
4.13 Histogram of the percent sediment thickness in the Paleocene. Zone II.....	33
4.14 Histogram of the percent sediment thickness in the Quaternary. Zone II.....	34
4.15 Histogram of the percent sediment thickness in the Pliocene. Zone III.....	35

4.16	Histogram of the percent sediment thickness in the Miocene. Zone III. DSDP: Deep Sea Drilling Project (Perch-Nielsen et al., (1977b, c, d, e), Baker et al., (1983a,b), Maxwell et al., (1970)), Samar Dx-1 and PIA (PIA: Intersection Point A represents the closest site along seismic line BGR87-1 to the oil drilling where the lithological contacts were extended). (Violante et al., 2010). Santos, Campos and Pelotas basin (Contreras et al., 2010)	36
4.17	Histogram of the percent sediment thickness in the Oligocene. Zone III .DSDP: Deep Sea Drilling Project (Perch-Nielsen et al., (1977d, e), Baker et al., (1983a, b), Maxwell et al., (1970)) Well Samar Dx-1 (Violante et al., 2010). Santos, Campos and Pelotas Basin (Contreras et al., 2010).....	37
4.18	Histogram of the percent sediment thickness in the Eocene. Zone III.	38
4.19	Histogram of the percent sediment thickness in the Paleocene. Zone III. DSDP: Deep Sea Drilling Project (Perch-Nielsen et al., (1977b,c,d,e), Baker et al., (1983b)), Samar Dx-1 and PIA (PIA: Intersection Point A represents the closest site along seismic line BGR87-1 to the oil drilling where the lithological contacts were extended). (Violante et al., 2010). Santos and Campos basin (Contreras et al., 2010)	39
4.20	Histogram of the percent sediment thickness in the Quaternary. Zone IV.....	40
4.21	Histogram of the percent sediment thickness in the Pliocene. Zone IV	41
4.22	Histogram of the percent sediment thickness in the Miocene. Zone IV.....	42
4.23	Histogram of the percent sediment thickness in the Oligocene. Zone IV.	43
4.24	Histogram of the percent sediment thickness in the Eocene. Zone IV	43
4.25	Histogram of percent sediment thickness in the Paleocene. Zone IV.	44
4.26	Localization Map of Offshore Sites. The colour scale is Topography/Bathymetry.....	50
4.27	Map of total Flexural Response due to sediment loads accumulated since the Quaternary (2.588-0 million years) for an effective elastic thickness of 40 km and a maximum harmonic degree of 2000.	51
4.28	Map of total Flexural Response due to sediment loads accumulated since the Quaternary (2.588-0 million years) for an effective elastic thickness of 80 km and a maximum harmonic degree of 2000	52
4.29	Contribution to lithospheric flexure, from sediments deposited in each geological epoch, at an offshore site in the Barracuda Abyssal Plain	62
4.30	Contribution to lithospheric flexure, from sediments deposited in each geological epoch, at an offshore site in the Cayos Basin.	63

4.31	Contribution to lithospheric flexure, from sediments deposited in each geological epoch, at an offshore site in the Colombia Basin.....	63
4.32	Contribution to lithospheric flexure, from sediments deposited in each geological epoch, at an offshore site in the Magdalena Delta	64
4.33	Contribution to lithospheric flexure, from sediments deposited in each geological epoch, at an offshore site in the Venezuela Basin	64
4.34	Contribution to lithospheric flexure, from sediments deposited in each geological epoch, at an offshore site in the Grenada Basin.....	65
4.35	Contribution to lithospheric flexure, from sediments deposited in each geological epoch, at an offshore site in the Tobago Basin	65
4.36	Contribution to lithospheric flexure, from sediments deposited in each geological epoch, at an offshore site in the Demerara Abyssal Plain.....	66
4.37	Contribution to lithospheric flexure, from sediments deposited in each geological epoch, at an offshore site in the Marin Guajira Basin.....	66
4.38	Contribution to lithospheric flexure, from sediments deposited in each geological epoch, at an offshore site in the Marin Sinú Basin	67
4.39	Contribution to lithospheric flexure, from sediments deposited in each geological epoch, at an offshore site in the Cariaco Basin	67
4.40	Contribution to lithospheric flexure, from sediments deposited in each geological epoch, at an offshore site in the Guiana.....	68
4.41	Contribution to lithospheric flexure, from sediments deposited in each geological epoch, at an offshore site in the Surinam	69
4.42	Contribution to lithospheric flexure, from sediments deposited in each geological epoch, at an offshore site in the French Guyana	69
4.43	Contribution to lithospheric flexure, from sediments deposited in each geological epoch, at an offshore site in the Amazon Delta	70
4.44	Contribution to lithospheric flexure, from sediments deposited in each geological epoch, at an offshore site in Brazil.....	70
4.45	Contribution to lithospheric flexure, from sediments deposited in each geological epoch, at an offshore site in Ceará	71
4.46	Contribution to lithospheric flexure, from sediments deposited in each geological epoch, at an offshore site in Potigar.....	71
4.47	Contribution to lithospheric flexure, from sediments deposited in each geological epoch, at an offshore site in Pernambuco	72

4.48	Contribution to lithospheric flexure, from sediments deposited in each geological epoch, at an offshore site in Sergipe-Alagoas.....	73
4.49	Contribution to lithospheric flexure, from sediments deposited in each geological epoch, at an offshore site in Bahia Sul.....	73
4.50	Contribution to lithospheric flexure, from sediments deposited in each geological epoch, at an offshore site in the Espiritu Santo Basin.....	74
4.51	Contribution to lithospheric flexure, from sediments deposited in each geological epoch, at an offshore site in the Campos Basin	74
4.52	Contribution to lithospheric flexure, from sediments deposited in each geological epoch, at an offshore site in the Santos Basin.....	75
4.53	Contribution to lithospheric flexure, from sediments deposited in each geological epoch, at an offshore site in the Pelotas Basin.....	75
4.54	Contribution to lithospheric flexure, from sediments deposited in each geological epoch, at an offshore site in the Punta del Este Basin	76
4.55	Contribution to lithospheric flexure, from sediments deposited in each geological epoch, at an offshore site in the Salado Basin	76
4.56	Contribution to lithospheric flexure, from sediments deposited in each geological epoch, at an offshore site in the Colorado Basin	77
4.57	Contribution to lithospheric flexure, from sediments deposited in each geological epoch, at an offshore site in the Rawson Basin	77
4.58	Contribution to lithospheric flexure, from sediments deposited in each geological epoch, at an offshore site in the San Jorge Basin.....	78
4.59	Contribution to lithospheric flexure, from sediments deposited in each geological epoch, at an offshore site in the San Julian Basin.....	78
4.60	Contribution to lithospheric flexure, from sediments deposited in each geological epoch, at an offshore site in the Argentina Basin	79
4.61	Contribution to lithospheric flexure, from sediments deposited in each geological epoch, at an offshore site in the Northern Falkland	79
4.62	Contribution to lithospheric flexure, from sediments deposited in each geological epoch, at an offshore site in the Eastern Falkland	80
4.63	Contribution to lithospheric flexure, from sediments deposited in each geological epoch, at an offshore site in the Western Falkland	81
4.64	Contribution to lithospheric flexure, from sediments deposited in each geological epoch, at an offshore site in the Southern Falkland	81

4.65	Map of total Flexural Response due to sediment loads accumulated since the Pliocene (5.332 – 0 million years) for an effective elastic thickness of 40 km and a maximum harmonic degree of 2000	82
4.66	Map of total Flexural Response due to sediment loads accumulated since the Pliocene (5.332 – 0 million years) for an effective elastic thickness of 80 km and a maximum harmonic degree of 2000	83
4.67	Map of total Flexural Response due to sediment loads accumulated since the Miocene (23.03 - 0 million years) for an effective elastic thickness of 40 km and a maximum harmonic degree of 2000	84
4.68	Map of total Flexural Response due to sediment loads accumulated since the Oligocene (33.9 - 0 million years) for an effective elastic thickness of 40 km and a maximum harmonic degree of 2000	85
4.69	Map of total Flexural Response due to sediment loads accumulated since the Eocene (55.8 - 0 million years) for an effective elastic thickness of 40 km and a maximum harmonic degree of 2000	86
4.70	Map of total Flexural Response due to sediment loads accumulated since the Paleocene (65.5 - 0 million years) for an effective elastic thickness of 40 km and a maximum harmonic degree of 2000	87
4.71	Time-dependence evolution of continental uplift due to the forebulge in South America continent (lat=10°S, lon = 60°W) since the Paleocene.....	88
4.72	Time-dependence evolution of continental uplift due to the forebulge along the eastern margin of South America (lat= 5°S, lon=45°W) since the Paleocene. .	89
4.73	Forebulge evolution at a representative location in Colombia (lat=8.5°N, lon= 74°W) from the Paleocene to the Present.	90
4.74	Forebulge evolution at a representative location in Venezuela (lat=7.5°N, lon=62°W) from the Paleocene to the Present.....	90
4.75	Forebulge evolution at a representative location in Guyana (lat=6.5°N, lon=60°W) from the Paleocene to the Present.....	91
4.76	Forebulge evolution at a representative location in Surinam (lat=4.5°N, lon=55.5°) from the Paleocene to the Present.	91
4.77	Forebulge evolution at a representative location in French Guyana (lat= 3.5°N, lon= 53°W) from the Paleocene to the Present.....	92
4.78	Forebulge evolution at a representative location in Brazil (lat= 21.4°S, lon= 43°W) from the Paleocene to the Present.	92
4.79	Forebulge evolution at a representative location in Uruguay (lat= 32.5°S, lon= 54°W) from the Paleocene to the Present.	93

4.80	Forebulge evolution at a representative location in Argentina (lat= 37°S, lon= 60° W) from the Paleocene to the Present.	93
4.81	Map of Flexural Response during the Pliocene-Quaternary interval (5.33 to 0 Ma). The effective elastic thickness is 40 km and a maximum harmonic degree of 2000 was employed.	102
4.82	Contribution to lithospheric flexure, from sediments deposited in each geological epoch, at an offshore site in the Barracuda Abyssal Plain	104
4.83	Contribution to lithospheric flexure, from sediments deposited in each geological epoch, at an offshore site in the Cayos Basin	104
4.84	Contribution to lithospheric flexure, from sediments deposited in each geological epoch, at an offshore site in Colombia Basin	105
4.85	Contribution to lithospheric flexure, from sediments deposited in each geological epoch, at an offshore site in the Magdalena Delta	105
4.86	Contribution to lithospheric flexure, from sediments deposited in each geological epoch, at an offshore site in the Venezuela Basin	106
4.87	Contribution to lithospheric flexure, from sediments deposited in each geological epoch, at an offshore site in the Grenada Basin	106
4.88	Contribution to lithospheric flexure, from sediments deposited in each geological epoch, at an offshore site in the Tobago Basin	107
4.89	Contribution to lithospheric flexure, from sediments deposited in each geological epoch, at an offshore site in the Demerara Abyssal Plain.....	107
4.90	Contribution to lithospheric flexure, from sediments deposited in each geological epoch, at an offshore site in the Marin Guajira.....	108
4.91	Contribution to lithospheric flexure, from sediments deposited in each geological epoch, at an offshore site in the Marin Sinú	108
4.92	Contribution to lithospheric flexure, from sediments deposited in each geological epoch, at an offshore site in the Cariaco Basin.....	109
4.93	Contribution to lithospheric flexure, from sediments deposited in each geological epoch, at an offshore site in the Guyana	110
4.94	Contribution to lithospheric flexure, from sediments deposited in each geological epoch, at an offshore site in the Surinam.....	110
4.95	Contribution to lithospheric flexure, from sediments deposited in each geological epoch, at an offshore site in the French Guyana	111
4.96	Contribution to lithospheric flexure, from sediments deposited in each geological epoch, at an offshore site in the Amazon Delta	111

4.97	Contribution to lithospheric flexure, from sediments deposited in each geological epoch, at an offshore site site in the Brazil	112
4.98	Contribution to lithospheric flexure, from sediments deposited in each geological epoch, at an offshore site site in the Ceará.....	112
4.99	Contribution to lithospheric flexure, from sediments deposited in each geological epoch, at an offshore site in the Potigar	113
4.100	Contribution to lithospheric flexure, from sediments deposited in each geological epoch, at an offshore site site in the Pernambuco.....	114
4.101	Contribution to lithospheric flexure, from sediments deposited in each geological epoch; at an offshore site in the Sergipe-Alagoas.....	114
4.102	Contribution to lithospheric flexure, from sediments deposited in each geological epoch, at an offshore site in the Bahia Sul.....	115
4.103	Contribution to lithospheric flexure, from sediments deposited in each geological epoch, at an offshore site in the Espírito Santo.....	115
4.104	Contribution to lithospheric flexure, from sediments deposited in each geological epoch, at an offshore site in the Campos	116
4.105	Contribution to lithospheric flexure, from sediments deposited in each geological epoch, at an offshore site in the Santos.....	116
4.106	Contribution to lithospheric flexure, from sediments deposited in each geological epoch, at an offshore site in Pelotas.....	117
4.107	Contribution to lithospheric flexure, from sediments deposited in each geological epoch, at an offshore site in the Punta Del Este.....	117
4.108	Contribution to lithospheric flexure, from sediments deposited in each geological epoch, at an offshore site in the Salado.....	118
4.109	Contribution to lithospheric flexure, from sediments deposited in each geological epoch, at an offshore site in the Colorado.....	118
4.110	Contribution to lithospheric flexure, from sediments deposited in each geological epoch, at an offshore site in the Rawson.....	119
4.111	Contribution to lithospheric flexure, from sediments deposited in each geological epoch, at an offshore site site in the San Jorge.	119
4.112	Contribution to lithospheric flexure, from sediments deposited in each geological epoch, at an offshore site site in the San Julian.	120
4.113	Contribution to lithospheric flexure, from sediments deposited in each geological epoch, at an offshore site in the Argentina Basin.	120

4.114	Contribution to lithospheric flexure, from sediments deposited in each geological epoch, at an offshore site shore site in the Northern Falkland.....	121
4.115	Contribution to lithospheric flexure, from sediments deposited in each geological epoch, at an offshore site in the Eastern Falkland.....	122
4.116	Contribution to lithospheric flexure, from sediments deposited in each geological epoch, at an offshore site in the Western Falkland	122
4.117	Contribution to lithospheric flexure, from sediments deposited in each geological epoch, at an offshore site in the Southern Falkland	123
4.118	Map of Flexural Response during the Miocene-Pliocene interval (23.03 to 2.588 Ma). The effective elastic thickness of 40 km and a maximum harmonic degree of 2000 was employed.	124
4.119	Map of Flexural Response during the Oligocene-Miocene interval (33.9 to 5.332 Ma). The effective elastic thickness of 40 km and a maximum harmonic degree of 2000 was employed.	125
4.120	Map of Flexural Response during the Eocene-Oligocene interval (55.8 to 23.03 Ma). The effective elastic thickness of 40 km and a maximum harmonic degree of 2000 was employed.	126
4.121	Map of Flexural Response during the Paleocene-Eocene interval (65.5 to 33.9 Ma). The effective elastic thickness of 40 km and a maximum harmonic degree of 2000 was employed.	127
4.122	Time-dependence of continental uplift due to the forebulge in South America (lat=10°S, lon= 60°W) during the Cenozoic	128
4.123	Time-dependence of continental uplift due to the forebulge along the eastern margin of South America (lat=20°S, lon= 43°W) during the Cenozoic.....	129
4.124	Time-dependent of continental uplift due to the forebulge along the eastern margin of South America (lat=7°S, lon= 39°W) during Cenozoic.....	130
4.125	Major River Basins of South America.	135
4.126	Magdalena River Basin. Taken from Restrepo & Kjerfve (2000).....	137
4.127	Orinoco River Basin. Taken from Warne et al., (2002).....	139
4.128	Amazon River Basin. Taken from Meade (1994).....	141
4.129	La Plata hydrographic Basin. Three hydrological units can be differentiated: Parana River, Paraguay River and the Uruguay River. Taken from Sallun & Suguio, (2010)	144
4.130	Map of the principal South-American Oceanic Currents.....	146

- 4.131 Malvinas Current and Brazil Current. Taken from Matano et al., (2010)..... 148
- 4.132 Map of the principal Oceanic Currents in the Atlantic Ocean between July and September, where the North Brazil current retroflects and goes eastward flowing in the North Equatorial countercurrent. Taken from Philander (2001)..... 150
- 6.1 Contributions to the changing topography of South America. (a) Flexural topography induced by loading of marine sediments deposited during the Quaternary (i.e. the past 2.5 Myr). An elastic thickness of 80 km is assumed for this calculation. (See chapter 4 for more details.) (b) The dynamic topography change over the past 1 Myr predicted on the basis of a tomography-based backward convection simulation carried out by Glišović & Forte (2014). This time-reversed convection simulation employs a quasi-reversible (QRV) treatment of thermal diffusion, with mobile surface plates, and the topography change is calculated in the mantle frame of reference. (For more details, see Glišović & Forte, 2014.)..... 168

LIST OF TABLES

Table	Page
4.1 Summary of the Percent Sediment Thicknesses Accumulated in the Cenozoic.	45
4.2 Parameters used to calculate flexure.....	47
4.3 Offshore flexural depression of South America in the Quaternary Period.....	58
4.4 Maximum Forebulge elevations along the eastern margin of South America during the Quaternary for T_e 40 km	60
4.5 Maximum Forebulge elevations along the eastern margin of South America during the Quaternary for T_e 80 km	61
4.6 Summary of Maximum Flexural depression (foredeep) and Forebulge Amplitudes since the Paleocene	94
4.7 Maximum Forebulge (uplift) over the Quaternary-Paleocene in the eastern region of the continent of South America	95
4.8 Flexural depression and forebulges amplitudes at the Mouths of Primary Rivers.	96
4.9 Maximum Forebulge (uplift) over the Cenozoic in the eastern region of the continent of South America. (Blank sections indicate that there was no uplift in the area during the time period).....	131
4.10 Summary of Maximum Foredeep and Forebulge Amplitudes during Cenozoic	132
4.11 Flexural Foredeep and forebulges amplitudes of Primary Rivers.....	133

LIST OF SYMBOLS AND ABBREVIATIONS

N	Force (Newtons)
M	Mass (Kilograms)
L	Length (Meters or Kilometers)
D	Flexural Rigidity (NL)
Te	Lithospheric Elastic Thickness (L)
P	Horizontal Stresses
δ	Flexure (L)
ρ_m	Density of mantle (M/V)
ρ_s	Density of sediments (M/V)
ρ_c	Density of crust (M/V)
g	Acceleration of gravity (L/T)
qa	Load (L)
E	Young's modulus (Pa)
v	Poisson's ratio (dimensionless)
S	Thickness of sediments (L)

ABSTRACT

The study of the flexure of the South-American lithosphere is of great importance for the understanding of the changes that were experienced by the continent throughout its geological evolution.

The underlying motivation of this research, was to determine: "What processes contributed to changes of South-American topography in the course of the last 65 million years?". The accumulation of vast quantities of sediment on the oceanic (especially Caribbean and Atlantic) margin of the South American continent is one such process. The research presented here will therefore explore and quantify the impact of this sediment accumulation on the flexural deformation of the South American lithosphere and its contribution to topography change during the Cenozoic. With this in mind, the investigation's preliminary step was the creation of a database that contains information about the thickness of the sediments deposited during the six geological epochs comprised by the Cenozoic era, which was prepared from data taken from articles of the drilling Campaign ODP (Ocean Drilling Program) and the DSDP (Deep Sea Drilling Program). In addition, the 2003 Divins global database was utilized for this study as well. These sediment data are employed to determine the thickness that is accumulated in each geological epoch, expressed as fraction of the total sediment thickness along the entire Atlantic margin of South America. Taking into consideration the preceding analysis, the flexural response was numerically calculated using a spectral treatment of the equations based on spherical harmonic basis functions. These calculations were performed using a group of algorithms generated in FORTRAN. The results were implemented on maps that show the change of the continental uplift (flexural forebulge) during the Cenozoic era. From the maps of the flexural response, we suggest that a maximum flexural depression of -2970 meters occurred in the Paleocene, yielding a maximum forebulge uplift of the continent of 153 meters, while the least flexural depression occurred in the Quaternary, prompting a forebulge of 12 meters. Similarly, during the Miocene-Pliocene interval occurred a maximum flexural depression of -1016 meters yielding a maximum continental uplift of 39 meters. Likewise, the Eocene-Oligocene interval experienced a maximum flexural depression of -831 meters, inducing a maximum forebulge of 47 meters. The Paleocene-Eocene interval is characterised by minor sediment-induced flexural depression, yielding a modest forebulge uplift of 21 meters. Finally, attention is given to the important question of the origin of the accumulated sediments in the oceanic margin, which are coming from the Andes, and the shields of Guyana, Brazil and Patagonia. Sediment transport to the oceanic margin is accomplished by different fluvial systems that drain to the continent. The primary river systems involved in this transport are the

Magdalena, Orinoco, Amazon and La Plata flowing into the Caribbean Sea and the Atlantic Ocean. Sediment deposition along the oceanic margin is modulated by a number of oceanographic process that include currents, wind, and tides.

Keys Words: South-America, Cenozoic sedimentary load, lithospheric flexure, fluvial system and oceanic currents.

RÉSUMÉ

L'étude de la flexion de la lithosphère Sud-américaine est de grande importance pour la compréhension des changements qui ont été expérimentés par le continent tout au long de son évolution géologique.

La principale motivation de cette recherche a été de déterminer : "Quels sont les processus qui ont contribué à des changements de la topographie de l'Amérique du Sud au cours des derniers 65 millions d'années ?". L'accumulation de vastes quantités de sédiments sur la marge océanique du continent sud-américain (surtout les Caraïbes et l'Atlantique) est un de ces processus. La recherche présentée ici donc explorera et quantifiera l'impact de cette accumulation de sédiments sur la déformation flexural de la lithosphère de l'Amérique du Sud et sa contribution au changement de la topographie durant le Cénozoïque. Dans cette optique, l'étape préliminaire de la recherche a été la création d'une base de données qui contient des informations sur l'épaisseur des sédiments déposés durant six époques géologiques qui constituent l'ère Cénozoïque. Les données ont été extraites des articles des campagnes de perforation ODP ("Ocean Drilling Program") et du DSDP ("Deep Sea Drilling Program"). La base de données mondiale de Divins 2003 a également été utilisée pour cette étude.

Ces données stratigraphiques sont utilisées pour déterminer l'épaisseur accumulée dans chaque époque géologique. Ils sont exprimés comme la fraction de l'épaisseur totale des sédiments sur toute la marge Atlantique de l'Amérique du Sud. La réponse de la flexion a été calculée numériquement utilisant un traitement spectral des équations basées sur les fonctions de base d'harmoniques sphériques. Ces calculs ont été effectués en utilisant un groupe d'algorithmes générés en FORTRAN. Les résultats ont été affichés sur des cartes qui montrent le changement du soulèvement continental (flexural forebulge) durant l'ère Cénozoïque. À partir des cartes de la réponse à la flexion, nous suggérons qu'une dépression flexurale maximale de -2970 mètres s'est produite dans le Paléocène, ce qui donne un soulèvement maximal (forebulge) du continent de 153 mètres, tandis que la plus faible dépression flexurale s'est produite dans le Quaternaire, provoquant un soulèvement (forebulge) de 12 mètres. De la même façon, durant l'intervalle du Miocène-Pliocène s'est produite une dépression flexural maximale de -1016 mètres produisant un soulèvement continental maximal de 39 mètres. De même, l'intervalle Éocène-Oligocène a expérimenté une dépression maximale de -831 mètres, induisant un soulèvement maximal (forebulge) de 47 mètres. L'intervalle Paléocène-Éocène est caractérisé par une dépression mineure; cette dépression induite par les sédiments, c'est qui donne un modeste soulèvement (forebulge) de 21 mètres. Enfin, l'attention est donnée à l'importante question de l'origine des sédiments accumulés dans la marge océanique, lesquels proviennent des

Andes, et des boucliers de Guyane, du Brésil et de la Patagonie. Le transport des sédiments à la marge océanique est accompli par différents systèmes fluviaux qui drainent le continent. Les principaux systèmes fluviaux impliqués dans ce transport sont le Magdalena, l'Orénoque, l'Amazone et La Plata qui se jettent dans la mer des Caraïbes et dans l'océan Atlantique. Le dépôt des sédiments le long de la marge océanique est modulé par un certain nombre de processus océanographiques qui comprennent les courants, les vents et les marées.

Mots clés: Amérique du Sud, la charge sédimentaire Cénozoïque, flexion lithosphérique, système fluvial et les courants océaniques.

CHAPTER I

INTRODUCTION

The lithosphere, which is considered to be the outermost layer of the mantle, rests on a low-viscosity layer called the asthenosphere, which flows to sustain the process of isostatic adjustment. (Barrell, 1914). The application of a load on the surface, generating vertical forces, gives rise to deformation or flexure of the lithosphere. This flexure is dependent on its flexural rigidity, which is a measure of the elastic resistance of the lithosphere (Walcott, 1970) and determines the amplitude and wavelength of the flexure caused by loads on the surface (Watts, 1978). Burov & Diament, (1992) suggest that the mechanical strength of the lithosphere, vertical and horizontal, are primarily controlled by the applied load, by restraining forces and by the thermal structure of the plate.

Numerous studies have elucidated the deformation of the lithosphere caused or induced by different surface loads such as volcanoes, ice, intrusion and sediment accumulation. In the case of the continental lithosphere, studies such as those conducted by Karner & Watts, (1983) show how the lithosphere is deformed by surface loads associated with fold/thrust belts and subsurface loads such as obducted blocks/flakes, which are developed during continental collision, convergence and suturing. Similarly, studies by Walcott, (1969) in Canada focused on the deformation of the lithosphere caused by ice sheets; where the lithosphere is treated as an elastic layer overlying a viscous layer. Garcia (2003) has shown that isostatic flexure may be induced by normal listric faulting of the crust, which is important to understand the geometry of sedimentary basins.

In the case of the oceanic lithosphere treated as a thin plate of elastic rheology, loads such as volcanoes flex the lithosphere thereby generating uplift with geological features near the area (islands, atolls). If the volcano continues to grow, flexure magnitude increases as the wavelength remains constant, with the exception of changes caused by the increase in the radius of the load (McNutt & Menard, 1978). Similarly Watts et al., (1975) and Watts and Cochran, (1974) analyzed and modelled flexure of the Hawaiian and Emperor chain that is maintained for long periods, employ data that constrain gravity and subsidence along the chain. Subsequent admittance analyses confirm that rigidity changes little with age of the lithosphere and that its effective elastic thickness is in the range of 20-30 km (Watts, 1978). Bodine et al, (1981) built a rheological model of the oceanic lithosphere based on results of experimental rock mechanics, in order to determine the relationship between flexure parameters and rheological properties. The results of the model suggest that, in responding to the loads of seamounts and oceanic islands, the lithosphere deflection is insensitive to the size and duration of the load for times greater than 1 to 10 million years. Based on the above, it can be inferred that the effective flexural rigidity of the oceanic lithosphere is a function of lithosphere age at the time of loading and therefore, depends on lithospheric temperature (Bodine et al, 1981; Watts, 1978), such that flexural rigidity increases with age. (Watts et al, 1980).

Finally, research on continental margin, such as that conducted by Karner & Watts (1982) which study the relationship between free-air gravity and topography, considered sedimentary loads and interpreted results in terms of a flexural isostatic model. These authors argue that if the mechanical properties of the oceanic lithosphere are similar to the lithosphere of the continental margin, then the sedimentary load on a young continental margin is associated with low elastic thickness (T_e) values while sediment loads on an old continental margin can be associated with higher T_e values.

For this reason the old continental margin of North America is associated with high values of T_e with values ranging from 10 to 20 Km. The opposite happens in the young Coral Sea/Lord Howe rise margin where T_e reaches values of about 5 km. The above shows that the elastic thickness T_e increases with the age of the lithosphere (Watts et al., 1980). The results of the elastic thickness were obtained using parameters such as Young's modulus with a value of 10^{12} Pa and Poisson's ratio of 0.25. (These values are referred in order to show how the elastic thickness changes if these values are modified)

Also, Pazzaglia & Gardner (1994) modeled the flexural isostatic deformation caused by sedimentary loads deposited offshore and the continental denudation experienced in the Middle US Atlantic Passive Margin. Their model describe the uplift of the Appalachian Piedmont, as well as the subsidence of the Salisbury Embayment. This study was developed using data from stratigraphic sections and fluvial deposits of the coastal plain, Susquehanna River terraces profiles, offshore load volumes and denudation rates. With this data, there were simulations that show the effects of different values of flexural rigidity and the rate of erosion over the flexural deformation. With this in mind, the authors found the best simulation was the one which had a good correlation between the erosion rate (10 mm/My), the stratigraphic and the terrace data using an average elastic thickness of 40 km, for which it was obtained a flexural rigidity of 4×10^{23} Nm.

Finally, research conducted by Driscoll & Karner (1994) in the passive continental margin of South America studied the deformation caused by the sedimentary load (Amazon Fan) and the uplift generated onshore, which is associated with the peripheral bulge that can modify the lower part of river networks. These authors employed a 2-D elastic plate loading formulation that assumed an elastic thickness of 38 km for the Amazon delta.

There is significant motivation in carrying out this research because few studies have focused on studying the temporal evolution of flexure caused by the sedimentary load on the continental margin of South America. Similarly, it is important to understand the change in the continent's topography over the Cenozoic (i.e. the past 65.5 My), in order to better understand geomorphological surface processes such as erosion, sediment transport, and river drainage that are strongly dependent on changes in topography. The Cenozoic era was characterized by episodes of major subduction-driven crustal shortening along the western margin of South America (e.g. Pearson et al., 2013), yielding substantial uplift of the central Andes that provides an important source for sediments that are ultimately deposited along the Atlantic margin.

The work presented below is therefore focused on determining the contribution to the topography of South America from flexural deformation caused by sediment accumulation on the continental shelves. This study will cover all the periods that make up the Cenozoic Era: Paleogene, Neogene and Quaternary (65.5 Ma- 0 Ma).

In carrying out this study, we divided the continental margin of South America into four main areas: The Caribbean Zone, the Amazon Zone, the Brazil-Argentina Zone and the Scotia Zone. This admittedly informal division was motivated by the recognition that the dynamics of sediment accumulation in these four areas is dependent on different river basin discharges into each of these zones. Data on sediment accumulation in each zone have been taken from various sources, including: well log information from drill cores obtained in the area by the Deep Sea Drilling Project (DSDP) and the Ocean Drilling Program (ODP), different publications, and especially the Total Sediment Thickness of the World's Oceans & Marginal Seas (Divins, 2003). In addition, sediment density data are taken from the Global Digital Map of Sediment Thickness on a $1^\circ \times 1^\circ$ scale. (Laske & Masters, 1997).

The elastic flexure model is determined by solving the differential equations that describe and govern elastic deformation of a thin 2-D plate (e.g. Turcotte & Schubert, 2002). These equations depend on flexural rigidity and, in turn, on the elastic thickness, the Young Modulus and the Poisson ratio. Flexural response is found numerically using a spectral treatment of the equations that is based on spherical harmonics. To accomplish these calculations a set of algorithms created in FORTRAN (Formula Translating System) were developed.

This thesis is presented in six chapters. Beginning with the current, the introduction. The second chapter describes the methodology, which shows each of the steps involved in the calculation of flexure. A brief description of the theory of flexure, as well as the equations and calculations based on spherical harmonics are discussed in the third chapter. Finally, the results are analyzed and interpreted in the fourth chapter, which includes a presentation of the sediment thickness database, the algorithm to find flexure and the flexure maps by age. These results are discussed and compared to previous studies in the fifth chapter and the main conclusions are presented in the final, sixth chapter.

CHAPTER II

METHODOLOGY

2.1 Database Construction

This study began with a search for sediment thickness calibrated on the geological timescale. In order to do so, data obtained from articles were compiled, in addition to information available on wells from the different campaign reports made by the Ocean Drilling Program (ODP) and the Deep Sea Drilling Project (DSDP). The data obtained were organized systematically in a table with the following parameters: age, latitude and longitude, thickness in meters, site, thickness from high spatial resolution global sediment database (Divins, 2003), relative thickness (expressed as a percentage of total thickness), penetration and source. (See Appendix B).

2.2 Development of Histograms

Based on the compiled sediment thickness data, and using the thickness from high spatial resolution global sediment database (Divins, 2003), the percent accumulation of sediment, relative to total thickness was determined as a function of time. Using this approach, histograms were concentrated showing the variation of percent sediment thickness with geologic age. This procedure was adopted in order to select the most representative thickness for each geological time period. A total of 24 histograms were

developed for a better understanding and interpretation of the evolution of sediment thickness with age.

Histograms were constructed for each of the zones comprised by the continental margin of South America: Zone I the Caribbean Zone, Zone II the Amazon, Zone III Brazil-Argentina and Zone IV Scotia Sea (Figure 4.1). Six histograms were developed for each geological epoch: Quaternary (2.588 to present Ma), Pliocene (5.332 to 2.588 Ma), Miocene (23.03 to 5.332 Ma), Oligocene (33.9 to 23.03 Ma) Eocene (55.8 to 33.9 Ma) and Paleocene (65.5 to 55.8 Ma).

2.3 Use of FORTRAN

All numerical work carried out in the course of this research was carried out using Fortran (Formula Translating System), a high-level programming language designed for the development and calculation of mathematical and scientific applications.

2.3.1 Numerical algorithm to find sediment densities

A Fortran code was written to take densities from a Global Digital Map of Sediment Thickness at a $1^{\circ} \times 1^{\circ}$ scale (Laske & Masters, 1997). This global map was originally developed using atlases and hand-made maps, as well as published high-resolution digital maps, such as the Map of the World provided by the Exxon research group (1985). The sediment densities as a function of depth were derived using the Ludwig, Nafe and Drake curves. (Ludwig et al., 1970). In this global map of sediment thickness, the sediment density is parameterized on the basis of three layers: the first layer is between 0 and 2000 meters thick, the second layer is between 2000 and 4000 meters

thick and the third layer is for all sediment columns with thickness greater than 4000 meters.

The Fortran code is organized in terms of a geographical grid with input given by latitude and longitude in degrees. As a result, the code prints the sediment thickness of each of the layers, the density of each of the layers, the total sediment thickness and the average density for the point required. Each point on the grid has a value of specific density. The values used for layer 1, layer 2 and layer 3 are 1500 Kg/m^3 , 2300 Kg/m^3 and 2545 Kg/m^3 respectively.

2.3.2 Algorithm to Find Sediment Load using the thickness from high spatial resolution Global sediment Database (Divins,2003)

Based on the most representative percent thickness for each geological age (See Table 2), obtained with the histograms, a Fortran code was created to extract the sediment thickness, as a function of age, from the global high-resolution data of Divins, (2003).

The output file is the total sediment load for each geological epoch, on a $5' \times 5'$ resolution grid.

2.3.3 Numerical Algorithm to Determine Flexure

Lithospheric flexure on the continental margin of South America is determined by calculating the spherical harmonic coefficients of the sedimentary loads in the different geological epoch from the Paleocene to the present.

The calculated time-dependent sediment loads are then used to calculate elastic flexure in spherical harmonics for the same geological periods, using the 2D extension of the equation of one-dimension flexure employed by Pazzaglia & Gardner (1994).

The following numerical codes were created to implement the basic steps required in the full flexure calculation:

- A code to calculate the spherical harmonic coefficients of the sediment loads distributed on a spatial grid.
- A code to calculate the 2-D elastic flexure on a spherical surface in terms of a spectral representation of the flexure equation. (Using an elastic thickness of 40 km and furthermore varying it to 80 km in the Pliocene and Quaternary ages)
- A code to read the harmonic coefficients of elastic flexure and output a spatial grid with values distributed as a function of latitude and longitude.

The elastic flexure code is presented in Appendix C.

2. 3.4 Use of Generic Mapping Tool GMT

The results output by the Fortran codes were graphically plotted by using the set of utilities of the GMT program: a free open-source collection of programs created and developed by Wessel & Smith., (1995)

CHAPTER III

ISOSTASY AND LITHOSPHERIC FLEXURE

The earth is composed of a set of concentric layers that are defined either in terms of their composition and/or phase or in terms of their rheology. From the rheological standpoint, they consist of the lithosphere (crust and part of the mantle), the asthenosphere, the upper mantle and the lower mantle.

The lithosphere is traditionally considered to be the outermost rheological layer of the earth, with long-term elastic strength overlying a viscous layer called the asthenosphere (Barrel 1914). The vertical balance of forces on the lithosphere gives rise to a condition of static equilibrium known as isostasy.

3.1 Isostasy

Isostasy is a principle that rests on the fundamental assumption of the hydrostatic equilibrium of the mantle. To achieve this equilibrium there is a balance between surface loads (e.g. topography) and deflections of the crust-mantle boundary and lithosphere such that at an equipotential surface such as in the compensation depth, the total pressure is everywhere constant. In practice, this requires that starting at the compensation depth, the mass of any vertical column above it is everywhere the same

independent of any lateral variations of densities and/or thickness in the overlying mantle and the crust.

3.1.1 Local Isostasy

The first models of isostatic compensation were proposed by Airy (1855) and Pratt (1855). These models were known as local compensation models. Airy's compensation model was based on the Archimedes principle, where the surface of the earth (crust) floats on a denser fluid substratum (asthenosphere). The thicker portions of the crust float higher than other thinner portions and they, in turn, have a correspondingly thicker root. These changes in crust thickness are necessary to maintain isostatic compensation (Figure 3.1a). Pratt's compensation model (1855) suggests that topography is produced by blocks of crust that have lateral variations in density, which all end at the same depth of the compensation. (Figure 3.1b)

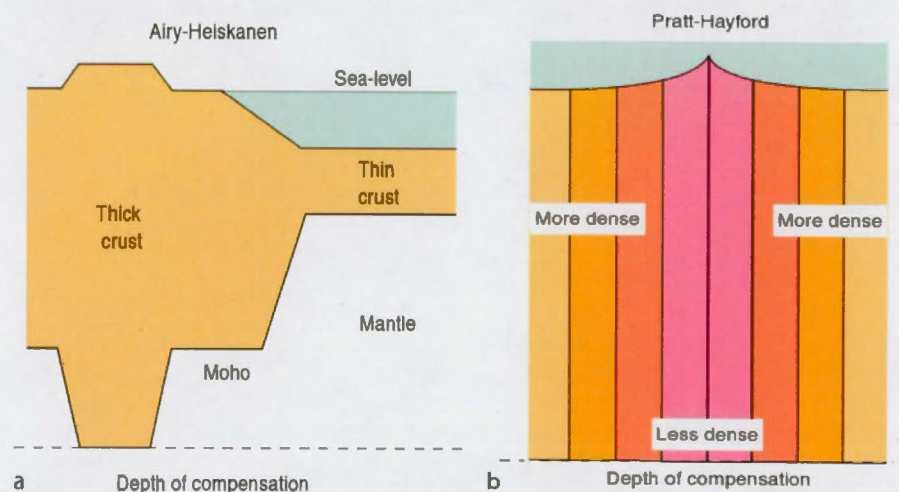


Figure 3.1 Local Compensation Models. (Taken from Gupta H. K. 2011)

The above local compensation models do not take into account rigidity (i.e. finite long-term strength) or lateral strain variations. The inclusion of finite rigidity leads to the concept of regional flexural isostasy model. In this flexural isostatic compensation the regional flexure is proportional to lithospheric rigidity and the size of the load.

3.1.2 Regional Flexural Isostasy

The first regional compensation model was described by Vening Meinesz (1939), who proposed that the crust and lithosphere behave like an elastic layer that flexes under the application of a surface load, giving rise to regional compensation. (Watts 2001). (Figure 3.2)

Similarly, theoretical treatments such as those developed by Turcotte & Schubert (2002) and Watts (2001) show that flexure may be modeled considering a system of forces or loads applied vertically on a thin elastic plate. These forces arise from a variety of surface loads, such as the accumulation of sediments, volcanoes, seamounts, ice and intrusions, cause vertical deflections of the solid surface.

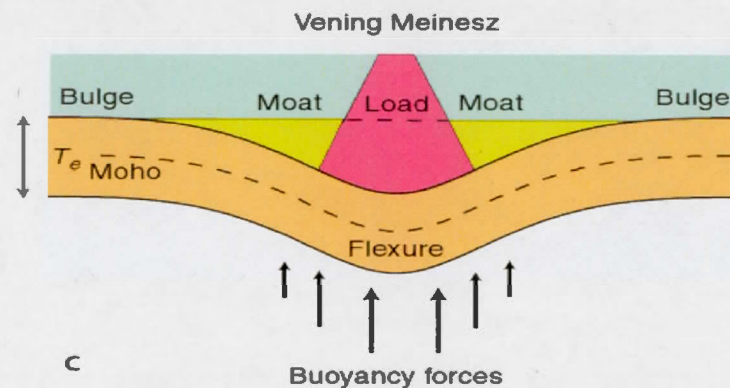


Figure 3.2 Lithospheric flexure caused by surface loads. (Taken from Gupta H. K. 2011)

It is important to add that these flexure models may be developed on the oceanic lithosphere and the continental lithosphere. On one hand, the flexure caused by the load on the oceanic lithosphere will be filled either with water or sediment (Figure 3.3a) and the fill material is less dense than the density of the lithospheric mantle it is replacing. On the other hand, the flexure caused by the load on the continental lithosphere will be filled by sediments from the crust. (Figure 3.3b)

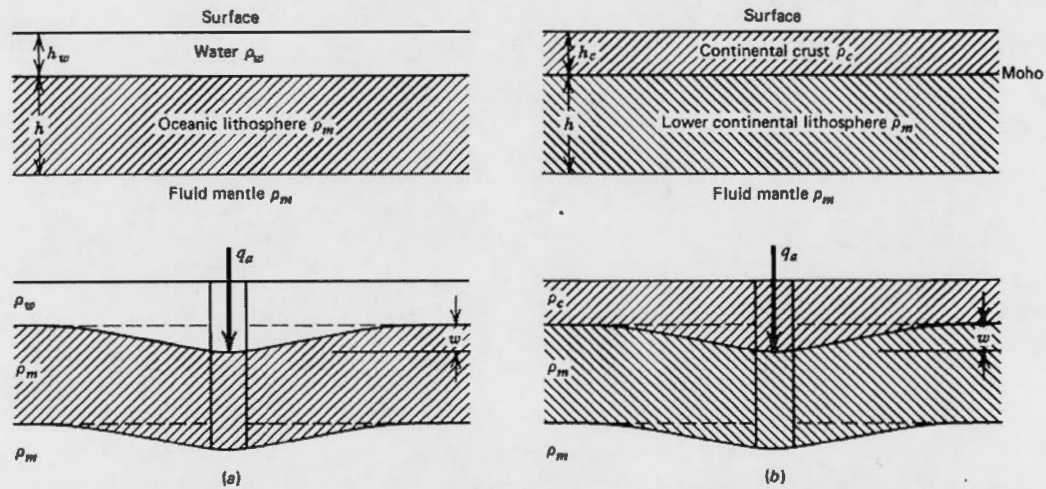


Figure 3.3 Models for calculating the hydrostatic restoring force on lithospheric plates deflected by an applied load q_a . (a) Oceanic Case. (b) Continental case. (Taken from Turcotte & Schubert, 2002).

According to Turcotte & Schubert (2002), the equation that describes lithospheric flexure in 2-D coordinate system is expressed as follows:

$$D \frac{d^4 \delta}{dx^4} + P \frac{d^2 \delta}{dx^2} + (\rho_m - \rho_s) g \delta = q_a \quad (3.1)$$

Where,

x: horizontal distance from the load to a point on the surface of the plate

δ : vertical deflection of the plate that varies with x

D: Flexural rigidity

P: Horizontal stresses

ρ_m : density of the mantle.

ρ_s : density of the sediments, or other infill material.

g: acceleration of gravity.

q_a : load applied on the lithosphere.

Horizontal stress P (here assumed constant) in the elastic plate gives rise to buckling if the elastic thickness is sufficiently small (Turcotte & Schubert, 2002). In general, however, the elastic thickness of the lithosphere is sufficiently large that the horizontal stress P has a small influence on the bending behavior (Turcotte & Schubert, 2002). For this reason, in the following calculations, it is assumed that $P=0$. In addition, the restorative hydrostatic force that compensates for the applied load was taken into consideration, by the 3rd term on the left-hand side of (3.1).

Finally, the equation of 2-D lithospheric flexure is governed by the following:

$$D \frac{d^4 \delta}{dx^4} + (\rho_m - \rho_w) g \delta = q_a \quad (3.2)$$

Where the first term of the equation represents elastic deformation and is proportional to the flexural rigidity of the plate. D determines the degree to which the elastic plate supports the load. When applying a load on a thin elastic plate, the flexure is greater than when the load is applied to a thicker plate with greater elastic rigidity.

The expression that relates flexural rigidity to elastic thickness is:

$$D = \frac{Eh^3}{12(1 - \nu^2)} \quad (3.3)$$

Where E is the Young Modulus, ν is the Poisson Ratio and h is elastic thickness.

In this study, a thin plate with elastic rheology is considered, which assumes that the flexure stresses are distributed linearly with depth and when the load is removed, the original state is recovered. One of the important characteristics of elastic flexure that are relevant to this study is that, with increasing distance from the load, flexure decreases and then changes sign, giving rise to an uplift known as forebulge.

3.1.3 2-D Lithospheric Flexure on a Sphere

We may rewrite the 1-D equation (3.2) describing elastic flexure as follows:

$$D \frac{d^4 \delta}{dx^4} + g(\rho_m - \rho_w) \delta = g(\rho_s - \rho_w) S \quad (3.4)$$

in which we again assumed that lithospheric flexure δ occurs under a water layer, thus generating an upward hydrostatic restoring force $g(\rho_m - \rho_w) \delta$, and the applied downward load $q_a(x) = g(\rho_s - \rho_w) S$ is due to sediments that have accumulated to a thickness S.

The equation governing the elastic deformation of a spherical shell is more complex owing to the surface curvature (e.g. Kraus 1967, Beuthe 2008). A major simplification is obtained by assuming the "thin shell" approximation which applies when the thickness h of the shell is much less than the radius R of the sphere (typically $h/R < 0.1$) and when the wavelength λ of the load applied to the shell is much larger than the shell thickness. The latter condition implies that $\lambda > 3h$ (Beuthe 2008); although in practice this condition is not important for the determination of displacements δ since they become small at small wavelengths (i.e. the rigidity of the shell entirely supports small-wavelength loads).

One further simplification is obtained from the "flat Earth" approximation which is valid when the wavelength λ of the load is small compared with the radius R (e.g. Turcotte 1979). In the latter limit the corresponding "flat Earth" flexure equation for a 2-D spherical surface reduces to the following expression (Turcotte 1979):

$$D\Delta_h^2\delta + g(\rho_m - \rho_w)\delta = g(\rho_s - \rho_w)S \quad (3.5)$$

Where Δ_h is the horizontal Laplace operator (see Appendix A):

$$\Delta_h f = \frac{1}{r^2 \sin\theta} \frac{\partial}{\partial\theta} \left(\sin\theta \frac{\partial f}{\partial\theta} \right) + \frac{1}{r^2 \sin^2\theta} \frac{\partial^2 f}{\partial\varphi^2} \quad (3.6)$$

We will employ equation (3.5) in all the sediment-induced flexure calculations presented below. One complication we must deal with in finding solutions to equation (3.5) arises from the recognition that the density of marine sediments ρ_s increases with depth owing to pressure-induced compaction and decreased porosity (e.g. Nafe & Drake 1957). The density profile in any given sediment column must therefore also vary laterally because of changing water depths and changes in total sediment thickness:

$$\rho_s = \rho_s(z, \theta, \varphi) \quad (3.7)$$

Where z is the depth in the sediment column and (θ, φ) are the geographical coordinates. In the calculations presented below, we employ the sediment-density profiles compiled by Laske & Masters (1997).

The sediment thickness S is, of course, a function of geographic position (θ, φ) and it also depends (as discussed in detail in section 4) on the period of time over which the sediments have accumulated. Denoting this time span, from some time in the geological past to the present, by the variable t , we may write:

$$S = S(t, \theta, \varphi) \quad (3.8)$$

By virtue of the dependence of sediment density and sediment thickness on position, space and time in expressions (3.7) & (3.8), the following time-dependent "load function" L may be defined:

$$L(t, \theta, \varphi) = \int_0^{S(t, \theta, \varphi)} [\rho_s(z, \theta, \varphi) - \rho_w] dz \quad (3.9)$$

For the purpose of subsequent numerical calculations, it is useful to employ a normalized load function that is defined as follows:

$$\hat{L}(t, \theta, \varphi) = (\rho_m - \rho_w)^{-1} L(t, \theta, \varphi) \quad (3.10)$$

With this time-dependent load function we rewrite the loading term on the right-hand side of equation (3.5) - which is only valid if sediment density does not vary with depth - finally yielding:

$$D\Delta^2\delta + g(\rho_m - \rho_w)\delta = g(\rho_m - \rho_w)\hat{L}(t, \theta, \varphi) \quad (3.11)$$

Expression (3.11) is the governing equation for sediment-induced lithospheric flexure that is employed in all calculations presented below.

3.1.4 Spherical Harmonic Solutions of the 2-D Flexure

In this study, we extensively exploit the properties of spherical harmonics described in Appendix A to employ the following forward and inverse harmonic representation of functions on a sphere:

$$f(\theta, \varphi) = \sum_{l=0}^{\infty} \sum_{m=-l}^l f_l^m Y_l^m(\theta, \varphi)$$

$$f_l^m = \frac{1}{4\pi} \int_0^{2\pi} d\varphi \int_0^{\pi} \sin \theta d\theta Y_l^{m*}(\theta, \varphi) f(\theta, \varphi)$$

Where f_l^m are the complex spherical harmonic coefficients of the bounded continuous function $f(\theta, \varphi)$.

Employing the above expression and using the 5min x 5min geographic grid of the sedimentary thickness for each geological epoch, the spherical harmonic coefficients of the sedimentary load $\hat{L}(\theta, \varphi)$ (where we have omitted the dependence on time t for notational convenience) are determined as follows:

$$\hat{L}_l^m = \frac{1}{4\pi} \int_0^{2\pi} d\varphi \int_0^\pi \sin \theta d\theta Y_l^m(\theta, \varphi) \hat{L}(\theta, \varphi) \quad (3.12)$$

In practice, the coefficients \hat{L}_l^m are determined to maximum harmonic degree $L_{\max}=2000$, corresponding to the spatial resolution of the data.

We begin by expressing both the normalized sediment load and lithospheric flexure in terms of spherical harmonics, as follows:

$$\hat{L}(\theta, \phi) = \sum_{l=0}^{L_{\max}} \sum_{m=-l}^l \hat{L}_l^m Y_l^m(\theta, \phi) \quad (3.13)$$

$$\delta(\theta, \phi) = \sum_{l=0}^{L_{\max}} \sum_{m=-l}^l \delta_l^m Y_l^m(\theta, \phi) \quad (3.14)$$

Where $L_{\max}=2000$. By substituting the spherical harmonic expansions (3.13) and (3.14) into the equation for lithospheric flexure (Equation 3.11), we obtain:

$$\left(\sum_{l=0}^{L_{\max}} \sum_{m=-l}^l \delta_l^m D \left[\frac{K^2}{r_e^2} \right] Y_l^m \right) + \left(\sum_{l=0}^{L_{\max}} \sum_{m=-l}^l \delta_l^m g(\rho_m - \rho_w) Y_l^m \right) = \left(\sum_{l=0}^{L_{\max}} \sum_{m=-l}^l g(\rho_m - \rho_w) \hat{L}_l^m Y_l^m \right) \quad (3.15)$$

Where the surface Laplacian operator is equal to
$$\left[\frac{\Lambda^2}{r_e^2} \right]^2 Y_l^m = \left[-\frac{l(l+1)}{r_e^2} \right]^2 Y_l^m \quad (3.16)$$

By substituting Equation (3.16) in Equation (3.15), we get:

$$\sum_{l=0}^{L_{\max}} \sum_{m=l}^l \left[\delta_l^m D \frac{l^2(l+1)^2}{r_e^4} + \delta_l^m g(\rho_m - \rho_w) \right] Y_l^m = \sum_{l=0}^{L_{\max}} \sum_{m=l}^l \left[g(\rho_m - \rho_w) \hat{L}_l^m \right] Y_l^m \quad (3.17)$$

Since the above expression is valid everywhere on the spherical surface, for any combination of l and m , we conclude that

$$\left[D \frac{l^2(l+1)^2}{r_e^4} + g(\rho_m - \rho_w) \right] \delta_l^m = g(\rho_m - \rho_w) \hat{L}_l^m \quad (3.18)$$

Finally, we obtain the following expression for the harmonic coefficients of elastic flexure, δ_l^m in terms of those for the sediments loads:

$$\delta_l^m = f_l \hat{L}_l^m \quad (3.19)$$

Where f_l is the wavelength-dependent elastic filter function that describes how the finite elastic strength of the lithosphere reduces the topography relative to that

calculated assuming pure isostasy. This filter function is given by the following mathematical expression:

$$f_l = \frac{1}{[1 + l^2(l+1)^2 \beta]} \quad (3.20)$$

Where the parameter β is defined to be:

$$\beta = \frac{D}{(\rho_m - \rho_w) g r_e^4} \quad (3.21)$$

The β parameter is a measure of the non-dimensional natural elastic wavelength for the flexure of the lithosphere (Turcotte & Schubert, 2002):

$$\beta = \left(\frac{\lambda_{elastic}}{2\pi r_e} \right)^4 \quad (3.22)$$

Where,

$$\lambda_{elastic} = 2\pi \left[\frac{D}{(\rho_m - \rho_w) g} \right]^{1/4} \quad (3.23)$$

It is important to emphasize that the above equations (3.13), (3.14), (3.19)–(3.23) are calculated numerically by the different FORTRAN codes outlined above in section 2-3-2 (see the Appendices for details).

CHAPTER IV

RESULTS

4.1 Database

For our study, we focussed on the sediment thicknesses deposited during the Cenozoic era, comprising the Paleogene, Neogene and Quaternary Periods, that is to say, from 65.5 million years ago to the present day. The sediment thickness data were taken from reports as well as biostratigraphic and stratigraphic columns based on cores obtained from the different campaigns of the Ocean Drilling Program (ODP) and Deep Sea Drilling Project (DSDP).

For the purpose of subsequent interpretations, we divided the sediment compilations into four main areas, whose geographic definition is shown in Figure 4.1: Zone I, Caribbean; Zone II, Amazon; Zone III, Brazil-Argentina, Zone IV, Scotia. The data we assembled consists of the following elements: age, latitude, longitude, sediment thickness, site, thickness from high spatial resolution global sediment database (Divins, 2003), percent sediment thickness with respect to the global high-resolution database of total thickness (Divins 2003), and source (see Appendix B).

Total Marine Sediment Thickness (5 min x 5min)

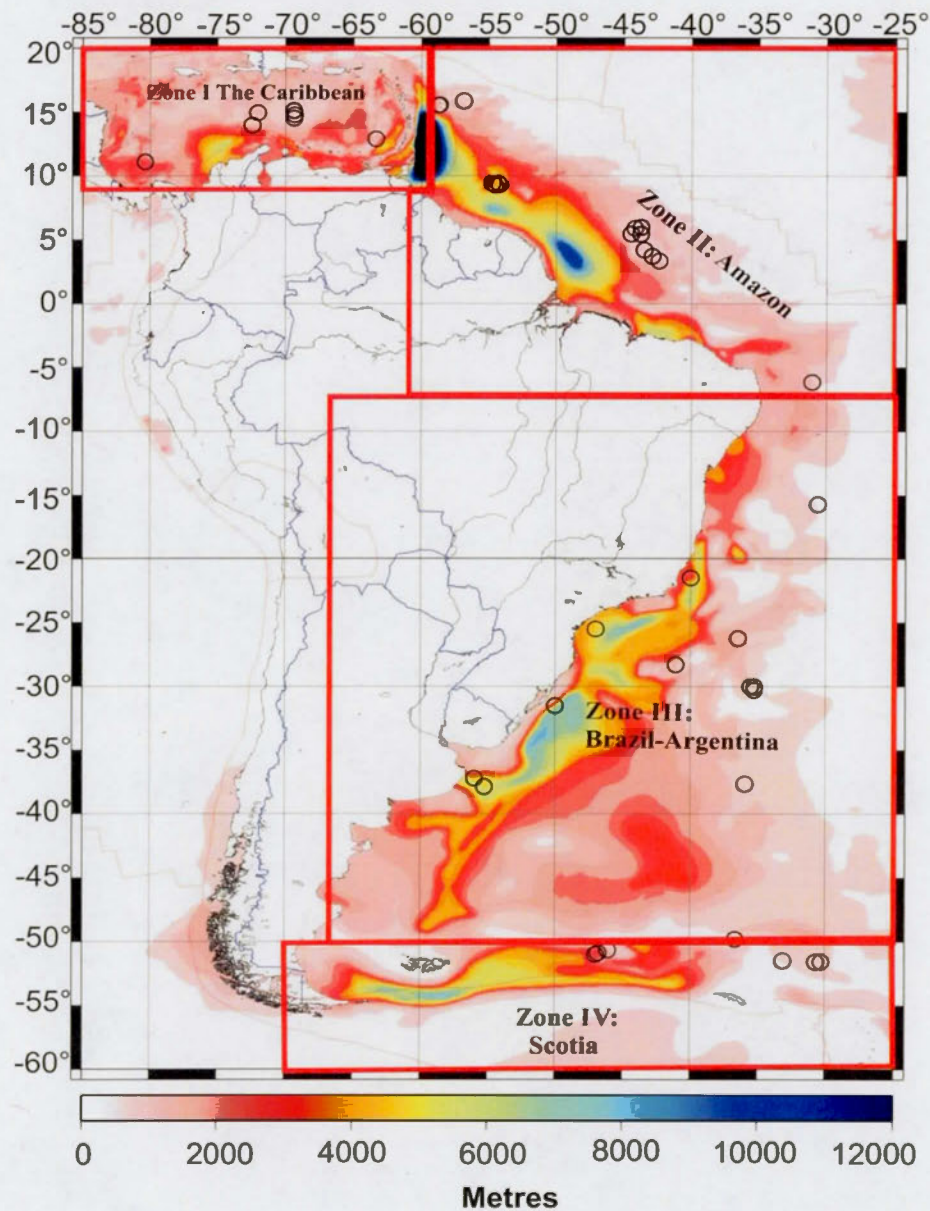


Figure 4.1 Location of four sediments deposition zones (I to IV) and the sites of wells utilized in different campaigns of the Ocean Drilling Program (ODP) and Deep Sea Drilling Project (DSDP).

4.2 Histograms

The total sediment thicknesses data we employ is extracted from previous studies, such as those conducted by Divins (2003). This database contains 5-minute resolution data for oceans and continental shelves. It was developed by the National Geophysical Data Center (NGDC), Marine Geology & Geophysics Division and was compiled from previous publications, isopach maps, drilling results, seismic reflection profiles and seismic data.

The global 5-minute sediment thickness data and the sediment thickness we compiled from ocean drilling data were compared. This comparison revealed some significant differences, where the thickness from local drill data was on average smaller than that given by global data.

In attempting to understand the origin of these differences, we must in the first place recognize that the sediment thickness in the global database come from different sources (isopach maps, seismic data, and different drilling campaigns) without taking into account the geologic ages. On the other hand, in the present investigation, we employ the data of drilling campaigns because the sediment thickness is calibrated on the geological time scale, which is of great importance for this research. A second issue to be considered, is the fraction of the total sediment column that is recovered by the drill cores, particularly when the deepest strata in the column are not sampled, thus leading to an incomplete age calibration. In this regard, we note that the maximum age horizon sampled by the drill-core data that we assembled corresponds to the Cretaceous. In contrast, the global high-resolution database, which extends down to the

acoustic basement, represents a much greater time span that dates back to the time of rifting between South America and Africa.

The combination of global data and drill-core data were used to quantify accumulation of sediments as a function of time. The database (Appendix B) shows the sediment thickness, expressed as a fraction (percent) of total thickness, classified by age. Six histograms were developed for each zone, one per age interval, with percent thickness represented on the x-axis (horizontal) and frequency (i.e. number of samples) are on the y-axis (vertical).

The most representative percentage was selected from each histogram for each age interval (See Table 4.1). The absolute thickness as a function of age was subsequently determined using the 5-minute-resolution total thickness database to obtain the sedimentary load to be used to find flexure.

In the following, we summarize the histograms for each of four zones:

4.2.1 Zone I: The Caribbean

The geographic area encompassed by Zone I, the Caribbean Zone, is shown in Figure 4.1.

4.2.1.1 Histogram of the percent sediment thickness in the Quaternary (2.588 to present Ma)

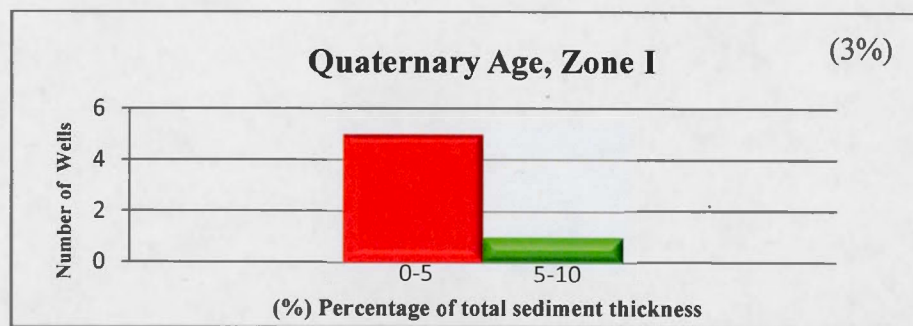


Figure 4.2 Histogram of the percent sediment thickness in the Quaternary. Zone I

Figure 4.2 shows the histogram of the percent sediment thickness for the Quaternary. This histogram shows an L-shaped distribution, where we can clearly distinguish the frequency of the percent sediment thickness from 0-5% compared to the next interval of 5-10%. The percentage with the highest frequency (or probability) is between 0 and 5%. We therefore selected this interval and simply employ the mean value of 3% assuming a rounding to the next-highest whole value.

4.2.1.2 Histogram of the percent sediment thickness in the Pliocene (5.332 to 2.588 Ma)

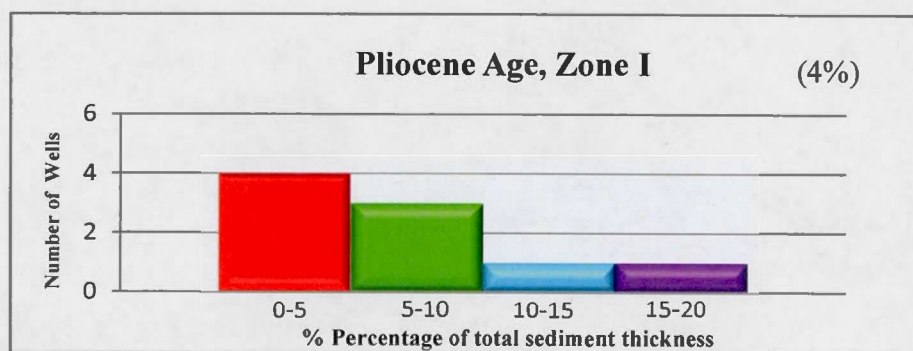


Figure 4.3 Histogram of the percent sediment thickness in the Pliocene. Zone I

Figure 4.3 shows the histogram of the percent sediment thickness for the Pliocene. This histogram has an elongated L-shaped distribution, where the interval with the highest frequency is from 0 to 5%. We thus select this interval, but also take into account the nearly equivalent frequency of the next highest interval, leading us to choose 4% as the value of the maximum frequency thickness.

4.2.1.3 Histogram of the percent sediment thickness in the Miocene (23.02 to 5.332 Ma)

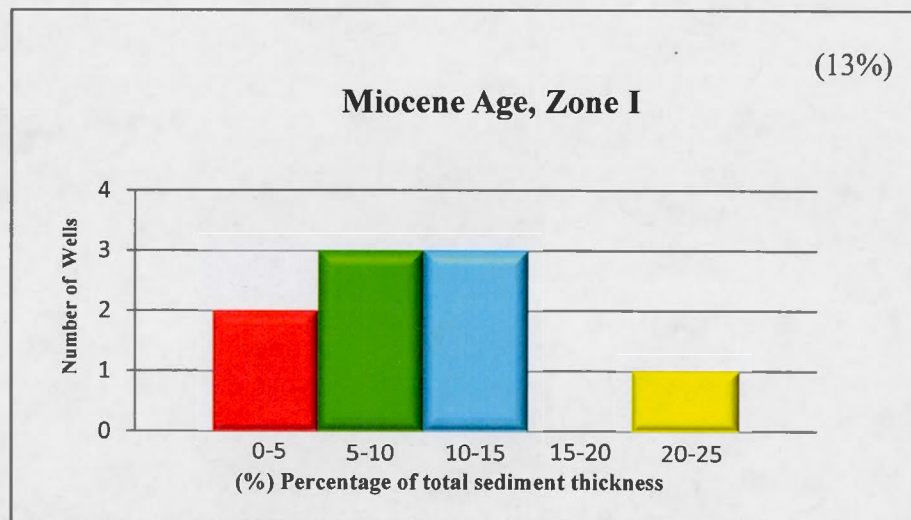


Figure 4.4 Histogram of the percent sediment thickness in the Miocene. Zone I

Figure 4.4 shows the histogram of the sediment thickness for the Miocene. This histogram has a nearly symmetric distribution, where two intervals have the same frequency: from 5 to 10% and from 10 to 15%. In this case, we selected the most probable thickness by also considering the penetration depth of the wells. The greatest core penetration depth corresponds to well data in the 10 to 15% interval and we thus select a most probable mean value of 13% thickness.

4.2.1.4 Histogram of the percent sediment thickness in the Oligocene (33.9 to 23.03

Ma)

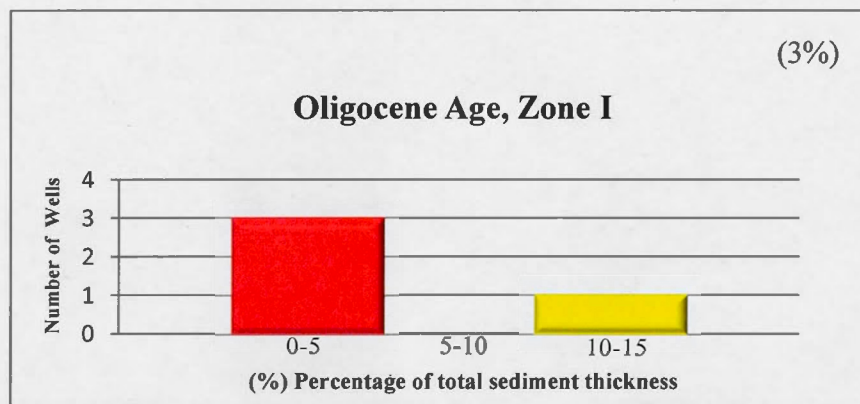


Figure 4.5 Histogram of the percent sediment thickness in the Oligocene. Zone I
 Figure 4.5 shows the histogram of the percent sediment thickness for the Oligocene. This histogram has an L-shaped distribution, with the highest frequency in the interval from 0 to 5%. In this case we again select a value of 3% for the maximum-frequency thickness.

4.2.1.5 Histogram of the percent sediment thickness in the Eocene (55.8 to 33.9 Ma)

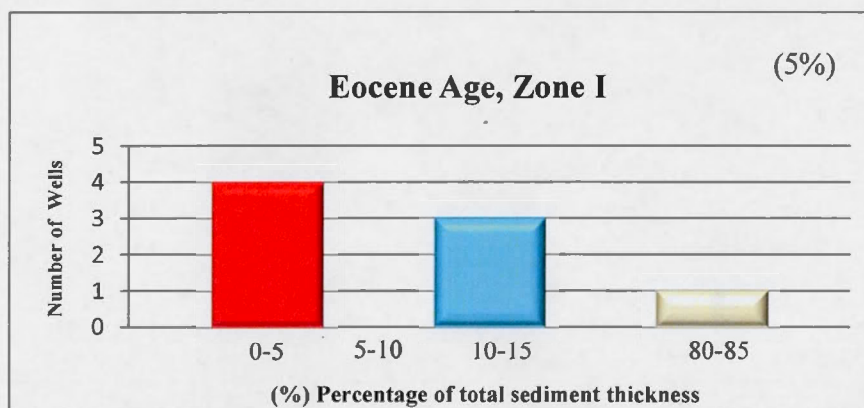


Figure 4.6 Histogram of the percent sediment thickness in the Eocene. Zone I

Figure 4.6 shows the histogram of the sediment thickness percentage for the Eocene. This histogram has an elongated L-shaped distribution, where the intervals 0-5% and 10-15% have the highest frequency. As in the case of the Pliocene (above), we select the interval 0-5% but recognizing that the interval from 10-15% has nearly the same frequency, we select a value of 5% for the thickness.

4.2.1.6 Histogram of the percent sediment thickness in the Paleocene (65.5 to 55.8 Ma)

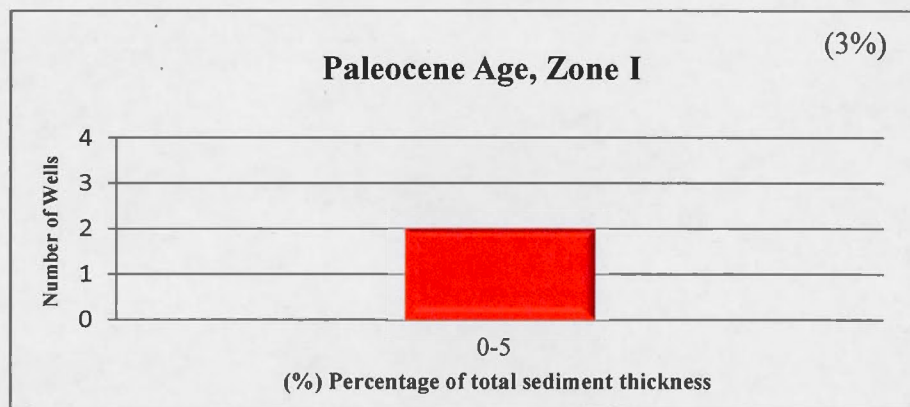


Figure 4.7 Histogram of the percent sediment thickness in the Paleocene. Zone I

Figure 4.7 shows the histogram of the percent sediment thickness for the Paleocene. For which there is just one interval from 0 to 5%. We thus select a value of 3% for the maximum – probability sediment thickness.

In summary, for the Caribbean region, the geological period with the greatest sediment accumulation (13%) is the Miocene and we find, on average, that 31% of the total thickness of sediments in this region was deposited during the Cenozoic.

4.2.2 Zone II: The Amazon

The geographic area encompassed by Zone II, the Amazon Zone, is shown in Figure 4.1.

4.2.2.1 Histogram of the percent sediment thickness in the Quaternary (2.588 to present Ma)

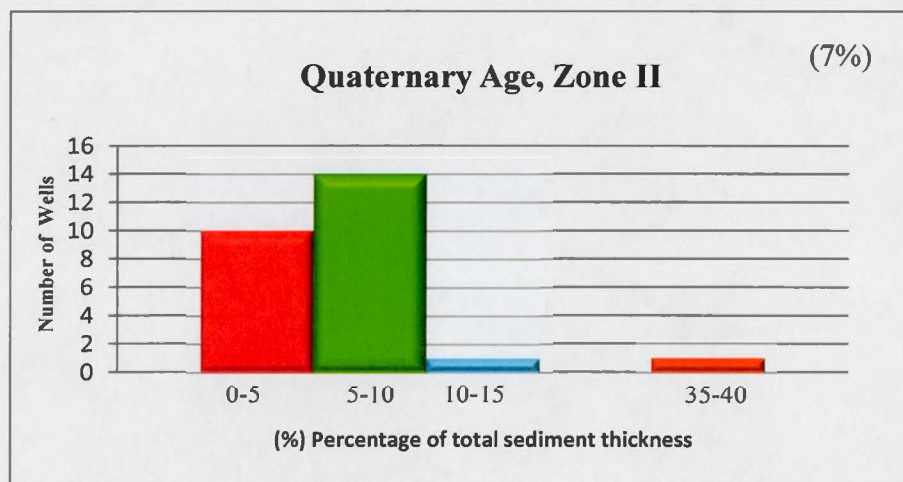


Figure 4.8 Histogram of the percent sediment percentage in the Quaternary.
Zone II

Figure 4.8 shows the histogram of the percent sediment thickness for the Quaternary. This histogram has a strongly skewed distribution and the interval with the highest frequency is between 5 and 10%. We thus selected the maximum probability value of 7% for sediment thickness in this period (where we rounded down, in recognition of the skewness).

4.2.2.2 Histogram of the percent sediment thickness in the Pliocene (5.332 to 2.588

Ma)

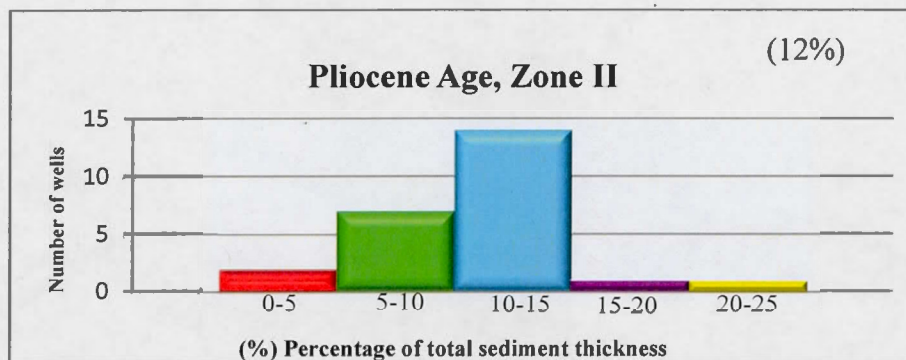


Figure 4.9 Histogram of the percent sediment thickness in the Pliocene. Zone II
 Figure 4.9 shows the histogram of the percent sediment thickness for the Pliocene. This histogram has a skewed distribution in the shape of an asymmetric bell. The interval with the highest frequency is between 10 and 15%. We thus adopt a value of 12% (rounded down, owing to the skewness) for the maximum likelihood sediment thickness

4.2.2.3 Histogram of the percent sediment thickness in the Miocene (23.02 to 5.332

Ma)

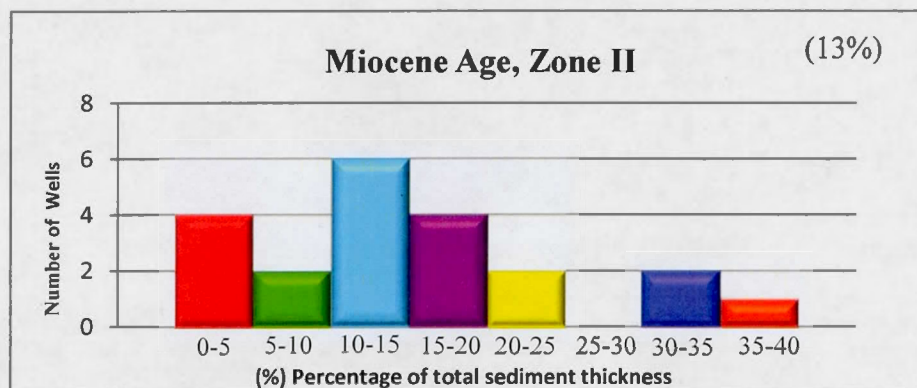


Figure 4.10 Histogram of the percent sediment thickness in the Miocene. Zone II

Figure 4.10 shows the histogram of the percent sediment thickness for the Miocene. This histogram has a distribution in the shape of an asymmetric bell and it is skewed towards higher thicknesses. We note that 0-5%, 10-15% and 15-20% have the highest frequency. The maximum probability thickness lies in the range 10-15% and owing to the skewness to higher values, we adopt a mean value of 13% for the Miocene.

4.2.2.4 Histogram of the percent sediment thickness in the Oligocene (33.9 to 23.03

Ma)

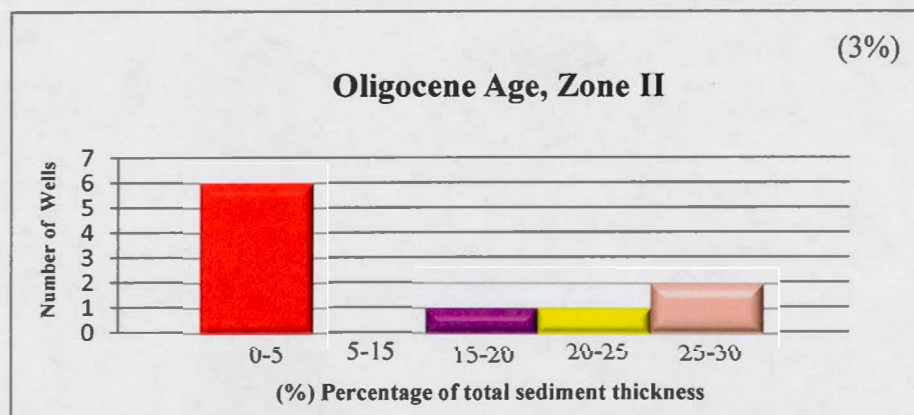


Figure 4.11 Histogram of the percent sediment thickness in the Oligocene. Zone

II

Figure 4.11 shows the histogram of the percent sediment thickness for the Oligocene. This histogram has an elongated L-shaped distribution, showing a high variability of thicknesses, where the intervals 0-5% and 25-30% have the highest frequency. The peak frequency is in the interval 0-5% and we thus adopt a mean thickness of 3% for the Oligocene.

4.2.2.5 Histogram of the percent sediment thickness in the Eocene (55.8 to 33.9 Ma)

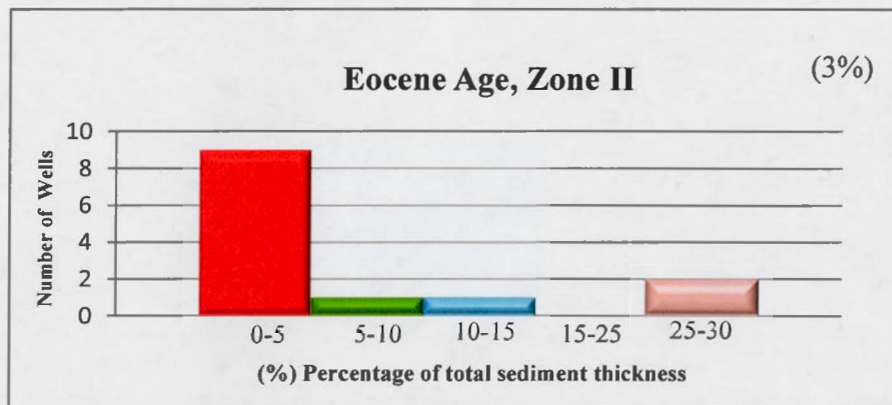


Figure 4.12 Histogram of the percent sediment thickness in the Eocene. Zone II

Figure 4.12 shows the histogram of the sediment thickness percentage for the Eocene. This histogram also has an elongated L-shaped distribution, but is clearly dominated by thicknesses in the interval 0-5%. We thus select a value of 3% (rounded up, owing to the skewness to higher values) as the mean thickness of the Eocene.

4.2.2.6 Histogram of the percent sediment thickness in the Paleocene (65.5 to 55.8 Ma)

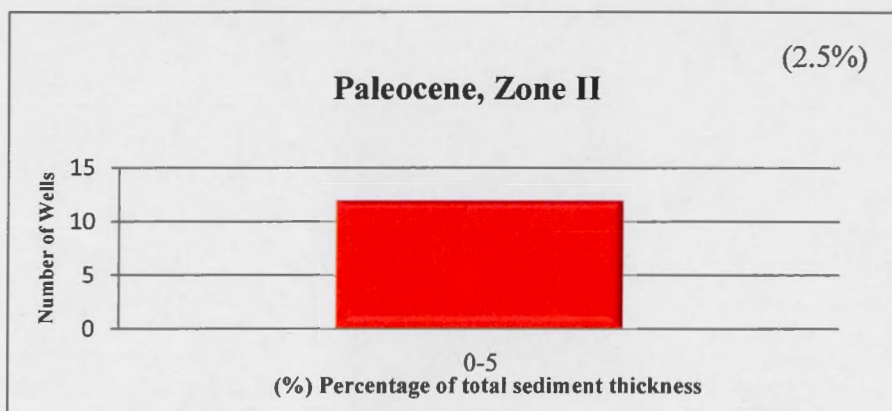


Figure 4.13 Histogram of the percent sediment thickness in the Paleocene.
Zone II

Figure 4.13 shows the histogram of the percent sediment thickness for the Paleocene. We find one thickness interval in the range 0-5%. We thus adopt a median sediment thickness of 2.5%.

4.2.3 Zone III: Argentina-Brazil

The geographic area encompassed by Zone III, the south-Atlantic margin of the continent that we call the Argentina-Brazil Zone is shown in Figure 4.1.

4.2.3.1 Histogram of the percent sediment thickness in the Quaternary (2.588 to present Ma)

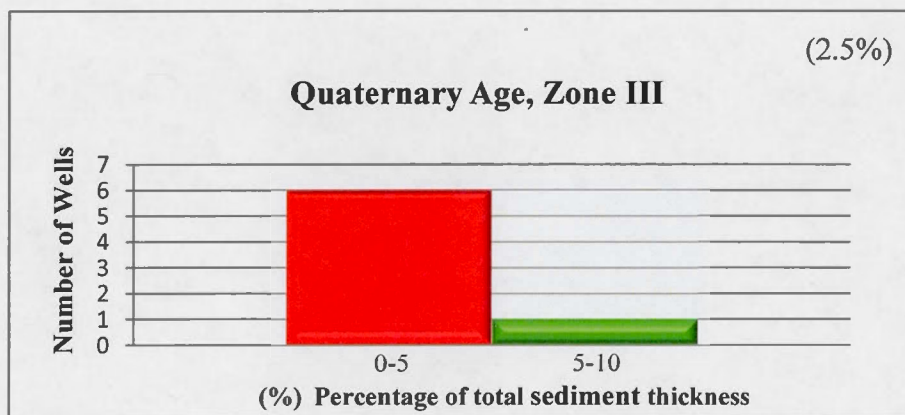


Figure 4.14 Histogram of the percent sediment thickness in the Quaternary.
Zone III

Figure 4.14 shows the histogram of the percent sediment thickness for the Quaternary. This histogram has a very slight L-shaped distribution, mainly dominated by thickness in the range 0 to 5%. We thus adopt a value of 2.5% for the mean thickness in the Quaternary.

4.2.3.2 Histogram of the percent sediment thickness in the Pliocene (5.332 to 2.588 Ma)

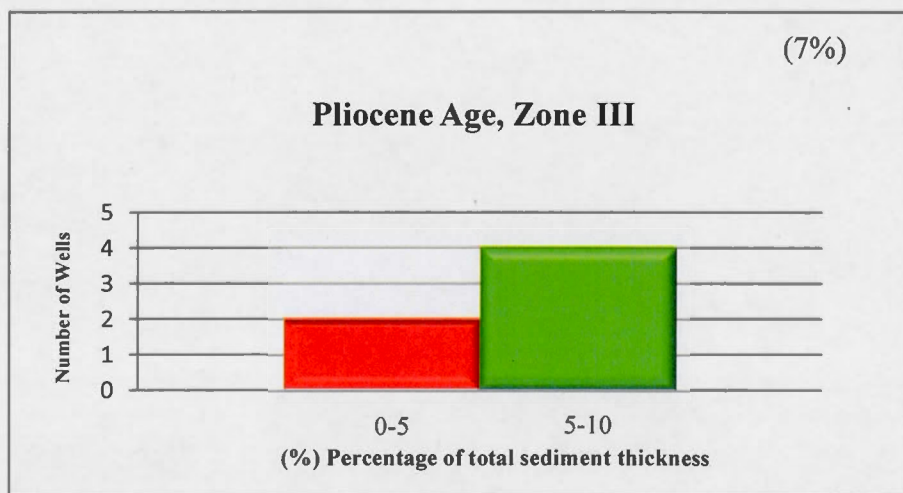


Figure 4.15 Histogram of the percent sediment thickness in the Pliocene. Zone III

Figure 4.15 shows the histogram of the percent sediment thickness for the Pliocene. This histogram has a skewed J-shaped distribution, where the percentage with the highest frequency is the interval from 5 to 10%. We thus adopt a maximum likelihood thickness of 7% (rounded down, owing to the skewness of the distribution) for the Pliocene.

4.2.3.3 Histogram of the percent sediment thickness in the Miocene (23.02 to 5.332 Ma)

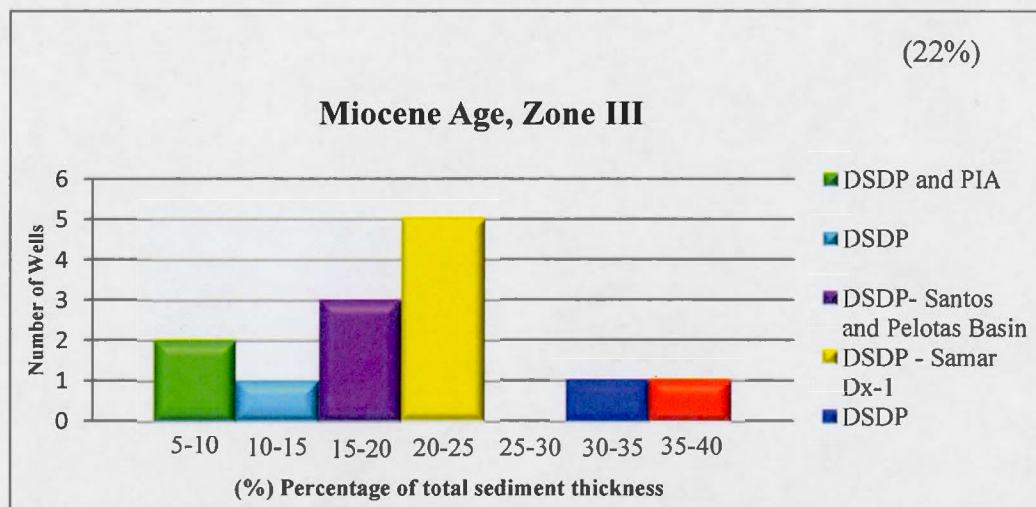


Figure 4.16 Histogram of the percent sediment thickness in the Miocene. Zone III. DSDP: Deep Sea Drilling Project (Perch-Nielsen et al., (1977b, c, d, e), Baker et al., (1983a,b), Maxwell et al., (1970)), Samar Dx-1 and PIA (PIA: Intersection Point A represents the closest site along seismic line BGR87-1 to the oil drilling where the lithological contacts were extended). (Violante et al., 2010). Santos, Campos and Pelotas basin (Contreras et al., 2010)

Figure 4.16 shows the histogram of the percent sediment thickness for the Miocene. This histogram has a distribution in the shape of an asymmetric bell. There is a wide range of thicknesses varying from 5% to 35-40%. The most probable thicknesses are in the range 15-20% and 20-25%, with highest frequency in 20-25%. We thus select 22% (rounded down, owing to the skewness) as the representative percent thickness for Miocene.

4.2.3.4 Histogram of the percent sediment thickness in the Oligocene (33.9 to 23.03

Ma)

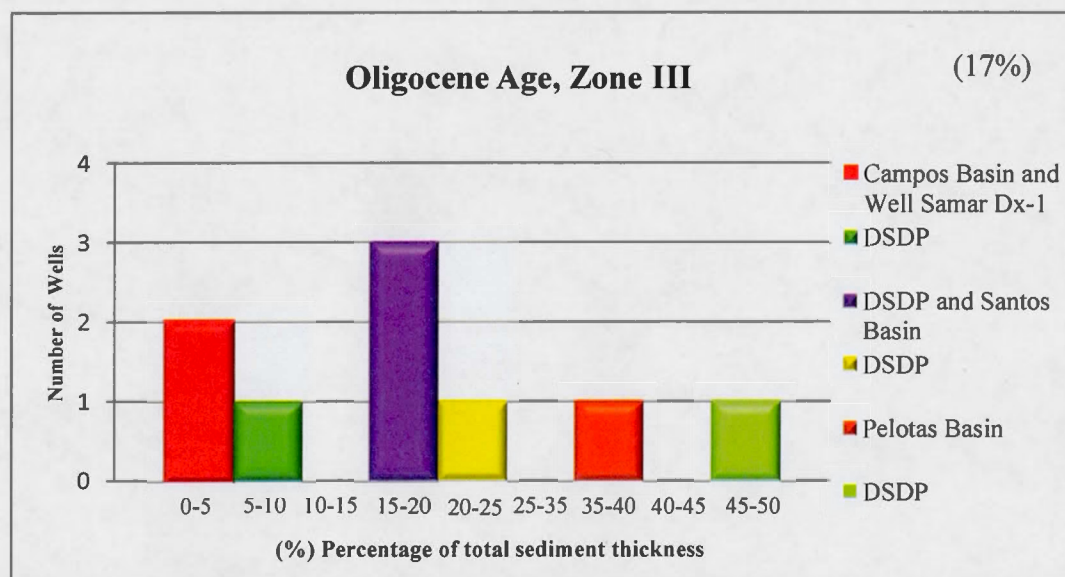


Figure 4.17 Histogram of the percent sediment thickness in the Oligocene. Zone III .DSDP: Deep Sea Drilling Project (Perch-Nielsen et al., (1977d, e), Baker et al., (1983a, b), Maxwell et al., (1970)) Well Samar Dx-1 (Violante et al., 2010). Santos, Campos and Pelotas Basin (Contreras et al., 2010)

Figure 4.17 shows the histogram of the percent sediment thickness for the Oligocene. This histogram has a distribution in the shape that roughly approximates an asymmetric bell but with considerable scatter of values. There is again a wide range of thicknesses, ranging from 0-5% to 45-50%. The interval with the highest frequency is between 15 and 20%. We thus select a mean percent sediment thickness of 17% (rounded down, owing to the skewness) for the Oligocene.

4.2.3.5 Histogram of the percent sediment thickness in the Eocene (55.8 to 33.9 Ma)

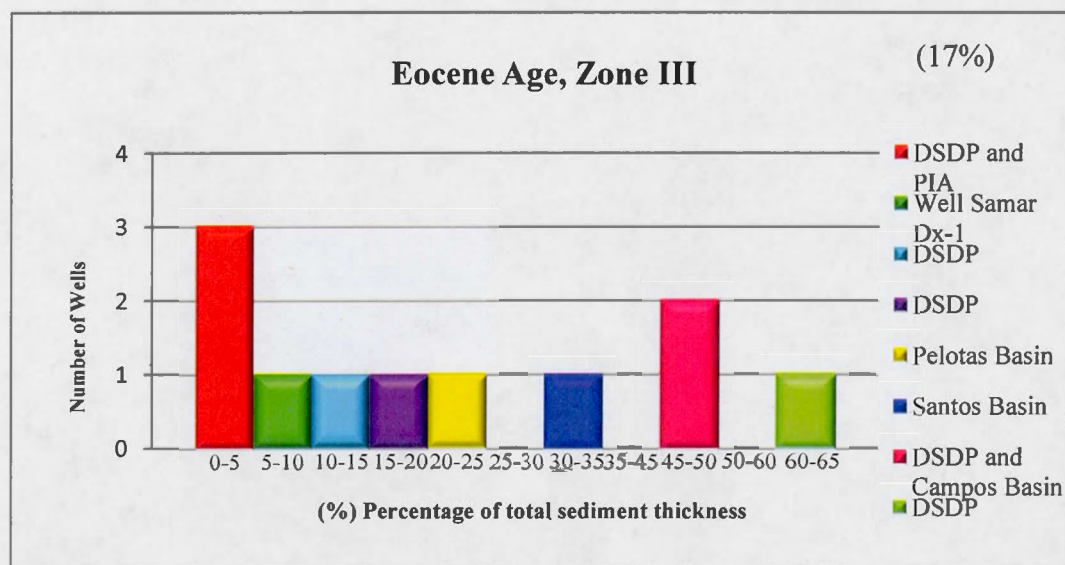


Figure 4.18 Histogram of the percent sediment thickness in the Eocene. Zone III.

DSDP: Deep Sea Drilling Project (Perch-Nielsen et al., (1977b,c,d,e), Baker et al., (1983a,b)), Well Samar Dx-1 and PIA (PIA: Intersection Point A represents the closest site along seismic line BGR87-1 to the oil drilling where the lithological contacts were extended). (Violante et al., 2010). Santos, Campos and Pelotas basin (Contreras et al., 2010)

Figure 4.18 shows the histogram of the percent sediment thickness for the Eocene. This histogram shows a bimodal distribution, since it has two peaks (intervals 0-5% and 45-50%). Due to the variability of thicknesses ranging from 0-5% to 60-65%, we selected an interval corresponding to the median of this highly irregular distribution. We therefore selected the interval 15-20% and hence a median value of 17% for the percent thickness in the Eocene.

4.2.3.6 Histogram of the percent sediment thickness in the Paleocene (65.5 to 55.8 Ma)

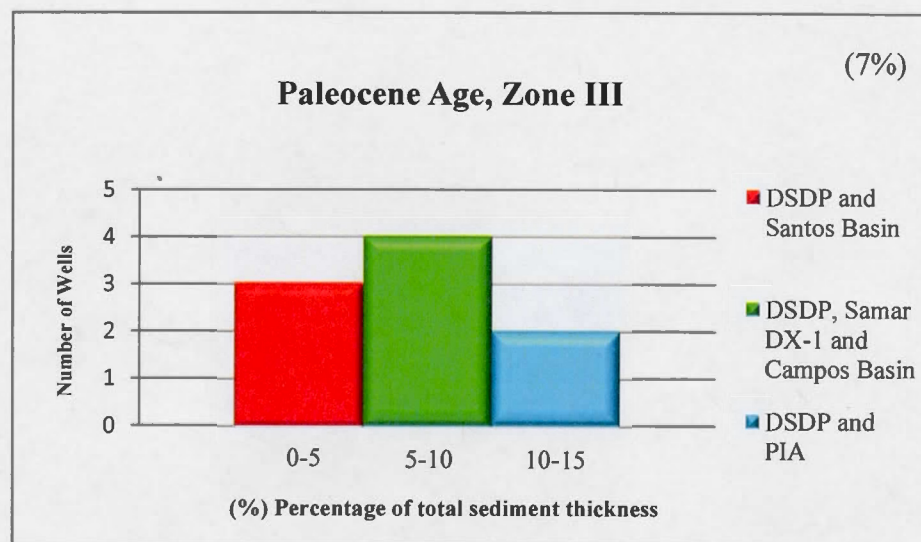


Figure 4.19 Histogram of the percent sediment thickness in the Paleocene. Zone III. DSDP: Deep Sea Drilling Project (Perch-Nielsen et al., (1977b,c,d,e), Baker et al., (1983b)), Samar Dx-1 and PIA (PIA: Intersection Point A represents the closest site along seismic line BGR87-1 to the oil drilling where the lithological contacts were extended). (Violante et al., 2010). Santos and Campos basin (Contreras et al., 2010)

Figure 4.19 shows the histogram of the percent sediment thickness for the Paleocene. This histogram has a distribution in the shape of an asymmetric bell. The thickness interval with maximum frequency is between 5 and 10%. We thus selected a mean sediment thickness of 7% (rounded down, owing to the asymmetry of the distribution)

In summary, we find that the peak sediment accumulations occur during the Miocene to Eocene periods, inclusively, and account for a sum total of about 56% of total sediment thickness in Zone III.

4.2.4 Zone IV: Scotia

The geographic area encompassed by Zone IV, the Scotia Zone, is shown in Figure 4.1.

4.2.4.1 Histogram of the percent sediment thickness in the Quaternary (2.588 to present Ma)

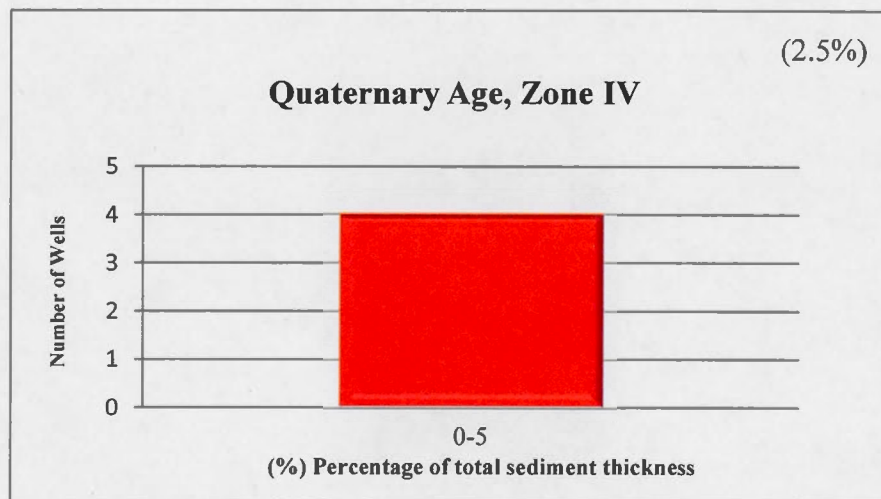


Figure 4.20 Histogram of the percent sediment thickness in the Quaternary.
Zone IV

Figure 4.20 shows the histogram of the sediment thickness percentage for the Quaternary. There is just one interval, 0 to 5% and we thus select a mean sediment thickness of 2.5%.

4.2.4.2 Histogram of the percent sediment thickness in the Pliocene (5.332 to 2.588 Ma)

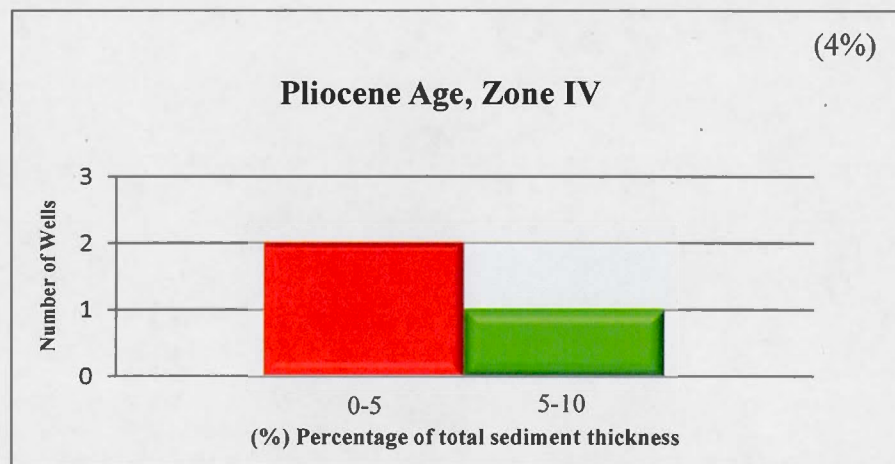


Figure 4.21 Histogram of the percent sediment thickness in the Pliocene. Zone IV

Figure 4.21 shows the histogram of the percent sediment thickness for the Pliocene. This histogram has an L-shaped distribution and the thickness with the highest frequency is between 0 and 5%. We thus select a sample mean value (owing to the limited number of wells) of 4% thickness for the Pliocene.

4.2.4.3 Histogram of the percent sediment thickness in the Miocene (23.02 to 5.332 Ma)

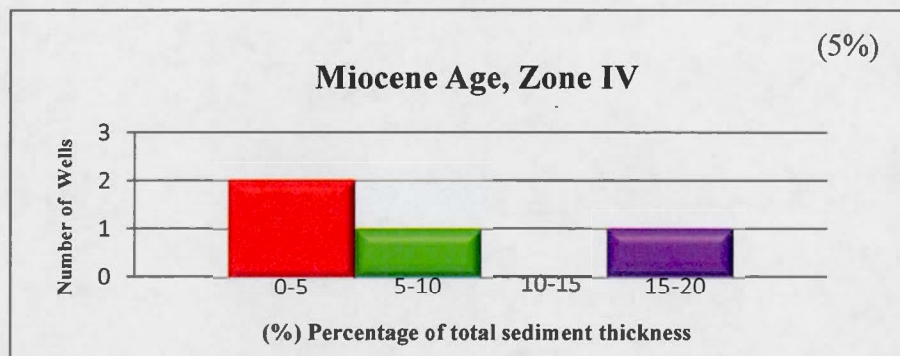


Figure 4.22 Histogram of the percent sediment thickness in the Miocene. Zone IV

Figure 4.22 shows the histogram of the percent sediment thickness for the Miocene Age. This histogram has an extended L-shaped distribution with thicknesses ranging from 0-5% to 15-20%. Owing to the limited number of samples, and the dispersion, we select a median value of 5%.

4.2.4.4 Histogram of the percent sediment thickness percentage in the Oligocene (33.9 to 23.03 Ma)

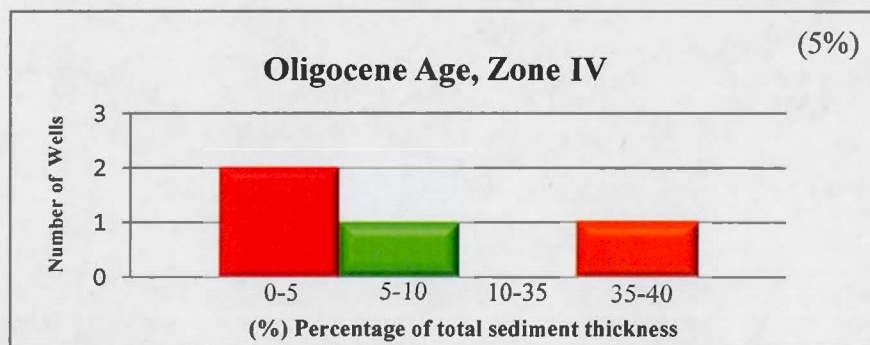


Figure 4.23 Histogram of the percent sediment thickness in the Oligocene. Zone IV

Figure 4.23 shows the histogram of the percent sediment thickness for the Oligocene. This histogram has an extended and dispersed L-shaped distribution, with wide variation. The percentage with the highest frequency is between 0 and 5%, but owing to the extended and dispersed range of values we select a median thickness of 5% for the Oligocene.

4.2.4.5 Histogram of the percent sediment thickness in the Eocene (55.8 to 33.9 Ma)

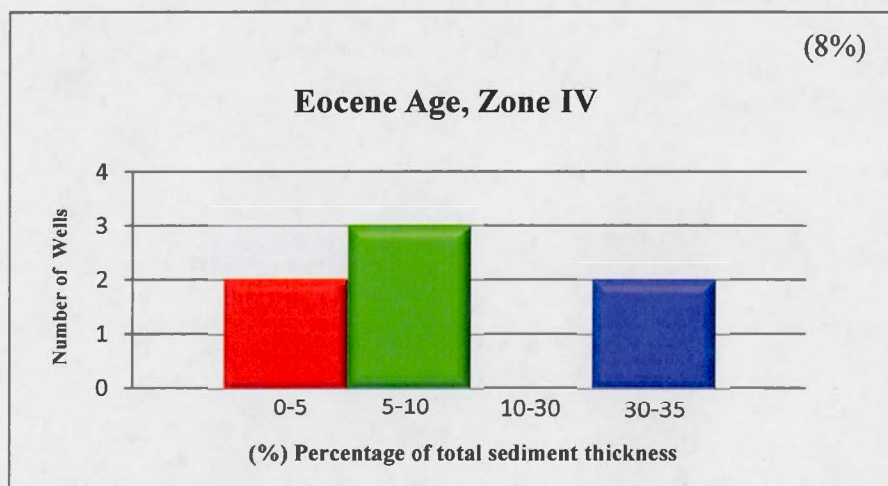


Figure 4.24 Histogram of the percent sediment thickness in the Eocene. Zone IV

Figure 4.24 shows the histogram of the percent sediment thickness for the Eocene. This histogram has a dispersed, asymmetric bell shape ranging from 0-5% to 30-35%. The

interval with the highest frequency is between 5 and 10% but owing to the limited sampling and dispersion, we select an approximate median value of 8% for the Eocene.

4.2.4.6 Histogram of the percent sediment thickness in the Paleocene (65.5 to 55.8 Ma)

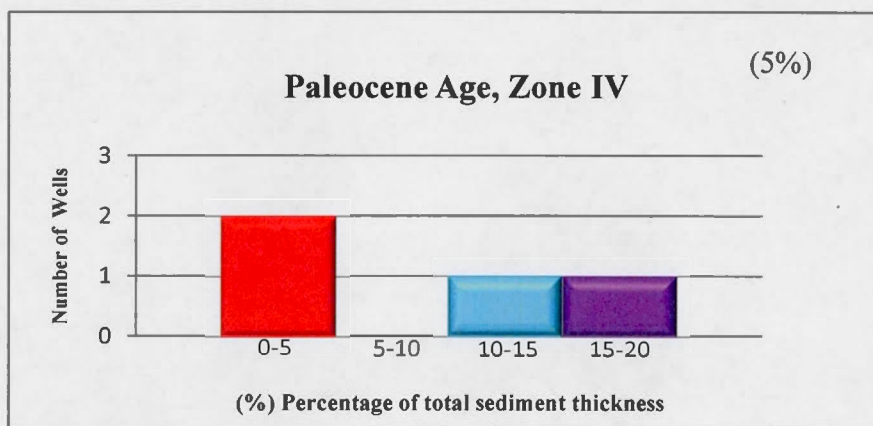


Figure 4.25 Histogram of percent sediment thickness in the Paleocene. Zone IV.

Figure 4.25 shows the histogram of the percent sediment thickness for the Paleocene. This histogram has a dispersed L-shaped distribution, showing a range of thickness extending from 0-5% to 15-20%. The interval with the highest frequency is between 0 and 5%, but owing to the dispersion, we selected a median value of 5%.

In summary, the Scotia region shows little variation in percent accumulations across the periods that span the Cenozoic and we find a total relative accumulation of almost 30% over this time interval.

Table 4.1 Summary of the Percent Sediment Thicknesses Accumulated in the Cenozoic. This table shows the percentages of sediment accumulated for the four areas in which the South American continent was divided (Zone I, Zone II, Zone III and Zone IV) into the Cenozoic . The percentages were taken from the histograms made to each area. The selected percentage was the percentage that was taken from the global database of high resolution for each age. (Divins, 2003)

Zone	Age	Percentage range	Percentage selected
I. Caribbean	Quaternary	0-5%	3%
	Pliocene	0-5%	4%
	Miocene	10-15%	13%
	Oligocene	0-5%	3%
	Eocene	0-5%	5%
	Paleocene	0-5%	3%
	Total		31%
II. Amazon	Quaternary	5-10%	7%
	Pliocene	10-15%	12%
	Miocene	10-15%	13%
	Oligocene	0-5%	3%
	Eocene	0-5%	3%
	Paleocene	0-5%	2.50%
	Total		40.5%
III. Argentina-Brazil	Quaternary	0-5%	2.50%
	Pliocene	5-10%	7%
	Miocene	20-25%	22%
	Oligocene	15-20%	17%
	Eocene	15-20%	17%
	Paleocene	5-10%	7%
	Total		72.5%
IV. Scotia	Quaternary	0-5%	2.50%
	Pliocene	0-5%	4%
	Miocene	0-5%	5%
	Oligocene	0-5%	5%
	Eocene	5-10%	8%
	Paleocene	0-5%	5%
	Total		29.5%

4.3 Lithospheric Flexure

4.3.1 Numerical calculation of Lithospheric Flexure

Elastic flexure, represented in terms of spherical harmonics, on the continental shelves of South America was calculated of the normalized sediment load L_l^n (equation 3.10) and by determining the harmonic coefficients of flexure based on Equation (3.19). In order to calculate the f_l in Equation (3.20). We first had to find flexural rigidity D using Equation (3.3). Data such as the Young modulus, effective elastic thickness and the Poisson ratio, were taken from Pazzaglia & Gardner (1994), using values of 70×10^9 Pa, 40 Km and 0.25 respectively. (Table 4.2). Replacing the above values in Equation (3.3) yields a flexural rigidity value of 3.98×10^{23} Nm.

We emphasize that in the calculation of the sediment loading we actually employ the depth-dependence of sediment density extracted from the global $1^\circ \times 1^\circ$ compilation by Laske & Masters (1997). This depth-dependence is taken into account in the numerical calculation of the normalized sediment load in equations (3.9) and (3.10).

Using this flexural rigidity and water density (1000 Kg/m^3) and mantle density (3300 Kg/m^3) (Table 2) in Equation (3.21), yields a β value of 1.12×10^{-08} for an elastic thickness of 40 Km. The β value is substituted in Equation (3.20), yields a f_l value of 5.57×10^{-6} .

Finally, the spherical harmonic coefficients of flexure are obtained by replacing the above results in Equation (3.19). (Assuming an elastic thickness of 40 km). These harmonic coefficients are calculated up to maximum degree $l=2000$, corresponding to

a spatial resolution of 5min x 5 min for each of the geological periods studied (Paleocene - Quaternary)

The spatial 5minx5min grid of flexure is calculated by the harmonic coefficients δ_l^m employing equation (3.14). All the maps were created using the tools from the GMT program. The Fortran code employed for the flexure calculations is presented in Appendix C.

Table 4.2 Parameters used to calculate flexure

Parameters	Symbols	Values	Units
Flexural Rigidity	D	$3,98 \cdot 10^{23}$	Nm
Young's modulus	E	70×10^9 *	Pa
Elastic Thickness	h	40 *	km
Poissons's ratio	v	0.25*	
Earth radius	r_e	6371	km
Mantle density	ρ_m	3300	kg/m^3
Water density	ρ_w	1000	kg/m^3

*Taken from Pazzaglia & Gardner 1994

4.4 Cumulative Flexural Response as a Function of Time

Figures 4.27, 4.28, 4.65, 4.66, 4.67, 4.68 4.69 and 4.70 show the maps of the flexural response caused by the weight of the offshore sedimentary load along the entire margin of South America. Flexure was found by using an effective elastic thickness of 40 km and, in some cases (discussed in the next section) we employed an elastic thickness of 80 km (Figures 4.26 and 4.63), up to a maximum harmonic degree of 2000.

In the following, we will first present a discussion of the sediment-induced flexural depression on the off-shore continental margins, followed by a discussion of uplift on land. The discussion below will focus on the flexural response at a number of representative offshore points that are shown in the map of figure 4.26.

4.4.1 Flexural Response of the Lithosphere during the Quaternary (0-2.588 million years)

In the following discussion, we explore the predicted flexural response between the present and 2.588 million years ago for an elastic thickness of 40 km and 80 km, which is illustrated in the maps of Figures 4.27 and 4.28, respectively.

To test the possibility of an effectively greater elastic thickness for loads applied over relatively short (<10 My) time spans (e.g. Watts & Zhong, 2000), owing to the viscoelasticity of the lithosphere, we explored the flexural response of an 80-km thick elastic lithosphere in addition to 40 km. Both thicknesses were included for the sediment loading calculations in the Quaternary and the Pliocene. In this regard we

note that the effective elastic thickness found in the estimations of the seismic thickness (Nishimura & Forsyth, 1989) is between 70-110 km. In accord with the value of 80 km we also employ here an elastic thickness of 80 km, was also used to model the variations of the forebulge that the continent experienced during 5.332 – 0 million years. This elastic thickness value was taken into account, following research from Pérez-Gussinye et al., (2007). The authors generated a map of elastic thickness (T_e) of South America using satellite data (GRACE and CHAMP mission) and terrestrial gravity data (EGM96 and SAGP), also the multitaper Bouguer coherence technique. Concluding that, in the platform, the elastic thickness values are generally high (> 70 km).

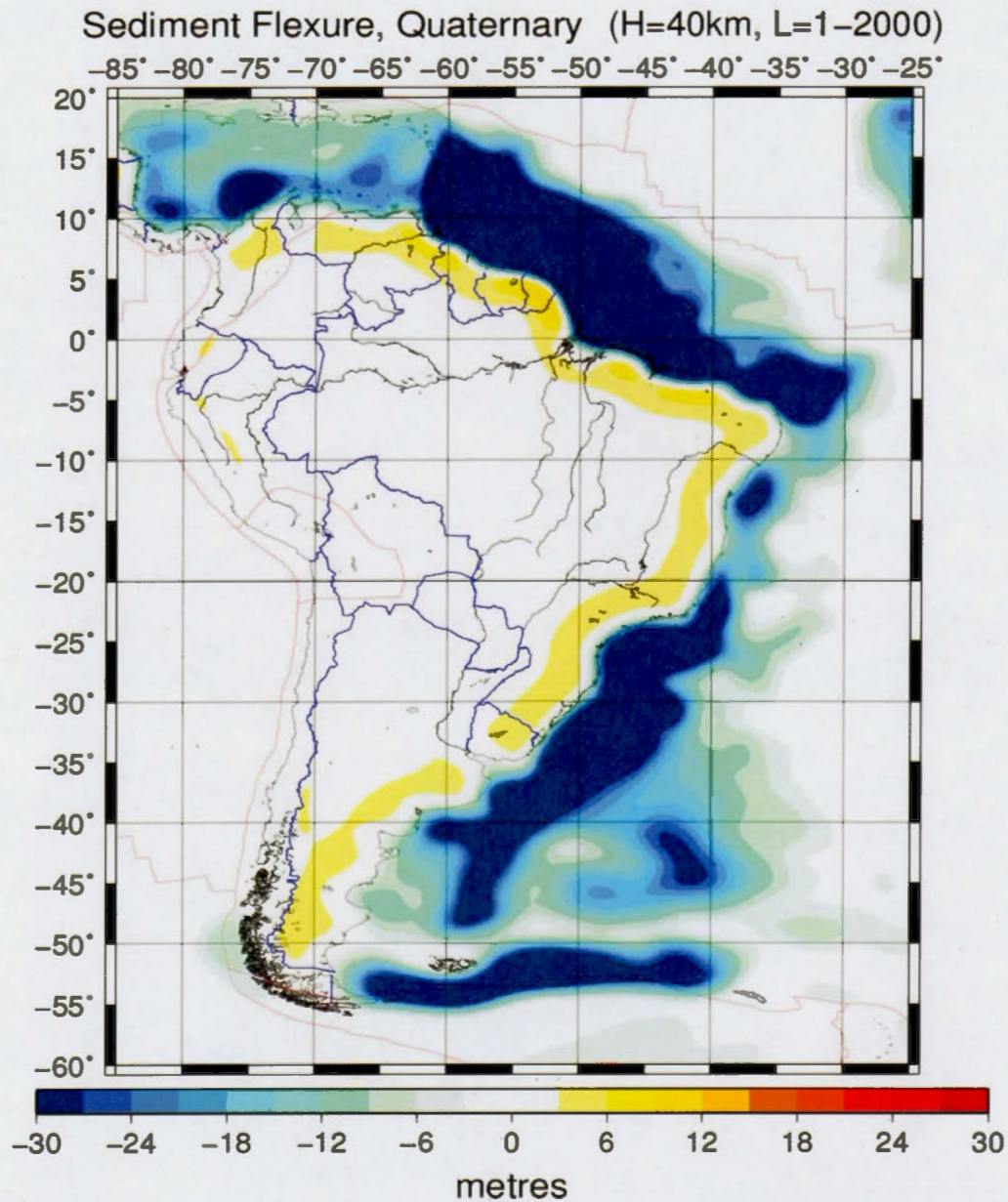


Figure 4.27 Map of total Flexural Response due to sediment loads accumulated since the Quaternary (2.588-0 million years) for an effective elastic thickness of 40 km and a maximum harmonic degree of 2000. Negative values indicate flexural depression and positive values indicate forebulge or uplift.

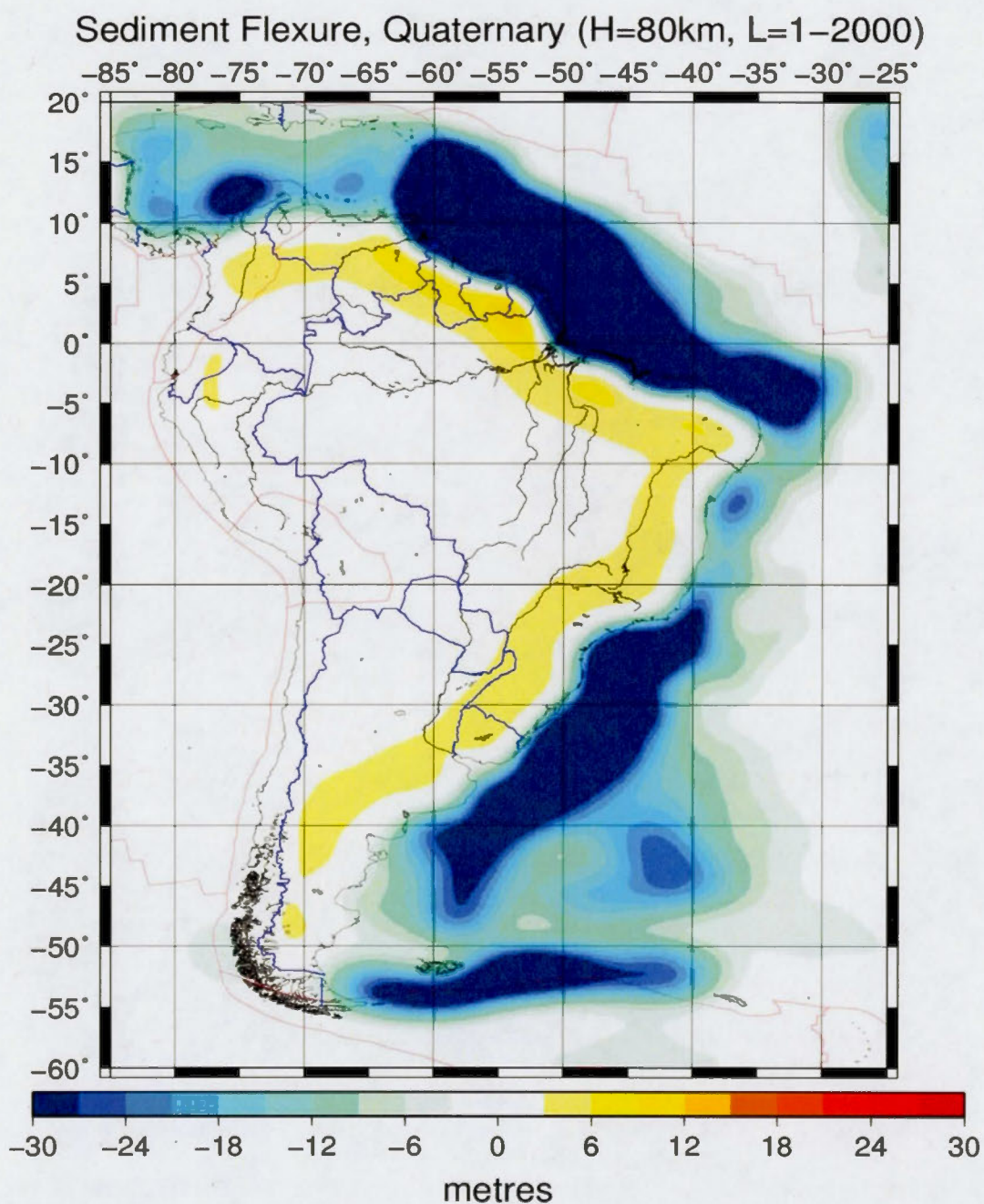


Figure 4.28 Map of total Flexural Response due to sediment loads accumulated since the Quaternary (2.588-0 million years) for an effective elastic thickness of 80 km and a maximum harmonic degree of 2000

In the following we present the results of our flexural calculations along the offshore margins in each of the four geographic zones (Figure 4.1). The discussion will primarily focus on the flexural response at a number of selected offshore points, shown in Figure 4.26, via a graphical representation of flexure versus time: from the Present to the Paleocene. In the interest of clarity we include an extended discussion for the Quaternary, and employ a purely graphical summary for all remaining geological periods.

4.4.1.1 Zone I. The Caribbean

In the following discussions we include results for both $T_e = 40$ km and $T_e = 80$ Km, where the latter are always enclosed in brackets.

In this zone on the continental margin of Colombia, the flexural depression of the lithosphere has amplitudes greater than -35 meters. More modest depressions of -26.71 meters [-24.78 meters] occurs in the area of the Offshore Guajira Marine Basin and between -6 and -33.39 meters [-26.2 meters] in the area covered by the offshore Sinú Marine Basin. This depression decreases near the mouth of the Magdalena River, where it is -26.9 meters [-25.77 meters] (Table 4.8), which in turn increases near the area of the Magdalena Delta, with values ranging between -30 and -50 meters [-36.16meters] . In the North and Northwest region of Zone I, flexural depressions range from -9 meters to above to -30 meters, such as in the area of the Cayos Basin, with -19.46meters [-17.58 meters] and, in turn, the Colombia Basin, where the depression is -42.79 meters [-33.29 meters] . (Table 4.3, Zone I)

On the other hand, on the continental margin of Venezuela, flexural depressions range from -12 to -18 meters, as is the case of the area of the offshore Cariaco Basin, with values of -17.24 meters [-9.48 meters]. This flexure decreases near the mouth of the Orinoco River with amplitudes of -2.42 meters [-19.47 meters] which increase offshore (Table 4.8). In Northern Venezuela, the flexure increases in the Venezuela Basin with flexure of -23.29 meters [-19.72 meters]. In addition, in the Minor Antilles arch, the amplitude of lithospheric flexure is greater than -30 meters, reaching values of more than -100 meters, such as in the area of the Grenada and Tobago Basin, where the depressions attain values of -48.82 meters [-38.23 meters] and -204.39 meters [-181.88 meters] respectively. (Table 4.3, Zone I)

4.4.1.2 Zone II. Amazon Zone

This zone is characterized by amplitudes greater than -100 meters in the area of the continental shelf and offshore the countries of Guyana, Surinam and French Guyana. The flexural depression caused by the sedimentary load in this area has major amplitudes of -161.27 [-165.99], -171.88 [-140.99] and -149.38 [-137.84] meters respectively.

Similarly, on the continental margin of Northeastern Brazil, the flexural depressions has small amplitudes along the coastline, which increase offshore to values greater than -100 meters, attaining a maximum of -119.14 meters. An example is the area of the mouth of the Amazon River, with amplitudes of -8.34 meters [-14.55 meter] (Table 4.8), which increases in the area of the Amazon Delta with amplitudes of -101.8 meters [-100.27 meter]. Similarly, in the Ceará Basin area, flexure amplitude increases to

values of up to -118.66 meters [-79.72 meter]. These amplitudes decreased in the area of the Potigar Basin, where flexure attains values of -60.86 meters [-48.02 meter], but at the same time, amplitude decreased to values of -54.9 meters [-39.24 meter] about 4°S and 37°W. (Table 4.3, Zone II)

4.4.1.3 Zone III. Brazil - Argentina

Along the continental margin of Brazil, the lithospheric depression varies from -10 to -70 meters. So in the area of the offshore Pernambuco and Espírito Santo Basins, lithospheric depressions are relatively modest with values of -15.76 [-18.01] and -15.79 [-14.32], meters, respectively. These amplitudes increase in the area of the offshore Sergipe-Alagoas, Bahía Sul and Campos Basins, where flexure attains values of -20.77 [-18.44], -31.7 [-24.28] and -39.36 [-27.39] meters respectively. Similarly, the areas that make up the offshore Santos and Pelotas Basins have values reaching -66.35 [-52, 41] and -57.85 [-48.49] meters, respectively. (Table 4.3, Zone III)

On the continental margin of Uruguay and in the area of the offshore Punta Del Este Basin, lithospheric depression reaches amplitudes of -30.66 [-36.41] meters. In addition, between the countries of Argentina and Uruguay, on the confluence of the Paraná and the Uruguay Rivers, there is a very modest inflection in the flexure yielding slightly positive values (see table 4.8).

On the other hand, on the extensional continental margin of Argentina, lithospheric depressions range over values that exceed -50 meters. In the case of the offshore San Julian and San Jorge Basins, the flexure is modest with values of -4.52 [-4.84] meters, and -10.53 [-7.47] meters, respectively. However, in the area of the offshore Argentina,

Rawson, Colorado and Salado Basins, flexure increases considerably, reaching values of -28.1 [-24.93] , -16.77 [-21.45] , -33.96 [-29.92] and -52.52 [-41.12] meters, respectively. (Table 4.3, Zone III). Finally, on the convergent sheared continental margin of Argentina, in the area of the Northern Falkland Basin, flexure varies between -1.32 [-7.38] and -13.55 [-12.17] meters (Table 4.3, Zone III).

4.4.1.4 Zone IV. Scotia

In this area, there are variations in flexure amplitude with values between -0 and -40 meters. For example, in the area of the offshore Western and Eastern Falkland Basins, the flexure values attains values of -29.42 [-26.64] meters and -48.03 [-37.48] meters, respectively. This flexure calculated for $T_e=40$ Km, uplifts the Falkland Islands approximately 2.71 meters. In contrast when $T_e=80$, the flexural depression continues on the Falkland Islands, with a value of -9.29 meters.

On the border between the South American and Scotia plates, the amplitude of lithospheric flexure ranges from -1 to -35 meters. Such as, on the area of the Southern Falkland where flexural depressions attain values of -34.17 [-29.36] (See Table 4.3, Zone IV). The flexure decreases gradually to minimum amplitudes, followed by uplifts in the eastern and western ends of the Scotia plate: 0.29 [0.54] meters and 1.99 [1.95] meters, respectively. In the middle of the plate, flexure increases progressively toward the south.

4.4.1.5 Uplift of the Continent of South America in the Quaternary

The map of the flexural response in the Quaternary (Figure 4.27 and Figure 4.28) shows that the sedimentary load accumulated on the continental margins of South America induces offshore depressions of the lithosphere, with values of more than -30 meters. This, in turn, induces a distinct pattern of continental uplift, known as forebulge, which is purely the consequence of the finite elastic strength of the lithosphere. No such forebulge will be produced in the traditional isostatic treatment of long-term fluid behavior of the lithosphere.

The forebulge or uplift (positive flexure) of the continent of South America in the Quaternary is between 2 and 3 [2.87] meters, increasing the elevation in the eastern region of the continent with values of 3.73 [3.47] meters near the coastline and increasing up to 4.43 [4.5] meters onshore. Similarly, countries such as Colombia, Venezuela, Guiana, Surinam, French Guiana, Brazil Uruguay and Argentina have higher uplifts, reaching values of 4.48, 6.64 [4.36], 7.73 [7.16], 7.26 [8.71], 11.56 [9.97], 6.99 [11.09], 4.79 [4.56] and 4.46 meters, respectively. These values are listed in Tables 4.4, 4.5.

Finally, during this geological interval, the maximum flexural depression was -309 [-244.34] meters, inducing a maximum onshore elevation of 11.93 [11.91] meters. (Table 4.7).

Table 4.3 Offshore flexural depression of South America in the Quaternary Period.

Zone	Offshore point	Coordinates		Flexure (m)	
		Latitude	Longitude	Quaternary	
				Te 40 km	Te 80 km
Zone I	Barracuda A.P	16.5°N	59°W	-27,35	-33,68
	Cayos	16°N	80°W	-19,46	-17,58
		15°N	81°W	-16,64	-17,93
	Colombia	16°N	74°W	-9,14	-11,29
		14.5°N	74°W	-15,06	-19,85
	Magdalena Delta	13°N	74°W	-42,79	-33,29
		11.5°N	75.5°W	-50	-36,16
	Venezuela	13°N	65°W	-23,29	-19,72
		12°N	67°W	-22,41	-20,08
	Grenada	14.5°N	62°W	-17,22	-34,28
	Tobago	11.5°N	62.5°W	-48,82	-38,23
	Demerara Abyssal Plain	12.5°N	60°W	-204,39	-181,88
		11°N	56°W	-123,41	-141,08
	Guajira Marino	13°N	57°W	-119,67	-139,59
	Sinú Marino	12°N	73°W	-26,71	-24,78
Cariaco	10.5°N	76°W	-33,39	-26,2	
Zone II	Guyana	10.5°N	65°W	-17,24	-9,48
		9.5 °N	57°W	-161,27	-165,99
	Surinam	8° N	58°W	-78,54	-93,88
		8°N	55°W	-171,88	-140,99
	French Guyana	7°N	56°W	-105,88	-93,2
		7°N	52°W	-149,38	-137,84
	Amazonas Delta	5.5°N	52.5°W	-81,43	-91,09
		1°N	49.5°W	-101,8	-100,27
	Brazil	1°S	46°W	-42,59	-50,86
		3°S	40°W	-53,17	-47,72
Ceará	2°S	43°W	-119,14	-79,84	
	2°S	41°W	-118,66	-79,72	
Potigar	2.5°S	37.5°W	-27,77	-36,11	
	3°S	37°W	-43,68	-40,93	

	4°S	36°W	-60,86	-48,02
	4°S	37°W	-54,9	-39,24
Pernambuco	8° S	34° W	-10,89	-13,87
	8° S	33° W	-15,76	-18,01
Sergipe-Alagoas	11° S	37.5° W	-7,34	-8,82
	11° S	36.5° W	-20,07	-14,44
Bahía Sul	12° S	35° W	-20,77	-18,44
	13° S	37° W	-31,7	-24,28
Espírito Santo	17° S	38.5° W	-11,98	-11,86
	16.5° S	38° W	-15,79	-14,32
Campos	21.5° S	41° W	-15,94	-16,67
	22° S	40° W	-39,36	-27,39
	23° S	41° W	-31,73	-28,21
Santos	25.5° S	48° W	-25,44	-23,45
	26° S	46° W	-66,35	-52,41
	27° S	46° W	-57,69	-52,65
Zone III Pelotas	32.5° S	51° W	-48,96	-41,8
	33° S	51° W	-57,85	-48,49
Punta del Este	35.5° S	53° W	-30,66	-36,41
Salado	37.5° S	57° W	-19,85	-18,91
	38° S	55° W	-52,52	-41,12
Colorado	40° S	61° W	-26,1	-17,9
	41° S	59° W	-33,96	-29,92
Rawson	43.5° S	60° W	-16,77	-21,45
San Jorge	46° S	65° W	-10,53	-7,47
	47° S	66° W	-9,44	-5,61
San Julián	49.5° S	64° W	-4,52	-4,84
	43° S	52° W	-7,65	-11,27
Argentina	41.5° S	43.5° W	-28,1	-24,93
	47° S	46° W	-18,26	-16,03
Northern Falkland	50.5° S	59.5° W	-1,32	-7,38
	49.5° S	59° W	-13,55	-12,17
Eastern Falkland	52.5° S	50° W	-43,68	-36,05
	52° S	55° W	-48,03	-37,48
Zone IV Western Falkland	52.5° S	65° W	-27,1	-20,4
	53° S	60° W	-21,5	-25,87
Southern Falkland	53° S	62° W	-29,42	-26,64
	54° S	55° W	-34,17	-29,36

Table 4.4 Maximum Forebulge elevations along the eastern margin of South America during the Quaternary for Te 40 km

Country	Latitude	Longitude	Forebulge (m)
			Te 40 km
Colombia	8.5° N	74°W	4.48
Venezuela	7.5° N	62°W	6.64
Guiana	6.5° N	60°W	7.73
Surinam	4.5°N	55.5° W	7.26
French Guiana	3.5° N	53° W	11.56
Brazil	1.5°N	51.5°W	4.65
	1.5°N	52.5°W	8.75
	3°S	46.5°W	6.99
	5°S	41.5°W	7.2
	7°S	37°W	5.52
	21.5°S	43°W	4.79
	28°S	51°W	4.9
Uruguay	32.5° S	54° W	4.79
Argentina	37° S	60° W	4.46

Table 4.5 Maximum Forebulge elevations along the eastern margin of South America during the Quaternary for T_e 80 km

Country	Latitude	Longitude	Forebulge (m)
			T_e 80 km
Venezuela	6.5°N	65.5°W	4.36
Guiana	4.5°N	59°W	7.16
Surinam	4°N	57°W	6.22
	3°N	55°W	8.71
French Guiana	7°N	54°W	9.97
	1.5°N	54°W	11.09
Brazil	0°	53°W	7.57
	4°S	48°W	6.89
	7.5°S	40°W	5.93
	18°S	43.5°W	4.11
	28.5°S	52.5°W	5.17
Uruguay	31.5°S	56.5°W	4.56

4.4.2 Flexural Response of the Lithosphere from the Paleocene to the Present

In the following, we present a graphical summary of the evolution of flexural response since Pliocene (5.332 to 0 Ma), Miocene (23.03 to 0 Ma), Oligocene (33.9 to 0 Ma), Eocene (55.8 to 0 Ma) and Paleocene (65.6 to 0 Ma) epochs

4.4.2.1 Zone I

Zone I, includes the following offshore points: Barracuda Abyssal Plain, Cayos, Colombia basin, Magdalena Delta, Venezuela Basin, Grenada, Tobago, Demerara Abyssal Plain, Marin Guajira, Marin Sinú and Cariaco for which flexural depression values are shown in Appendix D.

Figures 4.29 to 4.38 show evolution of flexural depression of lithosphere at each of these locations. In these figures is observed the changing of the flexural depression obtained using a $T_e = 40$ km (green line) and $T_e = 80$ km (blue line) through 0-65 million years and 5332-0 million years respectively.

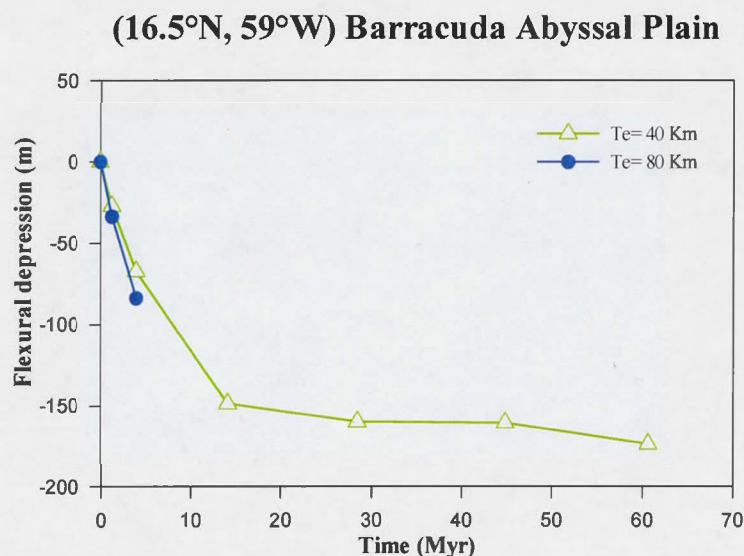


Figure 4.29 Contribution to lithospheric flexure, from sediments deposited in each geological epoch, at an offshore site in the Barracuda Abyssal Plain .

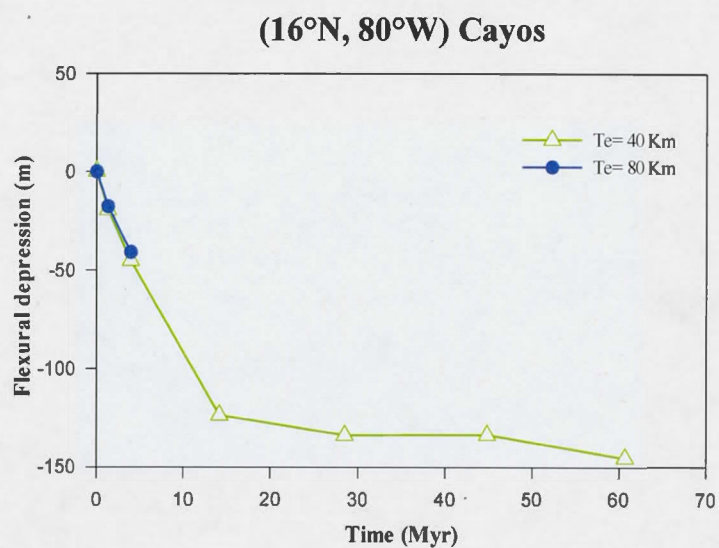


Figure 4.30 Contribution to lithospheric flexure, from sediments deposited in each geological epoch, at an offshore site in the Cayos Basin.

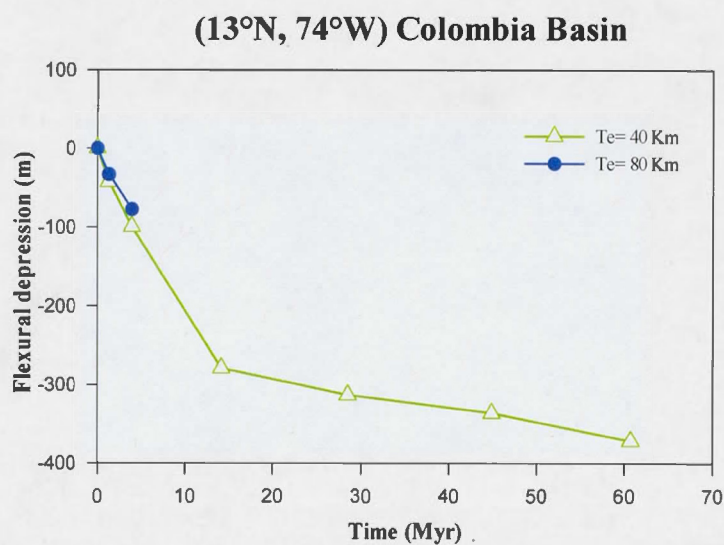


Figure 4.31 Contribution to lithospheric flexure, from sediments deposited in each geological epoch, at an offshore site in the Colombia Basin

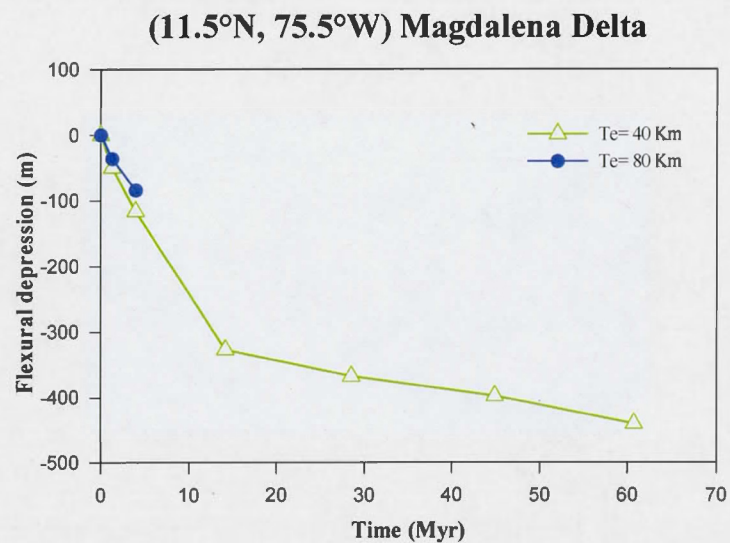


Figure 4.32 Contribution to lithospheric flexure, from sediments deposited in each geological epoch, at an offshore site in the Magdalena Delta

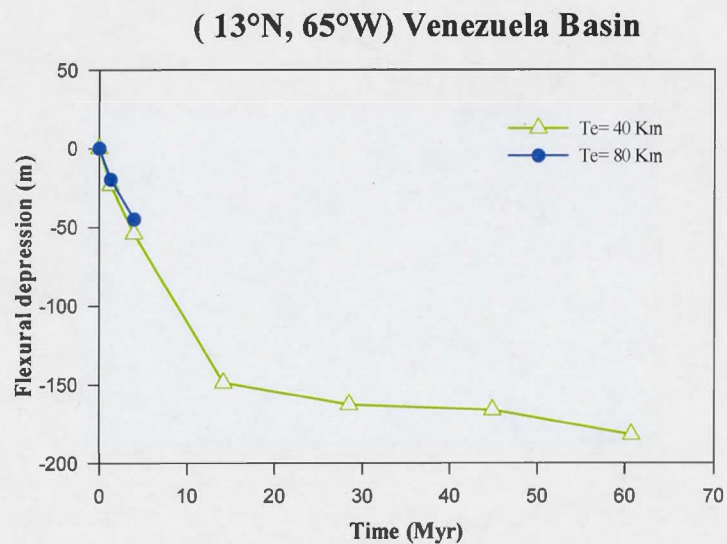


Figure 4.33 Contribution to lithospheric flexure, from sediments deposited in each geological epoch, at an offshore site in the Venezuela Basin

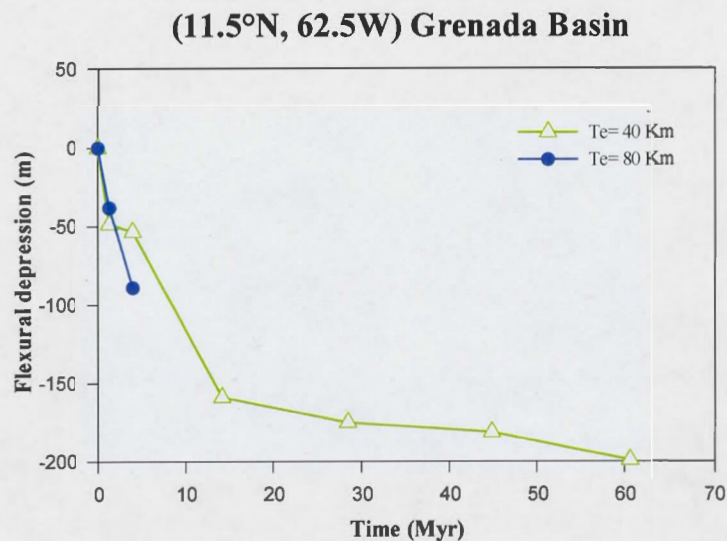


Figure 4.34 Contribution to lithospheric flexure, from sediments deposited in each geological epoch, at an offshore site in the Grenada Basin

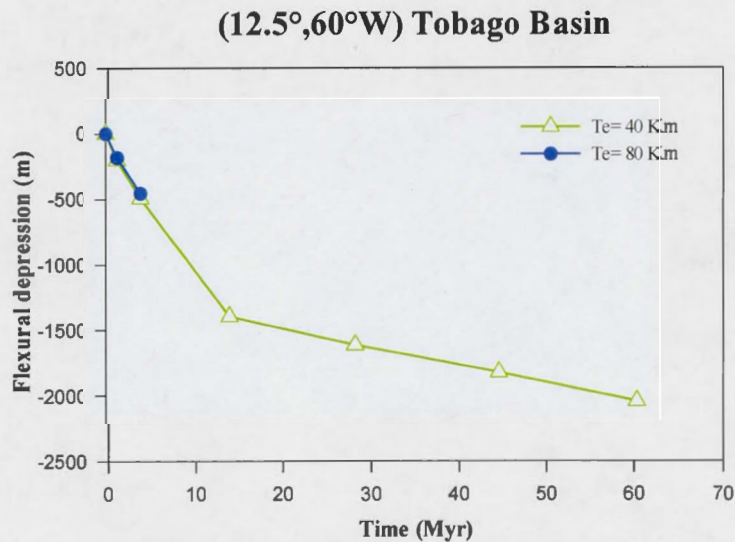


Figure 4.35 Contribution to lithospheric flexure, from sediments deposited in each geological epoch, at an offshore site in the Tobago Basin

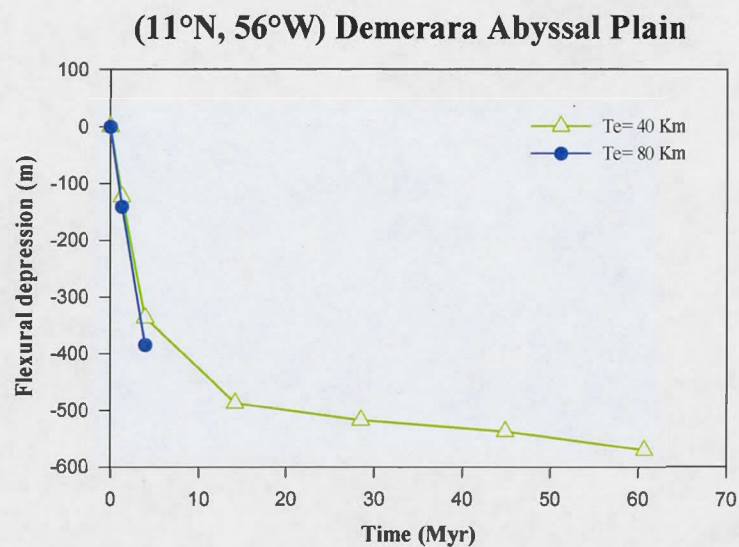


Figure 4.36 Contribution to lithospheric flexure, from sediments deposited in each geological epoch, at an offshore site in the Demerara Abyssal Plain

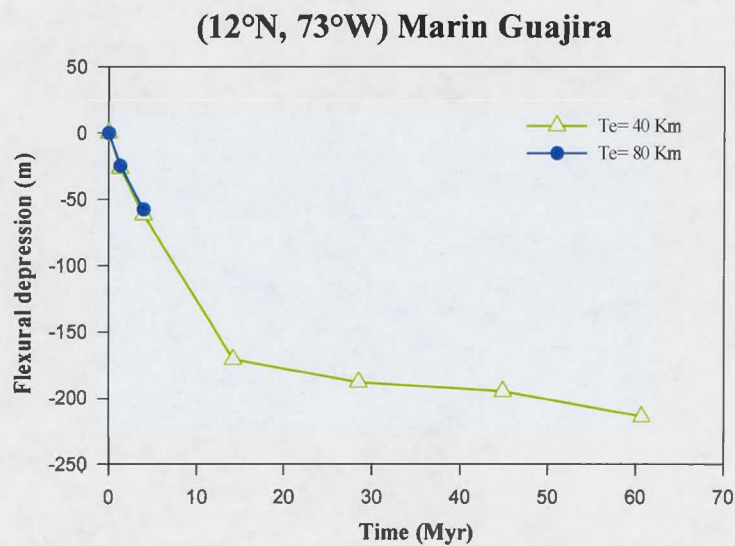


Figure 4.37 Contribution to lithospheric flexure, from sediments deposited in each geological epoch, at an offshore site in the Marin Guajira Basin

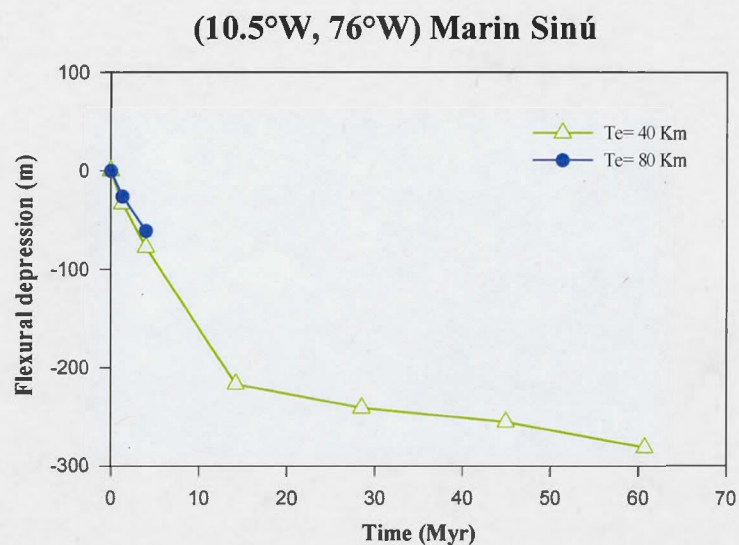


Figure 4.38 Contribution to lithospheric flexure, from sediments deposited in each geological epoch, at an offshore site in the Marin Sinú Basin

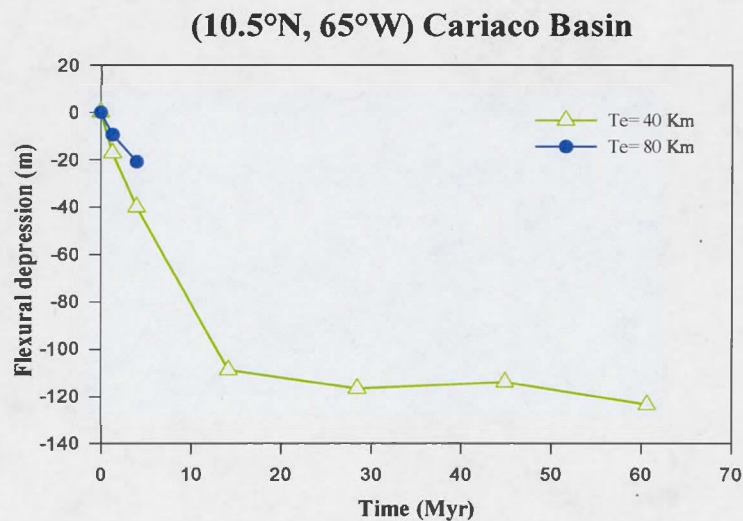


Figure 4.39 Contribution to lithospheric flexure, from sediments deposited in each geological epoch, at an offshore site in the Cariaco Basin

4.4.2.2 Zone II

Zone II, includes the following offshore points: Guiana, Surinam, French Guiana, Amazon Delta, Brazil, Ceará and Potiguar, for which flexural depression values are shown in Appendix D.

Figures 4.40 to 4.46 show evolution of flexural depression of lithosphere at each of these locations.

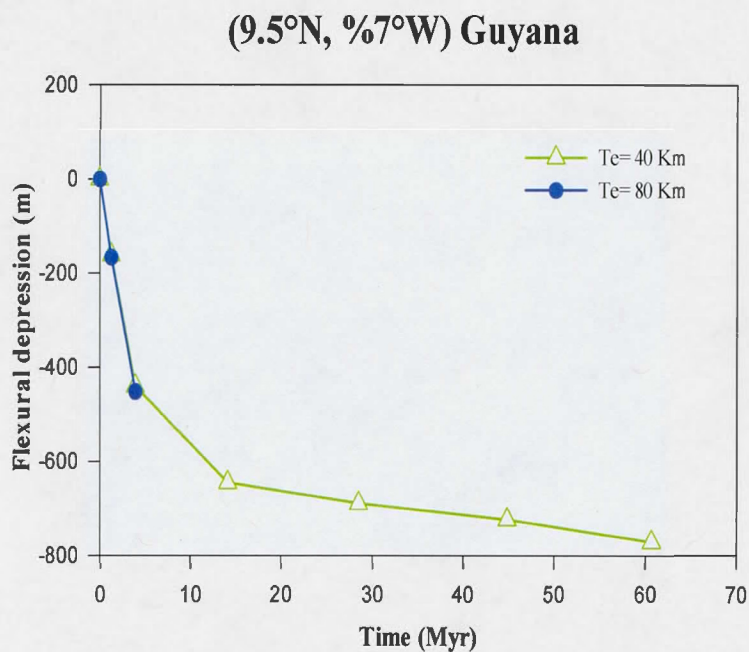


Figure 4.40 Contribution to lithospheric flexure, from sediments deposited in each geological epoch, at an offshore site in the Guiana

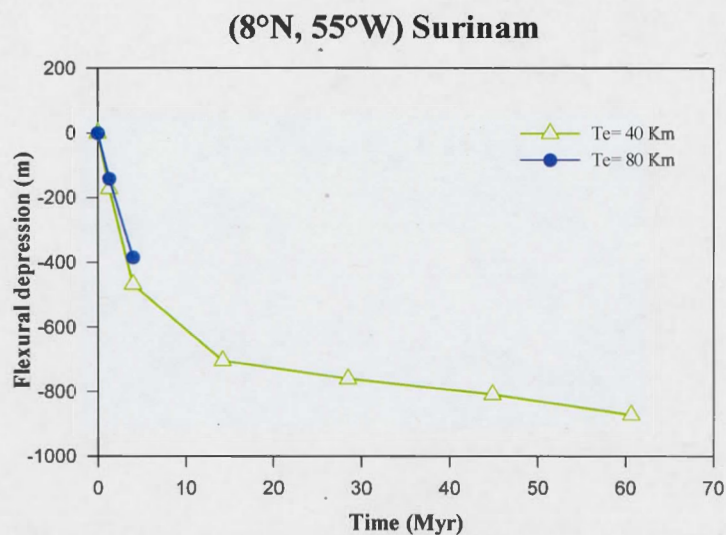


Figure 4.41 Contribution to lithospheric flexure, from sediments deposited in each geological epoch, at an offshore site in the Surinam

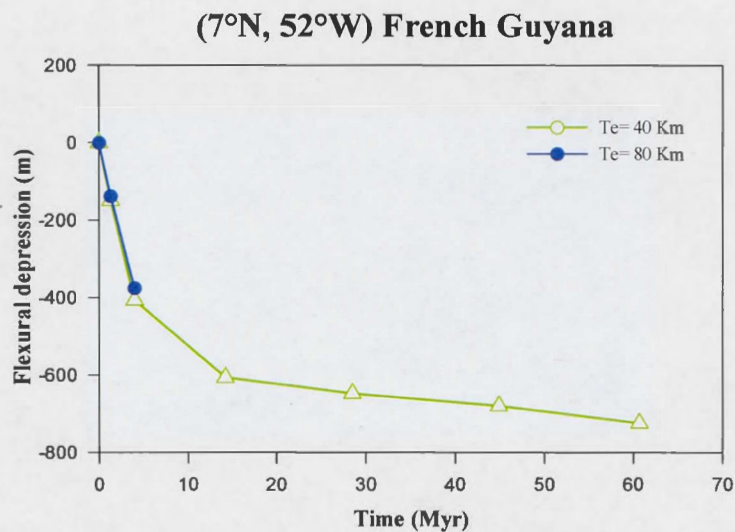


Figure 4.42 Contribution to lithospheric flexure, from sediments deposited in each geological epoch, at an offshore site in the French Guyana

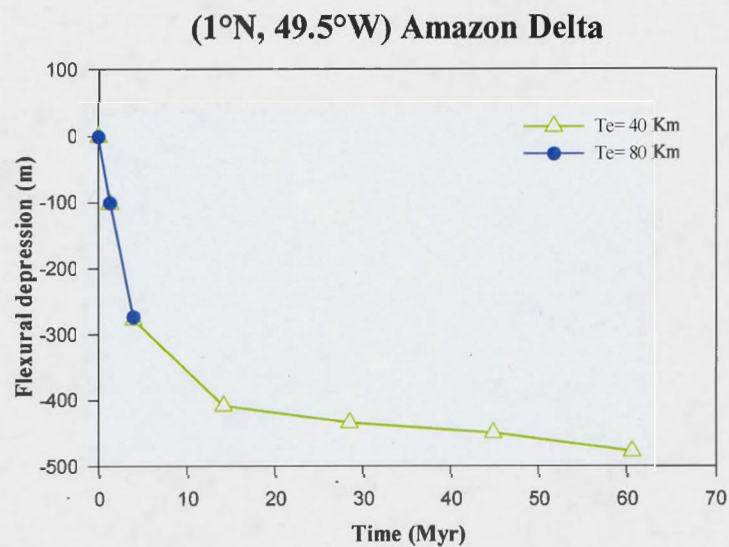


Figure 4.43 Contribution to lithospheric flexure, from sediments deposited in each geological epoch, at an offshore site in the Amazon Delta

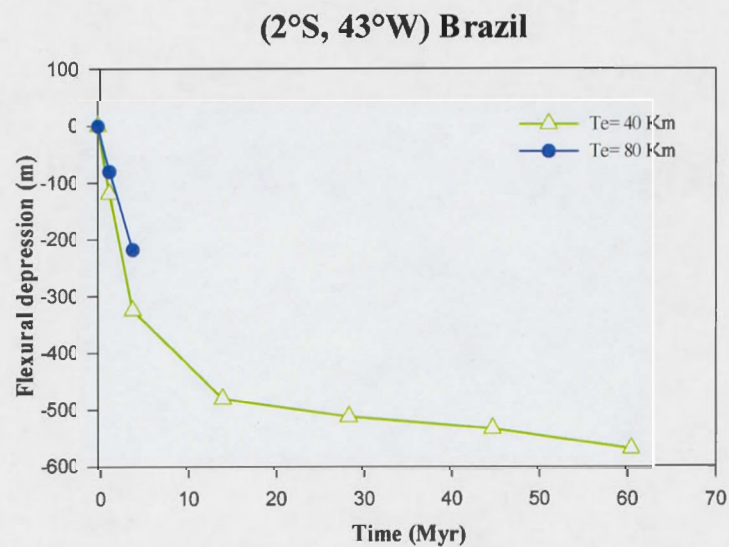


Figure 4.44 Contribution to lithospheric flexure, from sediments deposited in each geological epoch, at an offshore site in Brazil

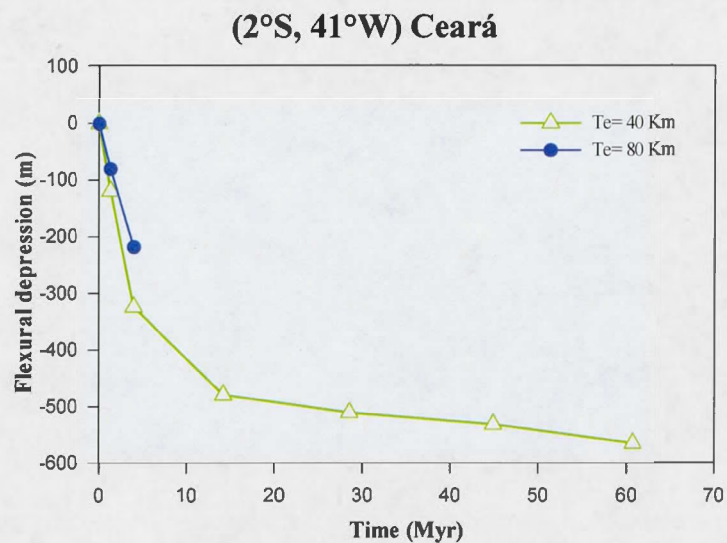


Figure 4.45 Contribution to lithospheric flexure, from sediments deposited in each geological epoch, at an offshore site in Ceará

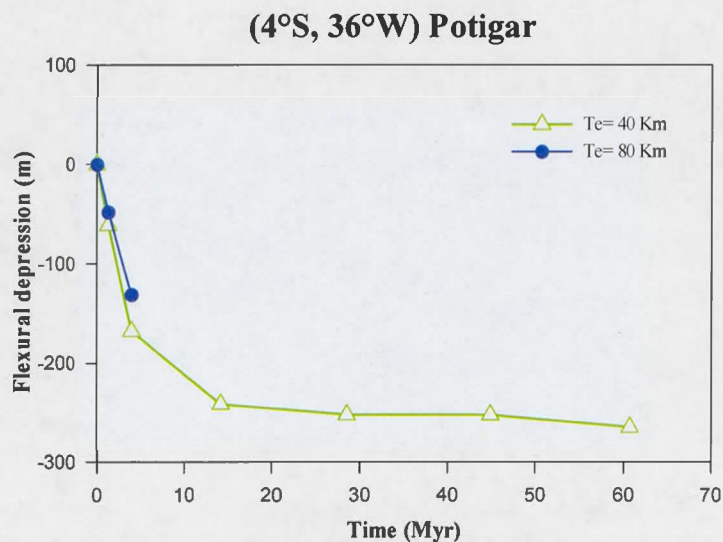


Figure 4.46 Contribution to lithospheric flexure, from sediments deposited in each geological epoch, at an offshore site in Potigarr

4.4.2.3 Zone III

Zone III, includes the following offshore points: Pernambuco, Sergipe-Alagoas, Bahia Sul, Espiritu Santo, Campos, Santos, Pelotas, Punta del Este, Salado, Colorado, Rawson, San Jorge, San Julian, Argentina and Northern Falkland, for which flexural depression values are shown in Appendix D.

Figures 4.47 to 4.61 show evolution of flexural depression of lithosphere at each of these locations.

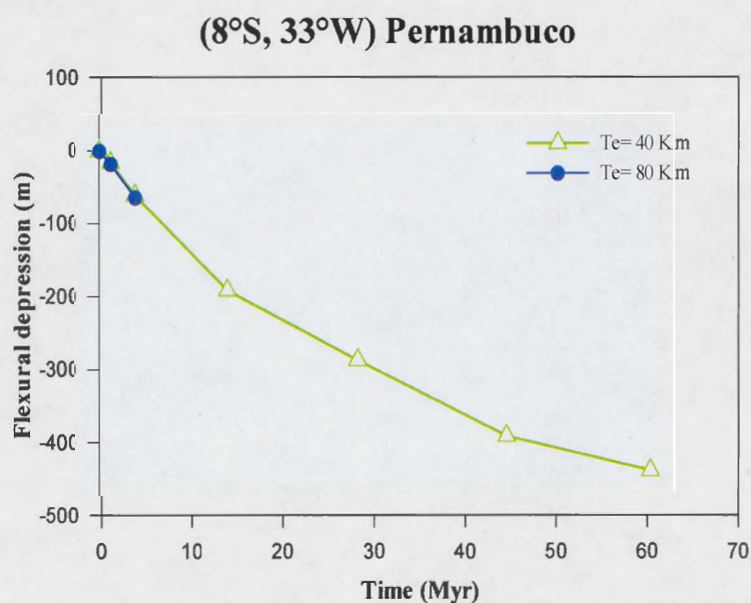


Figure 4.47 Contribution to lithospheric flexure, from sediments deposited in each geological epoch, at an offshore site in Pernambuco

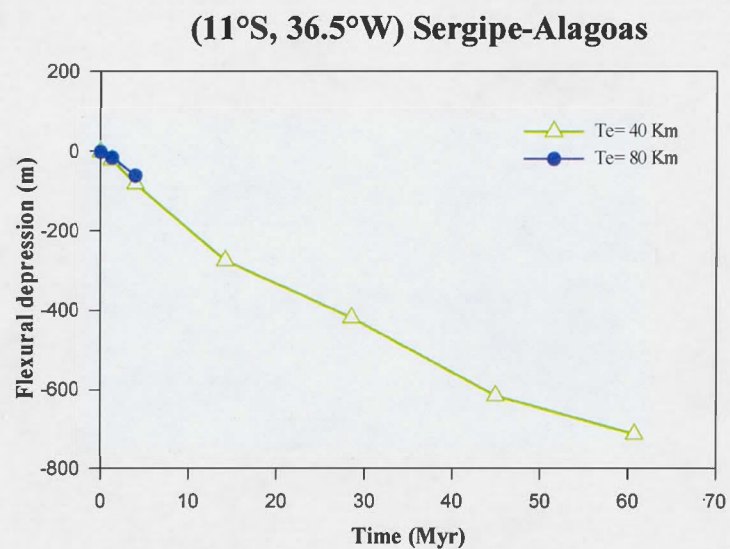


Figure 4.48 Contribution to lithospheric flexure, from sediments deposited in each geological epoch, at an offshore site in Sergipe-Alagoas

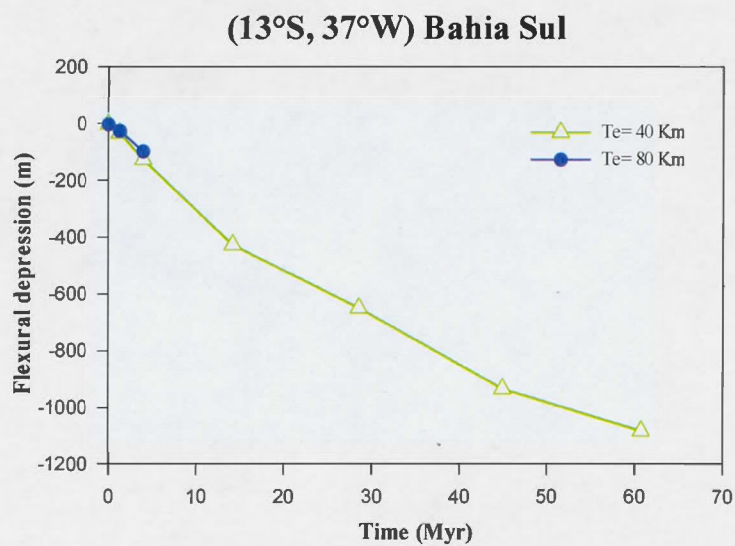


Figure 4.49 Contribution to lithospheric flexure, from sediments deposited in each geological epoch, at an offshore site in Bahia Sul

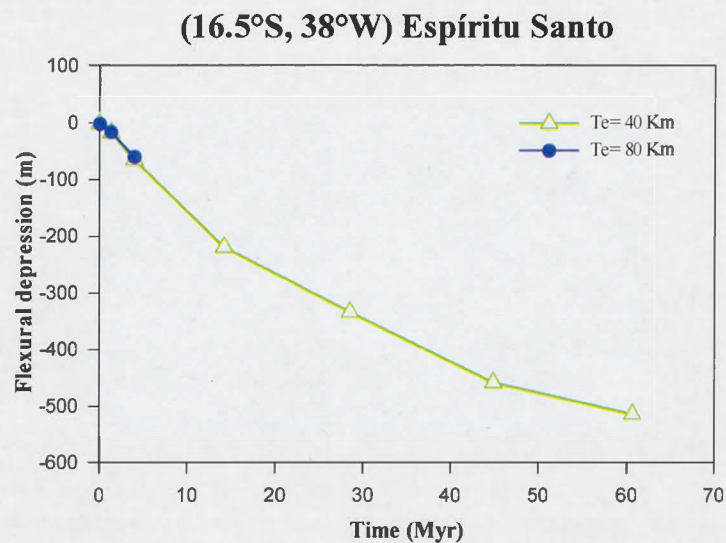


Figure 4.50 Contribution to lithospheric flexure, from sediments deposited in each geological epoch, at an offshore site in the Espírito Santo Basin

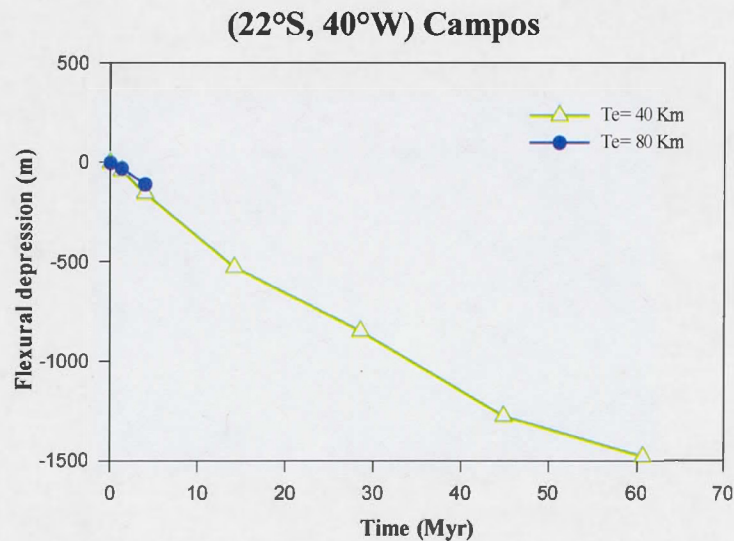


Figure 4.51 Contribution to lithospheric flexure, from sediments deposited in each geological epoch, at an offshore site in the Campos Basin

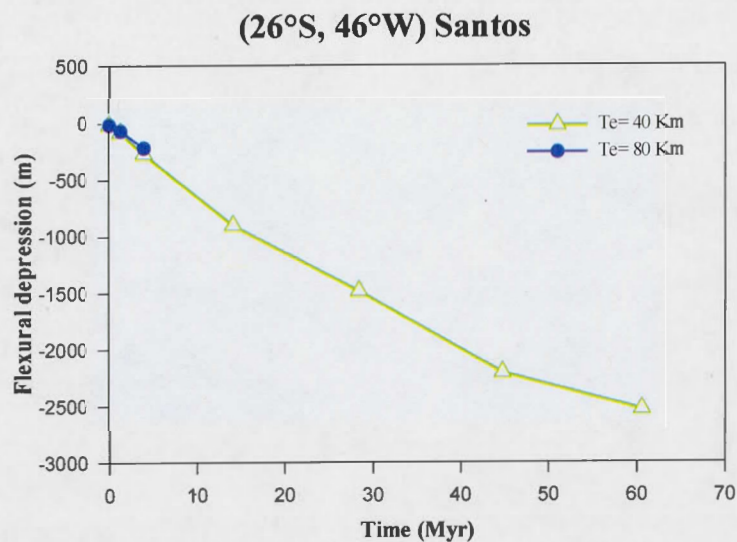


Figure 4.52 Contribution to lithospheric flexure, from sediments deposited in each geological epoch, at an offshore site in the Santos Basin

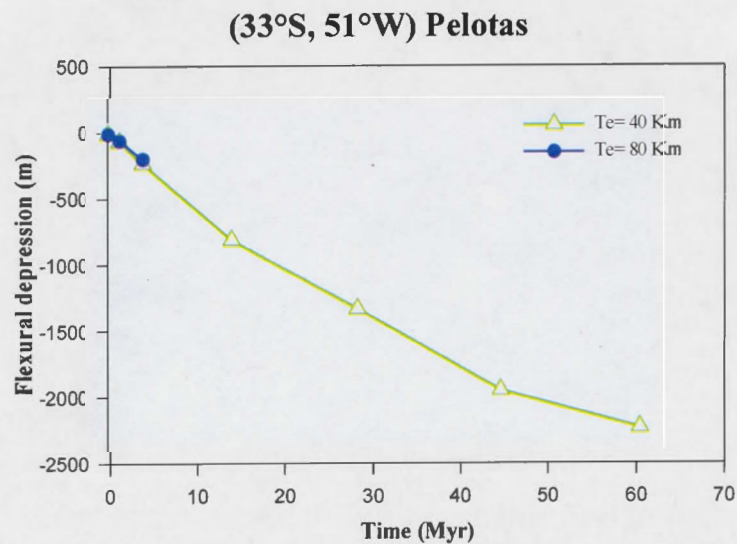


Figure 4.53 Contribution to lithospheric flexure, from sediments deposited in each geological epoch, at an offshore site in the Pelotas Basin

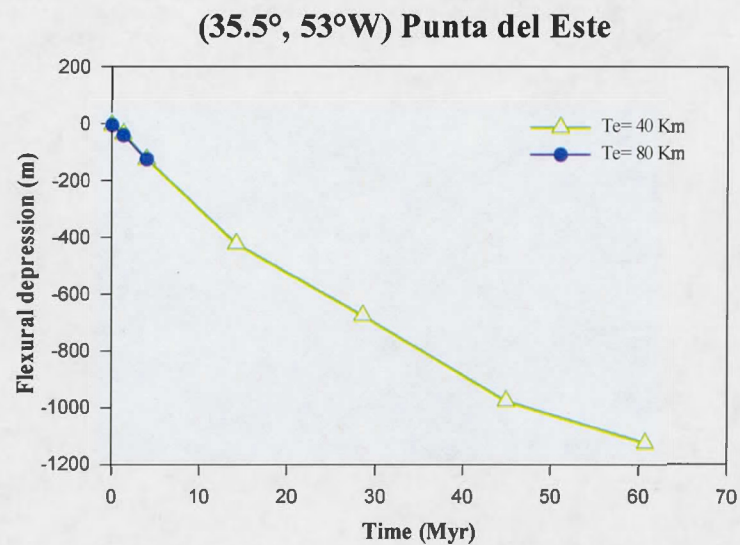


Figure 4.54 Contribution to lithospheric flexure, from sediments deposited in each geological epoch, at an offshore site in the Punta del Este Basin

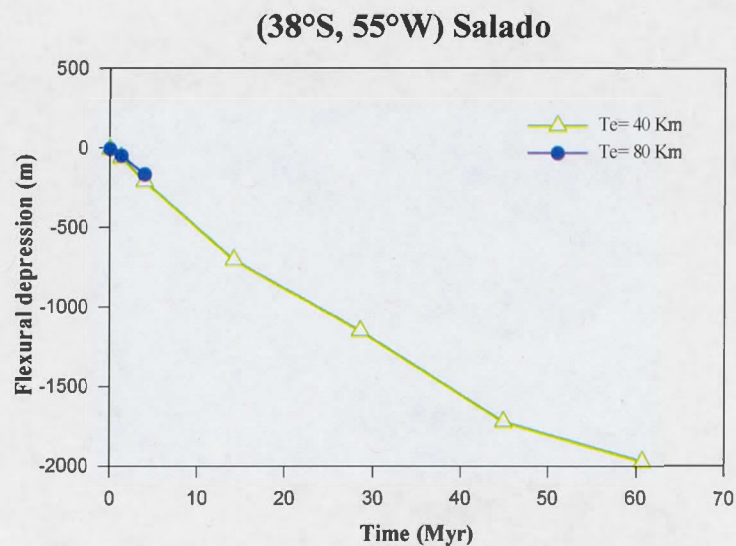


Figure 4.55 Contribution to lithospheric flexure, from sediments deposited in each geological epoch, at an offshore site in the Salado Basin

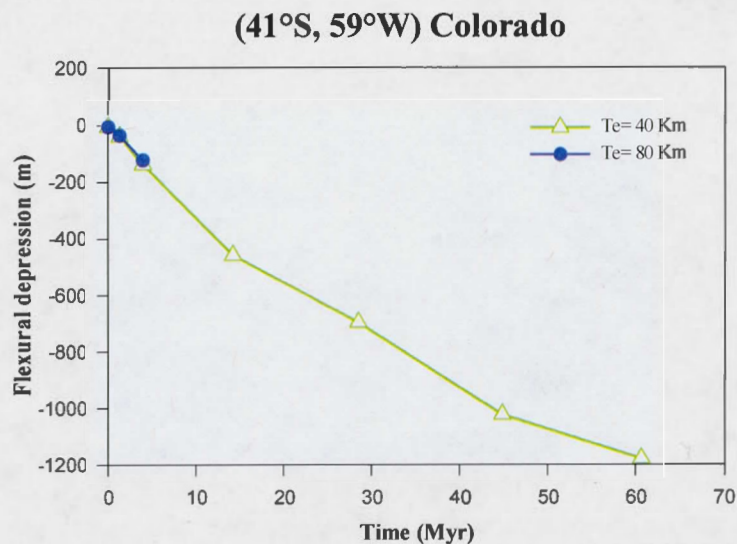


Figure 4.56 Contribution to lithospheric flexure, from sediments deposited in each geological epoch, at an offshore site in the Colorado Basin

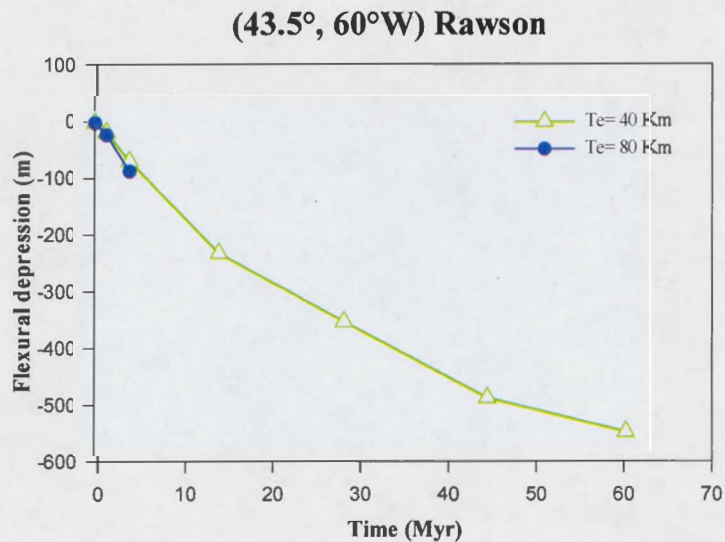


Figure 4.57 Contribution to lithospheric flexure, from sediments deposited in each geological epoch, at an offshore site in the Rawson Basin

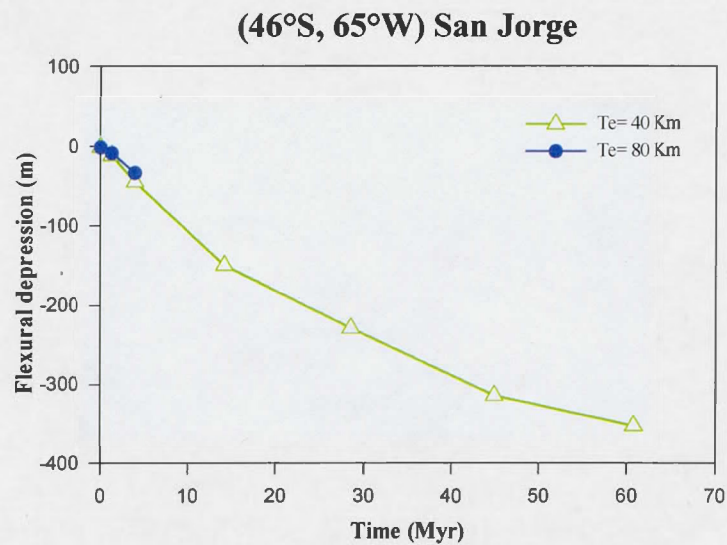


Figure 4.58 Contribution to lithospheric flexure, from sediments deposited in each geological epoch, at an offshore site in the San Jorge Basin

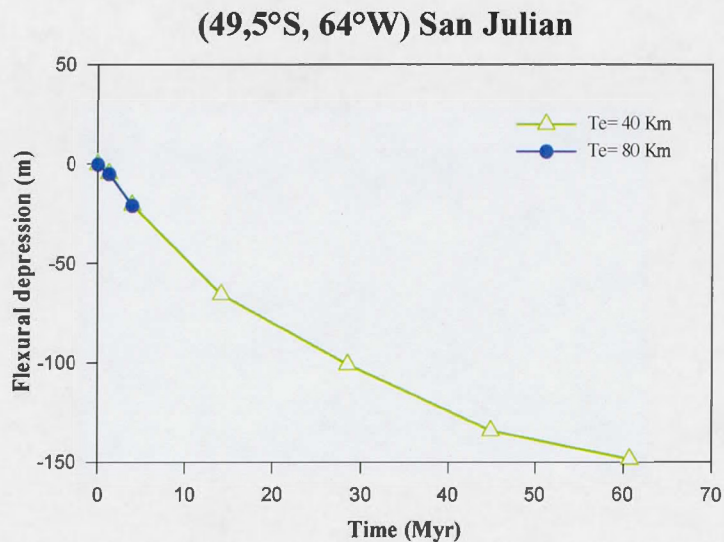


Figure 4.59 Contribution to lithospheric flexure, from sediments deposited in each geological epoch, at an offshore site in the San Julian Basin

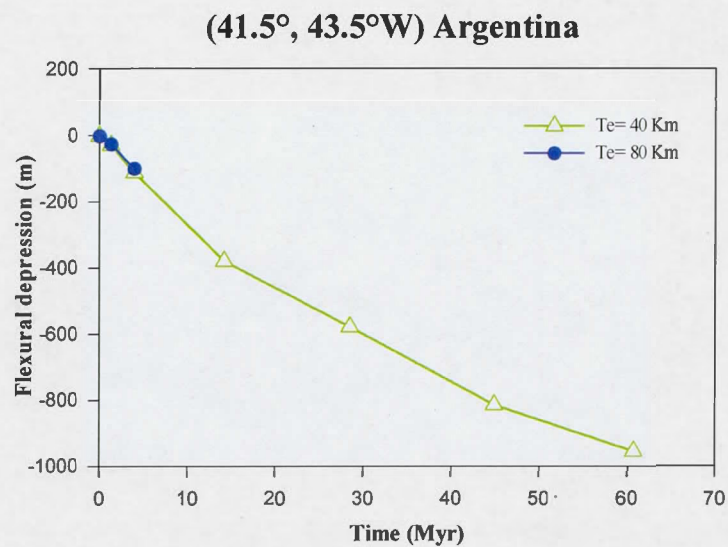


Figure 4.60 Contribution to lithospheric flexure, from sediments deposited in each geological epoch, at an offshore site in the Argentina Basin

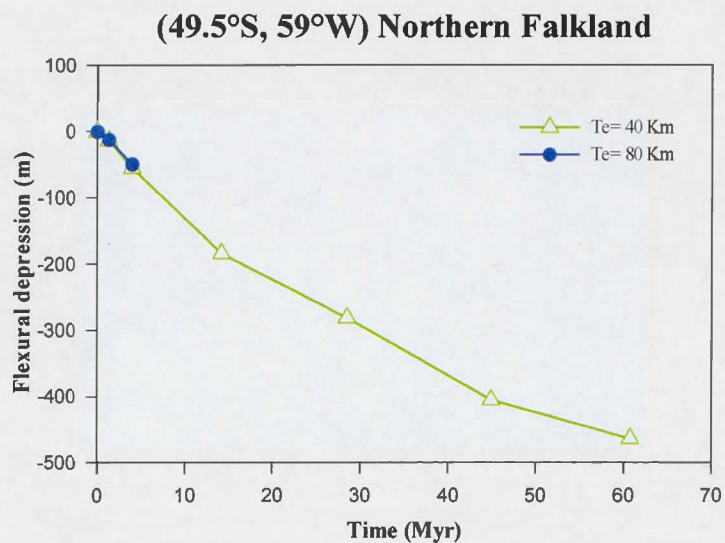


Figure 4.61 Contribution to lithospheric flexure, from sediments deposited in each geological epoch, at an offshore site in the Northern Falkland

4.4.2.4 Zone IV

Zone IV, includes the following offshore points: Eastern Falkland, Western Falkland and Southern Falkland, for which flexural depression values are tabulated in Appendix D.

Figures 4.62 to 4.64 show evolution of flexural depression of lithosphere at each of these locations.

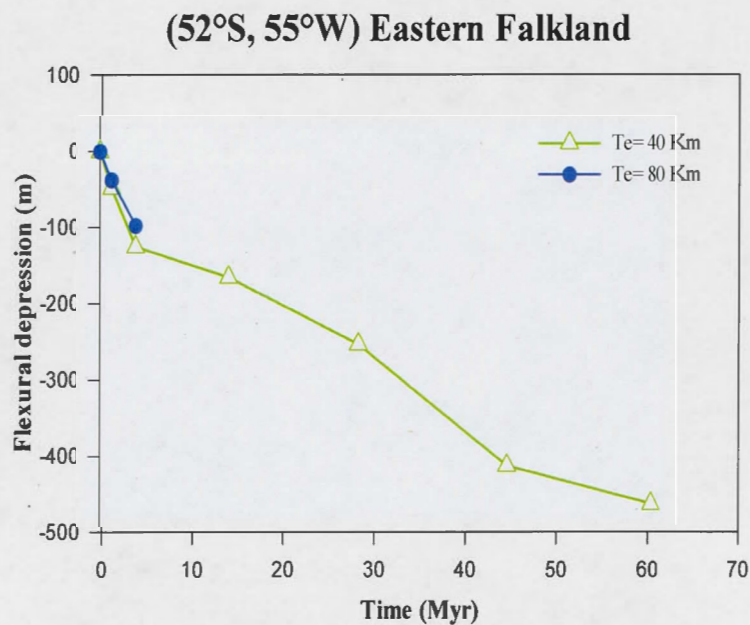


Figure 4.62 Contribution to lithospheric flexure, from sediments deposited in each geological epoch, at an offshore site in the Eastern Falkland

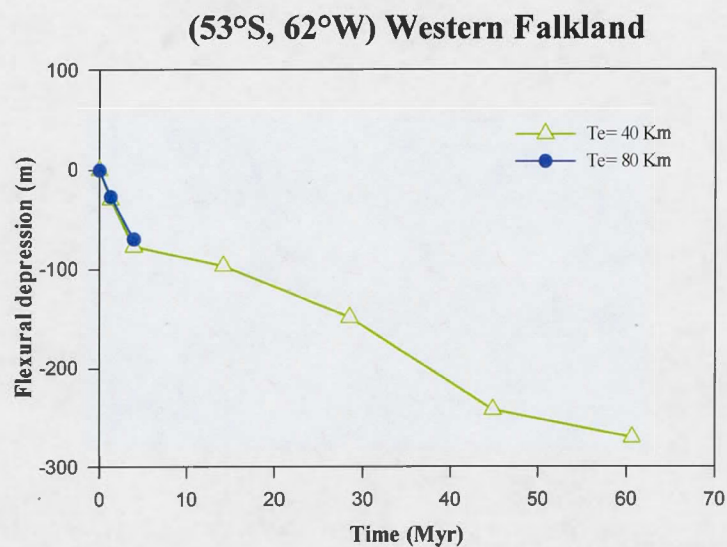


Figure 4.63 Contribution to lithospheric flexure, from sediments deposited in each geological epoch, at an offshore site in the Western Falkland

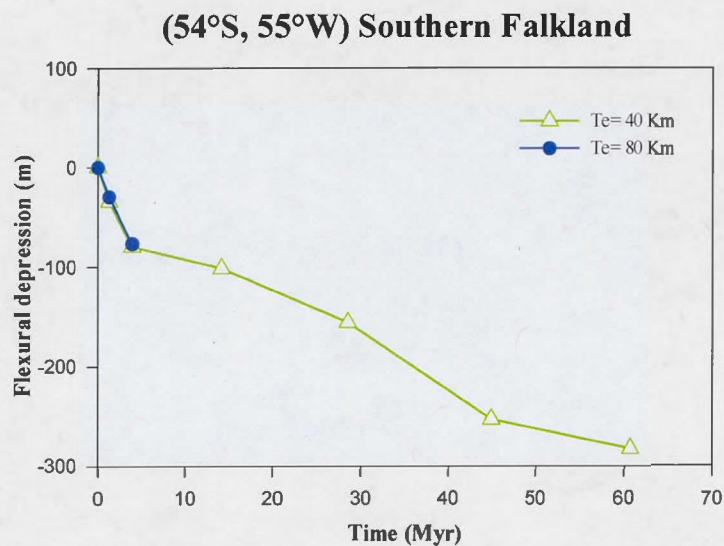


Figure 4.64 Contribution to lithospheric flexure, from sediments deposited in each geological epoch, at an offshore site in the Southern Falkland

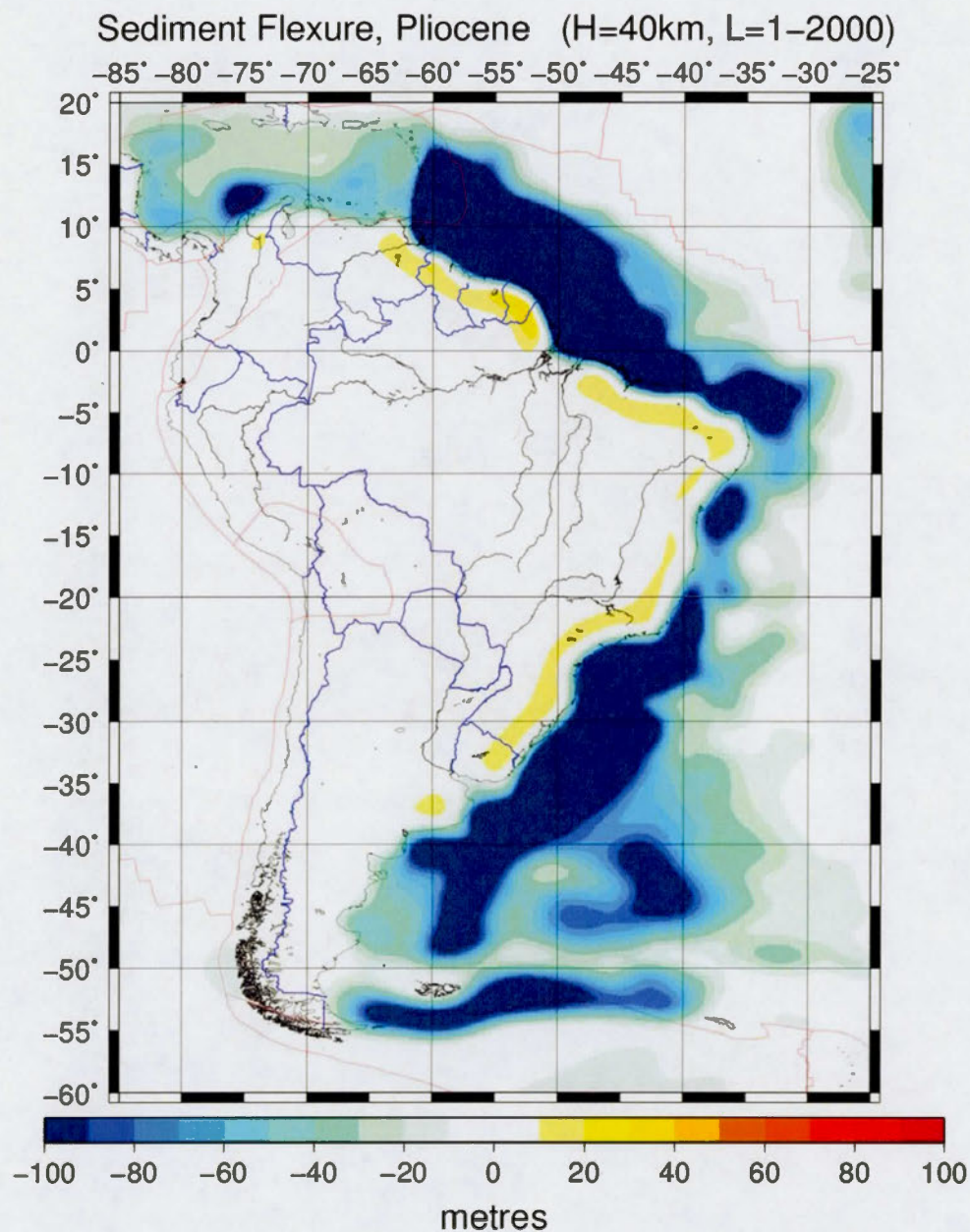


Figure 4.65 Map of total Flexural Response due to sediment loads accumulated since the Pliocene (5.332 – 0 million years) for an effective elastic thickness of 40 km and a maximum harmonic degree of 2000

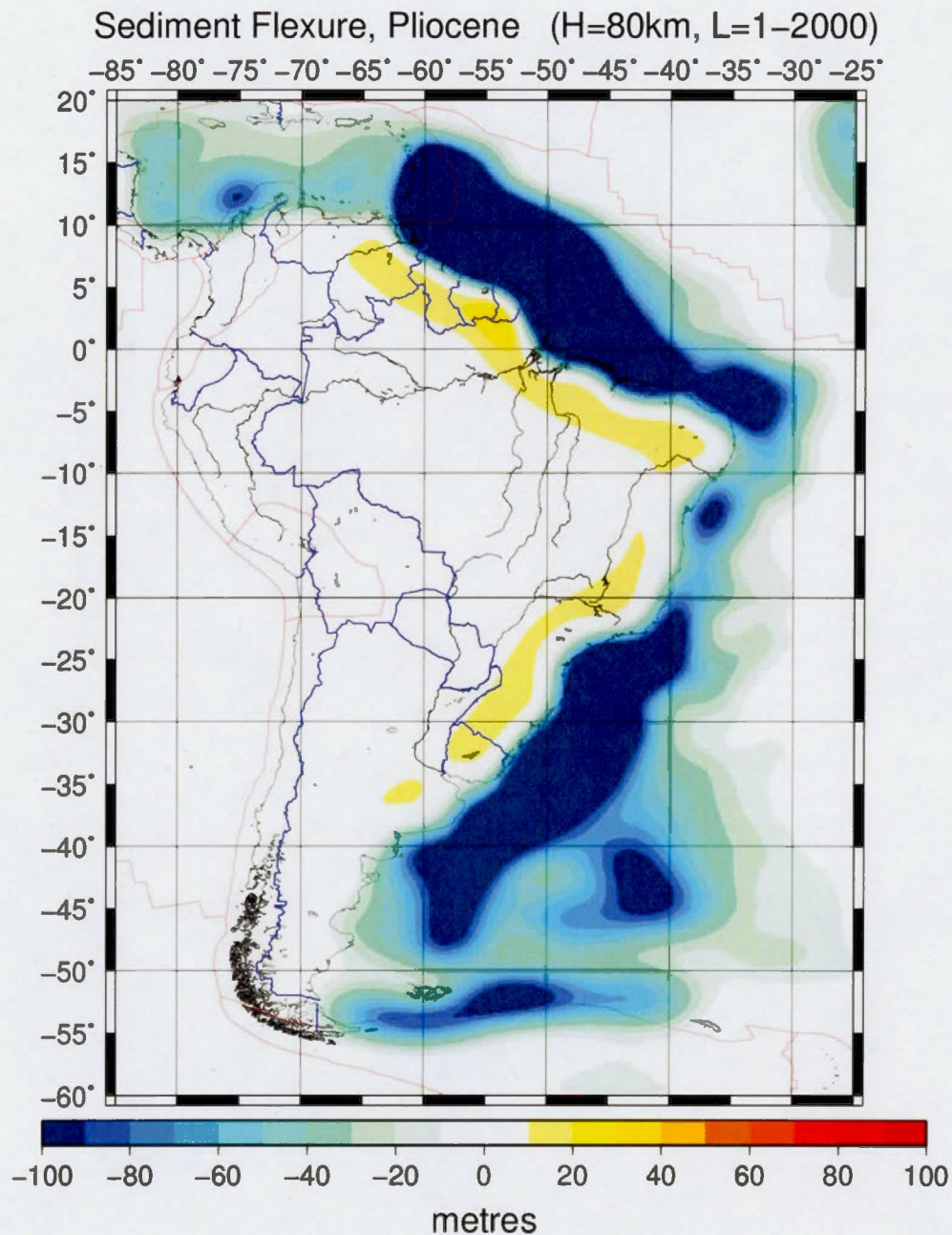


Figure 4.66 Map of total Flexural Response due to sediment loads accumulated since the Pliocene (5.332 – 0 million years) for an effective elastic thickness of 80 km and a maximum harmonic degree of 2000

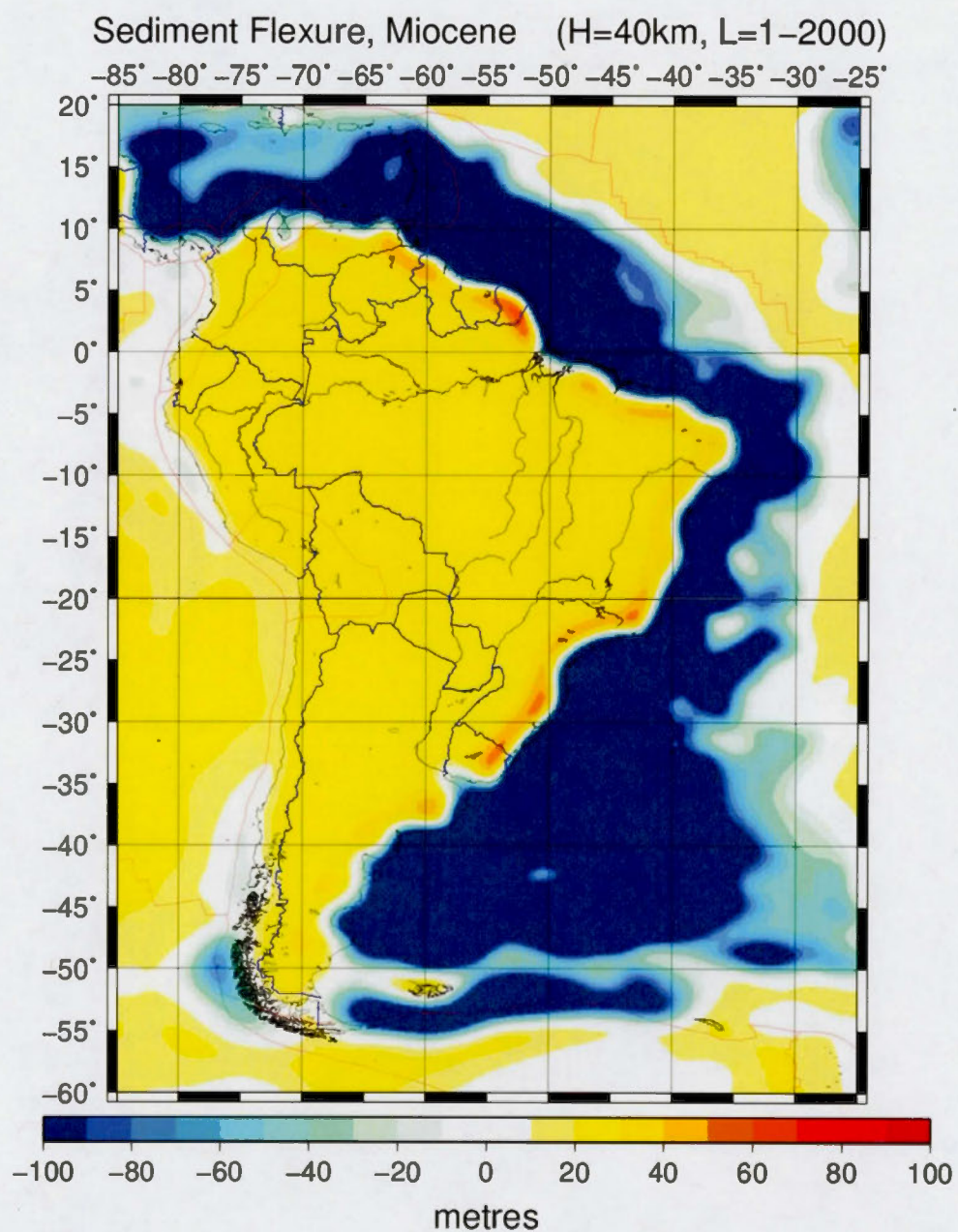


Figure 4.67 Map of total Flexural Response due to sediment loads accumulated since the Miocene (23.03 - 0 million years) for an effective elastic thickness of 40 km and a maximum harmonic degree of 2000

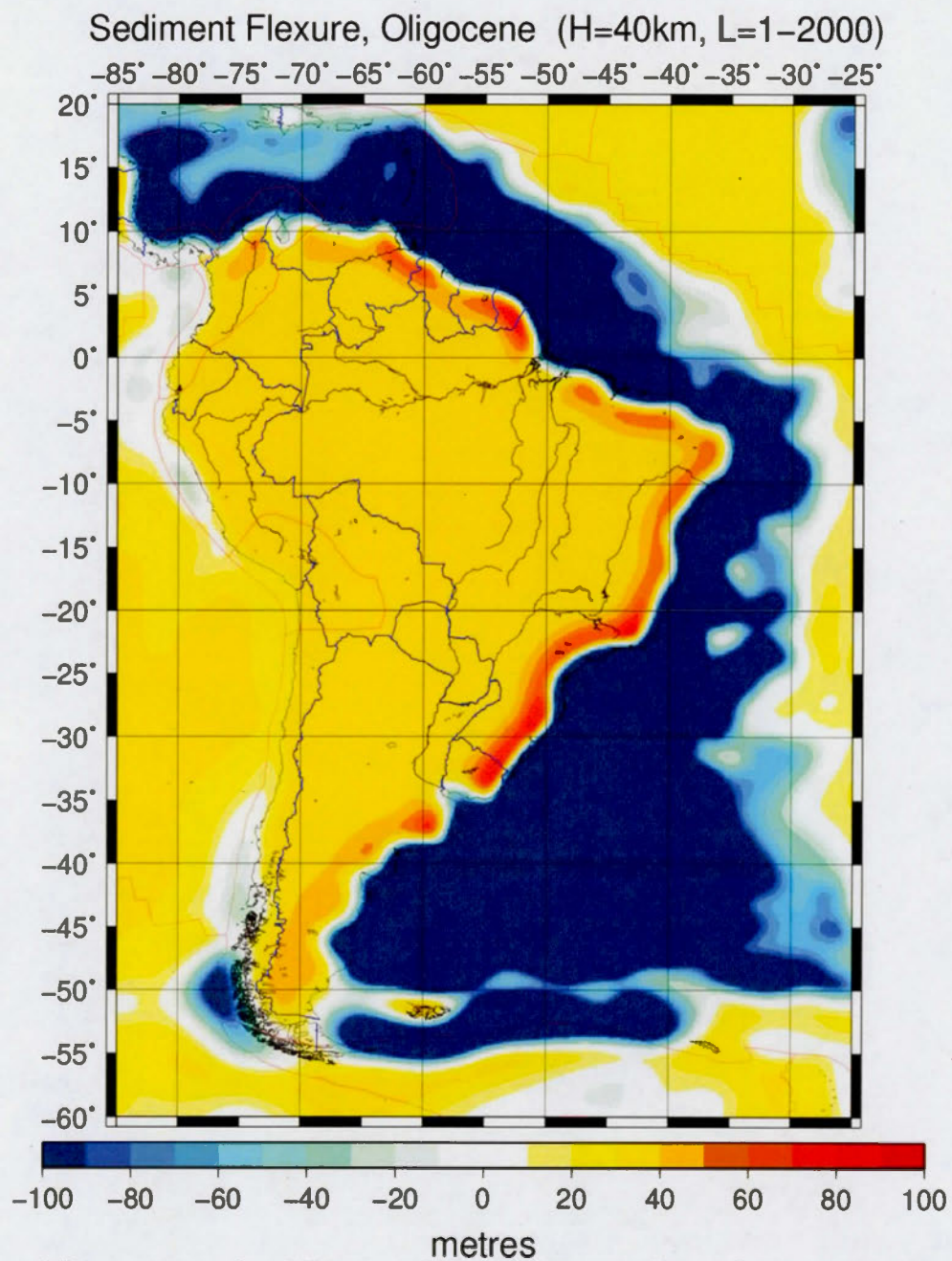


Figure 4.68 Map of total Flexural Response due to sediment loads accumulated since the Oligocene (33.9 - 0 million years) for an effective elastic thickness of 40 km and a maximum harmonic degree of 2000

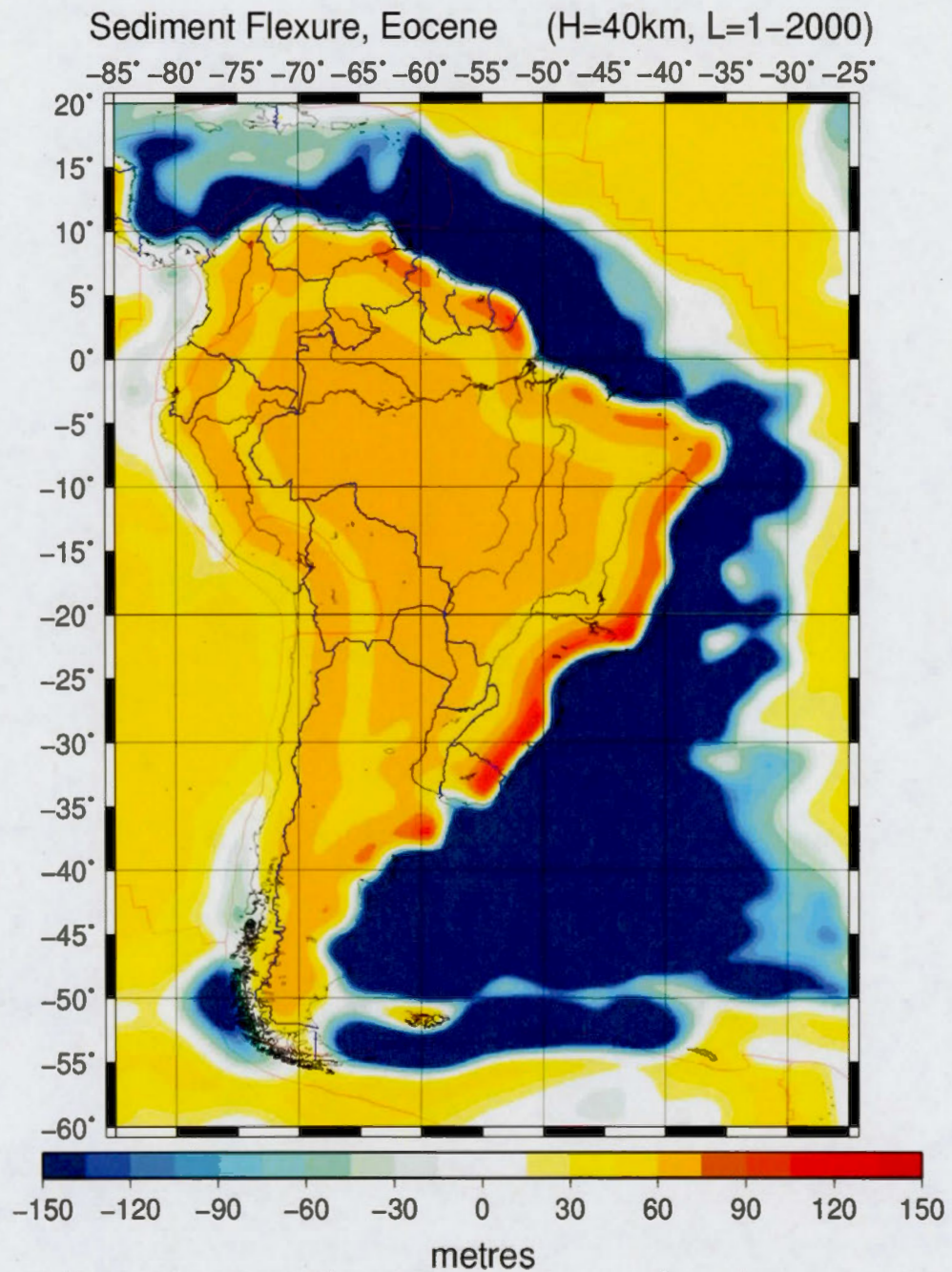


Figure 4.69 Map of total Flexural Response due to sediment loads accumulated since the Eocene (55.8 - 0 million years) for an effective elastic thickness of 40 km and a maximum harmonic degree of 2000

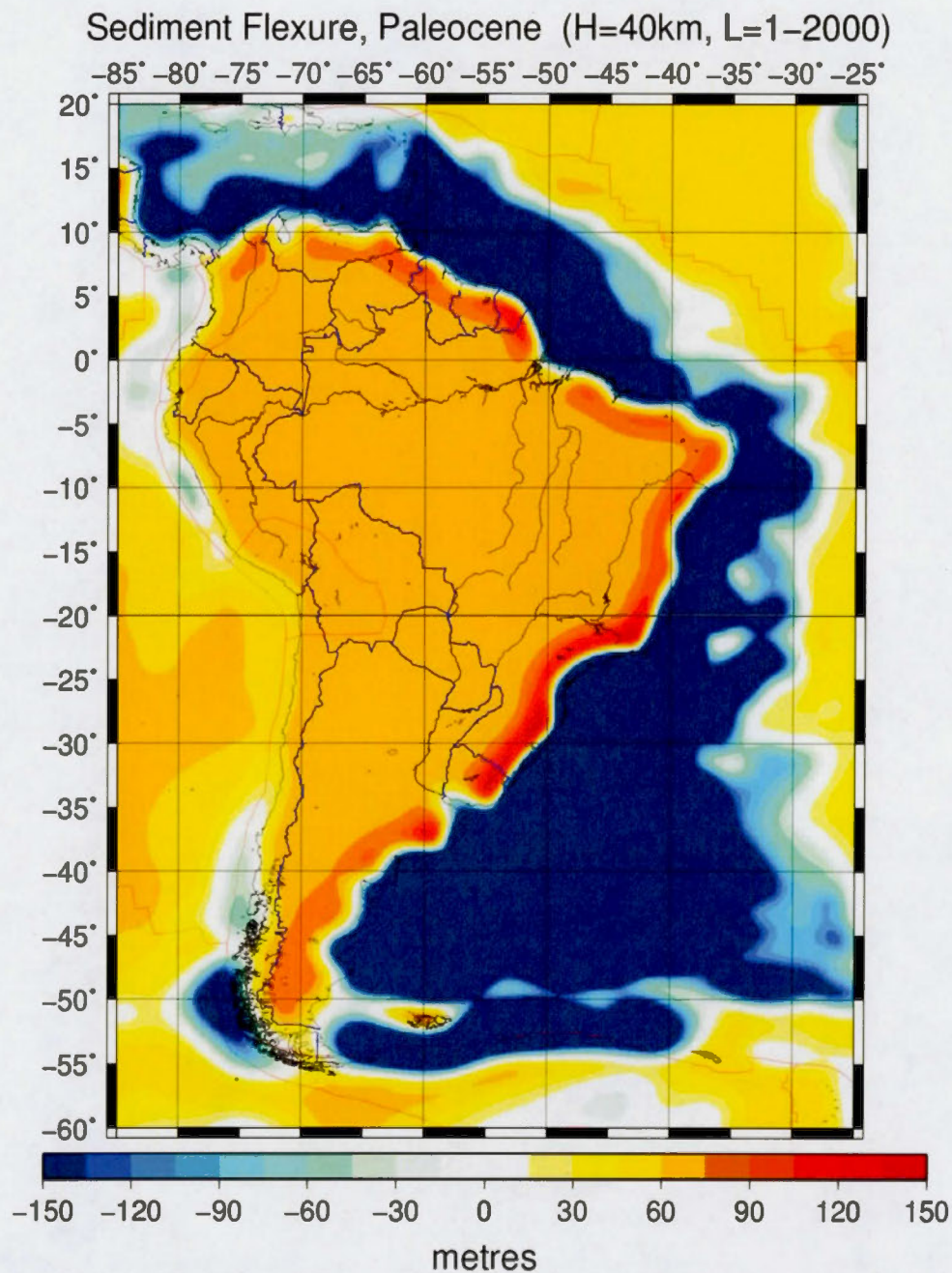


Figure 4.70 Map of total Flexural Response due to sediment loads accumulated since the Paleocene (65.5 - 0 million years) for an effective elastic thickness of 40 km and a maximum harmonic degree of 2000

4.4.3 Uplift of the Continent of South America since the Pliocene, the Miocene, the Oligocene, the Eocene and the Paleocene

The forebulge or uplift undergone by the continent of South America (at 10°S and 60°W) during the Cenozoic (Quaternary (Figure 4.27 and 4.28), Pliocene (Figure 4.65 and 4.66), Miocene (Figure 4.67), Oligocene (Figure 4.68), Eocene (Figure 4.69) and Paleocene (Figure 4.70) is between 2 and 70.66 meters.

The following graphic shows the uplift that South-American Continent has experience since the Paleocene until now:

Time-dependence evolution of continental uplift due to the forebulge in South America (lat= 10°S , lon= 60°W) since the Paleocene

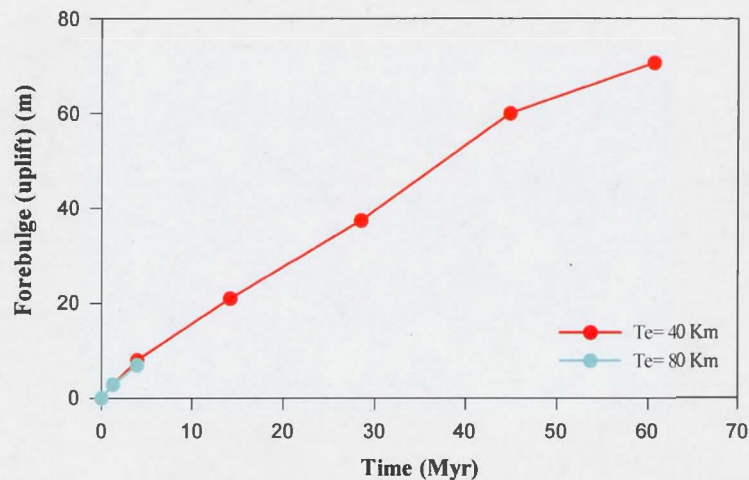


Figure 4.71 Time-dependence evolution of continental uplift due to the forebulge in South America continent (lat= 10°S , lon = 60°W) since the Paleocene.

The forebulge increases the elevation in the eastern region of the continent with values between 4.43 meters and 80 meters. The time-dependence of this uplift can be seen in the following figure, where the evolution of the forebulge from Paleocene to the Present is plotted.

Time-dependence evolution of continental uplift due to the forebulge along the eastern margin of South America (lat=5°S, lon= 45°W) since the Paleocene

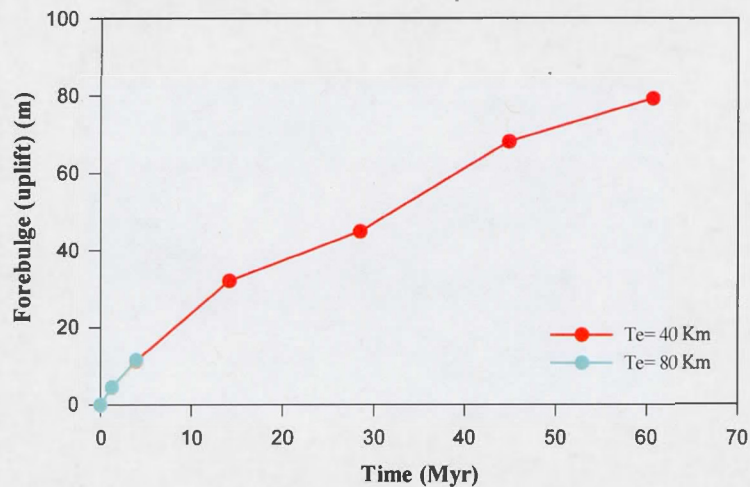


Figure 4.72 Time-dependence evolution of continental uplift due to the forebulge along the eastern margin of South America (lat= 5°S, lon=45°W) since the Paleocene.

In comparison to the uplift describe above, some portion of the continent such as in Venezuela, Guyana, Surinam, French Guyana, Brazil, Uruguay and Argentina showed greater elevation changes in some intervals. In the following graph, we present the evolution of forebulge during Quaternary, Pliocene, Miocene, Oligocene, Eocene and Paleocene ages for these countries with forebulge values summarized in Table 4.7.

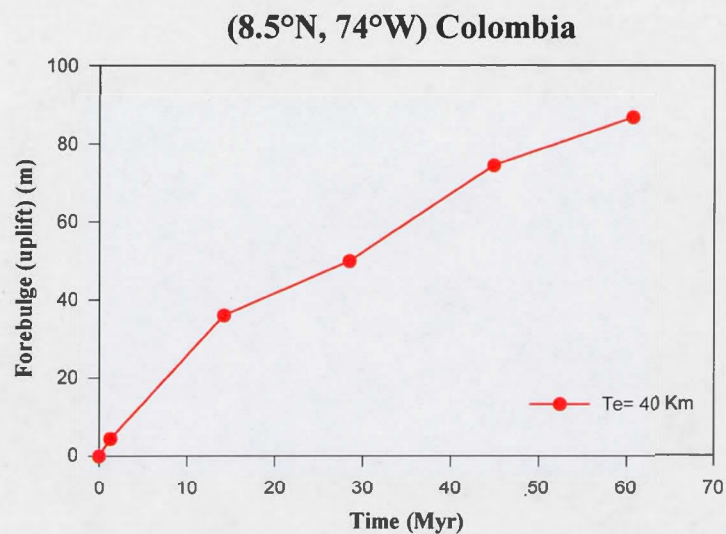


Figure 4.73 Forebulge evolution at a representative location in Colombia (lat=8.5°N, lon= 74°W) from the Paleocene to the Present.

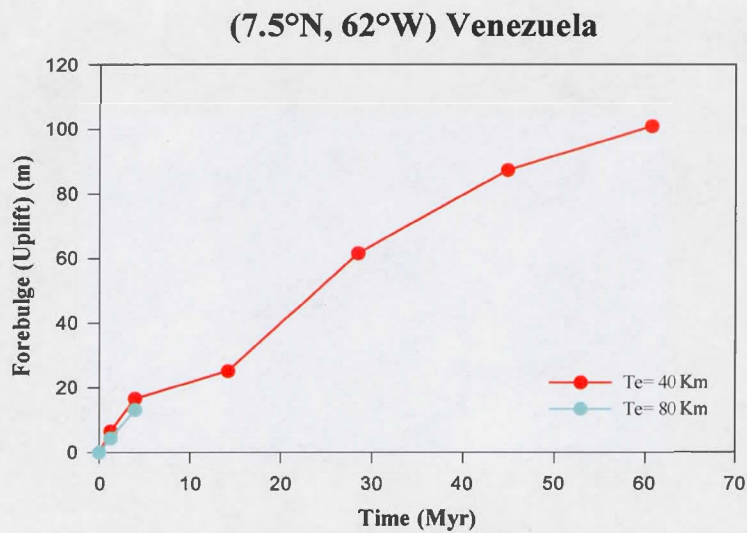


Figure 4.74 Forebulge evolution at a representative location in Venezuela (lat=7.5°N, lon=62°W) from the Paleocene to the Present.

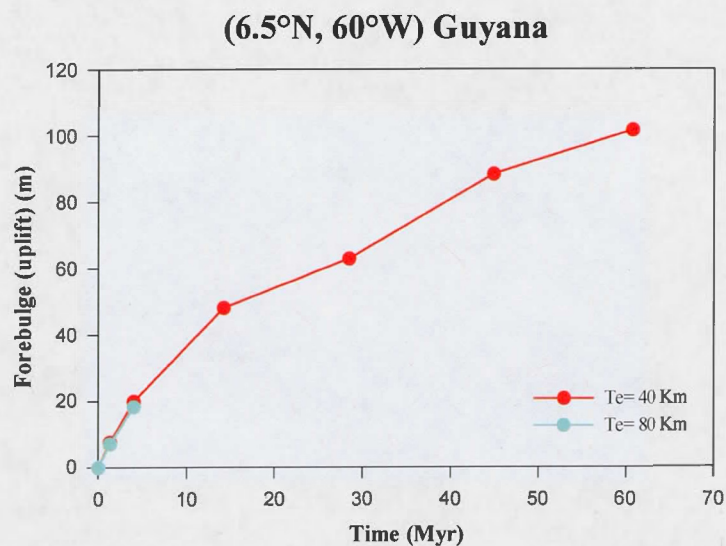


Figure 4.75 Forebulge evolution at a representative location in Guyana (lat=6.5°N, lon=60°W) from the Paleocene to the Present.

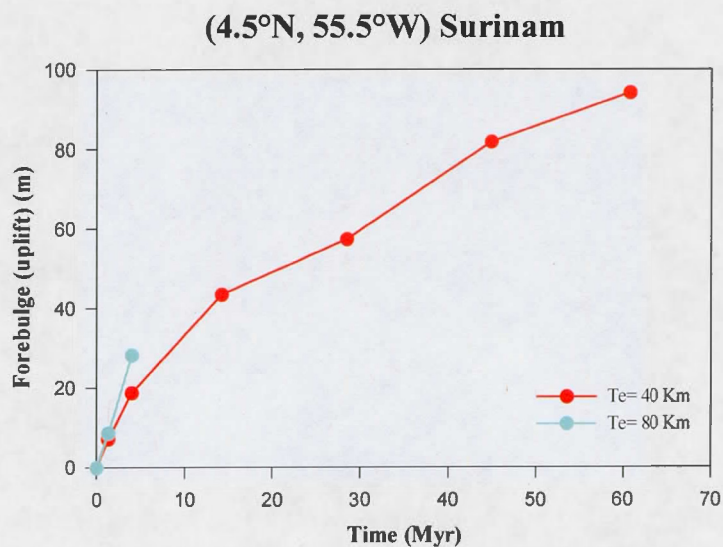


Figure 4.76 Forebulge evolution at a representative location in Surinam (lat=4.5°N, lon=55.5°) from the Paleocene to the Present.

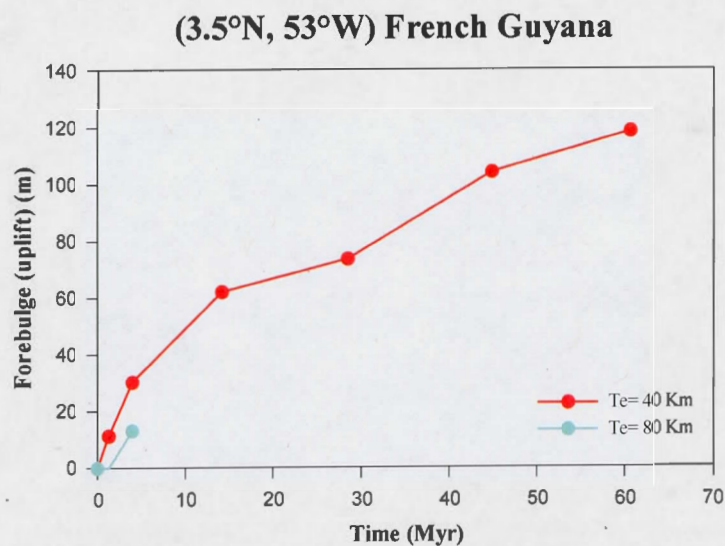


Figure 4.77 Forebulge evolution at a representative location in French Guyana (lat= 3.5°N, lon= 53°W) from the Paleocene to the Present.

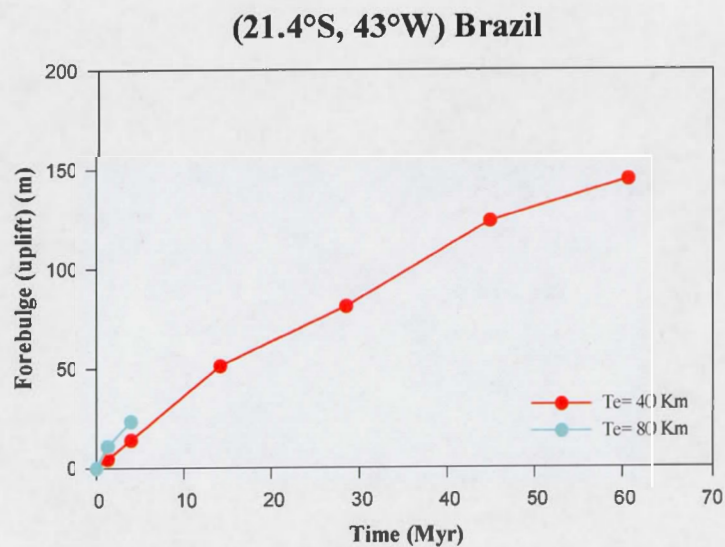


Figure 4.78 Forebulge evolution at a representative location in Brazil (lat= 21.4°S, lon= 43°W) from the Paleocene to the Present.

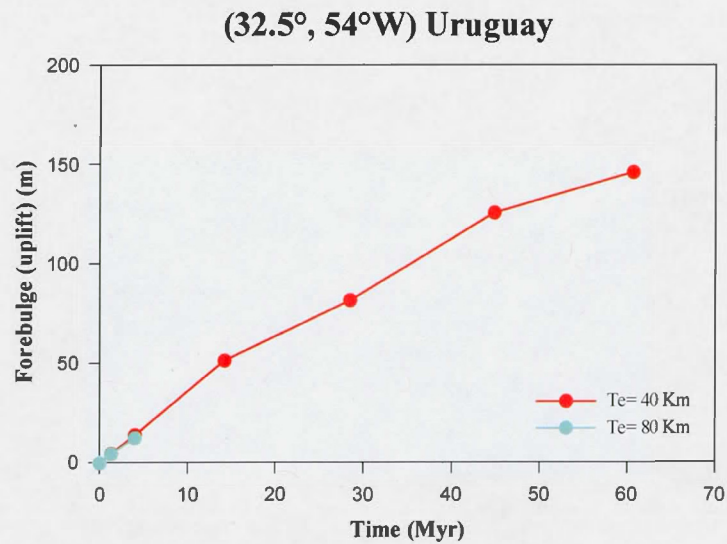


Figure 4.79 Forebulge evolution at a representative location in Uruguay (lat= 32.5°S, lon= 54°W) from the Paleocene to the Present.

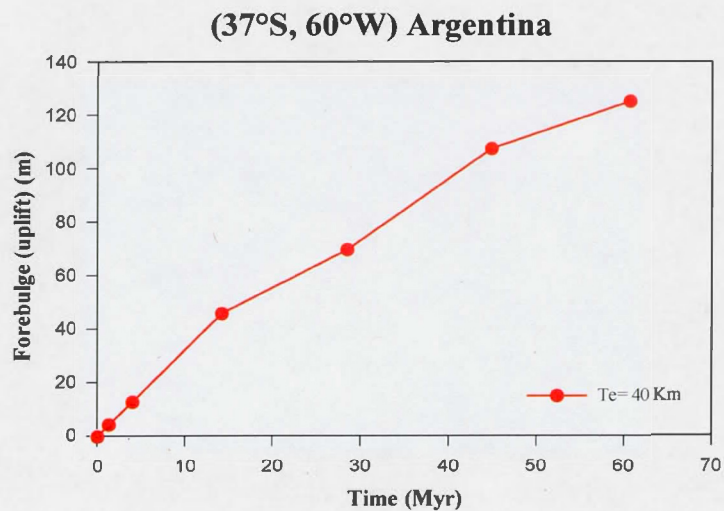


Figure 4.80 Forebulge evolution at a representative location in Argentina (lat= 37°S, lon= 60° W) from the Paleocene to the Present.

In Table 4.6 we summarize the age-dependent relation that exists between the maximum sediment-induced offshore depressions (the foredeep) and the resulting continental uplift (forebulge) since Paleocene.

Table 4.6 Summary of Maximum Flexural depression (foredeep) and Forebulge Amplitudes since the Paleocene

Age	Te (km)	Forebulge(m)	Flexural depression (m)
Quaternary	40	11.93	-309.04
	80	11.91	-244.34
Pliocene	40	31.51	-825.85
	80	31.49	-652.08
Miocene	40	64	-1726.42
Oligocene	40	84.56	-1967.28
Eocene	40	131.17	-2591.75
Paleocene	40	152.66	-2966.59

Table 4.7 Maximum Forebulge (uplift) over the Quaternary-Paleocene in the eastern region of the continent of South America

Age	Colombia	Venezuela	Guyana	Surinam	French Guyana	Brazil	Uruguay	Argentina
Quaternary	4,48	6,64	7,73	7,26	11,56	8,75	4,79	4,46
Quaternary 80 Km		4,36	7,16	8,71		11,09	4,56	
Pliocene		16,73	20,04	18,85	30,52	22,88	14,24	12,98
Pliocene 80 Km		13,12	18,33	28,26	13,19	23,52	12,55	
Miocene	36,09	46,52	48,27	43,53	62,28	55,56	51,65	46
Oligocene	50,02	61,72	63,11	57,44	73,83	81,43	81,88	69,82
Eocene	74,52	87,43	88,52	81,83	104,32	124,3	125,82	107,58
Paleocene	86,75	100,99	101,74	94,21	118,59	145,25	146,08	125,2

Table 4.8 Flexural depression and forebulges amplitudes at the Mouths of Primary Rivers

River mouth	Latitude	Longitude	Flexure-Forebulge (m)				
			Quaternary		Pliocene		Miocene
			40 km	80 km	40 km	80 km	40 km
Magdalena	11°N	74.5°W	-26,9	-25,77	-62,55	-59,91	-173,13
Orinoco	8.83°N	62°W	-2,42	-19,47	-7,46	-50,77	3.72*
	8.83°N	61.83°W	-6,74	-24,24	-19,08	-63,4	-16,85
Amazon	0.5°S	50.5°W	-8,34	-14,55	-23,51	-40,35	-81,92
	0.5°S	51°W	-3,03	-6,44	-9,09	-18,34	-10,3
Confluence Uruguay- Parana Rivers	34,16	58,5°W	0.95*	2.74*	-0,37	6.42*	0.31*
Mar del Plata	34,5°S	58°W	-0,54	1.8*	-6,01	2.86*	-18,99

Negative values indicate flexural depression (foredeep). * Forebulge or uplift

4.5 Flexural Response by Age Intervals

In the preceding section (4.4), flexure was calculated for the entire sediment column accumulated from a particular epoch in the past to present day. In the following, we instead present the flexure due to sediments deposited in each of the geological epochs.

Figures 4.81 4.118, 4.119, 4.120 and 4.121 show the maps of the flexural response generated by offshore sediment accumulation within different age intervals. Flexure was calculated using an effective elastic thickness of 40 km and a maximum harmonic degree of 2000.

Cenozoic Flexural Response of the Lithosphere

In the following we present the results of our flexural calculations in each of the four geographic zones (Figure 4.1) for the period of Cenozoic time, which includes the intervals of ages: Pliocene-Quaternary (5.332-0 Myr), Miocene-Pliocene (23.03-2.588 Myr), Oligocene-Miocene (33.9-5.332 Myr), Eocene-Oligocene (55.8-23.03 Myr) and Paleocene-Eocene (65.5-33.9 Myr). In the same manner as in section 4.4, the discussion will primarily focus on the flexural response at a number of selected offshore points shown in Figure 4.26, via a graphical representation of flexure versus time: Cenozoic time intervals. In the interest of clarity we include an extended discussion for the Quaternary-Pliocene interval, and employ a purely graphical summary for all remaining geological periods.

In the following discussion it should again be understood, as in section 4.4 that all values referring to flexural depression (foredeep) or uplift (forebulge) are induced by

the offshore sediment accumulations and do not refer to actual values of bathymetry or altitude.

4.5.1 Pliocene-Quaternary flexural response of the Lithosphere

The predicted flexural response between 5.332 and 0 million years ago in the Pliocene-Quaternary geological interval for an elastic thickness of 40 km is illustrated in figure 4.81.

4.5.1.1 Zone I. The Caribbean

In this zone on the continental margin of Colombia, the flexural depression (foredeep) has amplitudes greater than -10 meters, reaching values of -35 meters and -34 meters in the area of the Offshore Guajira and Sinú Marine Basins. The flexural depression (foredeep) begin to amplify at the mouth of the Magdalena River, where it is -35.65 meters (Table 4.11) and increases in the area of the Magdalena Delta, with values greater than -66 meters. In the North and Northwest region of Zone I, foredeep ranges from -10 and -30 meters, such as in the area of the Cayos Basin, with values of -25.73 meters. In certain areas of this sub-zone, the foredeep reaches values between -40 and -60 meters, such as in the southern part of the Colombia Basin, in where it is -56.85 meters. (Appendix E)

On the continental margin of Venezuela, the foredeep is greater than -20 meters, as is the case of the area of the offshore Cariaco Basin, with a value of -22.8 meters. These amplitudes increase beyond -30 meters, such as in the area of the offshore Venezuela

Basin where the foredeep is -34.13 meters. At the mouth of the Orinoco River, the depression is -5.04 meters, increasing offshore. Similarly, in the Lesser Antilles, the foredeep ranges between -25 and -35 meters, reaching values of more than -100 meters. For instance, in the Grenada Basin area, the depression is -29.6 meters, whereas in the Tobago Basin area, it increases to -289.64 meters. (Appendix E)

4.5.1.2 Zone II. Amazon Zone

This zone is characterized by depressions greater than -100 meters in the area of the continental margin and offshore in the countries of Guyana, Surinam and French Guyana. The flexural depression (foredeep) caused by the sedimentary loads in these areas attains values of -278.21, -295.48 and 256.95 meters respectively. (Appendix E)

Similarly, on the continental margin of Northeastern Brazil, the foredeep has small amplitudes along the coastline, which increase offshore reaching values of up to -187.74 meters. A noteworthy example is the area of the mouth of the Amazon River, with an amplitude of -6.07 meters (Table 4.11), which increases in the area of the Amazon Delta attaining a value of -175.38 meters. In addition, on the Ceará Basin area, the flexural depression (foredeep) increases to -204.28 meters. The foredeep shallows in the area of the Potigarr Basin, with a value of -105.99 meters. (Appendix E)

Finally, towards the Mid-Atlantic Ridge, the sediment induced depression decreases gradually to values of -7 meters.

4.5.1.3 Zone III. Brazil-Argentina

On the continental margin of Brazil of the sediment-induced flexural depressions range between approximately -30 and -100 meters. For example, for the offshore Pernambuco and Espírito Santo Basins the flexural depression (foredeep) attains values of -44.93 and -48.19 meters, respectively. These amplitudes increase in the area of the offshore Sergipe-Alagoas, Bahía Sul and Campos Basins, where the flexural depression (foredeep) has values of -62.09, -92.74 and -114.16 meters respectively. Similarly, in the offshore Santos and Pelotas Basins the flexural depression attains values of -189.73 and -165.95 meters, respectively. (Appendix E). On the continental margin of Uruguay and in the area of the offshore Punta del Este Basin, the flexural depression (foredeep) attains a maximum of -89.64 meters (Appendix E). In addition, between the countries of Argentina and Uruguay, on the confluence of the Paraná and the Uruguay Rivers, there a modest depression of -1.32 meters, which increases gradually towards the Mar del Plata River, with amplitudes of -5.47 meters (Table 4.11), and furthering increasing offshore.

Furthermore, on the extensional continental margin of Argentina, the flexural depressions are varied, ranging between -10 meters to more than -100 meters. For instance, the areas that comprise the offshore San Julian and San Jorge Basins attains values of -15.89 -33.28 meters, respectively. These amplitudes increase gradually in the area of the offshore Rawson, Argentina, Colorado and Salado Basins, where the foredeep amplitudes are -50.92, -82.82, -99.08 and -151.11 meters respectively. Finally, on the sheared continental margin of Argentina, in the area of the Northern Falkland Basin flexure varies between -6 meters and -41.27 meters. (Appendix E).

4.5.1.4 Zone IV. Scotia

In this area, there are variations in flexure amplitude with values between -5 and -70 meters. For example, in the area of the offshore Western and Eastern Falkland Basins, the flexure values attains values of -47.44 meters and -77.03 meters, respectively (Appendix E). Over the past 5 Myrs this flexure lifts the Falkland Islands by a very modest 0.13 meters, but this uplift is substantially larger during the subsequent age-intervals.

On the border between the South American and Scotia Plates, the amplitudes of the flexural depression range between -10 and -80 and meters. For example in the area of the Southern Falkland, the foredeep attains values of -49.16 meters. (Appendix E). In contrast, the eastern and western ends of the Scotia plate are uplifted by 3 meters and 0.97 meters, respectively.

Sediment Flexure, Pliocene-Quaternary ($H=40\text{km}$, $L=1-2000$)

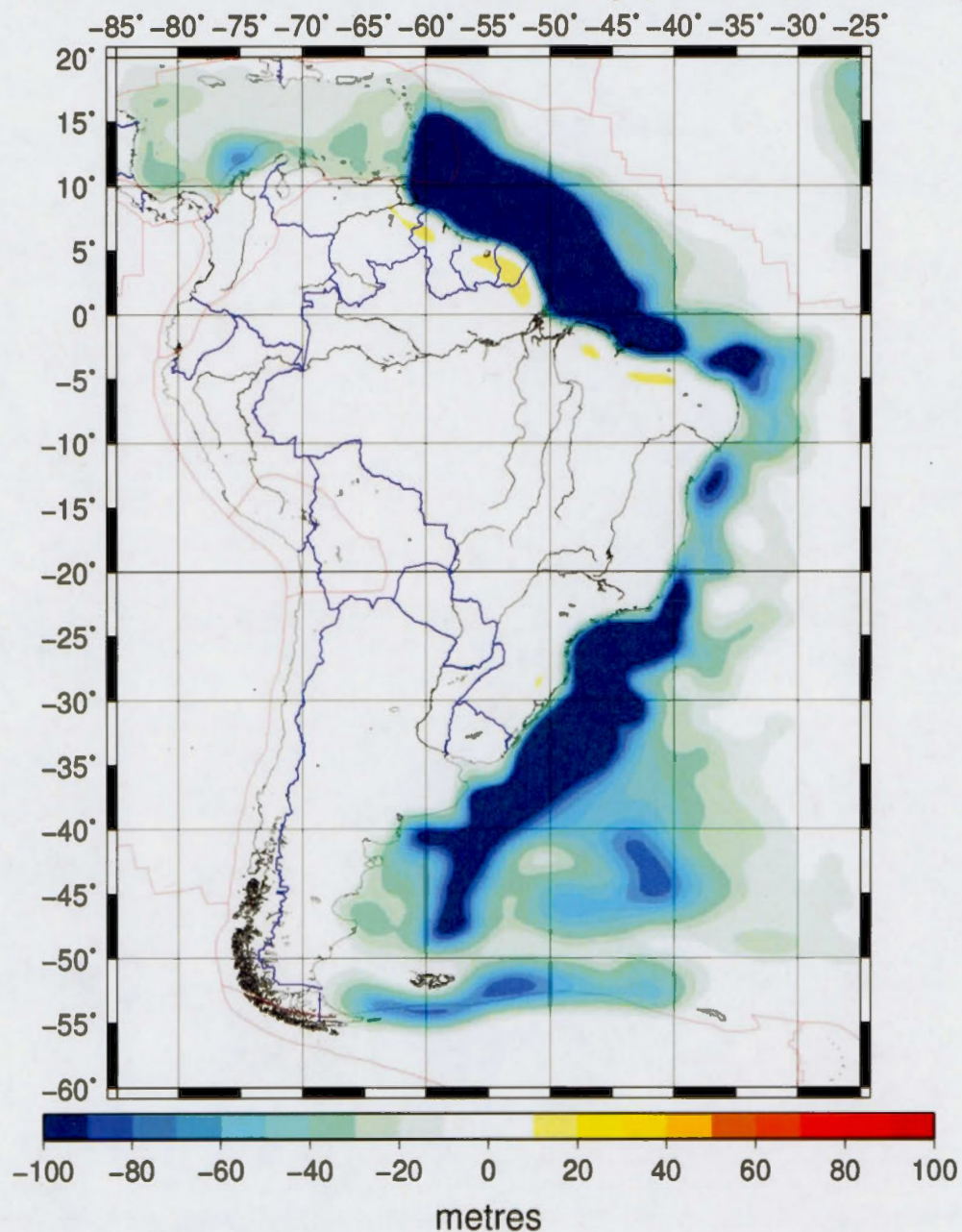


Figure 4.81 Map of Flexural Response during the Pliocene-Quaternary interval (5.33 to 0 Ma). The effective elastic thickness is 40 km and a maximum harmonic degree of 2000 was employed.

4.5.2 Flexural Response of the Lithosphere during the Pliocene-Quaternary, Miocene-Pliocene, Oligocene-Miocene, Eocene-Oligocene and Paleocene-Eocene interval ages.

In the following we present a graphical summary of the evolution of flexural response during the Pliocene-Quaternary (5.332 to 0 Ma), Miocene-Pliocene (23.03 -2.588 Ma), Oligocene-Miocene (33.9 to 5.332 Ma), Eocene-Oligocene (55.8 to 23.03 Ma) and Paleocene-Eocene (65.5 to 33.9 Ma) interval ages.

4.5.2.1 Zone I

Zone I, includes the following offshore points: Barracuda Abyssal Plain, Cayos, Colombia basin, Magdalena Delta, Venezuela Basin, Grenada, Tobago, Demerara Abyssal Plain, Marin Guajira, Marin Sinú and Cariaco, for which flexural depression values are shown in Appendix E.

Figures 4.82 to 4.92 show the contribution to lithospheric flexure, from sediments deposited in each geological epoch, at each of these locations.

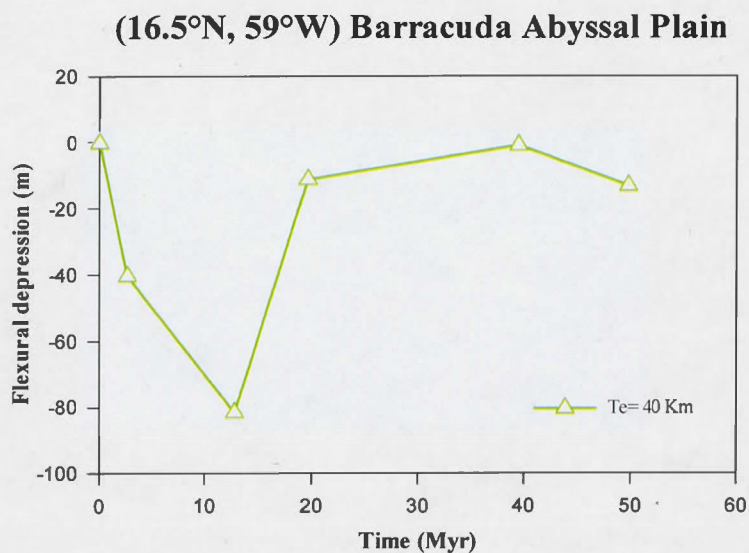


Figure 4.82 Contribution to lithospheric flexure, from sediments deposited in each geological epoch, at an offshore site in the Barracuda Abyssal Plain

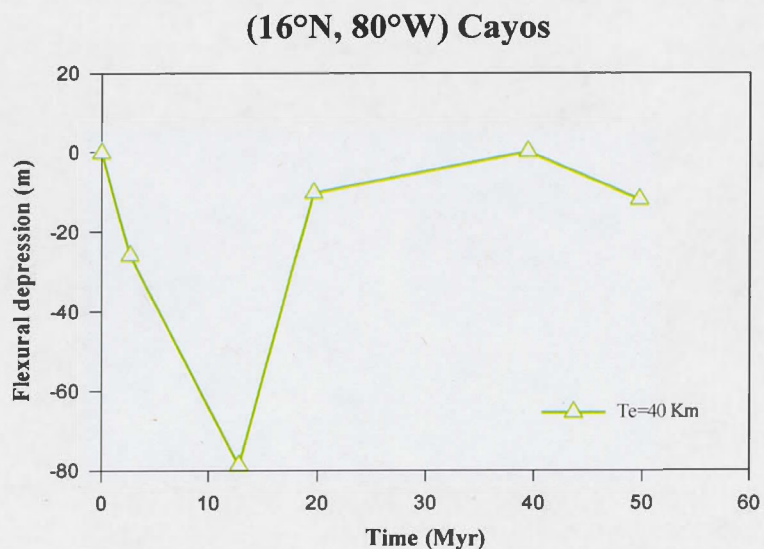


Figure 4.83 Contribution to lithospheric flexure, from sediments deposited in each geological epoch, at an offshore site in the Cayos Basin

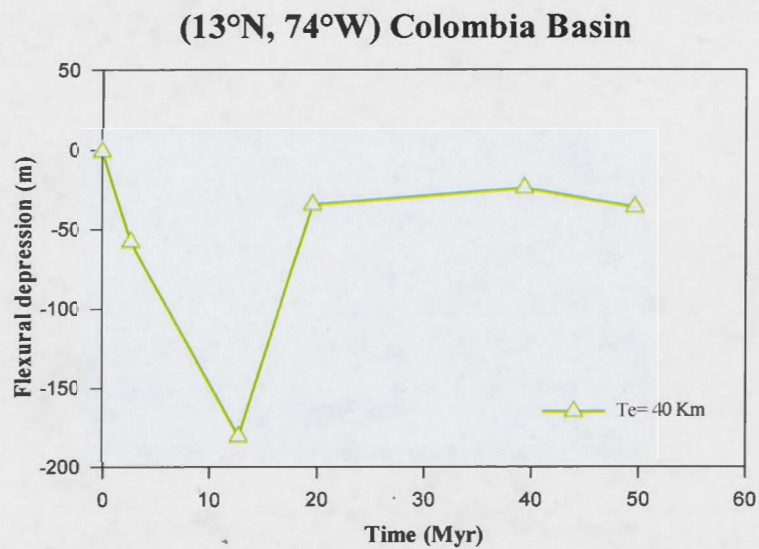


Figure 4.84 Contribution to lithospheric flexure, from sediments deposited in each geological epoch, at an offshore site in Colombia Basin

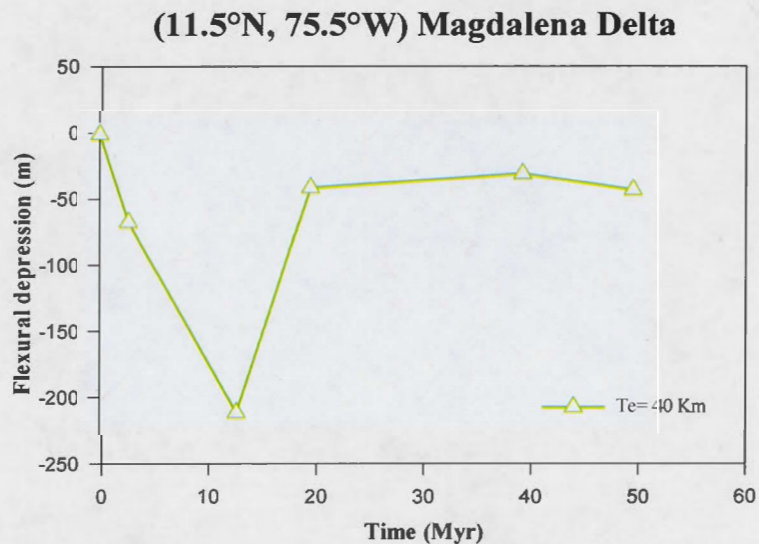


Figure 4.85 Contribution to lithospheric flexure, from sediments deposited in each geological epoch, at an offshore site in the Magdalena Delta

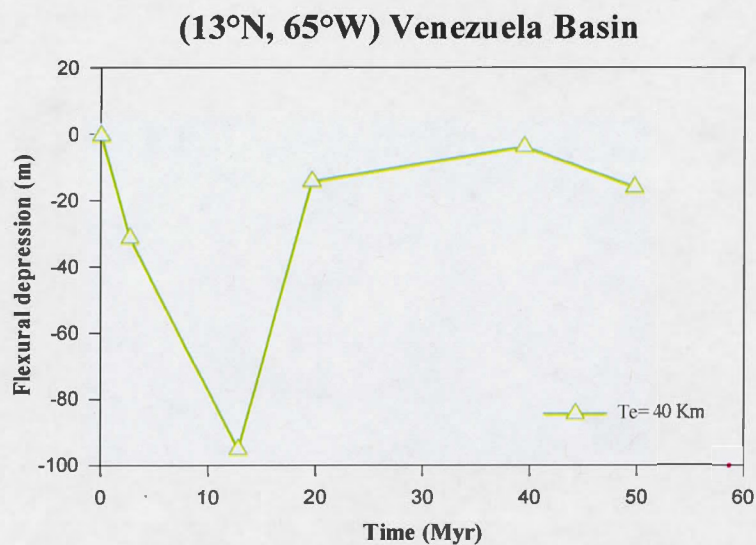


Figure 4.86 Contribution to lithospheric flexure, from sediments deposited in each geological epoch, at an offshore site in the Venezuela Basin

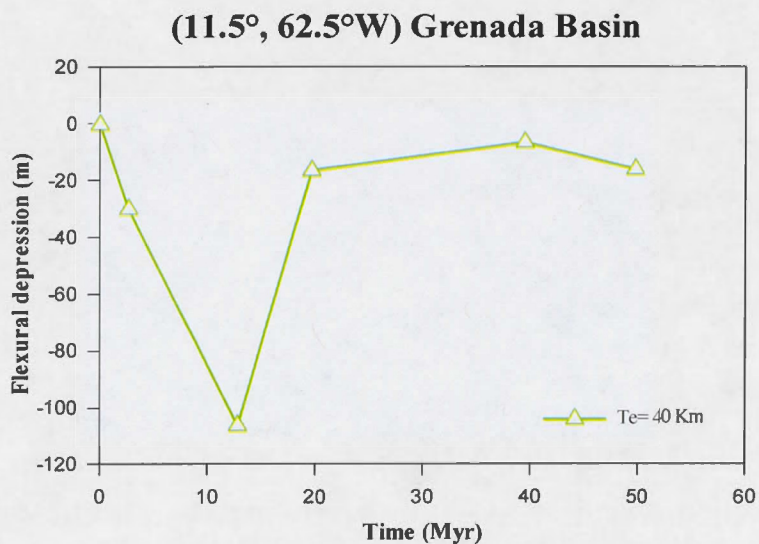


Figure 4.87 Contribution to lithospheric flexure, from sediments deposited in each geological epoch, at an offshore site in the Grenada Basin

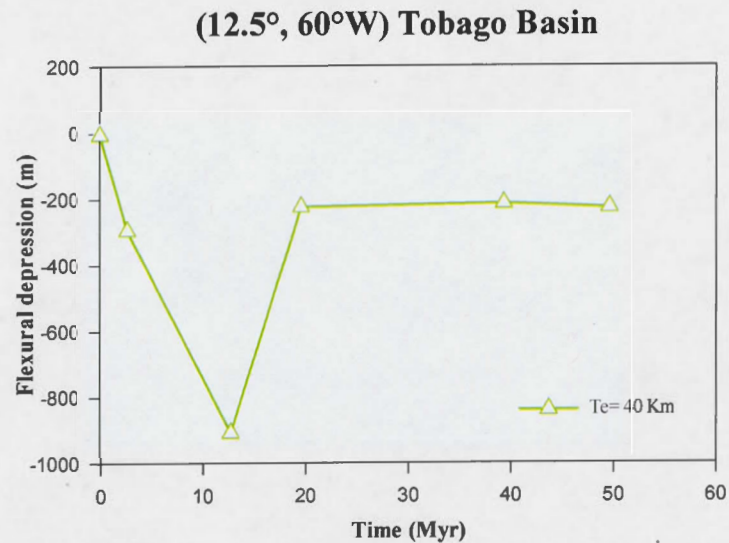


Figure 4.88 Contribution to lithospheric flexure, from sediments deposited in each geological epoch, at an offshore site in the Tobago Basin

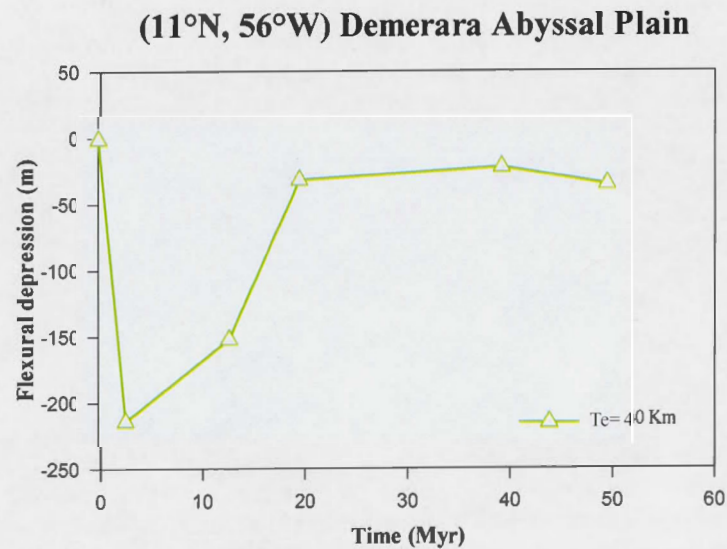


Figure 4.89 Contribution to lithospheric flexure, from sediments deposited in each geological epoch, at an offshore site in the Demerara Abyssal Plain

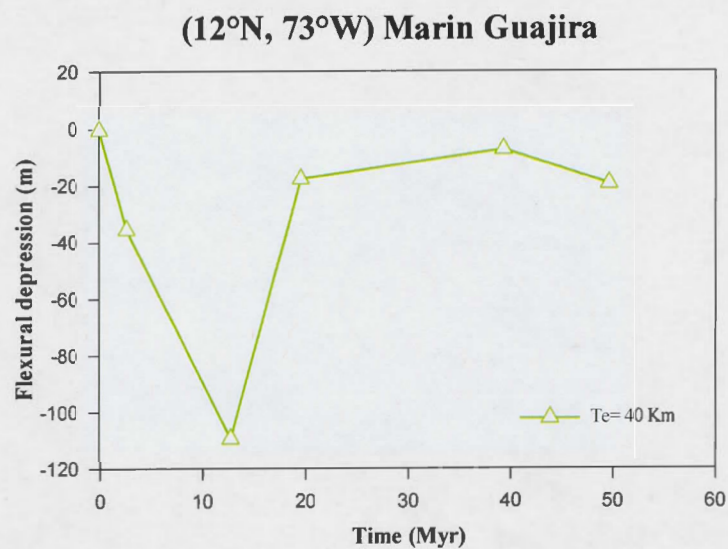


Figure 4.90 Contribution to lithospheric flexure, from sediments deposited in each geological epoch, at an offshore site in the Marin Guajira

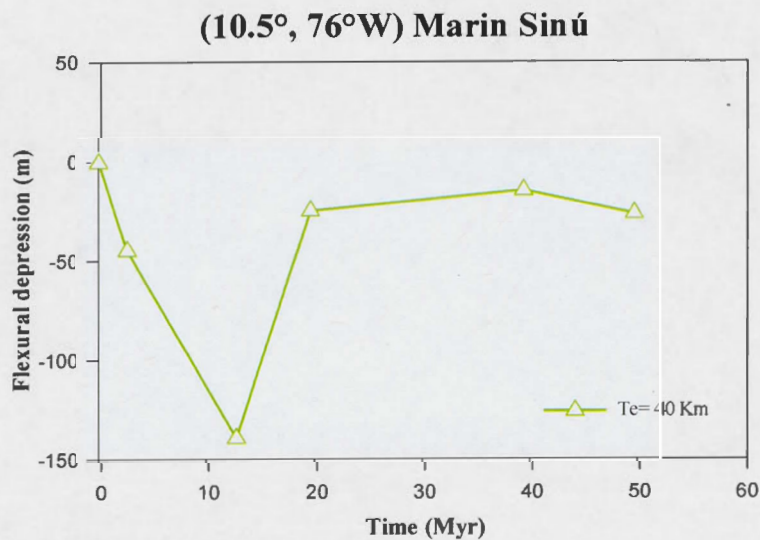


Figure 4.91 Contribution to lithospheric flexure, from sediments deposited in each geological epoch, at an offshore site in the Marin Sinú

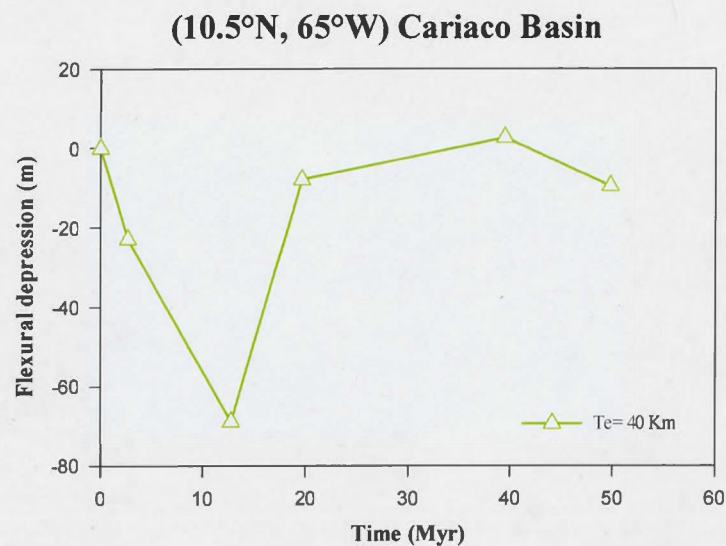


Figure 4.92 Contribution to lithospheric flexure, from sediments deposited in each geological epoch, at an offshore site in the Cariaco Basin

4.5.2.2 Zone II

Zone II, includes the following offshore points: Guiana, Surinam, French Guyana, Amazon Delta, Brazil, Ceará and Potigar, for which flexural depression values are shown in Appendix E.

Figures 4.93 to 4.99 show the contribution to lithospheric flexure, from sediments deposited in each geological epoch, at each of these locations.

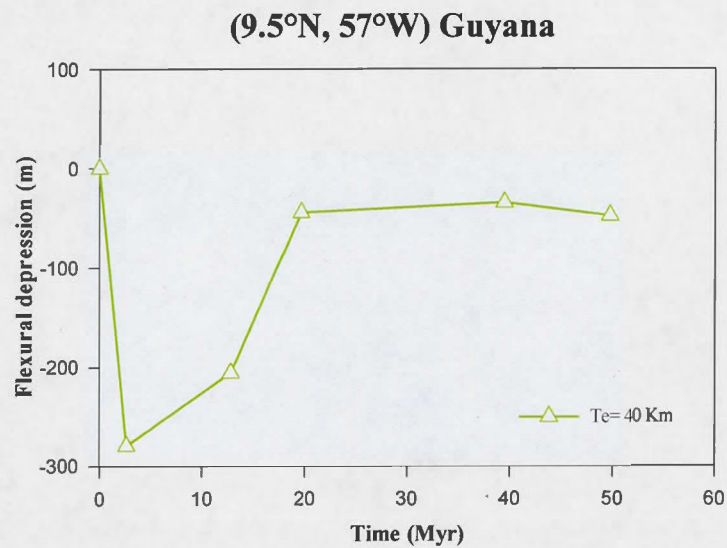


Figure 4.93 Contribution to lithospheric flexure, from sediments deposited in each geological epoch, at an offshore site in the Guyana

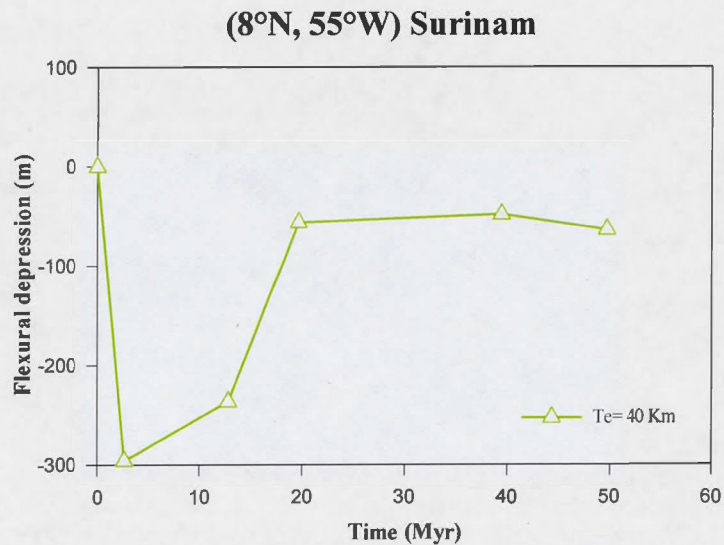


Figure 4.94 Contribution to lithospheric flexure, from sediments deposited in each geological epoch, at an offshore site in the Surinam

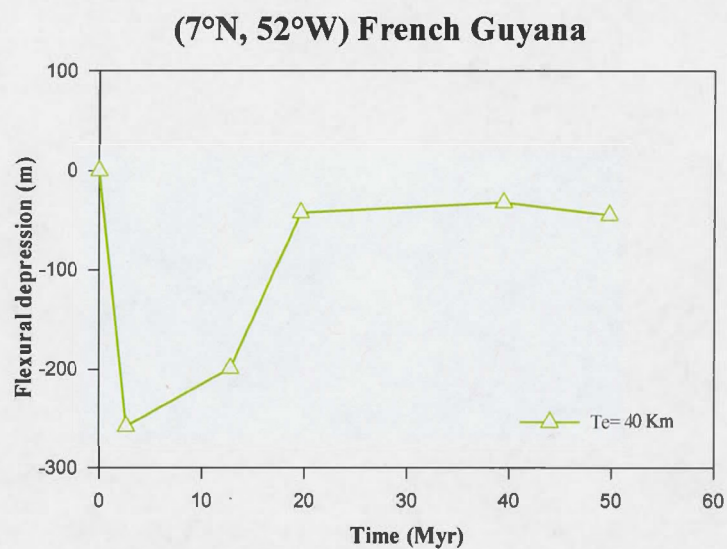


Figure 4.95 Contribution to lithospheric flexure, from sediments deposited in each geological epoch, at an offshore site in the French Guyana

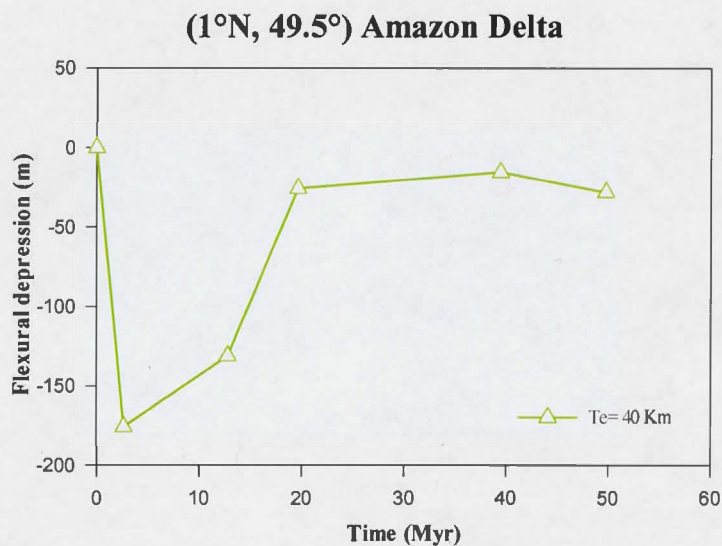


Figure 4.96 Contribution to lithospheric flexure, from sediments deposited in each geological epoch, at an offshore site in the Amazon Delta

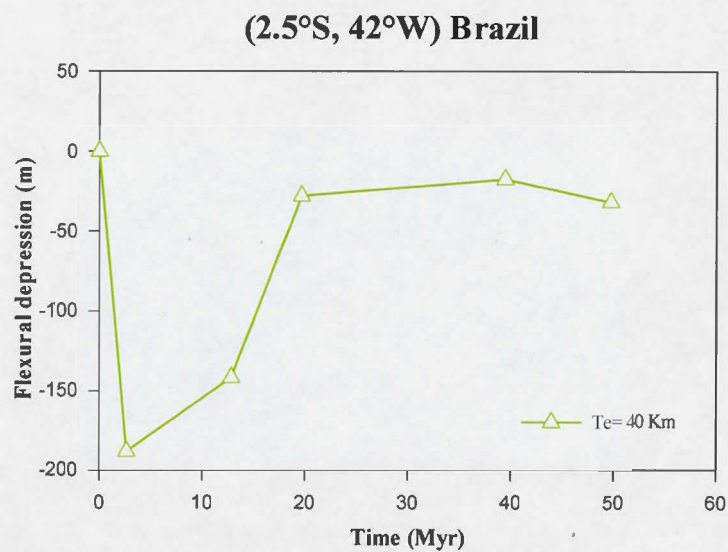


Figure 4.97 Contribution to lithospheric flexure, from sediments deposited in each geological epoch, at an offshore site site in the Brazil

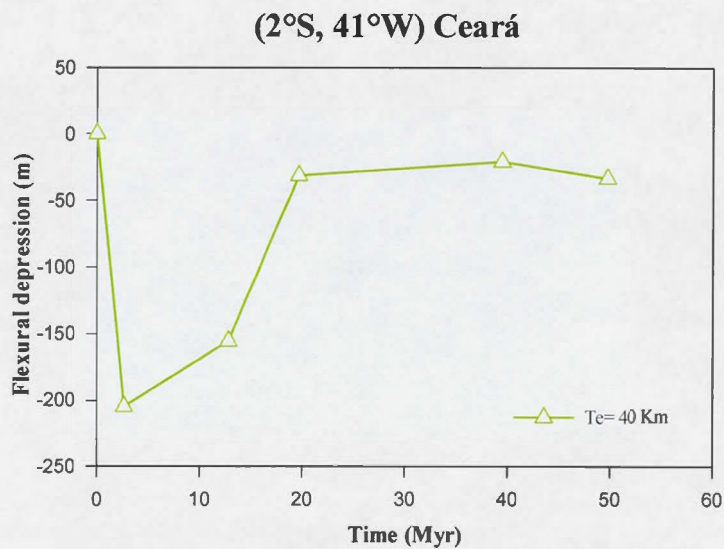


Figure 4.98 Contribution to lithospheric flexure, from sediments deposited in each geological epoch, at an offshore site site in the Ceará

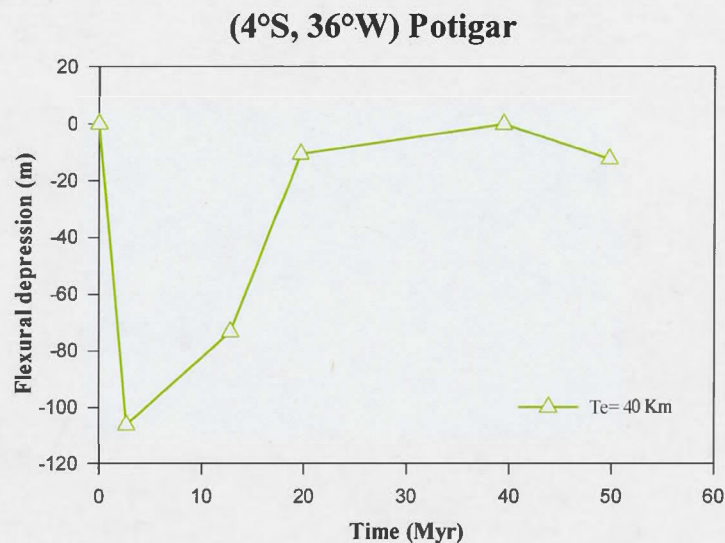


Figure 4.99 Contribution to lithospheric flexure, from sediments deposited in each geological epoch, at an offshore site in the Potigar

4.5.2.3 Zone III

Zone III, includes the following offshore points: Pernambuco, Sergipe-Alagoas, Bahia Sul, Espiritu Santo, Campos, Santos, Pelotas, Punta del Este, Salado, Colorado, Rawson, San Jorge, San Julian, Argentina and Northern Falkland, for which flexural depression values are shown in Appendix E.

Figures 4.100 to 4.114 show the contribution to lithospheric flexure, from sediments deposited in each geological epoch, at each of these locations.

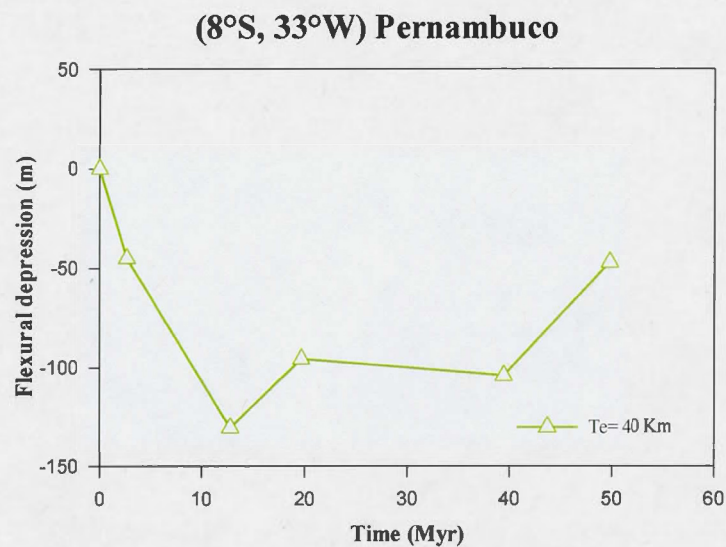


Figure 4.100 Contribution to lithospheric flexure, from sediments deposited in each geological epoch, at an offshore site site in the Pernambuco

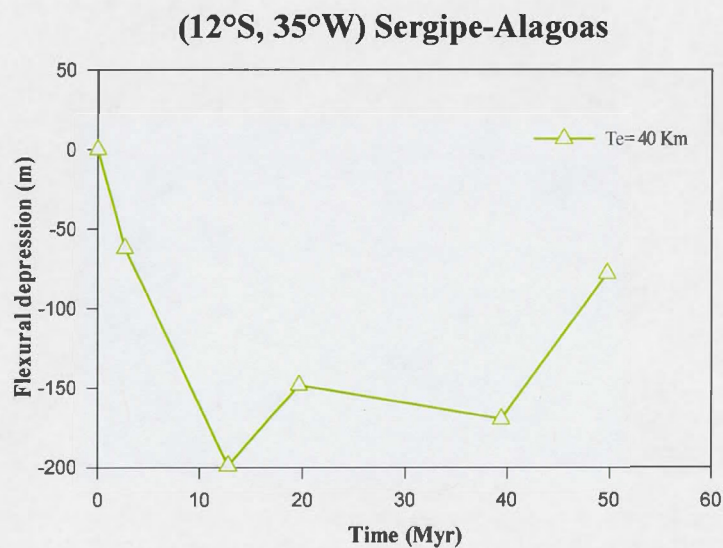


Figure 4.101 Contribution to lithospheric flexure, from sediments deposited in each geological epoch, at an offshore site in the Sergipe-Alagoas

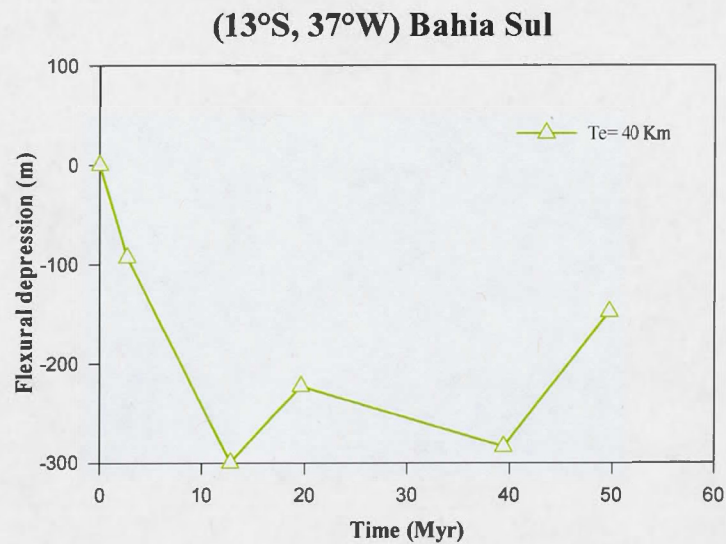


Figure 4.102 Contribution to lithospheric flexure, from sediments deposited in each geological epoch, at an offshore site in the Bahia Sul

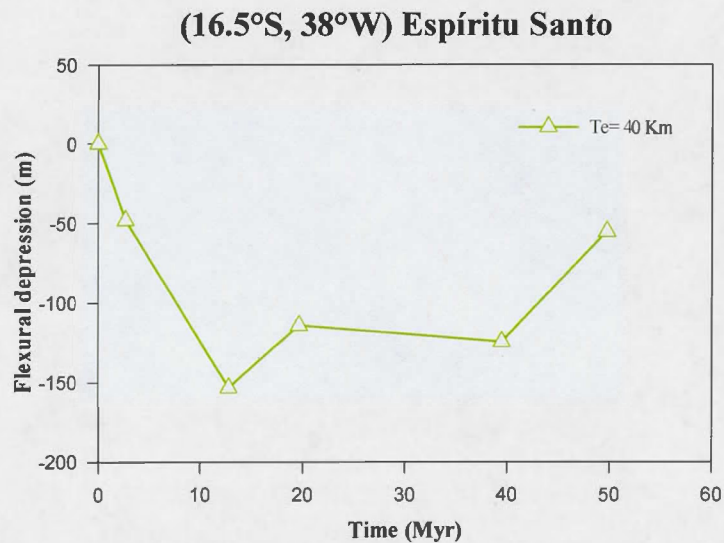


Figure 4.103 Contribution to lithospheric flexure, from sediments deposited in each geological epoch, at an offshore site in the Espírito Santo

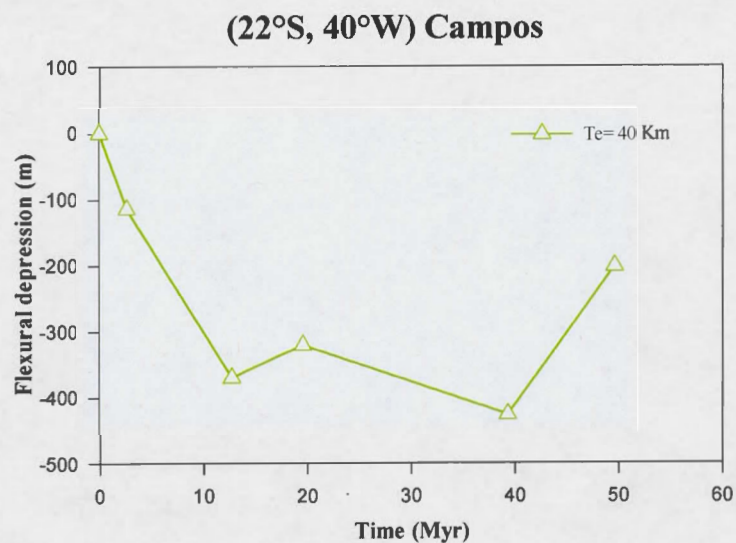


Figure 4.104 Contribution to lithospheric flexure, from sediments deposited in each geological epoch, at an offshore site in the Campos

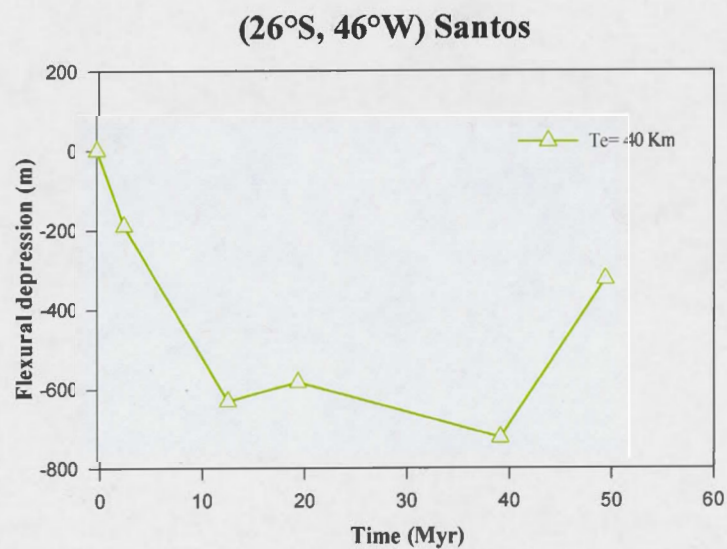


Figure 4.105 Contribution to lithospheric flexure, from sediments deposited in each geological epoch, at an offshore site in the Santos

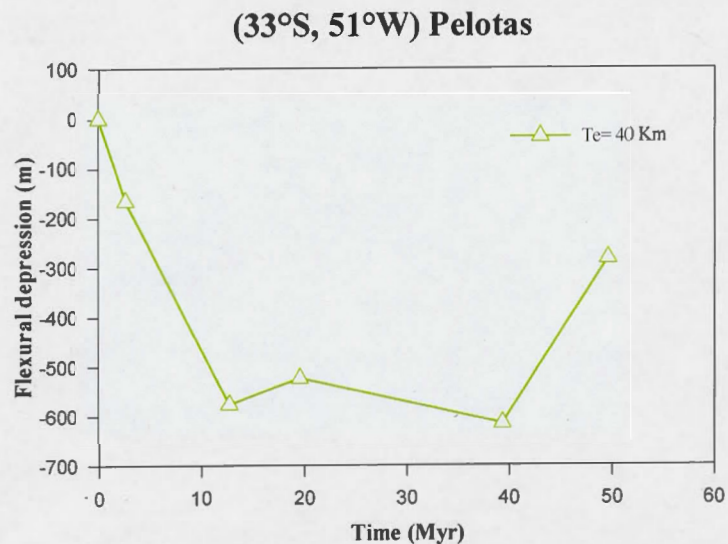


Figure 4.106 Contribution to lithospheric flexure, from sediments deposited in each geological epoch, at an offshore site in Pelotas.

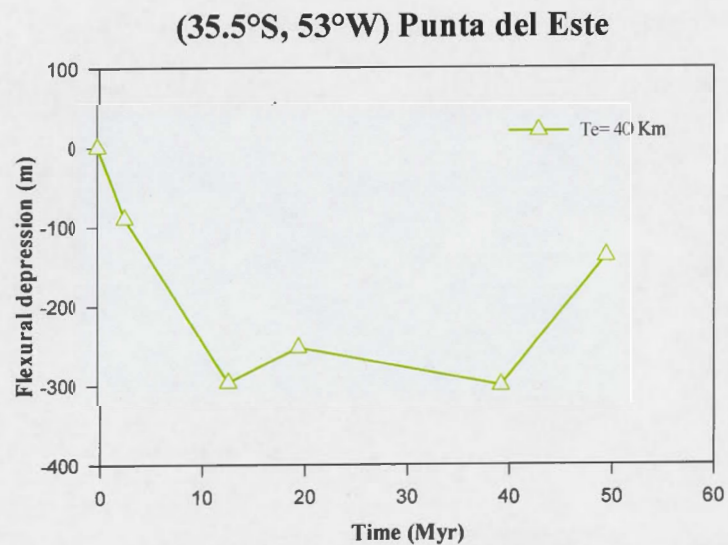


Figure 4.107 Contribution to lithospheric flexure, from sediments deposited in each geological epoch, at an offshore site in the Punta Del Este.

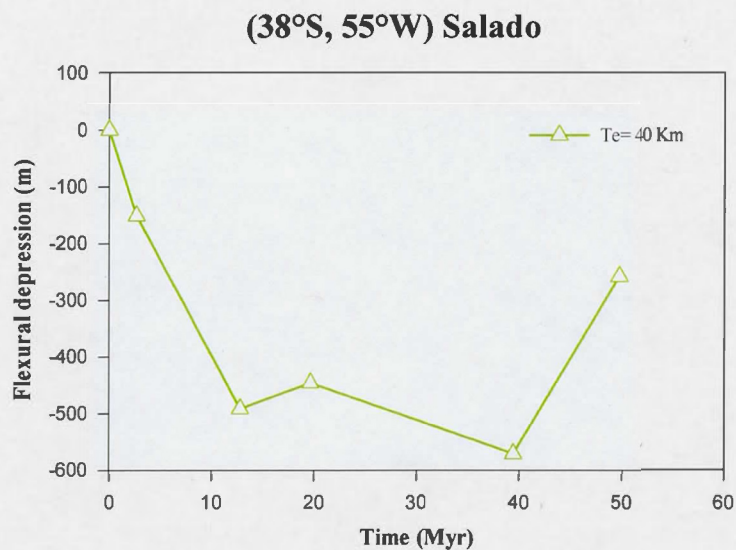


Figure 4.108 Contribution to lithospheric flexure, from sediments deposited in each geological epoch, at an offshore site in the Salado.

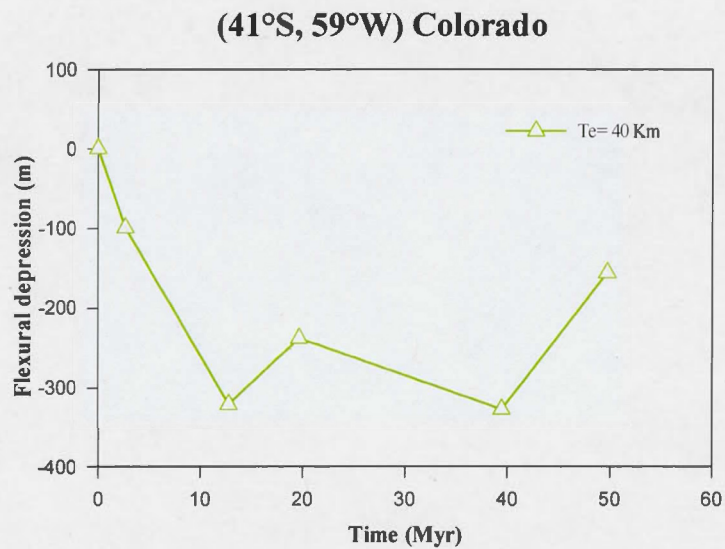


Figure 4.109 Contribution to lithospheric flexure, from sediments deposited in each geological epoch, at an offshore site in the Colorado.

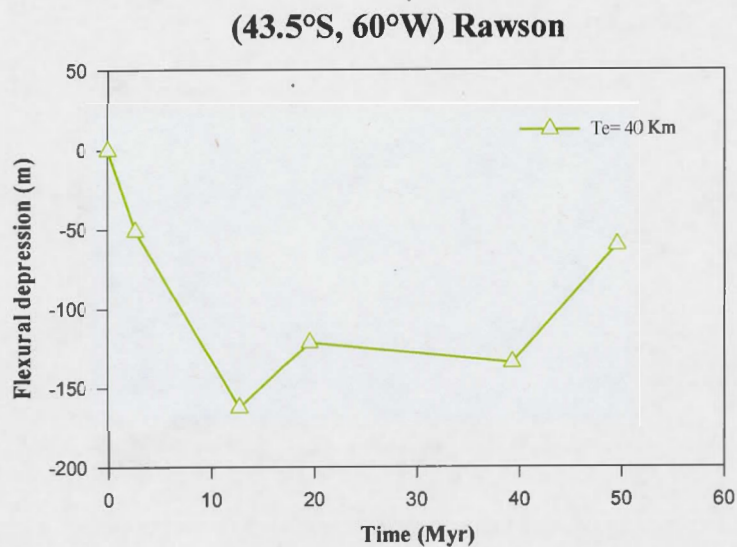


Figure 4.110 Contribution to lithospheric flexure, from sediments deposited in each geological epoch, at an offshore site in the Rawson.

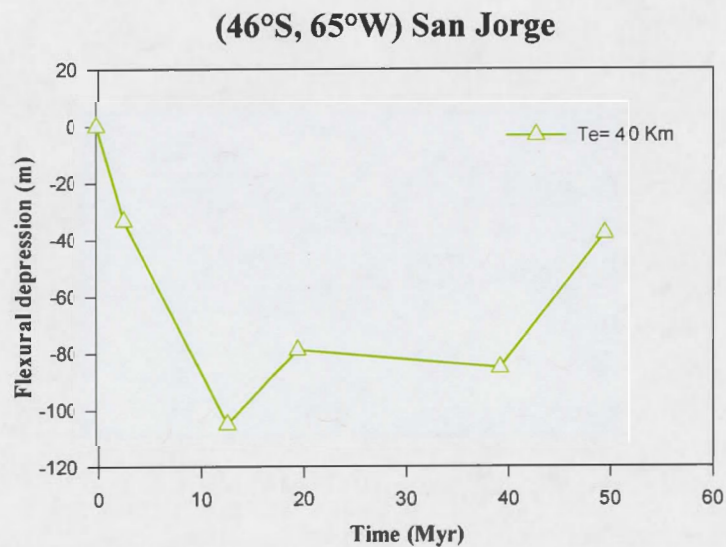


Figure 4.111 Contribution to lithospheric flexure, from sediments deposited in each geological epoch, at an offshore site site in the San Jorge.

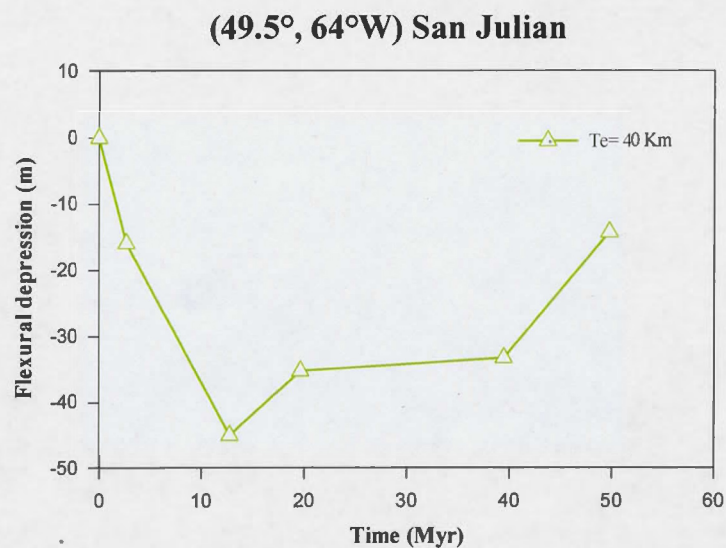


Figure 4.112 Contribution to lithospheric flexure, from sediments deposited in each geological epoch, at an offshore site site in the San Julian.

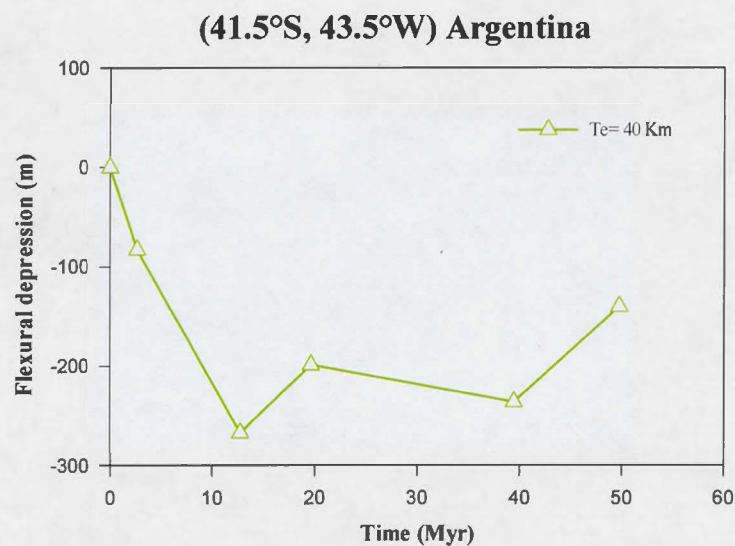


Figure 4.113 Contribution to lithospheric flexure, from sediments deposited in each geological epoch, at an offshore site in the Argentina Basin.

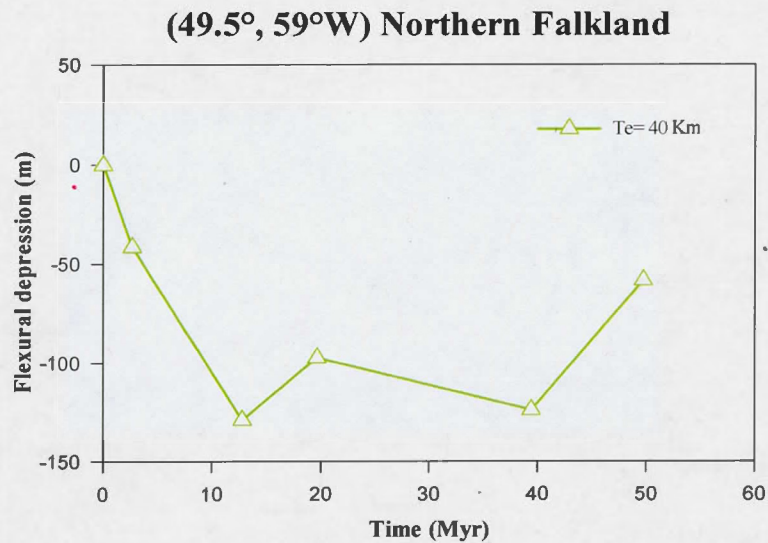


Figure 4.114 Contribution to lithospheric flexure, from sediments deposited in each geological epoch, at an offshore site shore site in the Northern Falkland.

4.5.2.4 Zone IV

Zone IV, includes the following offshore points: Eastern Falkland, Western Falkland and Southern Falkland, for which flexural depression values are tabulated in Appendix E.

Figures 4.115 to 4.117 shown evolution of flexural depression of lithosphere at each of these locations.

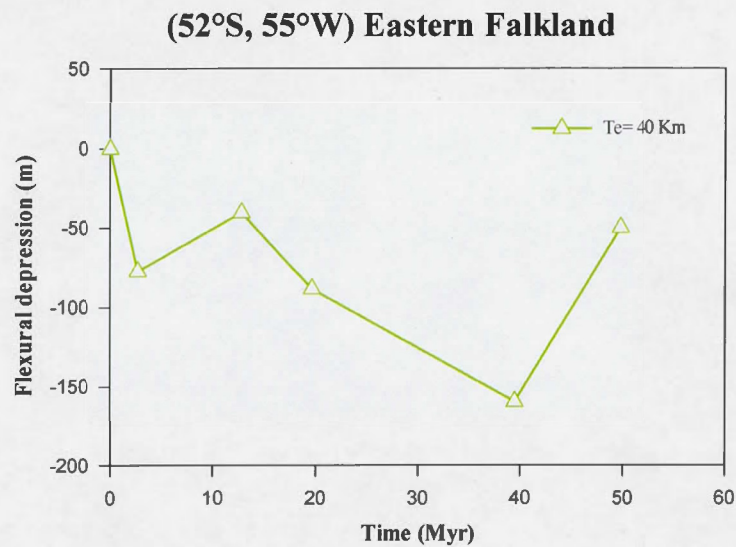


Figure 4.115 Contribution to lithospheric flexure, from sediments deposited in each geological epoch, at an offshore site in the Eastern Falkland

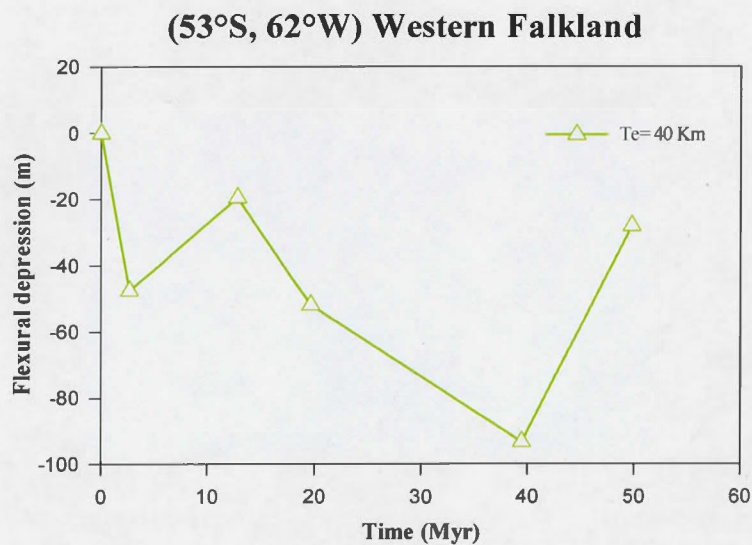


Figure 4.116 Contribution to lithospheric flexure, from sediments deposited in each geological epoch, at an offshore site in the Western Falkland

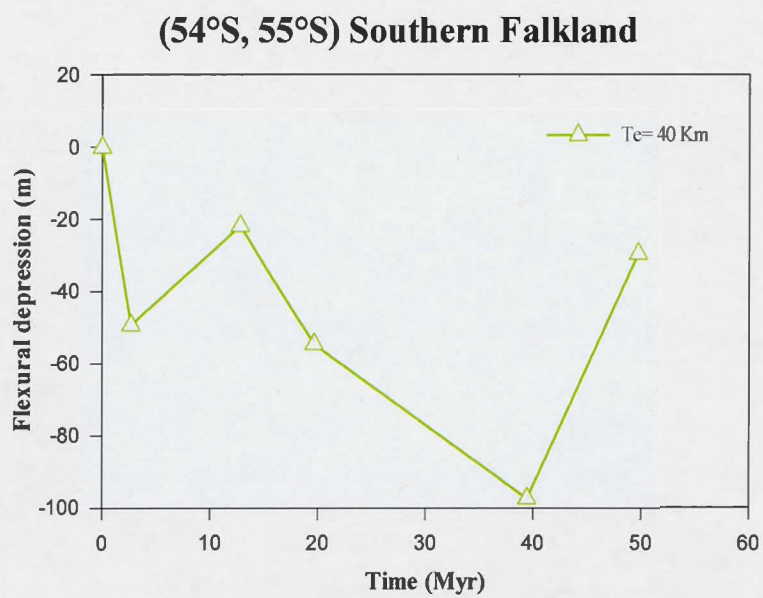


Figure 4.117 Contribution to lithospheric flexure, from sediments deposited in each geological epoch, at an offshore site in the Southern Falkland

Sediment Flexure, Miocene–Pliocene (H=40km, L=1–2000)

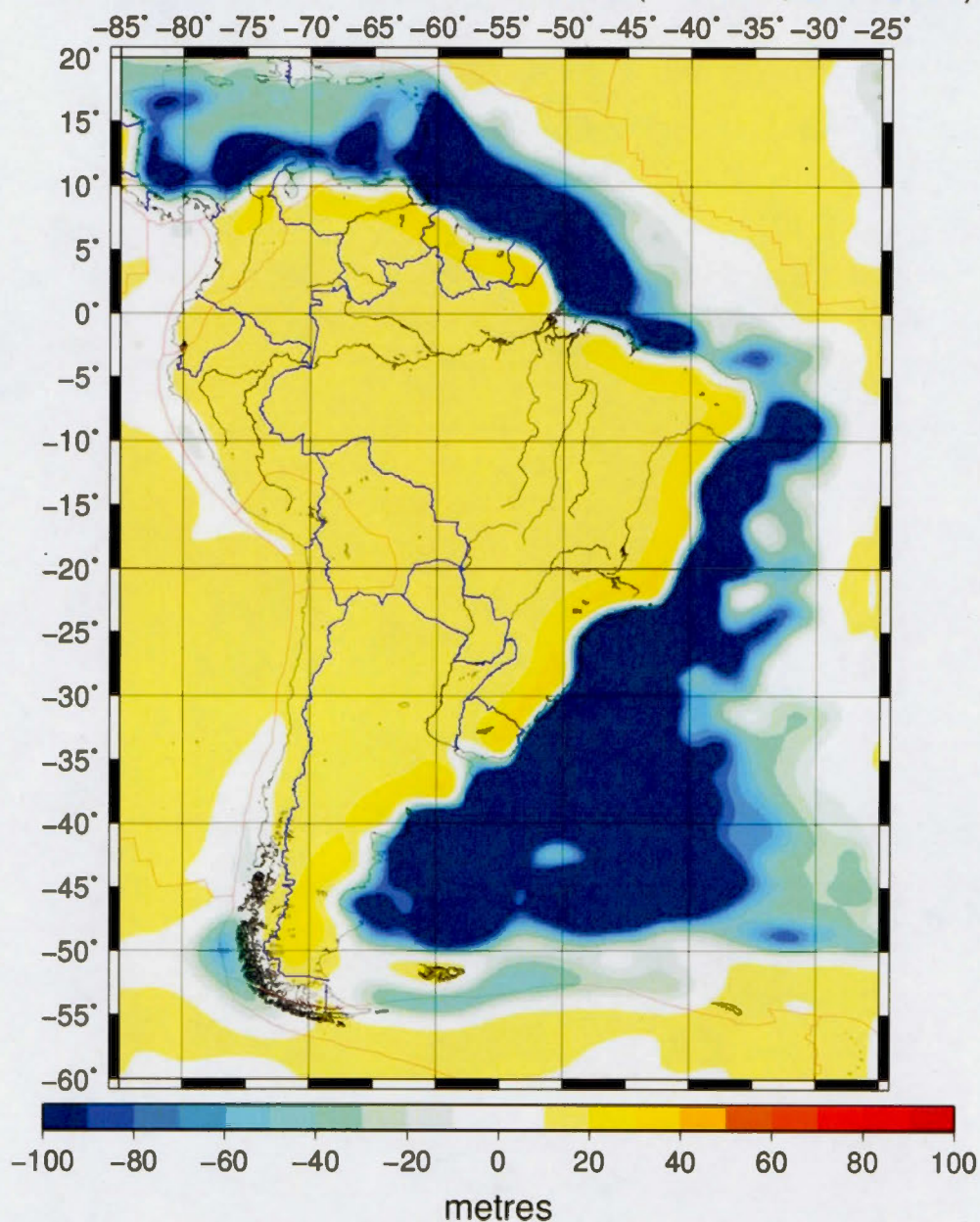


Figure 4.118 Map of Flexural Response during the Miocene-Pliocene interval (23.03 to 2.588 Ma). The effective elastic thickness of 40 km and a maximum harmonic degree of 2000 was employed.

Sediment Flexure, Oligocene–Miocene ($H=40\text{km}$, $L=1-2000$)

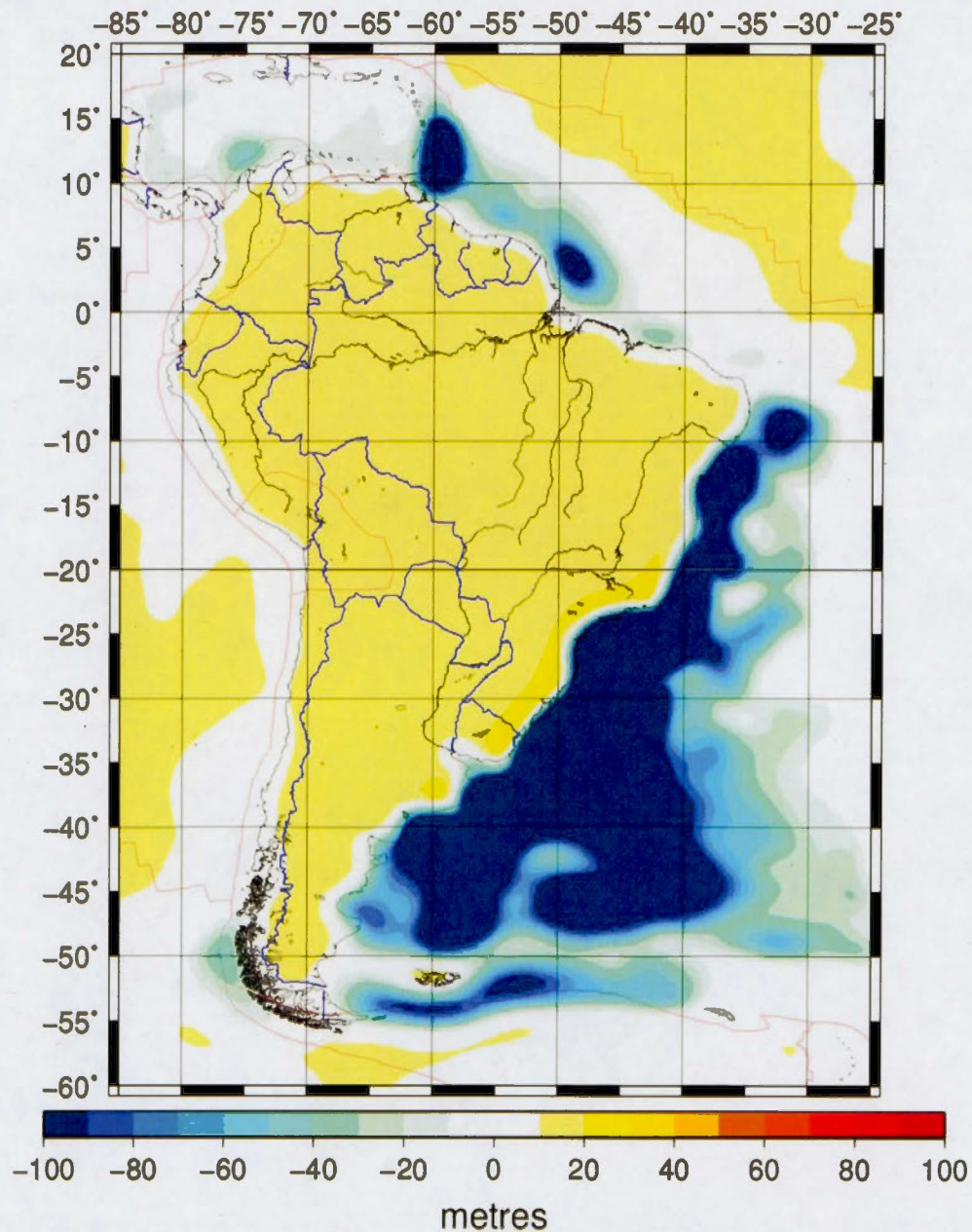


Figure 4.119 Map of Flexural Response during the Oligocene-Miocene interval (33.9 to 5.332 Ma). The effective elastic thickness of 40 km and a maximum harmonic degree of 2000 was employed.

Sediment Flexure, Eocene–Oligocene ($H=40\text{km}$, $L=1-2000$)

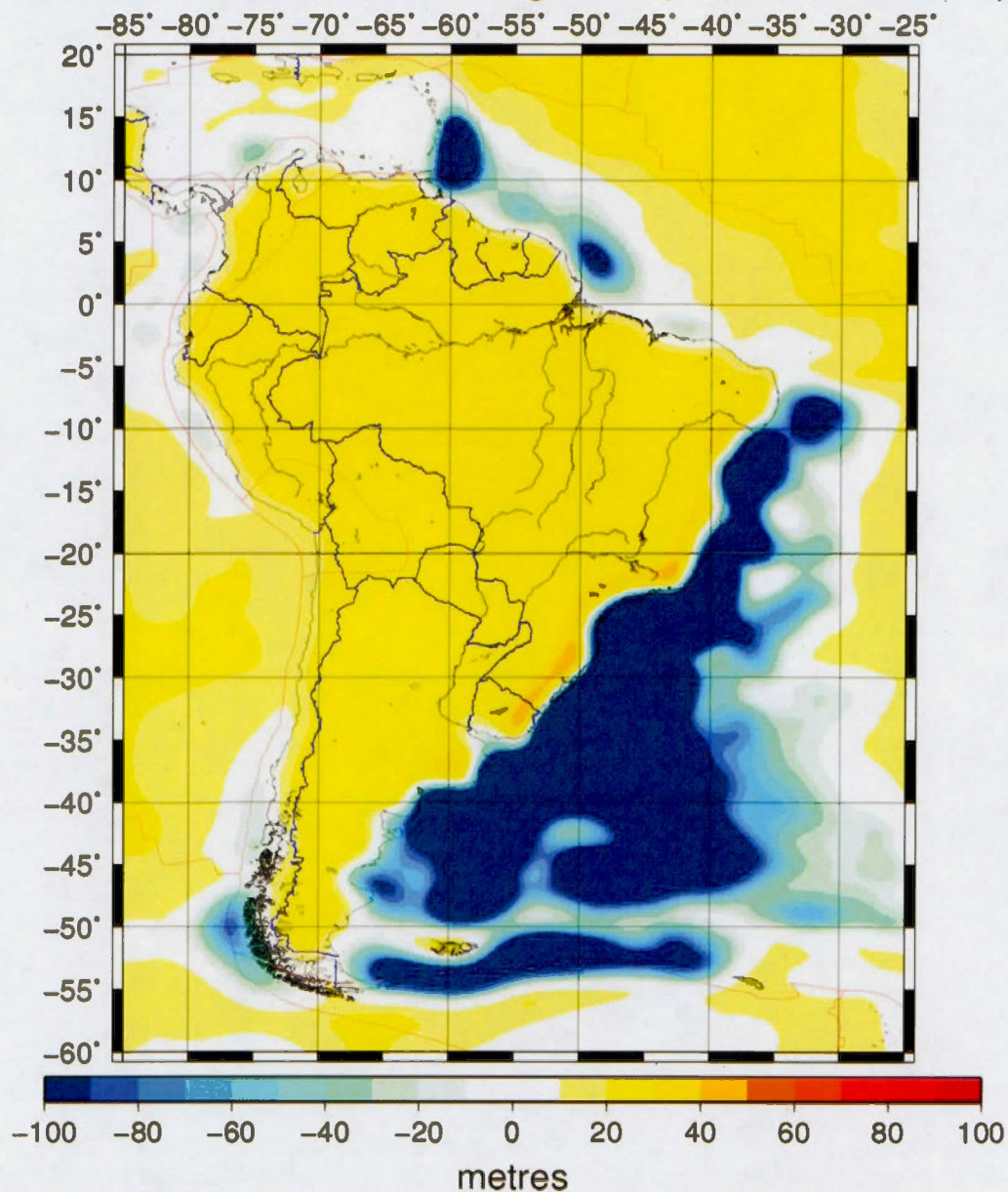


Figure 4.120 Map of Flexural Response during the Eocene-Oligocene interval (55.8 to 23.03 Ma). The effective elastic thickness of 40 km and a maximum harmonic degree of 2000 was employed.

Sediment Flexure, Paleocene–Eocene (H=40km, L=1–2000)

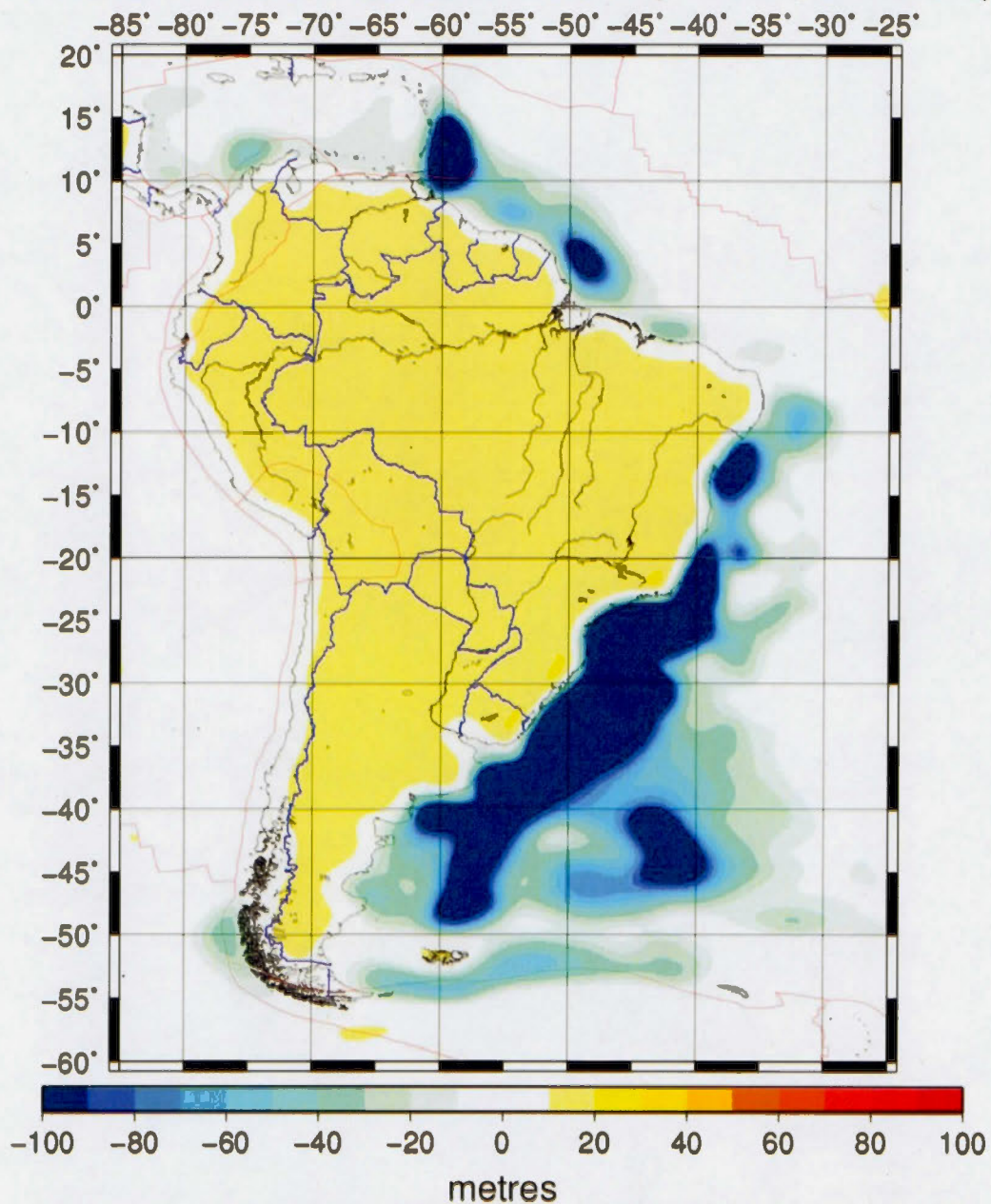


Figure 4.121 Map of Flexural Response during the Paleocene-Eocene interval (65.5 to 33.9 Ma). The effective elastic thickness of 40 km and a maximum harmonic degree of 2000 was employed.

4.5.3 Cenozoic Uplift of the Continent of South America

The sediment-induced flexural depressions discussed above also induce changes in the topography of South America, leading uplift along the continental margin, also called forebulge.

The forebulge or uplift undergone by the continent of South America (lat= 10°S, lon= 60°W) during the Cenozoic (Pliocene-Quaternary (figure 4.81), Miocene-Pliocene (Figure 4.118), Oligocene-Miocene (Figure 4.119), Eocene-Oligocene (Figure 4.120), Paleocene-Eocene (Figure 4.121)) is between 1 and 25 meters.

The following graphic, shows the forebulge change that was experienced in the South-American continent through the different intervals of ages:

Time-dependence evolution of continental uplift due to the forebulge in Sout America (lat= 10°S, lon= 60°W) during the Cenozoic

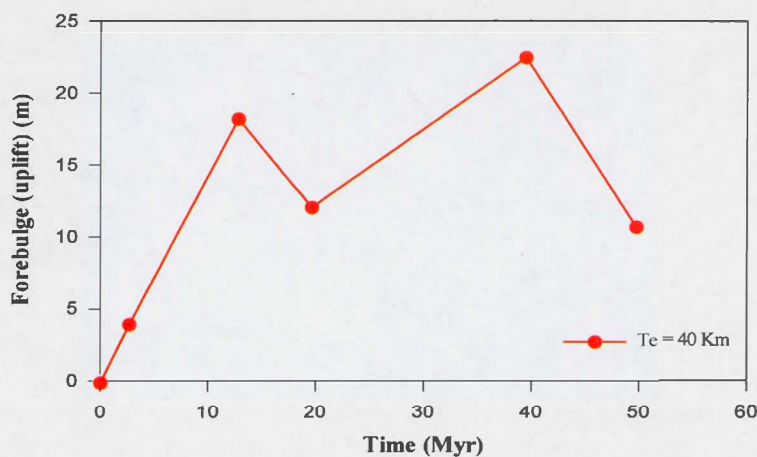


Figure 4.122 Time-dependence of continental uplift due to the forebulge in South America (lat=10°S, lon= 60°W) during the Cenozoic

The forebulge increases the elevation in the Eastern region of South America Continent (at lat=20°S, lon=43°W and lat=7°S, lon= 39°W) with values between 7 and 40 metres. This time-dependence of this uplift can be observed in the following figures, where the evolution of the forebulge from the Cenozoic is plotted.

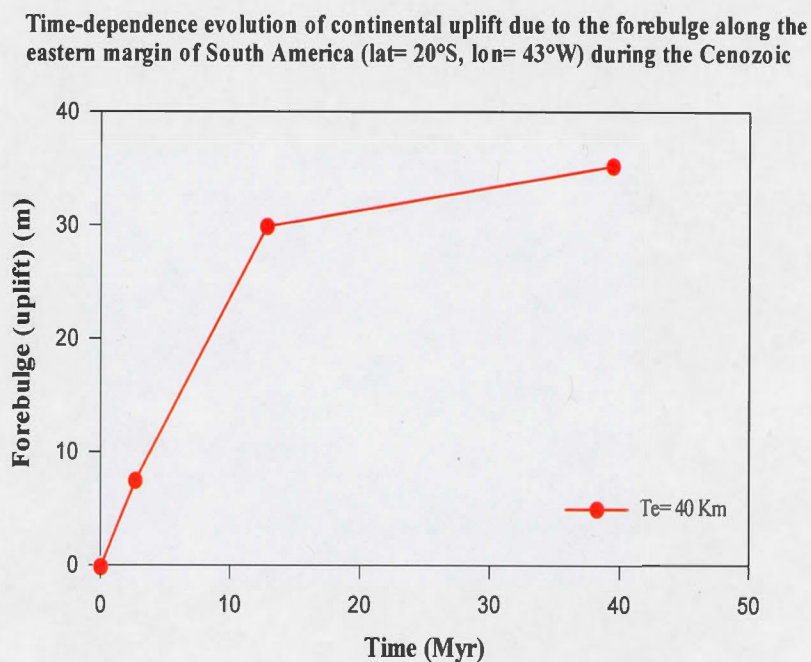


Figure 4.123 Time-dependence of continental uplift due to the forebulge along the eastern margin of South America (lat=20°S, lon= 43°W) during the Cenozoic

Time-dependence evolution of continental uplift due to the forebulge along the eastern of South America (lat=7°S, lon=39°W) during the Cenozoic

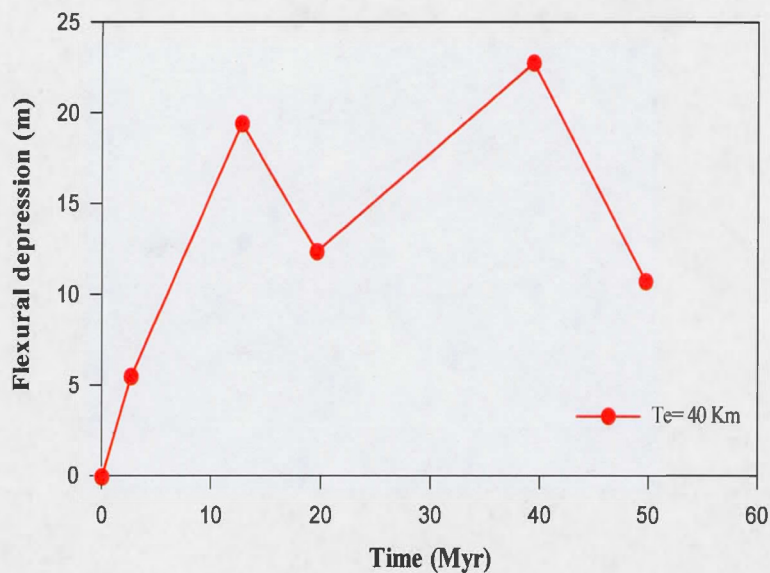


Figure 4.124 Time-dependent of continental uplift due to the forebulge along the eastern margin of South America (lat=7°S, lon= 39°W) during Cenozoic

In comparison to the uplift described above, some portion of the continent such as in, Venezuela, Guyana, Surinam, French Guyana, Brazil, Uruguay and Argentina showed greater elevation changes in some interval of ages. These elevations are summarized in Table 4.9.

Table 4.9 Maximum Forebulge (uplift) over the Cenozoic in the eastern region of the continent of South America. (Blank sections indicate that there was no uplift in the area during the time period)

Country	Quaternary- Pliocene	Miocene- Pliocene	Oligocene- Miocene	Eocene- Oligocene	Paleocene- Eocene
Venezuela	10,09	31,01			
Guyana	12,31				
Surinami	12,46				
French Guyana	18,95	31,76			
Brazil	10,78	36,96	22,81	36,93	20,95
	11,35	37,26	29,66	45,4	20,17
Uruguay		37,78	30,23	43,94	20,14
Argentina		33,02	22,07		

In Table 4.10 we summarize the age-dependent relation that exists between the maximum sediment-induced offshore depression (the foredeep) and the resulting continental uplift (forebulge) during Cenozoic.

Table 4.10 Summary of Maximum Foredeep and Forebulge Amplitudes during Cenozoic

Age	Forebulge	Flexural Depression
Pliocene-Quaternary	19.58	-521.9
Miocene-Pliocene	39.04	-1016.42
Oligocene-Miocene	30.86	-712.93
Eocene-Oligocene	46.62	-831.52
Paleocene-Eocene	21.49	-375.42

Table 4.11 Flexural Foredeep and forebulges amplitudes of Primary Rivers

River mouth	Latitude	Longitude	Flexure-Forebulge (m)	
			Pliocene- Quaternary	Miocene- Pliocene
Magdalena	11°N	74.5°W	-35,65	-110,58
Orinoco	8.83°N	62°W	-5,04	11,17*
	8.83°N	61.83°W	-12,35	2,23*
Amazon	0.5°S	50.5°W	-15,17	2,68*
	0.5°S	51°W	-6,07	10,1*
Confluence Uruguay- Parana Rivers	34,16	58,5°W	-1,32	0,68*
Mar del Plata	34,5°S	58°W	-5,47	-12,99

Negative values indicate flexural depression. * Forebulge or uplift

4.6 Where does the sediment come from?

South America has an extensive drainage network. Its primary rivers include the Magdalena River (Colombia), the Orinoco River (Venezuela), the Amazon River (Brazil) and the Mar del Plata River in Argentina. These rivers are in charge of draining and transporting the continent's sediments, which flow into the Caribbean Sea and the Atlantic Ocean, and deposit on the continental shelf of South America.

It is important to point out that the sediment flow reaching the coastal zone depends on geomorphological, tectonic, geographical and geological characteristics, as well as the anthropogenic factors of the area (Milliman and Syvitski, 1992; Syvitski et al, 2005a, b; Syvitski and Milliman, 2007).

Below we will discuss some of the primary rivers that make up the zones into which the continent of South American has been divided for this study. These rivers can be seen in the map of the figure 4.125, which shows the drainage basins and their respective main river.

In Zone I, the Caribbean Zone, the main river that flows into the Caribbean Sea is the Magdalena River.

4.6.1 The Magdalena River

The Magdalena is born in the Colombian massif of the Andes Mountain Range at an altitude of 3300 m and it is one of the largest rivers in Colombia, with a length of 1612

km, draining an area of 257,438 Km² (Kettner et al 2010)(Figure 4.126) . According to the sediment deposits extending into the Magdalena Valley, the initial age of the river is the Late Miocene. (Potter 1997)

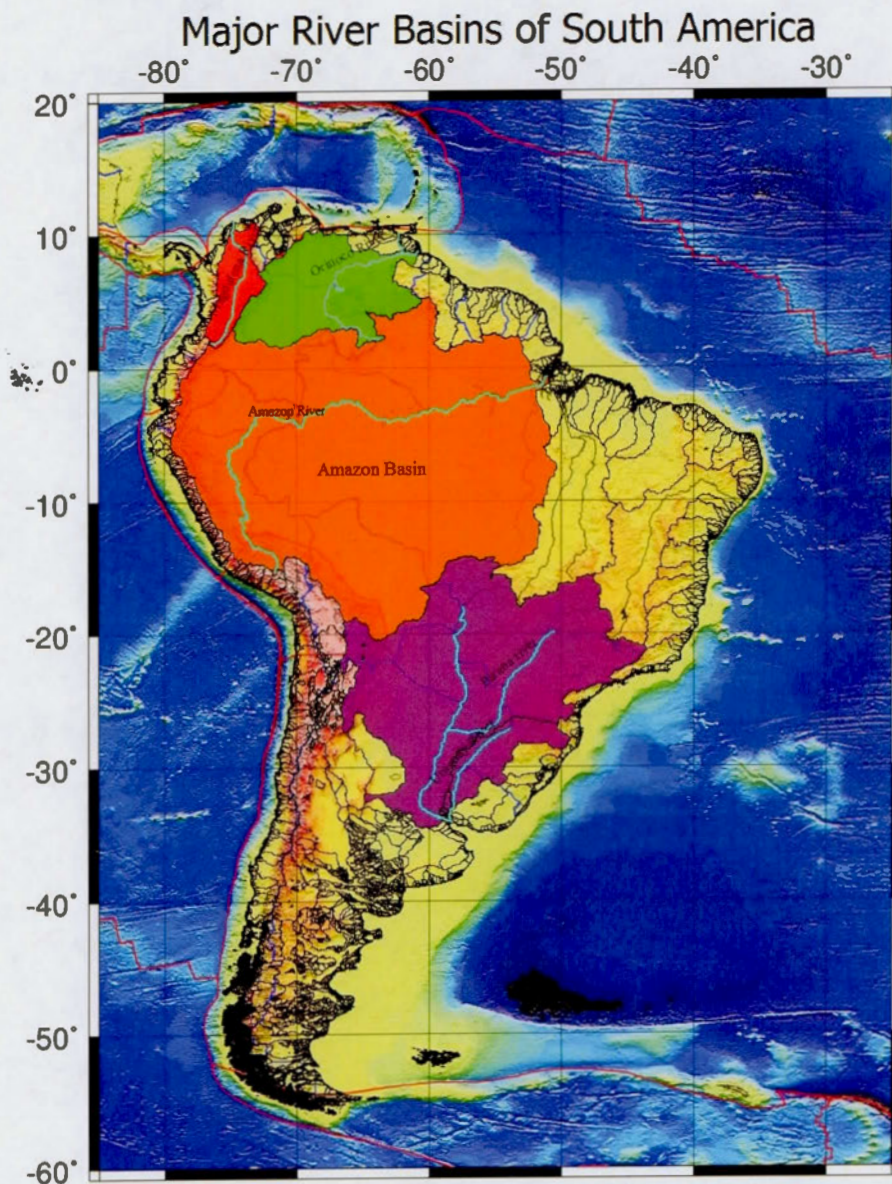


Figure 4.125 Major River Basins of South America. The figure shows the four principals hydrographic basins and their respective rivers. The Magdalena's basin is

Figure 4.126 Magdalena River Basin. Taken from Restrepo & Kjerfve (2000)

Based on the seasonal distribution, the Magdalena has two periods of high sediment load measured at the Calamar Station (located 112 km upstream from the Caribbean) with values of $690 \times 10^3 \text{ t day}^{-1}$ and $678 \times 10^3 \text{ t day}^{-1}$ during the months of November and December, and $443 \times 10^3 \text{ t day}^{-1}$ during the months of June and July. (Restrepo & Kjerfve 2000)

According to Restrepo et al (2006b) this river has the highest sediment yield at a value of $\sim 560 \text{ t km}^{-2} \text{ yr}^{-1}$ for the $257,438 \text{ km}^2$ basin, yielding $144 \times 10^6 \text{ t yr}^{-1}$: the annual sediment load transported to the ocean.

This river drains the Andes, the active orogenic mountain range characterized by its high relief ($>5000 \text{ m}$) and intense volcanic and seismic activity. In addition, the tributaries of the Magdalena Basin drain the three mountain ranges that make up the Andes mountain belt, which are separated by the Magdalena and Cauca Valleys. (Kettner 2010)

Two of the main rivers in Zone II are the Orinoco and the Amazon Rivers.

4.6.2 The Orinoco River

The basin of the Orinoco River covers approximately $1.1 \times 10^6 \text{ km}^2$ of northern South America. The basin consists of approximately 35% of the Guyana Shield, 15% of the orogenic belt of the Andes and coastal mountain ranges and finally 50% of the Eastern Plains of Colombia. (Warne A.G. et al 2002). (Figure 4.127)

The development of the Orinoco River system is strongly influenced by the Andean Orogeny, which began in the late Oligocene and peaked in the Pliocene. (Warne A.G. et al 2002)

The estimated annual average suspended sediment input of the Orinoco River at the Ciudad Bolívar Station is approximately 150×10^6 tons per year (Meade et al 1990). In the Orinoco River, the concentration of suspended sediments reaches two minimums and two maximums per year. The minimum concentration nearly matches the minimum and maximum water discharge. The maximum concentration occurs during the increases and drops in water discharge.

Meade et al (1990) have pointed out that the total sediment input in the ocean comes from the tributaries that drain the Andean Mountain Range. These tributaries, such as the Guaviare River and the Meta River contribute about 20% and 50% respectively of sediment discharge to the Orinoco River and drain the Andes and the Plains regions in Colombia. In addition, among the rivers that drain the eastern part of the Venezuelan Andes is the Apure River who contributes about 20% of sediment discharge, while the Caura and Caroni Rivers in Venezuela drain the Guyana Shield and contribute less than 5% of sediment discharge to the Orinoco River. (Figure 4.129)

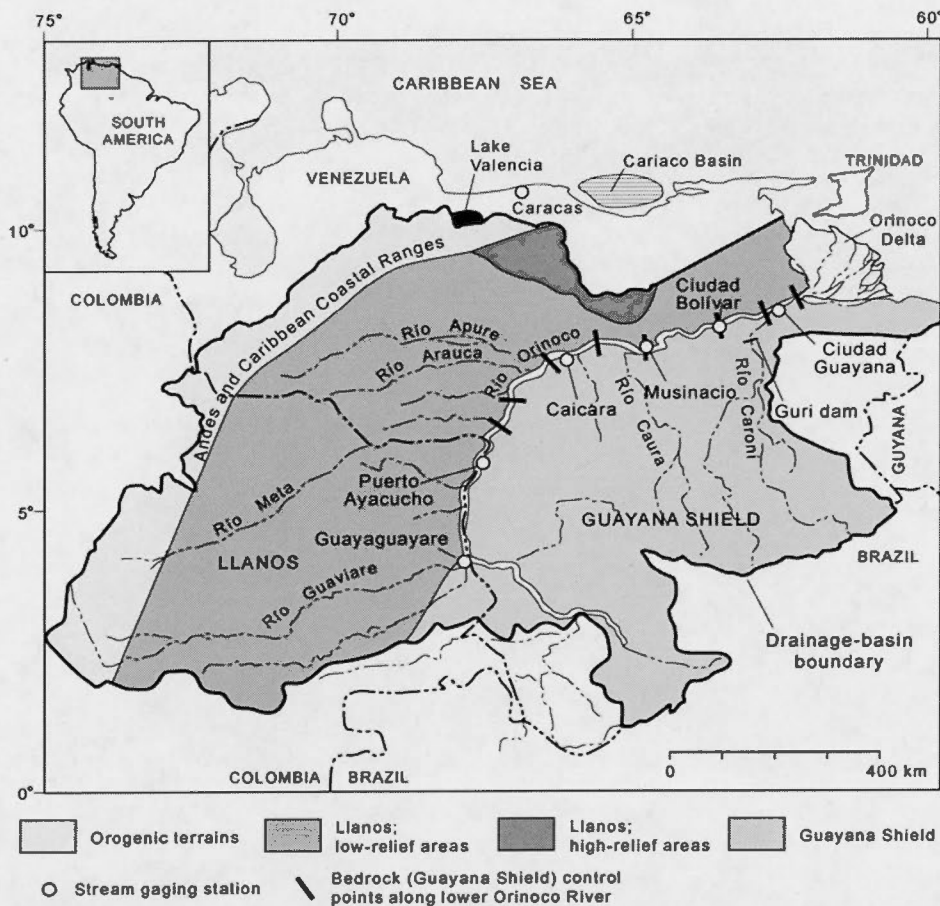


Figure 4.127 Orinoco River Basin. Taken from Warne et al., (2002)

4.6.3 The Amazon River

The Amazon River is the largest river in the world, in terms of water discharge with values of $100,000 - 220,000 \text{ m}^3 \text{ s}^{-1}$ and is also one of the three largest rivers in the world in terms of sediment discharge, with values of $13 \times 10^8 \text{ ton y}^{-1}$. (Milliman & Meade, 1983). It is born on the western ridge of the Andes, with a length of

approximately 4000 km from Peru to the Atlantic Ocean, flowing through different forms of reliefs and depositing sediments from the river itself as well as from its tributaries in river features such as floodplains, sandbars and fluvial terraces (Meade, 1994)

The Amazon basin extends to the eastern flank of the Andes mountain chain, and the mountainous relief and erosion associated therewith increases sediment discharge significantly (Nittrouer & Brunskill 1995). (Figure 4.128)

The rainy regions are found in the northeast and northwest of the Amazon Basin with more than 3000 mm/year. The area that makes up the northeastern section of the Basin is covered by the Amazon Delta near the Atlantic Ocean, while the northwestern portion of the Basin is made up of Colombia, the northern Amazon in Ecuador, northeastern Peru and northwestern Brazil. These regions are exposed to the Inter-Tropical Convergence Zone (ITCZ) (Espinoza et al 2010). Similarly, the southeastern portion of the Basin, near the middle of the Southern Atlantic Convergence Zone, has abundant rainfall. (Espinoza et al 2010, Lenters and Cook 1995). Rainfall decreases in the tropics, at values of 2000 mm/year in the southeastern region of Brazil, and approximately 1500mm/year in the Peruvian-Bolivian plains region and the Brazilian state of Roraima. The latter is sheltered from the humid flows from the Atlantic by the Guyana Shield. (Espinoza et al 2010).

Variations in water discharge from the Amazon River are closely linked to seasonal variations, so in mid-May, there is a maximum discharge of about $2.4 \times 10^5 \text{ m}^3 \text{ s}^{-1}$ and in mid-November, there is a minimum discharge of $0.8 \times 10^5 \text{ m}^3 \text{ s}^{-1}$. (Lentz, 1995a).

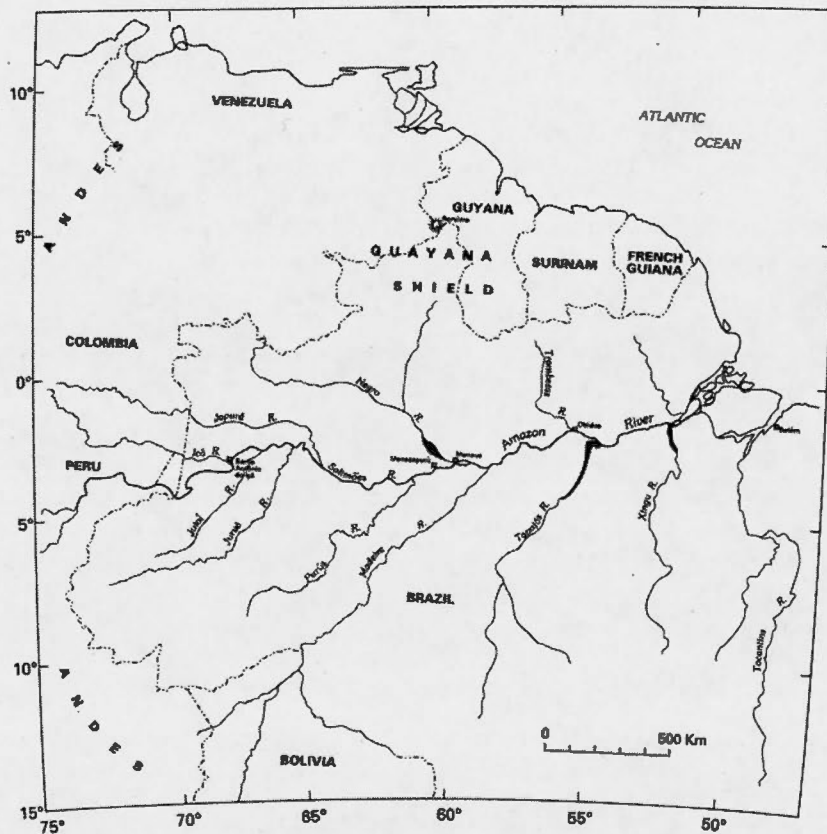


Figure 4.128 Amazon River Basin. Taken from Meade (1994).

This has a strong influence on the sediment input in the oceans. In the Amazon River, discharged sediments are trapped on the shelf and transported to the northwest. These sediments dominate the shelf and the coastline at around 100 km (Nittrouer & Demaster, 1986). Every year, the Amazon continental shelf accumulates approximately one quarter billion tons of sediments (Kuehl et al., 1986a). The majority

of suspended sediments originates in the tectonically active regions of the Andes. (Meade, 1994)

A large portion of the sediments come from the tributaries that drain the Andes, and the variations in sediment discharge are the result of the flow variations in these tributaries, as well as the accumulation and release cycles of the river bed (Meade et al 1985). According to records of the Obidos Measuring Station located 800 km from the Atlantic Ocean, the sediment discharge transported every year is approximately 1.3×10^9 tons. (Meade et al 1985). This is assumed as the amount discharged into the ocean (Nittrouer et al, 1995).

Sediment transport studies of the Amazon continental shelf conducted by Kineke et al 1996 revealed the presence of fluid mud as suspended sediment. The suspended sediment is also observed on the coast of Guyana and Suriname (Well and Coleman, 1981). This shows sediment migration due to factors such as wind-generated waves (Gratiot et al., 2007).

Zone III is strongly influenced by the drainage basin of La Plata River:

4.6.4 La Plata River System

The Rio de la Plata system is one of the major rivers in the world. It has a basin area of approximately 3.1×10^6 km², 45.6% of which is in Brazil, 29.7% in Argentina, 13.2% in Paraguay, 6.6% in Bolivia and 4.8% in Uruguay (OEA, 1971). Rio de la Plata is located on the eastern coast of South America between 34° S and 56°20' S and between

55°W and 58°30' W. It is 320 km long and its width ranges from 38 km in the upper region to 230 km at the mouth, between Punta Rasa and Punta del Este. (Framiñan and Brown, 1996). The main tributaries are the Paraná River and the Uruguay River. (Figure 4.129)

This system transports water and sediments from the interior of the continent and flows into the Atlantic Ocean. It contributes a total of 70×10^6 metric tons of dissolved solids to the southeastern portion of the Atlantic Ocean, 71% of which is provided by the upper basin of the Paraná-Paraguay River. A total of 129×10^6 metric tons of suspended solids are transported to the Atlantic Ocean, 68% of which is provided by the upper basin of the Paraná-Paraguay River. (Depetris and Griffin, 1968)

One of the most important tributaries of Rio de la Plata is the Paraná River. It is born at the confluence of the Grande and Paranaíba Rivers and is 4000 km long. Its main tributaries are the Paraguay, Iguazú and the Paranapanema Rivers. (Camilloni and Barros, 2003). The area of the drainage basin is 2.6×10^6 Km² and it is made up of the Andes mountain range, the Eastern Plains, Chaco-Pampa Plain, Jurassic-Cretaceous Highlands and the Brazilian Shield. (Iriondo 1988).

Basin climate is tropical to subtropical with an average annual rainfall of 1200 mm (Stevaux 1994). Rainfall varies depending on the season and ranges according to latitude and location within the basin. In the west, rainfall in the sub-basins amount to 700 mm per year, while in the east on the coastal mountain range, values reach 1800 mm per year. (Pochat 2010).

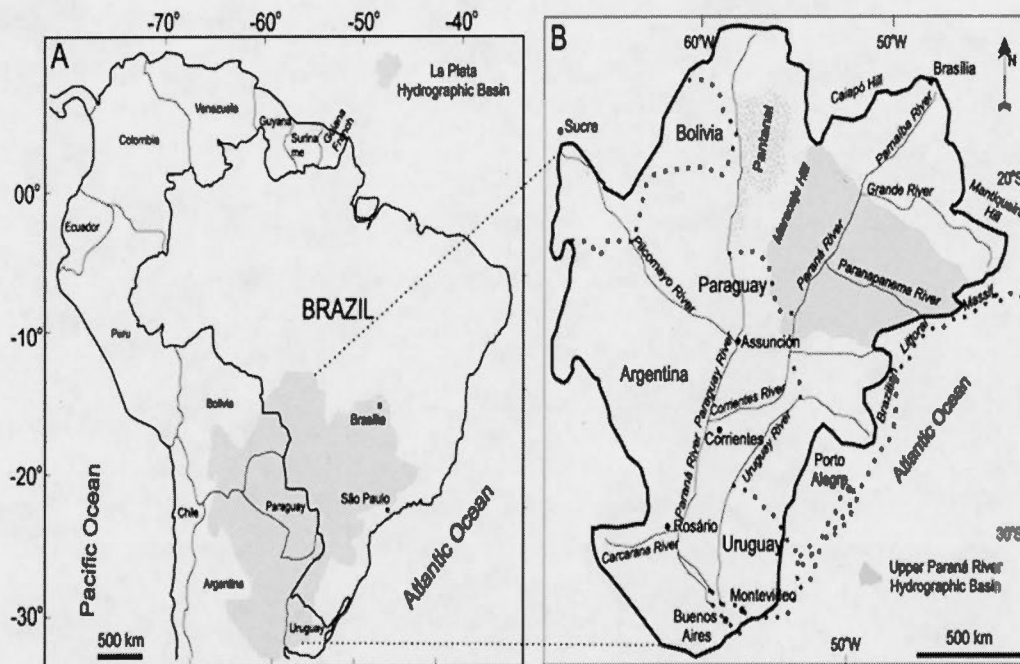


Figure 4.129 La Plata hydrographic Basin. Three hydrological units can be differentiated: Parana River, Paraguay River and the Uruguay River. Taken from Sallun & Suguio, (2010)

Considering discharge, the river has an average annual flow rate of approximately $17,700 \text{ m}^3\text{s}^{-1}$. (Pochat 2010). Annual discharge of suspended sedimentary load into the Atlantic Ocean at the mouth of the Paraná River is estimated at approximately 200×10^6 tons (Iriundo 2004, Depetris & Griffin, 1968). Studies conducted by Orfeo & Stevaux (2002), in the upper and middle segments of the Paraná River indicate suspended sediment values of $118.7 \times 10^6 \text{ tons year}^{-1}$ and an annual bed load discharge (sand, pebbles and stones) of $39.7 \times 10^6 \text{ ton year}^{-1}$.

This river drains the central-southern regions of South America from the edge of the Andes Mountain range to the Serra do Mar. The sediments flow into the Paraná River from the Bermejo River, transported from the Andes mountain range (Orfeo and Stevaux, 2002). The basin consist of sedimentary and volcanic rocks and come from the eastern ridge of the Andes and the Brazilian Shield in the north and east. (Stevaux 1994).

The large amount of sediment transported by the Paraguay River that reaches the Paraná River through the tributaries such as the Bermejo, Uruguay and La Plata Rivers give rise to the formation of the Paraná River Delta. (Pochat 2010)

The Uruguay River is the second most important in the Rio de la Plata Basin with a length of approximately 1600 km. The area of the drainage basin is 365,000 km² (Krepper et al., 2003). This River has headwaters in Sierra do Mar and Sierra Geral, near the Atlantic Ocean. Rainfall ranges from 1500 to 2000 mm in the upper basin, near the Santo Tome Station and drops to 1000 mm at the confluence (Garcia & Vargas., 1996). The suspended-sediment load at the Uruguaiiana station (lat - 29.750000; lon -57.083330 (Hidroweb.ana.gov.br) on the Uruguay River, was estimated to be 3.59×10^6 t year⁻¹ (Furquim et al, 2005)

4.7 South American Ocean Currents

Ocean currents are organized flows and water mass displacements caused by wind action and differences in temperature and salinity. They originate in geographic areas such as Equator or near the Poles, where they may be cold or warm. Between the main currents in the South Atlantic Ocean that influence water flow and sediment transport

along the east coast of South America, we found: The Falkland Current, the Brazil Current, the North Brazil Current, the Guiana Current and the Caribbean Current.
(Figure 4.130)

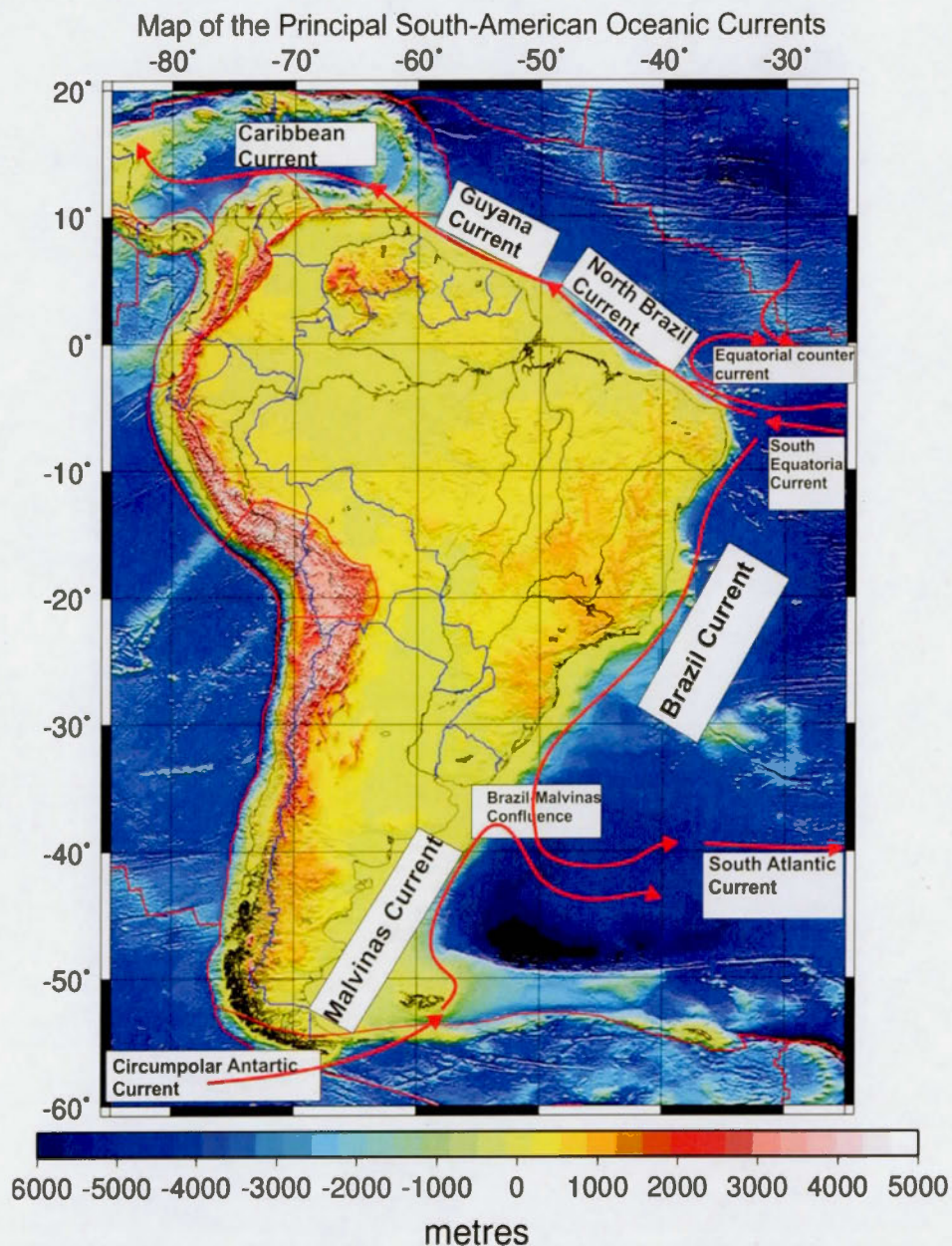


Figure 4.130 Map of the principal South-American oceanic Currents.

The Falkland Current is an arm of the Antarctic Circumpolar Current that flows north through the continental slope of Argentina at approximately 38°S (Matano et al., 2010) where it reaches the Brazil current offshore from La Plata River (Figure 4.130 and Figure 4.131). These currents converge, creating the Brazil-Falkland confluence, which falls between 33-38°S along the continental shelf of Brazil, Uruguay and Argentina (Olson et al, 1988), where one of the greatest eddies of the ocean is generated. (Palma et al 2008). The waters originate in the southeast Pacific, penetrating the southeast Atlantic through the Strait of Magellan, where it reaches the Falkland Current with a strong influence on the Patagonian Sea. (Piola & Falabella, 2009).

During the austral winter in the months from July to September, the Brazil-Falkland confluence tends to move to the north, while in the months from January to March, during the austral summer, it moves to the south. (Piola & Matano 2001). The above is due to the annual evolution of the winds which involve the subtropical basin.

Studies conducted by Palma et al (2008) infer that the transport of the Falkland Current at 45°S is 67Sv (Sverdrup, where $1\text{Sv} = 10^6\text{m}^3\text{s}^{-1}$), decreasing at 42°S with values of 43 Sv, down to values of 31Sv near 39°S.

In addition, the waters flowing toward the Brazilian coast flow from the South Equatorial Current (SEC), which divides at approximately 15°S into two main arms, giving rise to the North Brazil current and the Brazilian current. (Souza et al, 2011.)

The Brazil Current is an extension of the South Equatorial Current, which is divided between latitudes 7° and 17°S, depending on the time of year, and flows parallel to the southeast and south platform of Brazil, meeting in the form of meanders offshore. (Figure 4.129 and Figure 4.130) (Pimienta et al, 2005). Between 29° and 37°S of the

Southern Subtropical Zone, the weather is influenced by the Tropical Atlantic and Polar Atlantic air masses. In addition, the zone is characterized by the presence of the Southwest Atlantic Convergence Zone (SACZ), upwelling currents (Coastal and shelf-edge upwelling), nutrient-rich waters of South Atlantic Central Waters (SACW) and the input from the continent through La Plata River and the Estuary Patos lagoon. (Souza et al, 2011). Near 35°S, off the Uruguay shelf, it runs into the Falkland Current and they curve to the east (Brazil-Falkland Current) where they join the Southern Atlantic Current. (Boisvert, 1967). The strength of this current is due to the strength of the Southern Atlantic Equatorial Current, which depends on the season of the year. The current is more intense in July and August. (Boisvert, 1967)

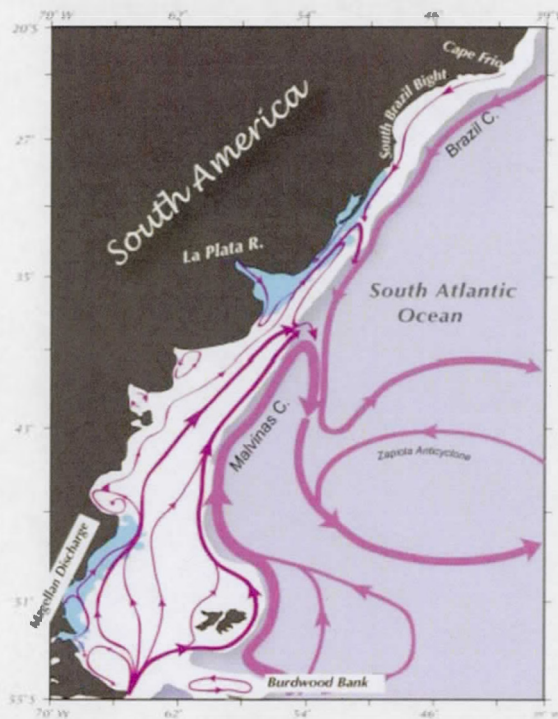


Figure 4.131 Malvinas Current and Brazil Current. Taken from Matano et al., (2010)

Just as the winds play an important role in the currents of the Southern Brazil shelf, mechanisms such as upwelling currents, eddy behavior, meandering processes and rotary currents are highly important components in controlling material transport in the area through which the Brazil Current flows. (Pimienta et al 2005). Similarly, Souza et al (2011) suggests that the meanders of the Brazil Current in form of eddies may be the most important mechanism contributing to the exchange of waters between the coastal shelf and the open ocean. These exchanges occur by means of the transport and mixing of different bodies of water. Furthermore, the rotary currents caused by tide activity may also be important for flow estimates through the shelf.

Simulations with winds and different discharges from La Plata River carried out by Pimienta et al (2005), demonstrated that the persistence of the winds along with a strong upwelling component are likely to be an effective mechanism in dispelling the Plata Plume and also in transferring shelf waters to the ocean. These upwelling currents, like the coastal upwelling, make the southeastern-southern part of the Brazil shelf more productive, in addition to dislodging major terrigenous sediments and organic matter contents as a result of the upwelling processes.

Last but not least, the tropical surface waters of the Brazil Current assist the water flow and transport sediment from rivers such as the Sao Francisco and medium ones such as the Requitinhonha, Doce, Mucuri and Paraiba do Sul these sediments are captured in the interior shelf of the current's area of confluence. (Souza et al 2011).

On another note, the North Brazil Current, one of the main currents flowing along the eastern coast of South America, is a western boundary current originated in the South Atlantic (Barbie et al, 2003), which transports warm waters from 5° S (Philander 2001) (Figure 4.132). The waters of the South Atlantic cross the equator through this North

Brazilian current in the form of rings (Fratantoni and Richardson, 2006), retroflexion eddies (Richardson et al., 1994) where the waters flow northeast through the continental shelf of South America, (Dessier and Donguy, 1994, Candela et al, 1992). In turn, the flow of these waters is divided on the way to the northern hemisphere and along the coast of Brazil, continuing to the south of the current. (Philander 2001). Between 7° and 17°S, this current is strongly influenced by an Equatorial Atlantic Air Mass (EAM) and the Inter-Tropical Convergence Zone (ITCZ). (Souza et al, 2011.)

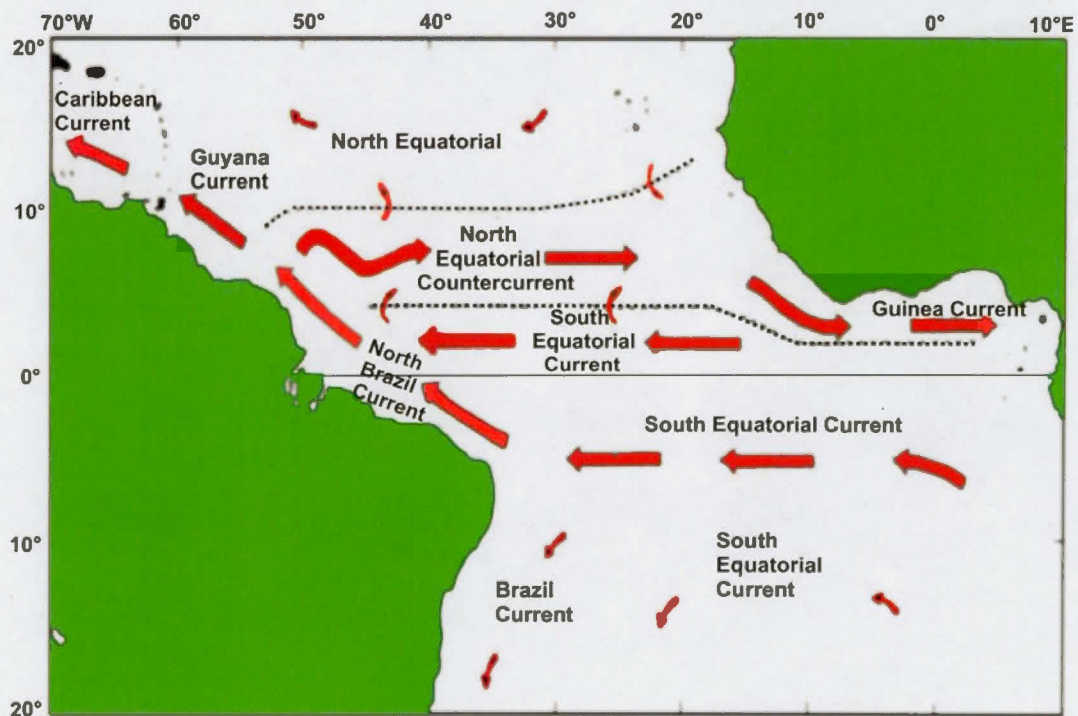


Figure 4.132 Map of the principal Oceanic Currents in the Atlantic Ocean between July and September, where the North Brazil current retroflects and goes eastward flowing in the North Equatorial countercurrent. Taken from Philander (2001).

When the waters from the North Brazil Current flow through the South American shelf at 5° N, they join the Guiana Current (Philander 2001) (Figure 4.132). The waters flowing in this current are strongly linked to the freshwater discharges of the Orinoco and Amazon Rivers (Morrison and Smith, 1990).

In the Amazon Plume, the waters flow and extend to the ocean currents and, depending on the time of year, the water either extends or changes direction. So from January to June, the water extends to the northwest that is to say, it goes to the Caribbean. In early May, the Amazon Water Plume is deflected to the east in the North Brazil Current Retroflexion (NBCR). Between July and October, nearly half of the water from the Amazon Plume is deflected to the northeast by the North Brazil Current Retroflexion (NBCR) (Lentz, 1995b) (Figure 4.132). Here, the rate of the North Brazil Current is linked to the season, with a maximum from August to September and a minimum in April (Nittrouer et al, 1995).

In addition, the duration of the water and sediments in the Amazon Plume also depend on easterly trade winds, which increase the flow along the shelf associated with the North Brazil Current when they blow from the southeast, and may inhibit it when they come from the northeast. (Lentz, 1995b). Winds are generally strong from January to March when they come from the northeast onshore, while they are weak from June to November, blowing along the southeastern shelf. (Nittrouer and Demaster, 1995)

The above comments show that the waters flowing along the Amazon Plume, as well as the sediments transported thereby, are likely driven by ocean currents. This can be analyzed by the studies conducted by Richardson et al, (1994), in which, based on the observation of salinity near the coastline, they demonstrated that a high percentage of the water from the Amazon Plume is taken to the northeast by the Guyana Current.

Discharge from the Amazon and Orinoco Rivers contributes a high percentage of fine-grained sediments. These sediments are deposited along the East Coast of South America between Venezuela and Brazil, giving rise to the formation of mud banks. Studies conducted by Gardel and Gratiot (2006) show the presence of mud banks on the coasts of French Guiana, Suriname, Brazil and Guiana, where the mud banks have been moved and migrate due to the action of certain processes and forces. This is why Allison et al (1995) suggest that the currents generated by trade winds, tidal currents and waves play an important role in sediment migration, maintaining suspended sediments in the coastal zone.

Similarly, Gratiot et al (2007) indicated that mud migration is caused by geostrophic forces associated with ocean currents such as the Guyana Current. In addition to its relation to the NE tidal currents, as well as factors such as the effect of the wind force with an impact on the coast, the energy wave and the generation of compensatory flows to the northwest due to N - NE winds during the trade wind season.

Finally, waters from the Guyana Current follow their course, extending to the Caribbean Current (Gordon 1967) (Figure 4.132). This major current transports water from the South Atlantic through the Caribbean. According to Chérubian and Richardson 2007, waters flowing from the South Atlantic Ocean up to 14°N in the Caribbean are transported by the rings of the North Brazil Current (NBC), which go through the windward Islands Passages, the Leeward Island passages and the Greater Antilles passages up to the Caribbean Sea. When these waters flow through the various passages, they do so through the Yucatan peninsula and continues into the Gulf of Mexico, exiting through the Florida Strait at a rate of $30 \times 10^6 \text{ m}^2 \text{ s}^{-1}$. (Schmitz and Richardson, 1991). In the Southern Caribbean, this current reaches an average speed of approximately 60 cm s^{-1} (Molinari et al, 1981).

According to the UNEP et al., (2006), the Magdalena River is the main source of discharge in the Caribbean, as well as the Orinoco River, which drains into the Atlantic Ocean, but has a significant impact on the southern shores of the Caribbean, due to the major impact of the ocean currents.

Other source of fresh water that strongly influence the Caribbean Sea is the Amazon River, where the discharges go to the tropical Atlantic Ocean and are conveyed to the Caribbean Sea. (Chérubin and Richardson. 2007)

Studies by Muller-Karger et al 1988, show the influence of the Amazon and Orinoco Rivers on the Caribbean sea, suggesting that water from the Amazon River is usually dispersed NW, parallel to the coast, during the months of June and July, entering the Caribbean Sea through the Minor Antilles. Whereas in the second half of the year, the waters from the Amazon Plume flows around the North Brazil Current Retroflexion and at the same time is directed in the form of meanders by the North Equatorial Counter Current (NECC). Similarly, the discharge from the Orinoco River flows into the Caribbean Sea after being transported and passing by Trinidad and Tobago, and is dispersed E and NE by the Ekman Drift, which is generated by trade winds. (Muller-Karger et al., 1989)

The above is demonstrated by the studies of Hu et al, (2004), where using colored water patterns such as Chlorophyll (Chl), colored dissolved organic matter (CDOM) correlated with salinity maps in the area, it is shown that discharges from the Orinoco and Amazon Rivers reach and influence the waters from the Caribbean sea depending on the season of the year. Therefore, in the months of July and August, the Amazon Plume goes NW through the Minor Antilles, while the freshwater plume of the Orinoco

river extends through the months of September through November, with a high discharge value in August.

In addition, Chérubin and Richardson (2007), by means of Sea Surface Salinity (SSS) maps, Colored Dissolved Organic Matter (CDOM) Maps, Surface Drifters and data from Sea-viewing Wide Field of View Sensor (Sea WiFs), demonstrated the development of the Caribbean Current is correlated to the influx of freshwater from the plumes of the Amazon and Orinoco Rivers.

In the case of the Orinoco River, its maximum discharge is in August, extending the plume to the north to later merge with the remnants of the Amazon Plume. Between August and November, the freshwater plume of the Orinoco River arrives at and dominates the eastern portion of the Caribbean with low salinities, Chérubin and Richardson (2007).

According to Field (2005), the arrival of fresh water is linked to the increase in surface temperature. Chérubin and Richardson (2007), correlated salinity with temperature and inferred that low salinity and temperature quality aid to accentuate the density front; the above intensify the Caribbean Current.

Last but not least, the complete rotation of the N-S circulation gives rise to the flow of warm surface water to the North. Returning a flow of deep cold water to the South, giving rise to heat transport from the South Atlantic that goes to the North Atlantic. (Philander 2001).

Finally, we can say that part of the sediments have been accumulated in South-American continental margin, and are given by the fluvial systems. According to

Milliman & Syvitski (1992), the rivers are considered as the principal channel that conducts the sediments towards the Coastal Ocean. Likewise, Milliman & Farnsworth, 2011 indicated that the majority of sediments and particles of organic matter that enter to the ocean are transported by tropical rivers. In addition, Syvitski, (2003) suggests that the sediments that stream toward the ocean are coming from the rivers, which represents around the 95% of the global flow of sediments to the ocean. These sediments that are transported are coming from the erosion occurred in range of mountains like los Andes and geographical regions like La Patagonia and the Escudos of Guyana and Brazil.

In the moment in which the rivers flow into the oceans, the fresh water is diffused over the salty water of the ocean, which is denser, given place a circulation pattern which will allow the initial development of plume. Further, taking into account the plume hydrographic parameters, such as: direction, speed, thickness and width that along with the speed of the sediments settling will determine where the river's sediments will discharge that will reach the seafloor. (Hill et al., 2009) These sediments will extend to the ocean and will acquire a behavior of sediments that according to Swift & Thorne (1991) are regulated by four variables, which are: sediment input rate, size of the given grain, change of the relative level of the sea and transportation of dispersed sediments. For this reason, it is a function of the potential of the tides, waves and the currents. As a result, the relation between sediment input rate and currents, tides and waves are fundamental to control the platform of sedimentation.

On the other hand, in the Amazon's continental platform where different process like the big releases of water with sediments that proceed from the Amazon River, the oceanic currents and the great physical energy that liberate the tides and the winds are

impacting enormously the distribution of sediments in this area and the process that occurred in the oceanographic coast.

Furthermore, oceanic process that take place such as flow of plume of the Amazon River and the creation of superficial waves of gravity are influenced by the Easterly trade winds. With that being said, when the winds blow towards the north, the plume is expanded over 200 km, while when the winds are going towards the south, the flow increases towards the north and the width of the plume decreases. (Nittrouer & Demaster, 1995). According to Nikiema et al, 2007, the structure and flow of the Amazon plume are strongly influenced by the North Brazilian Current. Consequently, this interaction causes that the Amazon system of dispersion continues towards the north. (Lentz, 1995b, Flagg et al., 1986). That is to say, the previous processes are very important to the diffusion of the release of freshwater and suspended sediments of the Amazon River in the South-American Continental Platform. (Nikiema et al, 2007).

Additionally, from the North Brazilian current, the Guyana's current continues transporting the sediments of the Amazon River toward the northeast throughout the coast. (Warne et al., 2002). These sediments have been transported and deposited all the way through the Guyana Coast by two principal processes: migration of the mud bank and mud cape accretion (Allison et al., 2000). The mud banks migrate by the combination generated between the current of Guyana that come from the East and the waves that are generated by the Trade Winds coming from the northeast where the waves shake, suspend and transport the mud towards the west-northeast. (Wells & Coleman, 1981). Lastly, the Amazonian sediments arrive until the Orinoco Coast, reaching around 1.0×10^8 tons/yr. of sediments, which are transported by the Guyana Current (Warne et al., 2002)

Correspondingly, studies done by Piola et al., (2005) and Huppertz et al., (2011) suggest that the sedimentation in the Argentina-Uruguay's North platform is principally governed by the plume of River La Plata where the sediments like bed load are trapped in the estuary (Violante & Parker, 2004), while the mud is transported towards the sea throughout the shoreline, where it mixes with platform waters (Piola et al., 2005). In addition, the sediments come from River La Plata. The sediments come from its runoff of the Patagonia and of the Antarctica, which are transported by the platform currents that act in the area (Mahiques et al., 2008) this means that the influence by the oceanic circulation caused in the zone of confluence Brazil-Malvinas.

In the final analysis, it can be said that the pattern of circulation of the oceanic currents have influence over the sediments. According McCave (1985), the transportation of sediments inside of an oceanic current to a scale of time of thousands of years gives the opportunity to build the contourite depositional sequences, which are closely related to a specific oceanic current. (Stow et al, 2002)

CHAPTER V

DISCUSSION

Based on the integration of the data and analyses set out above, over the course of the last 65 million years ago, South America has experienced substantial uplift on the Caribbean and South-Atlantic margin caused by the weight of the sediment deposited offshore. A clear example is the Amazon Fan where the flexure caused by the weight of the sedimentary load during the Miocene to Present generates a forebulge of 34.41 meters. These results are consistent with the studies conducted by Driscoll & Karner, (1994), who predicted forebulge amplitudes between 25-50 meters, which are the result of the load exerted by the sediments accumulated on the Amazon Fan in the Middle Miocene to Present. The values of Driscoll & Karner (1994) were obtained using an elastic thickness of 38 km, a constant sediment density of 2450 kg/m^3 , a Young Modulus of $6.5 \times 10^{10} \text{ Pa}$ and Poisson's ratio of 0.25.

It is important to pointed out that the amplitudes identified near the Amazon Fan, at 1.5°N and 52.5°W , reaching values of 50.23 meters in the Miocene, 22.85 meters in the Pliocene and 8.75 meters in the Quaternary, which suggests an increase in uplift amplitudes with regard to the studies by Driscoll & Karner (1994).

Similarly, the sediments deposited in the offshore basin of Sergipe-Alagoas cause deformation in the area, generating uplifts along the coastal margin, in the states of Sergipe and Alagoas. At 11.5° South Latitude and 39° West Longitude onshore, the uplift generated during the Paleocene-Quaternary interval was 54.42 meters. It is of

interest to compare this value to that obtained by Da Silva et al (1999), in the same location, where they show that the continental region was lifted 230 meters during the period of total thermal subsidence that started in the Albian. This value was obtained using an elastic thickness of 20 Km. When using an elastic thickness of 40 km, the above value of the amplitude of the flexural bulge decreases to approximately 10% to 207 meters. We also note that at sites further inland, such as for example at 11.5° South Latitude and 40° West Longitude, the uplifts increase, reaching values of 103.23 meters for the Paleocene-Quaternary interval.

The comparison with the Da Silva et al., (1999) results for uplift reveals evident differences, and we may in part attribute this to differing estimates of the accumulated offshore sediment load, and in part to the greater time interval they considered (the Albian corresponds to ages between 100 and 113 Ma). However, the topographic changes are obvious, which result in the modification of the geomorphology of the coastline and, in turn, changes in the small drainage networks as inferred by Da Silva et al, (1999).

Changes in coastal and inland topography due to uplift driven by offshore sediment loading lead to geomorphological modifications that also result in the reorganization of the drainage systems. One example is the drainage system of Parnaíba do Sul in Brazil, where the lifting of the Serra do Mar coastal mountain ranges during the Late Cretaceous strongly affected the organization of the system and influenced the filling history of the Santos Basin, which was the most significant event in the stratigraphic evolution of this Basin throughout the Late Cretaceous and the Tertiary. During the Late Cretaceous - Paleocene, the sediment flow from the ancestral Parnaíba do Sul was concentrated in the Northern and Central portions of the Santos Basin. Millions of years later, in the Early Oligocene, there was a transgression and a sea level highstand, where

the ancestral Parnaíba do Sul changed direction, flowing into the Northern portion of the Campos Basin. This change in direction is reported as a thick sequence of marine shale that overlaps deltaic marine sands. (Modica & Brush, 2004).

CHAPTER VI

CONCLUSIONS

The main purpose of this research was to develop a flexural model of the South American continent, in order to contribute to the knowledge of the temporal evolution of its topography during the past 65 million years. The flexural response was calculated numerically using a spectral treatment of the equations, based on the spherical harmonics. The lithosphere was treated as a thin elastic plate having long-term rigidity. The corresponding flexural rigidity was determined using an elastic thickness of 40 km and 80 km in some cases (Quaternary and Pliocene). Based on the above, the main results stemming from our analysis of the flexural response of the South American continent and offshore margin due to marine sediment loading are as follows.

- The accumulation of offshore sediment loads induces the lifting of the continent that is known as forebulge. The existence of this forebulge is a unique consequence of the assumed long-term elastic strength of the lithosphere. It was observed that since the Quaternary and since the Pliocene, the South American continent is raised from 2 – 4 meters and 6-11 meters, respectively. These uplifts increase due to the greater sediment load deposited since the Miocene and Oligocene, with elevations between 21-25.5 m and 30 -37, meters respectively. Likewise, since the Eocene epoch the uplift increases with elevation to 60 meters. Finally, since the Paleocene, the continent experiences uplifting between 65 and 71 meters. The above values

are the representative of a continent-wide summary. The eastern portion of South America shows greater uplift of 4.54 [4.6] meters since the Quaternary , 11.46 [11.59] meters since the Pliocene , 32 meters since the Miocene , 44.95 meters since Oligocene, 68.15 meters since the Eocene and 79.28 meters since the Paleocene . In turn, certain areas of some countries such as Colombia, Venezuela , Guyana, French Guyana, Surinam , Brazil, Uruguay and Argentina exceed the values set forth above , these values can be observed in Tables 4.4, 4.5, and 4.7.

- The uplift experienced by the eastern part of South America contributes to an overall NE -SW tilt of the continent.
- The results of the flexural depression and of the forebulge obtained for the Quaternary period and the Pliocene epoch using an effective elastic thickness of 80 Km, differs little with the results obtained using an elastic thickness of 40 Km. The maps in the figures 4.27 and 4.28, as well as the values obtained from the flexural depression in offshore points show no significant change (see Appendix D and graphs 4.29 to 4.64). Likewise, the uplift in the continental interior at these times show that since the Quaternary, the continent was elevated 2.86-4.54 [2.87-4.59] meters and since the Pliocene 8-11.46 meters [6.91-11.59 meters]. With the above, it is evident that there is no significant difference using an elastic thickness of 80 km.
- In the Quaternary-to-Paleocene interval, the South American continent experienced cumulative (i.e. time-integrated) maximum flexural depressions and maximum uplifting or forebulges with the following values: since the Quaternary , the greatest flexural depression was -309.04 meters [-244.34 meters] which in turn induces a maximum uplift or forebulge of 11.93 meters [11.91 meters] . These values

increased since the Pliocene reaching flexural depressions of -825.85 meters [-652.08 meters] and inducing a forebulge of 31.51 meters [31.49 meters]. Since the Miocene, the flexural depression increases to -1725.42 meters and induces a forebulge of 64 meters. The flexural depression since the Oligocene increases to -1967.28 meters generating a forebulge of 84.56 meters. Since the Eocene, flexural depression reaches -2591.75 meters and generates a forebulge of 131.27 meters. Finally, since the Paleocene, the maximum flexural depression created is -2966.58 meters generating a maximum forebulge of 152.66 meters.

- The flexural depression experienced by the South American continent in the individual geological epochs comprised by Cenozoic Era shows the greatest flexural depression in the Miocene - Pliocene interval in zone I. The Pliocene - Quaternary and Miocene - Pliocene interval show a greater flexural depression in zone II. The Miocene - Pliocene and Eocene - Oligocene intervals show greatest flexural depression in zone III. And finally, in zone IV, the intervals that show a greater flexural depression are Oligocene - Miocene and Eocene - Oligocene. The values are summarized in the Appendix E.
- The above flexural depressions induce uplift in the continent of 1-4 meters in the Pliocene - Quaternary interval, and increases in the Miocene - Pliocene interval with 18-20 meters. The Oligocene - Miocene, Eocene - Oligocene and Paleocene - Eocene intervals are characterized by an uplift of 11-13 meters 20-23 meters and 10 meters respectively. Likewise, the eastern part of South America experienced uplift of 5-8 meters, 20-30 meters and 35 meters in the Pliocene - Quaternary, Miocene - Pliocene and Eocene - Oligocene intervals respectively. Some countries such as Venezuela, Brazil, Guyana, French Guyana, Surinam, Uruguay and Argentina, have higher uplift, which can be seen in Table 4.9.

- The Pliocene – Quaternary interval experiences a maximum flexural depression of -521.9 meters inducing a maximum forebulge of 19.58 meters. These values increase in the Miocene - Pliocene interval -1016.42 meters of flexural depression and inducing a maximum forebulge of 39.04 meters. During the Oligocene - Miocene interval, the flexural depression decreases reaching values of -712.93 meters and generating a forebulge of 30.86 m. In the Eocene – Oligocene interval, the flexural depression increases from the previous age interval, reaching a flexural depression of -831.52 meters and inducing a forebulge of 46.62 meters. Finally, during the Paleocene -Eocene interval, the flexural depression is lower compared to the previous age intervals, reaching values of -375.42 meters and generating a forebulge of 21.49 meters.
- The flexural depression, caused elevation changes in the coastline and in the mouth of Rivers. The results show that as a consequence of the sediment load transported by the Magdalena river, the mouth was depressed during the Miocene - Quaternary interval, with values of flexural depressions -173.13 meters in the Miocene, -62.55 [-59.91] meters in the Pliocene and -26.9 [-25.77] meters in the Quaternary. At the mouth of the Orinoco River (8.83°N, 61.83°W), the mouth was depressed -16.85 meters in the Miocene, -19.08 meters [-63.4 meters] in the Pliocene and -6.74 meters [-24.24 meters] in the Quaternary. At the mouth of the Amazon River (05°S, 51°W), the flexural depression is -10.3 meters in the Miocene, -9.09 [-18.34] meters in the Pliocene and -3.03 [-6.44] in the Quaternary. The confluence of the Uruguay -Paraná river is uplifted in the Miocene, Pliocene ($T_e = 80\text{Km}$) and Quaternary, with values of 0.31 meters, 6.42 meters and 0.95 [2.74] meters respectively. In the Pliocene ($T_e = 40\text{ Km}$) it experienced a minor flexural depression of -0.37 meters. Finally, in Mar del Plata (34.5°N, 58°W), the flexural depressions were -18.99

meters in the Miocene , -6.01 meters in the Pliocene and -0.54 meters in the Quaternary . The Quaternary Period and Pliocene epoch using an elastic thickness of 80 km, provided small uplifting of 1.8 meters and 2.86 meters respectively.

- The results show that in the Miocene - Pliocene and Pliocene - Quaternary intervals, the mouth of the Magdalena River experienced flexural depressions of -110.50 m and -35.65 m respectively. At the mouth of the Orinoco River (8.83°N, 61.83°W) there was a flexural depression of -12.35 m in the Pliocene - Quaternary interval , while in the Miocene - Pliocene interval it was 2.23 meters. The mouth of the Amazon River (0.5°S, 51°W) experienced an uplift in the Miocene - Pliocene interval of 10.1 meters and later in the Pliocene - Quaternary interval there was a flexural depression of -6.07 meters. At the confluence of the Uruguay - Paraguay Rivers in the Miocene - Pliocene interval there was a small uplift of 0.68 meters and later in the Pliocene – Quaternary there was a flexural depression of -1.32 meters. Finally in Mar del Plata, the Miocene - Pliocene and Pliocene - Quaternary intervals experienced flexural depressions of -12.99 m and -5.47 m respectively.
- This research shows that the forebulge generated in the continental area, caused by the Amazonian fan in the Miocene –Present time interval has a value of 34.41 meters. This result is in agreement with the previous estimates from Driscoll & Karner, 1994. But at the same time, at a nearby site (1.5°N, 52.5°W) the forebulge increases, with values of 50.23 meters in the Miocene, 22.85 meters in Pliocene and 8.75 meters in the Quaternary. Likewise , the flexural uplift due to the accumulation of sediments in the Sergipe- Alagoas basin , has a value of 103.23 meters in the Paleocene - Quaternary interval.

- The delivery of sediments from the continent to the ocean can be divided into two phases: the first, before the lifting of the Northern Andes, where the sediments come from the Shields of Brazil and Guyana, and are led by the rivers Orinoco and Amazonas to the north of the continent. The second phase, with the lifting of the northern Andes, in middle -Late Miocene (Hoorn, 1993), where the flow of sediments of the Orinoco and Amazon Rivers path changes eastward and the major sediment provenance are derived from the Andes.
- Part of the sediments that have been accumulated on the continental margin of South America come from river systems. According to Milliman & Syvitski (1992) the rivers are considered as the main channel that conducts the sediments towards the Coastal Ocean. In the same way, Milliman & Farnsworth, (2011) indicate that most of the sediments and particulate organic matter entering the ocean are transported by tropical rivers. Another important component that contributes to the transport and distribution of sediments are ocean currents. Factors such as winds, upwelling currents, eddy behavior, meandering processes and rotary currents are important elements that control the transport of material between the continental margin and the open sea, in the area where the oceanic current is flowing. (Pimienta et al 2005).
- The sediments that are found in the continental margins of South America are transported by the various rivers that make up the continent. First, the Magdalena River is a major vector for sediment transport into the Caribbean Sea. This river drains the three mountain ranges that make up Andes, so the provenance of the sediments come from this tectonic source in addition to the old craton (Figueiredo, 2009). Moreover, the Orinoco River traversing Venezuela and portions of Colombia, and the Amazon River traversing Brazil, both flow into the Atlantic Ocean. Sediments transported by the Orinoco River come from tributaries draining

the Guayana Shield, the orogenic belt of the Andes and the eastern plains of Colombia (Warne et al., 2002). While, sediments carried by the Amazonas river, have their main source in the Andes. The sediments that are carried by Rio de la Plata, come from runoff from Patagonia. Finally, the sediments deposited on the continental margin of Argentina come from Antarctic, and are carried by currents following along the continental shelf of this area. (Mahiques et al., 2008)

- As noted above, an important motivation for determining topography changes due to marine sediment loading is to assess their importance with respect to other processes that contribute to the overall evolution of the topography and bathymetry of the South American plate. One such process is the dynamic topography of Earth's solid surface driven by the convective circulation in the mantle (e.g. Moucha et al., 2008). What is the relative importance of these two different contributors to topography change? We can obtain an initial response to this fundamental question by considering recent calculations of the Cenozoic evolution of 3-D mantle structure using tomography-based, backward (i.e. time-reversed) convection simulations (Glišović & Forte, 2014).
- Convection-driven changes in the distribution of mantle buoyancy will directly lead to changes in the vertical stresses that maintain the dynamic topography of Earth's solid surface (e.g. Forte et al., 1993; Moucha et al., 2008). The most recent determinations of the Cenozoic evolution of mantle buoyancy distribution by Glišović & Forte (2014) allow us to quantify the rate-of-change of internally driven dynamic topography changes. The predicted dynamic topography change of South America over the past one million years is mapped in Figure 6.1. In this same figure, we also present the change of topography due to offshore sediment loads that accumulated during the Quaternary (i.e. over the past 2.5 Myr).

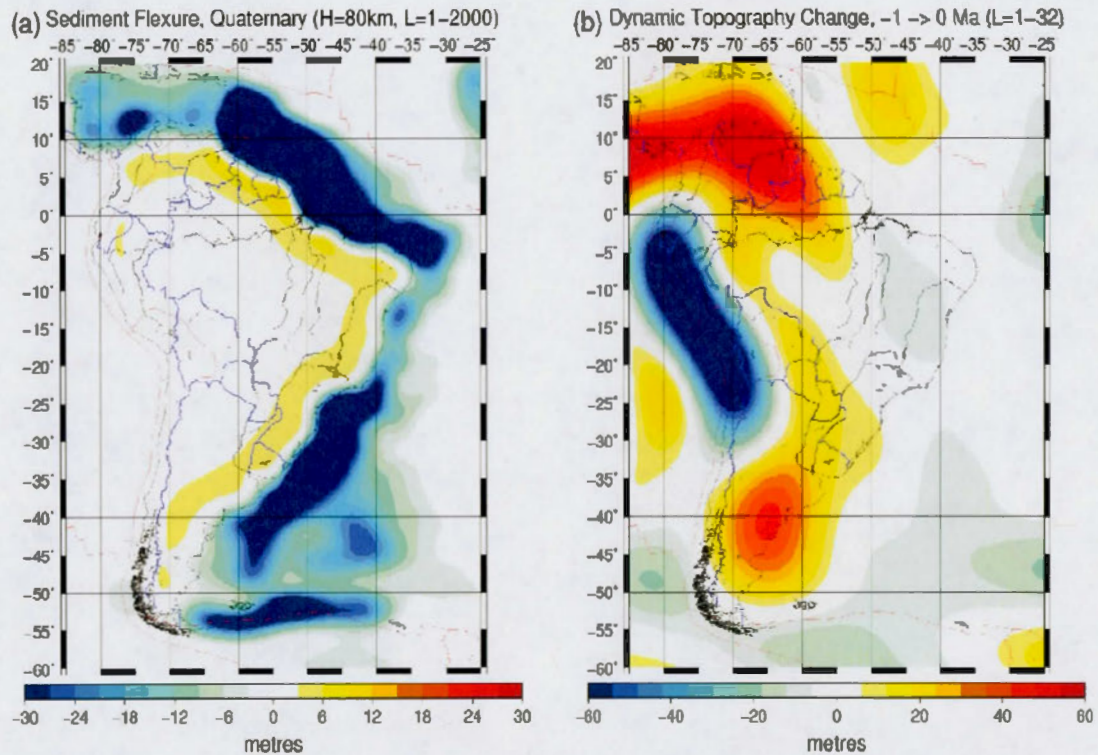


Figure 6.1 Contributions to the changing topography of South America. (a) Flexural topography induced by loading of marine sediments deposited during the Quaternary (i.e. the past 2.5 Myr). An elastic thickness of 80 km is assumed for this calculation. (See chapter 4 for more details.) (b) The dynamic topography change over the past 1 Myr predicted on the basis of a tomography-based backward convection simulation carried out by Glišović & Forte (2014). This time-reversed convection simulation employs a quasi-reversible (QRV) treatment of thermal diffusion, with mobile surface plates, and the topography change is calculated in the mantle frame of reference. (For more details, see Glišović & Forte, 2014.)

The contributions to South American topography change from surface sediment loading and internal convective forcing are complementary (Fig. 6.1). We first note that while dynamic topography changes dominate in the tectonically active western half of South America, the sediment-induced flexural changes dominate in the eastern half of the continent and along the Atlantic platform. We also note that the amplitudes of topography change over million-year time windows are also comparable. For example, the change in forebulge topography just north west of the Amazon delta is about 5 m/Myr and this is of the same order, or larger, than dynamic topography changes in the same region. Moreover, along most of the length of the Brazilian coast, it is the sediment-induced forebulge that dominates dynamic topography changes. These initial results thus show that an understanding of the changing topography of South America during the Cenozoic requires that we not only consider mantle convective forcing (i.e. dynamic topography) but also the important sediment-induced flexure of the plate.

APPENDIX A

SPHERICAL HARMONIC FUNCTIONS

Elastic flexure on a spherical surface can be greatly simplified in a spectral treatment based on spherical harmonic functions. The objective of a spherical harmonic analysis is to determine the harmonic coefficients of the measurements of a signal $f(\theta, \phi)$. These measurements vary with position θ and ϕ (colatitude and longitude respectively) and consist of values at discrete locations on a geographic grid (point data). As shown below a harmonic spherical expansion is analogous to a 2-D Fourier series.

Spherical harmonics functions are solutions of the Laplace equation in spherical coordinates, where the Laplace operator is defined in terms of three variables r , Θ , and Φ . The spherical harmonic solution of Laplace's equation outlined below follow Jackson (1962).

The equation of the Laplace operator in a system of spherical coordinates has the form:

$$\nabla^2 f = \frac{1}{r} \frac{\partial^2}{\partial r^2} (rf) + \frac{1}{r^2 \sin \theta} \frac{\partial}{\partial \theta} \left(\sin \theta \frac{\partial f}{\partial \theta} \right) + \frac{1}{r^2 \sin^2 \theta} \frac{\partial^2 f}{\partial \phi^2} \quad (\text{A.1})$$

The above expression can be rewritten as follows:

$$\nabla^2 f = \frac{1}{r} \frac{\partial^2}{\partial r^2} (rf) + \frac{\Lambda^2}{r^2} f \quad (\text{A.2})$$

Where $\frac{\Lambda^2}{r^2} f$ is the surface Laplacian defined as:

$$\frac{\Lambda^2}{r^2} f = \frac{1}{r^2 \sin \theta} \frac{\partial}{\partial \theta} \left(\sin \theta \frac{\partial f}{\partial \theta} \right) + \frac{1}{r^2 \sin^2 \theta} \frac{\partial^2 f}{\partial \varphi^2} \quad (\text{A.3})$$

As will be shown below, the spherical harmonic basis functions we seek have the fundamental property of being eigenfunctions of the surface Laplace operator:

$$\frac{\Lambda^2}{r^2} Y_l^m(\theta, \varphi) = -\frac{l(l+1)}{r^2} Y_l^m(\theta, \varphi) \quad (\text{A.4})$$

When comparing equation (3.7) with the equation for the 1-D Laplace operator

$$\frac{d^2}{dx^2} e^{i\kappa_n x} = -(\kappa_n)^2 e^{i\kappa_n x}. \text{ It is observed that the Cartesian wave number } \kappa_n \text{ is equivalent}$$

to the spherical wave number $\sqrt{l(l+1)}/r$. The above equivalence leads to the

deduction that horizontal wavelength λ_l of the spherical harmonic function $Y_l^m(\theta, \varphi)$

on a spherical surface of radius r is:

$$\lambda_l = \frac{2\pi r}{\sqrt{l(l+1)}} \approx \frac{2\pi r}{l + \frac{1}{2}} \quad \text{valid for } l \gg 1 \quad (\text{A.5})$$

6.0.0.1 Solving the Laplace Equation in Spherical Coordinates

Following the equations presented in Jackson (1962) and based on lecture notes prepared by Forte, we show how the solution of Laplace's equation in spherical coordinates naturally leads to the derivation of the spherical harmonic functions:

The spherical-geometry Laplace equation (Equation 3.4), has the form:

$$\nabla^2 f = \frac{1}{r} \frac{\partial^2}{\partial r^2} (rf) + \frac{1}{r^2 \sin \theta} \frac{\partial}{\partial \theta} \left(\sin \theta \frac{\partial f}{\partial \theta} \right) + \frac{1}{r^2 \sin^2 \theta} \frac{\partial^2 f}{\partial \phi^2}$$

Using the separation of variables method, we write:

$$f(r, \theta, \phi) = \frac{U(r)}{r} P(\theta) Q(\phi) \quad (\text{A.6})$$

The above expression is substituted in (3.4), yielding:

$$PQ \frac{d^2 U}{dr^2} + \frac{UQ}{r^2 \sin \theta} \frac{d}{d\theta} (\sin \theta) \frac{dP}{d\theta} + \frac{UP}{r^2 \sin^2 \theta} \frac{d^2 Q}{d\phi^2} = 0 \quad (\text{A.7})$$

By multiplying the above equation by $\frac{r^2 \sin \theta}{UPQ}$, we get:

$$r^2 \sin^2 \theta \left[\frac{1}{U} \frac{d^2 U}{dr^2} + \frac{1}{r^2 \sin \theta P} \frac{d}{d\theta} \left(\sin \theta \frac{dP}{d\theta} \right) \right] = - \frac{1}{Q} \frac{d^2 Q}{d\phi^2} \quad (\text{A.8})$$

We see that the term on the left depends only on r and Θ , while the term on the right depends only on Φ . Therefore, both terms of the equation have to be equal to a constant. Writing this constant as m^2 , we obtain:

$$-\frac{1}{Q} \frac{d^2 Q}{d\phi^2} = m^2$$

$$Q = e^{\pm im\phi}$$
(A.9)

In order for Q to be single-valued in the range $0 \leq \phi \leq 2\pi$, m must be an integer. Considering the above, we rewrite Equation (3.12) as follows:

$$\frac{1}{P \sin \theta} \frac{d}{d\theta} \left(\sin \theta \frac{dP}{d\theta} \right) - \frac{m^2}{\sin^2 \theta} = -\frac{r^2}{U} \frac{d^2 U}{dr^2}$$
(A.10)

In this equation, it is observed that the terms on the left depend only on Θ , while the terms on the right depend only on r . For this to be possible, both sides again have to be equal to a constant, which we write for convenience as $-l(l+1)$, where l can be any real number.

Considering the right side of the (3.13), we get:

$$-\frac{r^2}{U} \frac{d^2 U}{dr^2} = -l(l+1)$$

$$U(r) = Ar^{l+1} + Br^{-l}$$
(A.11)

Where A and B are any integration constants.

By substituting (3.14) in (3.13), we get:

$$\frac{1}{\sin \theta} \frac{d}{d\theta} \left(\sin \theta \frac{dP}{d\theta} \right) - \left[l(l+1) - \frac{m^2}{\sin^2 \theta} \right] P = 0 \quad (\text{A.12})$$

Expressing the dependence of P (θ) in terms of $x = \cos \theta$, the above equation is rewritten as:

$$\frac{d}{dx} \left[(1-x^2) \frac{dP}{dx} \right] + \left[l(l+1) - \frac{m^2}{1-x^2} \right] P = 0 \quad (\text{A.13})$$

This equation is known as the generalized Legendre equation and the solutions are called the "Associated Legendre functions". To solve this equation, P may be expanded in terms of a power series in x:

$$P(x) = (1-x^2)^{m/2} \sum_{n=0}^{\infty} a_n x^n \quad (\text{A.14})$$

The solution must be finite and, continuous in the interval $-1 \leq x \leq +1$ (corresponding to $0 \leq \theta \leq \pi$). By replacing the power series (Equation 3.17) into Equation 3.16, we get a recursion relation for a_n . It is found (proof not shown here) that the series diverge at $x = \pm 1$ unless l is a non-negative integer and $l \geq |m|$.

When $n > l - |m|$, then $a_n = 0$, which means that the power series truncates to a finite order polynomial at x. When $m=0$, the polynomial solutions are called "Legendre

polynomials" and are in the form of $P(x) \equiv P_l(x)$. These Legendre polynomials are represented in compact form as:

$$P_l(x) = \frac{1}{2^l} \frac{1}{l!} \frac{d^l}{dx^l} (x^2 - 1)^l \quad (\text{A.15})$$

Where the multiplicative factor dependent on l is just a normalization constant.

On the other hand, when $m \neq 0$, the polynomial solutions are called "Associated Legendre functions" expressed as: $P(x) \equiv P_l^m(x)$

These functions are represented in compact form by the formula:

$$P_l^m(x) = (-1)^m (1-x)^{m/2} \frac{d^m}{dx^m} P_l(x) \quad (\text{A.16})$$

When using Equation (3.18) to represent $P_l(x)$, for positive and negative values of m , we get:

$$P_l^m(x) = \frac{(-1)^m}{2^l l!} (1-x)^{m/2} \frac{d^{l+m}}{dx^{l+m}} (x^2 - 1)^l \quad (\text{A.17})$$

Since (3.16), depends on m^2 being an integer, then $P_l^m(x)$ and $P_l^{-m}(x)$ are proportional:

$$P_l^{-m}(x) = (-1)^m \frac{(l-m)!}{(l+m)!} P_l^m(x) \quad (\text{A.18})$$

For fixed values of m , $P_l^m(x)$ are orthogonal with respect to the index l , over the interval $-1 \leq x \leq +1$. The orthogonality relationship obtained is:

$$\int_{-1}^1 P_l^m(x) P_l^m(x) dx = \frac{2}{2l+1} \frac{(l+m)!}{(l-m)!} \delta_{ll} \quad (\text{A.19})$$

The Associated Legendre functions can be normalized as follows:

$$X_l^m(x) = \sqrt{2l+1} \sqrt{\frac{(l-m)!}{(l+m)!}} P_l^m(x) \quad (\text{A.20})$$

Such that,

$$\int_{-1}^1 X_l^m(x) X_l^m(x) dx = \delta_{ll} \quad (\text{A.21})$$

These functions $X_l^m(x)$ thus form an orthogonal set in index l over the interval $-1 \leq x \leq +1$ (i.e. $0 \leq \theta \leq \pi$).

Returning to function $Q_m(\phi) = e^{im\phi}$, it forms a complete set of orthogonal functions over the interval $0 \leq \phi \leq 2\pi$:

$$\frac{1}{2\pi} \int_0^{2\pi} Q_m(\phi) Q_m^*(\phi) d\phi = \delta_{m,m} \quad (\text{A.22})$$

Where * indicates complex conjugation.

Finally, by combining the complete (θ, ϕ) -dependence of the solution to the Laplace equation (Equation 3.9) in just one function, we obtain finally the “Spherical Harmonic” function:

$$Y_l^m(\theta, \phi) = X_l^m(\cos \theta) e^{im\phi} \quad (\text{A.23})$$

Where l is the harmonic degree and m is the azimuthal order, such that $|m| \leq l$. Spherical harmonic functions are widely used to represent and analyze physical phenomena that occur on the Earth's surface or within. Important applications include potential fields such as gravitation, geomagnetism and, in the current study, surface loads in flexural Earth models

APPENDIX B

DATABASE OF CENOZOIC SEDIMENT THICKNESS

Zone	Age	lat	lon	Thickness (m)	Site	Thickness high resolution	%	Penetration (mbsf)	Source
Zone I	Q	15.1042	-69.3641	41	149	932.25	4	390	Edgar, N. T. et al., (1973a)
		14.9433	-72.0271	18	31	1001	2	279	Bader, R. G. et al., (1970f)
		14.785	-69.3227	14	29	935.5	1	230	Bader, R. G. et al., (1970d)
		13.4187	-63.7208	120	148	1163	10	272	Edgar, N. T. et al., (1973b)
		12.882	-63.3833	128	30	1321.5	10	430	Bader, R. G. et al., (1970e)
		11.0852	-80.3791	80	154	2543.5	3	278	Edgar, N. T. et al., (1973e)
		11.0845	-80.3803	75	154A	2543.5	3	127	Edgar, N. T. et al., (1973e)
		15.1042	-69.3641	52	149	932.25	6	390	Edgar, N. T. et al., (1973a)
		14.9433	-72.0271	37	31	1001	4	279	Bader, R. G. et al., (1970f)
		14.785	-69.3227	22	29	935.5	2	230	Bader, R. G. et al., (1970d)
	P		14.5115	-69.3558	80	150	948.5	8	180
		13.9722	-72.4346	195	153	992.25	20	776	Edgar, N. T. et al., (1973d)
		13.4187	-63.7208	129	148	1163	11	272	Edgar, N. T. et al., (1973b)

	12.882	-63.3833	67	30	1321.5	5	430	Bader, R. G. et al., (1970e)
	11.0852	-80.3791	169	154	2543.5	7	278	Edgar, N. T. et al., (1973e)
	11.0845	-80.3803	97	154A	2543.5	4	127	Edgar, N. T. et al., (1973e)
	15.1165	-69.3778	128	146	932.25	14	762	Edgar, N. T. et al., (1973a)
	15.1042	-69.3641	130	149	932.25	14	390	Edgar, N. T. et al., (1973a)
	14.9433	-72.0271	66	31	1001	7	279	Bader, R. G. et al., (1970f)
	14.785	-69.3227	85	29	935.5	9	230	Bader, R. G. et al., (1970d)
	14.785	-69.3227	67	29B	935.5	7	231	Bader, R. G. et al., (1970d)
	14.5115	-69.3558	115	150	948.5	12	180	Edgar, N. T. et al., (1973c)
	13.9722	-72.4346	215	153	992.25	22	776	Edgar, N. T. et al., (1973d)
	12.882	-63.3833	64	30	1321.5	5	430	Bader, R. G. et al., (1970e)
	11.08516667	-80.3791	28	154	2543.5	1	278	Edgar, N. T. et al., (1973e)
	14.9433	-72.0271	9	31	1001	1	279	Bader, R. G. et al., (1970f)
	15.1165	-69.3778	25	146	932.25	3	762	Edgar, N. T. et al., (1973a)
	15.1042	-69.3641	47	149	932.25	5	390	Edgar, N. T. et al., (1973a)
	13.9721	-72.4346	140	153	992.25	14	776	Edgar, N. T. et al., (1973d)
	20.5865	-65.6221	286	28	343	83	404	Bader, R. G. et al., (1970c)
	15.1165	-69.3778	34	146	932.25	4	762	Edgar, N. T. et al., (1973a)
	15.1042	-69.3641	111	149	932.25	12	390	Edgar, N. T. et al., (1973a)
	14.785	-69.3227	113	29	935.5	12	230	Bader, R. G. et al., (1970d)
	14.785	-69.3227	107	29B	935.5	11	231	Bader, R. G. et al., (1970d)
	14.5115	-69.3558	30	150	948.5	3	180	Edgar, N. T. et al., (1973c)
	13.9722	-72.4346	25	153	992.25	3	776	Edgar, N. T. et al., (1973d)
Pa	15.1165	-69.3778	37	146	932.25	4	762	Edgar, N. T. et al., (1973a)

Zone
I.

	13.9722	-72.4346	25	153	992.25	3	776	Edgar, N. T. et al., (1973d)
	15.8565	-56.8793	21	27A	729	3	474.6	Bader, R. G. et al., (1970b)
	15.5398	-58.6412	30	1044	712.5	4	685	Shipboard Scientific Party, (1998). Site 1044
	15.5338	-58.6763	30	1048	857.25	3	337	Shipboard Scientific Party, (1998). Site 1048
	15.5305	-58.7032	65	1047	857.25	8	633	Shipboard Scientific Party, (1998). Site 1047
	15.5260	-58.7323	9.5	948C	857.25	1	592	Shipboard Scientific Party, (1995). Site 948
	15.5200	-58.7283	90	541	857.25	11	459	Biju-Duval, B. et al., (1984a)
	15.5200	-58.7133	88	542	857.25	10	240	Biju-Duval, B. et al., (1984b)
	9.2658	-54.5439	9.3	1260A	3901	0.2	491.9	Shipboard Scientific Party, (2004). Site 1260
	5.9763	-43.7397	51	929B	1210.5	4	229	Shipboard Scientific Party, (1995). Site 929
	5.9762	-43.7399	52	929A	1210.5	4	527.5	Shipboard Scientific Party, (1995). Site 929
	5.8992	-44.1963	75	354	775.25	10	886	Perch-Nielsen, K. et al., (1977a)
	5.4630	-44.4806	66	927C	828.25	8	358	Shipboard Scientific Party, (1995). Site 927
Zone	5.4629	-44.4806	66	927B	828.25	8	261.5	Shipboard Scientific Party, (1995). Site 927
II	5.4627	-44.4806	66	927A	828.25	8	312.5	Shipboard Scientific Party, (1995). Site 927
	5.4553	-43.7481	51	928A	822	6	246.7	Shipboard Scientific Party, (1995). Site 928
	5.45525	-43.7484	52	928C	822	6	181.5	Shipboard Scientific Party, (1995). Site 928
	5.4552	-43.7482	51	928B	822	6	531.9	Shipboard Scientific Party, (1995). Site 928
	4.2043	-43.4894	50	925D	699.5	7	354	Shipboard Scientific Party, (1995). Site 925
	4.2043	-43.4892	51	925C	699.5	7	360.1	Shipboard Scientific Party, (1995). Site 925
	4.2041	-43.4892	51	925B	699.5	7	318	Shipboard Scientific Party, (1995). Site 925
	3.7191	-42.9084	49	926B	892.5	5	605.8	Shipboard Scientific Party, (1995). Site 926
	3.7191	-42.9081	49	926A	892.5	5	327	Shipboard Scientific Party, (1995). Site 926
	3.7188	-42.9085	50	926C	892.5	6	398.3	Shipboard Scientific Party, (1995). Site 926

3.3692	-42.3915	367	142	957.5	38	626	Hayes, D. E. et al., (1972)
-6.1458	-31.0433	4.3	23	575.75	1	208	Bader, R. G. et al, (1970a)
15.5398	-58.6412	80	1044	712.5	11	685	Shipboard Scientific Party, (1998). Site 1044
15.8565	-56.8793	36	27A	729	5	474.6	Bader, R. G. et al., (1970b)
15.5338	-58.6763	80	1048	857.25	9	337	Shipboard Scientific Party, (1998). Site 1048
15.5305	-58.7032	85	1047	857.25	10	633	Shipboard Scientific Party, (1998). Site 1047
15.5200	-58.7283	105	541	857.25	12	459	Biju-Duval, B. et al., (1984a)
15.5200	-58.7133	138	542	857.25	16	240	Biju-Duval, B. et al., (1984b)
15.5196	-58.7134	183	542A	857.25	21	325.5	Biju-Duval, B. et al., (1984b)
5.9763	-43.7397	51	929B	1210.5	4	229	Shipboard Scientific Party, (1995). Site 929
5.9762	-43.7399	84	929A	1210.5	7	527.5	Shipboard Scientific Party, (1995). Site 929
5.9761	-43.7398	84	929C	1210.5	7	155.2	Shipboard Scientific Party, (1995). Site 929
5.8992	-44.1963	74	354	775.25	10	886	Perch-Nielsen, K. et al., (1977a)
5.4630	-44.4806	104	927C	828.25	13	358	Shipboard Scientific Party, (1995). Site 927
5.4629	-44.4806	104	927B	828.25	13	261.5	Shipboard Scientific Party, (1995). Site 927
5.4627	-44.4806	104	927A	828.25	13	312.5	Shipboard Scientific Party, (1995). Site 927
5.4553	-43.7481	90	928A	822	11	246.7	Shipboard Scientific Party, (1995). Site 928
5.4552	-43.7484	90	928C	822	11	181.5	Shipboard Scientific Party, (1995). Site 928
5.4552	-43.7482	90	928B	822	11	531.9	Shipboard Scientific Party, (1995). Site 928
4.2043	-43.4894	100	925D	699.5	14	354	Shipboard Scientific Party, (1995). Site 925
4.2043	-43.4892	100	925C	699.5	14	360.1	Shipboard Scientific Party, (1995). Site 925
4.2041	-43.4892	100	925B	699.5	14	318	Shipboard Scientific Party, (1995). Site 925
3.7191	-42.9085	96	926B	892.5	11	605.8	Shipboard Scientific Party, (1995). Site 926
3.7191	-42.9081	96	926A	892.5	11	327	Shipboard Scientific Party, (1995). Site 926

P

3.7188	-42.9085	96	926C	892.5	11	398.3	Shipboard Scientific Party, (1995). Site 926
3.3692	-42.3915	70	142	957.5	7	626	Hayes, D. E. et al., (1972)
-6.1458	-31.0433	3	23	575.75	0.5	208	Bader, R. G., et al., (1970a)
15.8565	-56.8793	105	27A	729	14	474.6	Bader, R. G., et al (1970)
15.5398	-58.6412	100	1044	712.5	14	685	Shipboard Scientific Party, (1998). Site 1044
15.5338	-58.6763	108	1048	857.25	13	337	Shipboard Scientific Party, (1998). Site 1048
15.5305	-58.7032	150	1047	857.25	17	633	Shipboard Scientific Party, (1998). Site 1047
9.4538	-54.3420	2.6	1257A	4177.25	0.1	284.7	Shipboard Scientific Party, (2004). Site 1257
9.4333	-54.7333	5	1258A	3264.25	0.2	447.5	Shipboard Scientific Party, (2004). Site 1260
9.43333	-54.7330	7	1258B	3264.25	0.2	460.9	Shipboard Scientific Party, (2004). Site 1260
9.2999	-54.1999	74	1259A	4264	2	558.8	Shipboard Scientific Party, (2004). Site 1259
5.9763	-43.7397	51	929B	1210.5	4	229	Shipboard Scientific Party, (1995). Site 929
5.9762	-43.7399	195	929A	1210.5	16	527.5	Shipboard Scientific Party, (1995). Site 929
5.8992	-44.1963	251	354	775.25	32	886	Perch-Nielsen, K. et al., (1977a)
4.2042	-43.4889	237	925A	699.5	34	930.4	Shipboard Scientific Party, (1995). Site 925
4.2041	-43.4892	168	925B	699.5	24	318	Shipboard Scientific Party, (1995). Site 925
3.7191	-42.9085	340	926B	892.5	38	605.8	Shipboard Scientific Party, (1995). Site 926
3.7191	-42.9081	180	926A	892.5	20	327	Shipboard Scientific Party, (1995). Site 926
3.7188	-42.9085	70	926C	892.5	8	398.3	Shipboard Scientific Party, (1995). Site 926
3.3692	-42.3915	125	142	957.5	13	626	Hayes, D. E. et al., (1972)
5.4630	-44.4806	96	927C	828.25	12	358	Shipboard Scientific Party, (1995). Site 927
5.4629	-44.4806	91	927B	828.25	11	261.5	Shipboard Scientific Party, (1995). Site 927
5.4627	-44.4806	142	927A	828.25	17	312.5	Shipboard Scientific Party, (1995). Site 927
5.45522	-43.7482	208	928B	822	25	531.9	Shipboard Scientific Party, (1995). Site 928

M

Zone II	15.8565	-56.8793	221	27A	729	30	474.6	Bader, R. G., et al., (1970b)
	15.5398	-58.6412	150	1044	712.5	21	685	Shipboard Scientific Party, (1998). Site 1044
	9.4538	-54.3420	29	1257A	4177.25	1	284.7	Shipboard Scientific Party, (2004). Site 1257
	9.4536	-54.3418	5	1257B	4177.25	0.1	225.7	Shipboard Scientific Party, (2004). Site 1257
	9.3008	-54.1991	10	1259B	4264	0.2	556.2	Shipboard Scientific Party, (2004). Site 1259
	9.2999	-54.1999	44	1259A	4264	1	558.8	Shipboard Scientific Party, (2004). Site 1259
	9.2658	-54.5439	19	1260A	3901	0.5	491.9	Shipboard Scientific Party, (2004). Site 1260
	5.9762	-43.7399	199	929A	1210.5	16	527.5	Shipboard Scientific Party, (1995). Site 929
	5.9761	-43.7400	20	929E	1210.5	2	808.9	Shipboard Scientific Party, (1995). Site 929
	5.8992	-44.1963	215	354	775.25	28	886	Perch-Nielsen, K.et al., (1977a)
	15.8565	-56.8793	92.6	27A	729	13	474.6	Bader, R. G., et al., (1970b)
	9.4538	-54.3420	42	1257A	4177.25	1	284.7	Shipboard Scientific Party, (2004). Site 1257
	9.4536	-54.3418	44	1257B	4177.25	1	225.7	Shipboard Scientific Party, (2004). Site 1257
	9.4534	-54.3416	9.6	1257C	4177.25	0.2	234.17	Shipboard Scientific Party, (2004). Site 1257
	9.4333	-54.7333	168	1258A	3264.25	5	447.5	Shipboard Scientific Party, (2004). Site 1258
9.43333	-54.7330	162	1258B	3264.25	5	460.9	Shipboard Scientific Party, (2004). Site 1258	
9.4333	-54.7328	58	1258C	3264.25	2	485	Shipboard Scientific Party, (2004). Site 1258	
9.3008	-54.1991	63	1259B	4264	1	556.2	Shipboard Scientific Party, (2004). Site 1259	
9.3004	-54.1995	56	1259C	4264	1	533.7	Shipboard Scientific Party, (2004). Site 1259	
9.2658	-54.5439	245	1260A	3901	6	491.9	Shipboard Scientific Party, (2004). Site 1260	
9.2655	-54.5442	137	1260B	3901	4	509	Shipboard Scientific Party, (2004). Site 1260	
5.9761	-43.7400	318	929E	1210.5	26	808.9	Shipboard Scientific Party, (1995). Site 929	
5.8992	-44.1963	205	354	775.25	26	886	Perch-Nielsen, K.et al., (1977a)	
9.4538	-54.3420	67	1257A	4177.25	2	284.7	Shipboard Scientific Party, (2004). Site 1257	

	9.4536	-54.3418	62	1257B	4177.25	1	225.7	Shipboard Scientific Party, (2004). Site 1257
	9.4534	-54.3416	42	1257C	4177.25	1	234.17	Shipboard Scientific Party, (2004). Site 1257
	9.4333	-54.7333	82	1258A	3264.25	3	447.5	Shipboard Scientific Party, (2004). Site 1258
	9.4333	-54.7330	77	1258B	3264.25	2	460.9	Shipboard Scientific Party, (2004). Site 1258
	9.4333	-54.7328	38	1258C	3264.25	1	485	Shipboard Scientific Party, (2004). Site 1258
Pa	9.3008	-54.1991	39	1259B	4264	1	556.2	Shipboard Scientific Party, (2004). Site 1259
	9.3004	-54.1995	19	1259C	4264	0.4	553.7	Shipboard Scientific Party, (2004). Site 1259
	9.2999	-54.1999	96	1259A	4264	2	558.8	Shipboard Scientific Party, (2004). Site 1259
	9.2658	-54.5439	63	1260A	3901	2	491.9	Shipboard Scientific Party, (2004). Site 1260
	9.2655	-54.5442	58	1260B	3901	1	509	Shipboard Scientific Party, (2004). Site 1260
	5.8992	-44.1963	25	354	775.25	3	886	Perch-Nielsen, K. et al., (1977a)
	-37.6552	-35.9637	50	358	926.75	5	842	Perch-Nielsen, K. et al., (1977e)
	-30.005	-35.2520	9.1	22	541.75	2	242.2	Maxwell, A. E. et al., (1970)
	-30.0041	-35.55998	28	357	754.25	4	797	Perch-Nielsen, K. et al., (1977d)
Q	-30.2765	-35.2850	11	516	587.75	2	182.3	Baker, P. F., et al., (1983b)
	-26.385	-36.5028	41	515A	1278.75	3	107.9	Baker, P. F., et al., (1983a)
	-37.85	-55.25	20	PIA	4980	0.4	2500	Violante et al., (2010)
	-15.7098	-30.6005	80	355	443	18	460	Perch-Nielsen, K. et al., (1977b)
	-37.6552	-35.9637	50	358	926.75	5	842	Perch-Nielsen, K. et al., (1977e)
	-30.2765	-35.2850	40	516	587.75	7	193	Baker, P. F., et al., (1983b)
P	-28.2870	-41.0880	38	356	940.25	4	741	Perch-Nielsen, K. et al., (1977c)
	-37.85	-55.25	400	PIA	4980	8	2500	Violante et al., (2010)
	-37.2	-56	200	Samar Dx-1	4326	5	3200	Violante et al., (2010)
	-26.2387	-36.5032	19	515B	1278.75	1	636.4	Baker, P. F., et al., (1983a)

	-37.6552	-35.9637	308	358	926.75	33	842	Perch-Nielsen, K.et al., (1977e)
	-30.2765	-35.2850	131	516	587.75	22	182.3	Baker, P. F., et al., (1983b)
	-30.2765	-35.2850	76	516F	587.75	13	1271	Baker, P. F., et al., (1983b)
	-30.005	-35.2520	96	22	541.75	18	242.2	Maxwell, A. E. et al., (1970)
	-30.0041	-35.55998	155	357	754.25	21	797	Perch-Nielsen, K.et al., (1977d)
	-28.2870	-41.0880	77	356	940.25	8	741	Perch-Nielsen, K.et al., (1977c)
M	-26.2387	-36.5032	304	515B	1278.75	24	636.4	Baker, P. F., et al., (1983a)
	-15.7098	-30.6005	110	355	443	25	460	Perch-Nielsen, K.et al., (1977b)
	-37.85	-55.25	500	PIA	4980	10	2500	Violante et al., (2010)
	-21.5	-40	1000	Campos	2778	36	2778	Contreras J. et al., (2010)
	-25.5	-47	722	Santos	3867	19	3867	Contreras J. et al., (2010)
	-31.5	-50	900	Pelotas	4851	19	4851	Contreras J. et al., (2010)
	-37.2	-56	993	Samar Dx-1	4326	23	3200	Violante et al., (2010)
Zone	-37.6552	-35.9637	230	358	926.75	25	842	Perch-Nielsen, K.et al., (1977e)
III.	-30.2765	-35.2850	285	516F	587.75	48	1271	Baker, P. F., et al., (1983b)
	-30.005	-35.2520	55	22	541.75	10	242.2	Maxwell, A. E. et al., (1970)
	-30.0041	-35.55998	141	357	754.25	19	797	Perch-Nielsen, K.et al., (1977d)
	-37.2	-56	91	Samar Dx-1	4326	2	3200	Violante et al., (2010)
	-21.5	-40	1000	Campos	2778	36	2778	Contreras J. et al., (2010)
	-25.5	-47	600	Santos	3867	16	3867	Contreras J. et al., (2010)
	-31.5	-50	400	Pelotas	4851	8	4851	Contreras J. et al., (2010)
	-26.2387	-36.5032	200	515B	1278.75	16	636.4	Baker, P. F., et al., (1983a)
	-37.6552	-35.9637	28	358	926.75	3	842	Perch-Nielsen, K.et al., (1977e)

	-30.2765	-35.2850	371	516F	587.75	63	1271	Baker, P. F., et al., (1983b)
	-30.0041	-35.55998	86	357	754.25	11	797	Perch-Nielsen, K. et al., (1977d)
	-28.2870	-41.0880	180	356	940.25	19	741	Perch-Nielsen, K. et al., (1977c)
	-26.2387	-36.5032	19	515B	1278.75	1	636.4	Baker, P. F., et al., (1983a)
E	-37.2	-56	347	Samar Dx-1	4326	8	3200	Violante et al., (2010)
	-37.85	-55.25	200	PIA	4980	4	2500	Violante et al., (2010)
	-21.5	-40	1400	Campos	2778	50	2778	Contreras J. et al., (2010)
	-25.5	-47	1200	Santos	3867	31	3867	Contreras J. et al., (2010)
	-31.5	-50	1000	Pelotas	4851	21	4851	Contreras J. et al., (2010)
	-15.7098	-30.6005	200	355	443	45	460	Perch-Nielsen, K. et al., (1977b)
	-37.6552	-35.9637	49	358	926.75	5	842	Perch-Nielsen, K. et al., (1977e)
	-30.2765	-35.2850	57	516F	587.75	10	1271	Baker, P. F., et al., (1983b)
	-30.0041	-35.55998	50	357	754.25	7	797	Perch-Nielsen, K. et al., (1977d)
	-28.2870	-41.0880	126	356	940.25	13	741	Perch-Nielsen, K. et al., (1977c)
Pa	-37.2	-56	428	Samar Dx-1	4326	10	3200	Violante et al., (2010)
	-37.85	-55.25	600	PIA	4980	12	2500	Violante et al., (2010)
	-21.5	-40	290	Campos	2778	10	2778	Contreras J. et al., (2010)
	-25.5	-47	60	Santos	3867	2	3867	Contreras J. et al., (2010)
	-15.7098	-30.6005	9	355	443	2	460	Perch-Nielsen, K. et al., (1977b)
	-51.5423	-30.6770	18	699A	601	3	518.1	Shipboard Scientific Party, (1988). Site 699
	-50.8713	-46.7836	9	327A	3028.25	0.3	469.5	Barker, P. F., et al., (1977a)
	-50.6552	-46.0955	5	329	1359	0.3	464.5	Barker, P. F., et al., (1977c)
Q	-49.8112	-36.6588	10	328A	199	5	397	Barker, P. F., et al., (1977b)

P	-51.5423	-30.6770	43	699A	601	7	518.1	Shipboard Scientific Party, (1988). Site 699
	-51.4585	-33.0993	4	698	575.75	1	237	Shipboard Scientific Party, (1988). Site 698
	-49.8112	-36.6588	10	328B	199	5	397	Barker, P. F., et al., (1977b)
M	-51.5423	-30.6770	31	699A	601	5	518.1	Shipboard Scientific Party, (1988). Site 699
	-50.6552	-46.0955	266	329	1359	20	464.5	Barker, P. F., et al., (1977c)
	-49.8112	-36.6588	19	328	199	10	397	Barker, P. F., et al., (1977b)
	-49.8112	-36.6588	9.5	328B	199	5	471	Barker, P. F., et al., (1977b)
O	-51.5423	-30.6770	215	699A	601	36	518.1	Shipboard Scientific Party, 1988. Site 699
	-51.0047	-46.9717	150	511	2981.5	5	632	Ludwig, W. J. et al., (1983)
	-50.6552	-46.0955	70	329	1359	5	464.5	Barker, P. F., et al., (1977c)
	-49.8112	-36.6588	19	328B	199	10	471	Barker, P. F., et al., (1977b)
	-51.5423	-30.6770	193	699A	601	32	518.1	Shipboard Scientific Party, (1988). Site 699
E	-51.5329	-30.2781	202	700B	602	34	489	Shipboard Scientific Party, (1988). Site 700
	-51.4585	-33.0993	48	698	575.75	8	237	Shipboard Scientific Party, (1988). Site 698
	-50.8713	-46.7836	10	327A	3028.25	0.3	469.5	Barker, P. F., et al., (1977a)
	-50.6552	-46.0955	10	329	1359	1	464.5	Barker, P. F., et al., (1977c)
	-49.8112	-36.6588	19	328	199	10	397	Barker, P. F., et al., (1977b)
	-49.8112	-36.6588	19	328B	199	10	471	Barker, P. F., et al., (1977b)
	-51.5329	-30.2781	98	700B	602	16	489	Shipboard Scientific Party, (1988). Site 700
Pa	-51.4585	-33.0993	67	698	575.5	12	237	Shipboard Scientific Party, (1988). Site 698
	-50.8713	-46.7836	48	327A	3028.25	2	469.5	Barker, P. F., et al., (1977a)
	-49.8112	-36.6588	10	328	199	5	397	Barker, P. F., et al., (1977b)

Zone
IV.

APPENDIX C

FORTRAN ALGORITHM TO CALCULATE LITHOSPHERIC FLEXURE

```
c   Calculates the Elastic-Flexure topography
c
  implicit real*8 (a-h,o-z)
  parameter (lmax = 2048)
  parameter (nharm = (lmax+1)*lmax-(lmax**2+lmax)/2 +lmax+2)
  character*80 name
  complex*16 vmn(nharm)
  data vmn/nharm*(0.d0,0.d0)/
c
  mn(m,n) = (lmax+1)*m-(m*m+m)/2+n+1
c
  write(6,*)
& 'harmonic coefficient file with normalized sediment thickness = '
  read(5,'(a)') name
  open(10,file=name)
  print *, 'max harmonic degree in file = '
  read *, lmx
  do 1 m=0,lmx
  do 1 n=m,lmx,2
  k1=mn(m,n)
  k2=k1+1
```

```

read(10,*) cr1,ci1,cr2,ci2
vmn(k1) = dcplx( cr1, ci1 )
vmn(k2) = dcplx( cr2, ci2 )
1 continue
close(10)
c
! zero out L = 0
vmn(1) = 0.d0
c
c Elastic parameters (from Pazzaglia & Gardner 1994]
c
print *,'elastic lithosphere thickness [in km] = ?'
read *, h
h = h * 1.d3 ! convert to meters
E = 70.d9 !Pascals
v = 0.25d0 ! Poisson's ratio
D = E * h**3 / 12.d0 / (1.d0 - v**2) ! flexural rigidity
! print *,'average sediment density [in gm/cm**3] = ?'
! read *, den_sed
! den_sed = 2.d0
! density of sea water
den_wat = 1030.d0 ! kg/m^3
! density of lithospheric mantle
den_man = 3200.d0 ! kg/m^3
g = 9.82d0 ! mean surface gravity
r_e = 6368.d3 ! mean solid-surface radius
beta = D / ( g * r_e**4 * (den_man - den_wat) )

```

```

c
! apply flexure filter
!   fac = (den_sed - den_wat)/(den_man - den_wat)
      fac = 1.d0
      do l = 1, lmx
!*****
! Using the following causes an integer overflow error for l > 214
!   fl4 = l*(l+1) * l*(l+1)
!*****

      fl = dble(l)
      fl4 = (fl*(fl+1.d0))**2
      denom = fl4 * beta + 1.d0
      filt = -fac / denom
      do m = 0, 1
        k = mn(m,l)
        vmn(k) = filt * vmn(k)
      enddo
    enddo

c   write(6,*) 'output file = '
      read(5,'(a)') name
      open(11,file=name)
      do 30 m=0, lmx
        do 31 n=m, lmx ,2
          k1=mn(m,n)
          k2=k1+1

31 write(11,32) vmn(k1),vmn(k2)
32 format(e14.7,1x,e14.7,4x,e14.7,1x,e14.7)
30 continue

      Stop end

```

APPENDIX D

FLEXURAL TOPOGRAPHY OF SOUTH AMERICA CONTINENT CUMULATIVE SINCE THE PALEOCENE

Zone	Offshore point	Coordinates		Flexure (m)		Flexure (m)		Flexure (m)		Flexure (m)		Flexure (m)		Flexure (m)	
		Latitude	Longitude	Quaternary		Pliocene		Miocene	Oligocene	Eocene	Paleocene	Miocene	Oligocene	Eocene	Paleocene
				Te 40 km	Te 80 km	Te 40 km	Te 80 km								
Zone I	Barracuda A.P	16.5°N	59°W	-27,35	-33,68	-67,4	-83,75	-148,59	-159,62	-160,33	-173,28	-148,59	-159,62	-160,33	-173,28
	Cayos	16°N	80°W	-19,46	-17,58	-45,19	-40,85	-123,62	-133,77	-133,55	-145,36	-123,62	-133,77	-133,55	-145,36
		15°N	81°W	-16,64	-17,93	-38,58	-41,64	-104,81	-112,15	-109,14	-118,14	-104,81	-112,15	-109,14	-118,14
		16°N	74°W	-9,14	-11,29	-21,11	-26,18	-54,84	-54,69	-44,21	-45,73	-54,84	-54,69	-44,21	-45,73
	Colombia	14.5°N	74°W	-15,06	-19,85	-34,92	-46,12	-94,26	-100,02	-95,41	-102,84	-94,26	-100,02	-95,41	-102,84
		13°N	74°W	-42,79	-33,29	-99,64	-77,46	-279,19	-312,88	-335,76	-370,91	-279,19	-312,88	-335,76	-370,91
	Magdalena Delta	11.5°N	75.5°W	-50	-36,16	-116,46	-84,14	-327,16	-367,74	-397,74	-439,99	-327,16	-367,74	-397,74	-439,99
		13°N	65°W	-23,29	-19,72	-54,2	-44,94	-148,86	-162,76	-166,24	-181,82	-148,86	-162,76	-166,24	-181,82
	Venezuela	12°N	67°W	-22,41	-20,08	-52,06	-46,58	-143,26	-156,37	-159,07	-173,85	-143,26	-156,37	-159,07	-173,85
		14.5°N	62°W	-17,22	-34,28	-38,79	-78,71	-112,81	-121,78	-120,37	-131,07	-112,81	-121,78	-120,37	-131,07
Grenada	11.5°N	62.5°W	-48,82	-38,23	-53,54	-89,15	-159,13	-175,25	-181,49	-199,29	-159,13	-175,25	-181,49	-199,29	

Tobago	12.5°N	60°W	-204,39	-181,88	-494,03	-455,76	-1397,72	-1616,7	-1825,76	-2047,39
Demerara	11°N	56°W	-123,41	-141,08	-336,43	-384,55	-487,21	-517,37	-537,42	-570,13
Abysal Plain	13°N	57°W	-119,67	-139,59	-328,33	-376,75	-473,52	-503,35	-523,15	-555,43
Marin Guajira	12°N	73°W	-26,71	-24,78	-61,65	-57,6	-170,65	-187,86	-194,64	-213,52
Marin Sinú	10.5°N	76°W	-33,39	-26,2	-77,66	-60,86	-216,62	-240,93	-255,12	-281,05
Cariaco	10.5°N	65°W	-17,24	-9,48	-40,04	-20,95	-108,73	-116,54	-113,83	-123,32
Guyana	9.5°N	57°W	-161,27	-165,99	-439,49	-451,35	-644,66	-688,76	-723,04	-770,61
Surinam	8°N	58°W	-78,54	-93,88	-214,62	-256	-303,49	-317,86	-321,68	-337,67
French Guyana	8°N	55°W	-171,88	-140,99	-467,36	-383,91	-703,67	-759,8	-807,97	-871,27
Amazonas	7°N	56°W	-105,88	-93,2	-288,22	-254,18	-427,09	-455,91	-475,38	-508,07
Delta	7°N	52°W	-149,38	-137,84	-406,33	-374,98	-604,73	-646,63	-678,23	-722,34
Brazil	5.5°N	52.5°W	-81,43	-91,09	-221,91	-248,09	-322,84	-340,3	-347,4	-366,8
Ceara	1°N	49.5°W	-101,8	-100,27	-277,18	-273,04	-408,06	-433,68	-449,17	-477,1
Potigar	1°S	46°W	-42,59	-50,86	-116,47	-138,92	-163,06	-167,06	-160,63	-166,23
Pernambuco	3°S	40°W	-53,17	-47,72	-145,18	-130,41	-206,91	-214,74	-212,15	-221,63
Alagoas	2°S	43°W	-119,14	-79,84	-324,23	-217,56	-480,19	-511,57	-532,63	-567,68
Sergipe	2°S	41°W	-118,66	-79,72	-322,95	-217,27	-478,24	-509,45	-530,27	-563,61
Bahia Sul	2.5°S	37.5°W	-27,77	-36,11	-76,27	-98,87	-101,74	-100,52	-88,88	-89,33
Espiritu Santo	3°S	37°W	-43,68	-40,93	-119,43	-111,88	-167,65	-172,13	-166,22	-172,35
Campos	4°S	36°W	-60,86	-48,02	-167,33	-130,89	-240,54	-251,15	-251,31	-263,66
	4°S	37°W	-54,9	-39,24	-149,88	-107,13	-214,11	-222,59	-220,66	-230,8
	8° S	34° W	-10,89	-13,87	-42,99	-49,32	-134,12	-201,28	-271,75	-303,5
	8° S	33° W	-15,76	-18,01	-60,69	-63,79	-190,91	-286,46	-390,42	-437,42
	11° S	37.5° W	-7,34	-8,82	-31,86	-37,85	-107,22	-164,26	-243,85	-284,08
	11° S	36.5° W	-20,07	-14,44	-80,18	-59,43	-272,51	-415,98	-611,78	-707,7
	12° S	35° W	-20,77	-18,44	-82,86	-74,35	-281,76	-430,08	-599,72	-677,9
	13° S	37° W	-31,7	-24,28	-124,45	-96,19	-424,13	-646,98	-930,33	1078,13
	17° S	38.5° W	-11,98	-11,86	-49,51	-49,03	-167,85	-256,2	-350,91	-392,99
	16.5° S	38° W	-15,79	-14,32	-63,98	-58,4	-217,34	-331,63	-456,28	-511,77
	21.5° S	41° W	-15,94	-16,67	-64,53	-67,32	-219,17	-345,88	-506,44	-589,31

Zone
IIZone
III

	22° S	40° W	-39,36	-27,39	-153,52	-108,05	-523,63	-844,21	-1270,67	-1472,78
	23° S	41° W	-31,73	-28,21	-124,55	-111,18	-424,32	-677,8	-1014,68	-1173,66
Santos	25.5° S	48° W	-25,44	-23,45	-100,65	-93,09	-342,68	-538,5	-810,6	-934,69
	26° S	46° W	-66,35	-52,41	-256,08	-203,12	-886,91	-1469,42	-2191,76	-2516,39
	27° S	46° W	-57,69	-52,65	-222,44	-204,05	-762,95	-1249,38	-1888,14	-2175,13
	32.5° S	51° W	-48,96	-41,8	-182,49	-162,83	-648,92	-1069,6	-1564,39	-1790,88
Pelotas	33° S	51° W	-57,85	-48,49	-223,8	-188,23	-800,59	-1324,34	-1939,78	-2222,66
Punta del Este	35.5° S	53° W	-30,66	-36,41	-120,24	-142,33	-416,98	-669,78	-970,49	-1118,43
	37.5° S	57° W	-19,85	-18,91	-79,37	-75,83	-269,9	-442,17	-659,02	-758,15
Salado	38° S	55° W	-52,52	-41,12	-203,65	-160,22	-695,05	-1140,69	-1711,29	1960,7
	40° S	61° W	-26,1	-17,9	-103,18	-71,98	-351,41	-536,14	-765,33	-877,68
Colorado	41° S	59° W	-33,96	-29,92	-133,04	-117,66	-453,57	-691,32	-1018,08	-1173,91
Rawson	43.5° S	60° W	-16,77	-21,45	-67,79	-85,43	-229,97	-351,31	-485,46	-545,48
	46° S	65° W	-10,53	-7,47	-43,81	-32,33	-148,72	-227,49	-312,59	-350,52
San Jorge	47° S	66° W	-9,44	-5,61	-39,37	-43,79	-134,33	-205,65	-282,66	-316,97
	49.5° S	64° W	-4,52	-4,84	-20,4	-20,69	-65,32	-100,48	-133,69	-147,94
San Julian	43° S	52° W	-7,65	-11,27	-33,03	-46,72	-111,42	-170,78	-230,23	-255,94
	41.5° S	43.5° W	-28,1	-24,93	-110,92	-98,78	-377,84	-576,43	-812,3	-952,5
Argentina	47° S	46° W	-18,26	-16,03	-73,66	-66,29	-251,65	-384,25	-531,64	-597,41
Northern	50.5° S	59.5° W	-1,32	-7,38	-7,45	-26,56	-17,75	-28,07	-34,06	-36,27
Falkland	49.5° S	59° W	-13,55	-12,17	-54,82	-49,06	-183,39	-280,53	-404,04	-462,25
Eastern	52.5° S	50° W	-43,68	-36,05	-113,95	-93,63	-150,54	-230,87	-375,29	-420,35
Falkland	52° S	55° W	-48,03	-37,48	-125,08	-97,48	-165,21	-253,25	-412,38	-462,08
Western	52.5° S	65° W	-27,1	-20,4	-70,83	-53,34	-87,17	-134,16	-218,67	-243,71
Falkland	53° S	60° W	-21,5	-25,87	-56,27	-67,14	-65,96	-101,79	-166,21	-184,66
	53° S	62° W	-29,42	-26,64	-76,87	-69,2	-96,33	-148,14	-241,23	-269,18
Southern	54° S	55° W	-34,17	-29,36	-79,54	-76,43	-101,24	-155,62	-252,78	-282,23
Falkland										

Zone
IV

APPENDIX E

FLEXURAL TOPOGRAPHY DURING THE CENOZOIC EPOCH

Zone	Offshore point	Coordinates		Flexure (m)						
		Latitude	Longitude	Pliocene- Quaternary	Miocene - Pliocene	Oligocene - Miocene	Eocene - Oligocene	Eocene - Eocene	Paleocene - Eocene	
Zone I	Barracuda	16.5°N	59°W	-40,06	-81,19	-11,03	-0,71	-12,96		
	A.P Cayos	16°N	80°W	-25,73	-78,43	-10,15	0.22*	-11,81		
		15°N	81°W	-21,95	-66,23	-7,35	3.02*	-9		
	Colombia	16°N	74°W	-11,96	-33,73	0.14*	10.48*	-1,52		
		14.5°N	74°W	-19,86	-59,34	-5,76	4.61*	-7,43		
		13°N	74°W	-56,85	-179,55	-33,49	-23,08	-35,15		
	Delta Magdalena	11.5°N	75.5°W	-66,46	-210,7	-40,57	-30	-42,25		
	Venezuela	13°N	65°W	-30,91	-94,65	-13,91	-3,48	-15,68		
		14°N	66°W	-34,13	-105,8	-16,47	-6,08	-18,15		

	12°N	67°W	-29,65	-91,21	-13,11	-2,7	-14,77
Grenada	14.5°N	62°W	-21,57	-74,02	-8,97	1.42*	-10,7
	11.5°N	62.5°W	-29,64	-105,58	-16,12	-6,24	-15,68
Tobago	12.5°N	60°W	-289,64	-903,69	-218,98	-209,06	-221,63
Demerara Abyssal Plain	11°N	56°W	-213,01	-150,78	-30,16	-20,06	-32,71
	13°N	57°W	-208,67	-145,18	-29,83	-19,8	-32,27
Marin Guajira	12°N	73°W	-35,14	-108,99	-17,21	-6,79	-18,88
Marin Sinú	10.5°N	76°W	-44,27	-138,96	-24,31	-14,19	-25,93
Cariaco	10.5°N	65°W	-22,8	-68,69	-7,81	2.71*	-9,48
Zone II	9.5°N	57°W	-278,21	-205,18	-44,09	-34,28	-47,57
Guyana	8°N	58°W	-136,07	-88,88	-14,36	-3,82	-15,99
Surinami	8°N	55°W	-295,48	-236,31	-56,13	-48,17	-63,6
	7°N	56°W	-182,34	-138,87	-28,82	-19,47	-32,69
French Guayana	7°N	52°W	-256,95	-198,4	-41,9	-31,62	-44,11
	5.5°N	52.5°W	-140,47	-100,94	-17,46	-7,1	-19,39
Amazonas Delta	1°N	49.5°W	-175,38	-130,88	-25,62	-15,49	-27,93
Brazil	1°S	46°W	-73,88	-46,59	-4	6.42*	-5,6
	3°S	40°W	-92,01	-61,73	-7,82	2.59*	-9,48
	2°S	43°W	-205,09	-155,96	-31,39	10.01*	-35,05
	2.5°S	42°W	-187,74	-141,5	-27,77	-17,43	-31,58
Ceara	2°S	41°W	-204,28	-155,29	-31,21	-20,83	-33,33
Potigar	2.5°S	37.5°W	-48,5	-25,47	1.22*	11.64*	-0,44
	3°S	37°W	-75,5	-48,22	-4,49	5.92*	-6,13
	4°S	36°W	-105,99	-73,22	-10,61	-0,16	-12,35
	4°S	37°W	-94,97	-64,24	-8,48	1.93*	-10,14
Zone III	8°S	34°W	-32,1	-91,13	-67,16	-70,47	-31,74

	8° S	33° W	-44,93	-130,22	-95,55	-103,96	-47
Sergipe-Alagoas	11° S	36.5° W	-60,12	-192,33	-143,47	-195,8	-95,92
	12° S	35° W	-62,09	-198,91	-148,32	-169,63	-78,18
Bahia Sul	13° S	37° W	-92,74	-299,68	-222,85	-283,5	-147,8
Espirito Santo	17° S	38.5° W	-37,53	-118,34	-88,34	-94,71	-42,09
	16.5° S	38° W	-48,19	-153,36	-114,29	-124,65	-55,49
Campos	21.5° S	41° W	-48,6	-154,64	-126,7	-160,56	-82,87
	22° S	40° W	-114,16	-370,11	-320,58	-426,46	-202,11
	23° S	41° W	-92,82	-299,77	-253,48	-336,89	-158,98
Santos	25.5° S	48° W	-75,21	-242,03	-195,82	-272,11	-124,08
	26° S	46° W	-189,73	-630,83	-582,61	-722,24	-324,63
	27° S	46° W	-104,79	-540,51	-486,43	-638,76	-286,99
Pelotas	32.5° S	51° W	-135,51	-466,43	-420,68	-494,79	-226,48
	33° S	51° W	-165,95	-576,79	-523,75	-615,44	-282,89
Punta del Este	35.5° S	53° W	-89,64	-296,74	-252,8	-300,71	-137,94
Salado	37.5° S	57° W	-59,53	-190,53	-172,27	-216,85	-99,12
	38° S	55° W	-151,11	-491,39	-445,65	-570,6	-258,41
Colorado	40° S	61° W	-77,08	-248,23	-184,63	-229,2	-112,35
	41° S	59° W	-99,08	-320,53	-237,75	-326,76	-155,83
Rawson	43.5° S	60° W	-50,92	-162,28	121,33	-134,15	-60,03
San Jorge	46° S	65° W	-33,28	-104,91	-78,77	-85,1	-37,93
	47° S	66° W	-29,93	-94,95	-71,32	-77,01	-32,13
San Julian	49.5° S	64° W	-15,89	-44,91	-35,17	-33,21	-14,24
Argentina	43° S	52° W	-25,38	-78,39	-59,36	-59,45	-25,72
	41.5° S	43.5° W	-82,82	-266,92	-198,59	-235,86	-140,2
	47° S	46° W	-55,41	-177,98	-132,6	-147,4	-65,77

Northern Falkland	50.5° S	59.5° W	-6,13	-10,3	-10,32	-5,99	-2,21
	49.5° S	59° W	-41,27	-128,57	-97,13	-123,51	-58,21
Eastern Falkland	52.5° S	50° W	-70,27	-36,59	-80,32	-144,42	-45,07
	52° S	55° W	-77,03	-40,13	-88,05	-159,13	-49,7
Western Falkland	52.5° S	65° W	-43,73	-16,34	-46,99	-84,51	-25,04
	53° S	60° W	-34,77	-9,7	-35,83	-64,42	-18,45
Southern Falkland	53° S	62° W	-47,44	-19,47	-51,81	-93,09	-27,95
	54° S	55° W	-49,16	-21,7	-54,38	-97,17	-29,44

Negative values indicate flexure. * Positive flexure or uplift

REFERENCES

- Airy, G.B. 1855. *On the computation of the Effect of the Attraction of Mountain-Masses, as disturbing the Apparent Astronomical Latitude of Stations in Geodetic Surveys*. Philosophical Transactions of the Royal Society of London, Vol 145, pp 101-104. Doi: 10.1098/rstl.1855.0003
- Allison, M.A., Lee, M.T., Ogston, A.S., Aller, R.C., 2000. *Origin of Amazon mudbanks along northeastern coast of South America*. Mar. Geol. 163, 241 – 256
- Allison, M.A., Nittrouer, C.A., Faria, L.E.C., 1995. *Rates and mechanisms of shoreface progradation and retreat downdrift of the Amazon River mouth*. Mar. Geol. 125, 373-392
- Barbie B., Arthur J. M., Edward H. R. (2003). "*The North Brazil Current*." Ocean Surface Currents. <http://oceancurrents.rsmas.miami.edu/atlantic/north-brazil.html>.
- Boisvert William E. 1967. *Major Currents in the North and South Atlantic Oceans between 64°N and 60°S*. Oceanographic Analysis Division. Naval Oceanographic Office.
- Barrell, J., 1914. *The Strength of the Earth's crust*. The Journal of Geology.
- Bader, R. G., Robert, D.G., Benson, W.E., Bolli, H. M., Hay, W.W., Rothwell, T. J., Ruef, M. H., Riedel, W.R & Sayles, F. L. (1970a). Site 23. *In* Bader, R.G., et al, 1970. *Initial Reports of the Deep Sea Drilling Project*. Vol IV, pp 17-35. doi:10.2973/dsdp.proc.4.102.1970
- Bader, R. G., Robert, D.G., Benson, W.E., Bolli, H. M., Hay, W.W., Rothwell, T. J., Ruef, M. H., Riedel, W.R & Sayles, F. L. (1970b). Site 27. *In* Bader, R.G., et al, 1970. *Initial Reports of the Deep Sea Drilling Project*. Vol IV, pp 93-123. doi:10.2973/dsdp.proc.4.106.1970
- Bader, R. G., Robert, D.G., Benson, W.E., Bolli, H. M., Hay, W.W., Rothwell, T. J., Ruef, M. H., Riedel, W.R & Sayles, F. L. (1970c). Site 28. *In* Bader, R.G., et al,

1970. *Initial Reports of the Deep Sea Drilling Project*. Vol IV, pp 125-143. doi:10.2973/dsdp.proc.4.107.1970
- Bader, R. G., Robert, D.G., Benson, W.E., Bolli, H. M., Hay, W.W., Rothwell, T. J., Ruef, M. H., Riedel, W.R & Sayles, F. L. (1970d). Site 29. *In* Bader, R.G., et al, 1970. *Initial Reports of the Deep Sea Drilling Project*. Vol IV, pp 145-213. doi:10.2973/dsdp.proc.4.108.1970
- Bader, R. G., Robert, D.G., Benson, W.E., Bolli, H. M., Hay, W.W., Rothwell, T. J., Ruef, M. H., Riedel, W.R & Sayles, F. L. (1970e). Site 30. *In* Bader, R.G., et al, 1970. *Initial Reports of the Deep Sea Drilling Project*. Vol IV, pp 215-241. doi:10.2973/dsdp.proc.4.109.1970
- Bader, R. G., Robert, D.G., Benson, W.E., Bolli, H. M., Hay, W.W., Rothwell, T. J., Ruef, M. H., Riedel, W.R & Sayles, F. L. (1970f). Site 31. *In* Bader, R.G., et al, 1970. *Initial Reports of the Deep Sea Drilling Project*. Vol IV, pp 243-263. doi:10.2973/dsdp.proc.4.110.1970
- Baker, P. F., Johnson, D.A., Carslson, R.L., Cepek, P., Coulbourn, W.T., Gamboa, L.A., Hamilton, N., De Melo, U., Pujol, C., Shor, A.N., Suzyumov, A.E., Ljalsma, R. C & Walton, W.H. (1983a). Site 515 Brazil Basin. *In* Baker, P. F et al 1980. *Initial Reports of the Deep Sea Drilling Project*, Vol 72, pp 53-154. doi:10.2973/dsdp.proc.72.104.1983
- Baker, P. F., Johnson, D.A., Carslson, R.L., Cepek, P., Coulbourn, W.T., Gamboa, L.A., Hamilton, N., De Melo, U., Pujol, C., Shor, A.N., Suzyumov, A.E., Ljalsma, R. C & Walton, W.H. (1983b). Site 516 Rio Grande Rise. *In* Baker, P. F et al 1980. *Initial Reports of the Deep Sea Drilling Project* Vol 72, pp. 53-154. doi:10.2973/dsdp.proc.72.105.1983
- Barker, P. F., Dalziel, I.W.D., Dinkelman, M.G., Elliot, D. H., Gombos, A.M., Lonardi, A., Plafker, G., Tarney, J., Thompson, R.W., Tjalma R.C., Von der Borch, C.C., Wise, S.W. & Harris, W. K. (1977a). Site 327. *Initial Reports of the Deep Sea Drilling Project*, Volume 36, pp 27-86. doi:10.2973/dsdp.proc.36.103.1977
- Barker, P. F., Dalziel, I.W.D., Dinkelman, M.G., Elliot, D. H., Gombos, A.M., Lonardi, A., Plafker, G., Tarney, J., Thompson, R.W., Tjalma R.C., Von der Borch, C.C.,

- Wise, S.W. & Harris, W. K. (1977b). Site 328. *Initial Reports of the Deep Sea Drilling Project*, Volume 36, pp 87-141. doi:10.2973/dsdp.proc.36.104.1977
- Barker, P. F., Dalziel, I.W.D., Dinkelman, M.G., Elliot, D. H., Gombos, A.M., Lonardi, A., Plafker, G., Tarney, J., Thompson, R.W., Tjalma R.C., Von der Borch, C.C., Wise, S.W. & Harris, W. K. (1977c). Site 329. *Initial Reports of the Deep Sea Drilling Project*, Volume 36, pp 143-206. doi:10.2973/dsdp.proc.36.105.1977
- Beuthe, M., 2008. *Thin elastic shells with variable thickness for lithospheric flexure of one-plate planets*. *Geophysical Journal International* 172 , 817-841.
- Biju-Duval, B., Moore, J. C., Bergen, J. A., Blackinton, G., Claypool, G.E., Cowan, D. S., Davis, D. M., Guerra, R.T., Hemleben, C. H.J., Marlow, M.S., Pudsey, C. J., Renz, G. W., et al.(1984a). Site 541 Toe of the Barbados Ridge complex. *In Init. Repts of Deep Sea Drilling Project*,: Washington (U.S. Govt. Printing Office), Vol 78A, pp 107-186. doi:10.2973/dsdp.proc.78a.108.1984
- Biju-Duval, B., Moore, J. C., Bergen, J. A., Blackinton, G., Claypool, G.E., Cowan, D. S., Davis, D. M., Guerra, R.T., Hemleben, C. H.J., Marlow, M.S., Pudsey, C. J., Renz, G. W., et al (1984b). Site 542 Toe of the Barbados Ridge complex. *In Init. Repts of Deep Sea Drilling Project*,: Washington (U.S. Govt. Printing Office), Vol 78A, pp 187-225. doi:10.2973/dsdp.proc.78a.109.1984
- Bodine J. H., Steckler M.S & Watts A.B. 1981. *Observations of Flexure and the Rheology of the Oceanic Lithosphere*. *Journal of Geophysical Research*, Vol 86, No B5, pp 3695-3707.
- Burov E.B & Diament M. 1992. *Flexure of the continental lithosphere with multilayered rheology*. *Geophys. J. Int* 109, pp 449-468
- Candela, J., Beardsley, R.C & Limeburner, R. 1992. *Separation of tidal and subtidal currents in ship-mounted acoustic doppler current profiler observations*. *J. Geophys. Res.*, 97: 769-788.
- Camilloni I. A., Barros V. R. 2003. *Extreme discharge events in the Paraná River and their climate forcing*. *Journal of Hydrology* 278. 94-106
- Contreras J., Zuhlke R., Bowman S. & Bechstads Thilo. 2010. *Seismic Stratigraphy and subsidence analysis of the southern Brazilian margin (Campos, Santos and Pelotas Basins)*. *Marine and Petroleum Geology* 27. Pp 1952-1980

- Chérubin, L. M., Richardson, P. L., 2007. *Caribbean current variability and the influence of the Amazon and Orinoco Freshwater plumes*. Deep-Sea Research I, 54, 1451-1473
- Da Silva A.C., Landim J.M & Ussami N.1999. *Flexure as a tectonic control on the Large Scale Geomorphic Characteristics of the Eastern Brazil Coastal Zone*. Journal of Coastal Research, Vol 15, No 2. Pp 505-519
- Depetris P. J., Griffin JJ. 1968. *Suspended load in the Rio de la Plata drainage basin*. Sedimentology 11, pp 53-60
- Dessier A., Donguy J. R., 1994. *The sea surface salinity in the tropical Atlantic between 10°S and 30°N- Seasonal and interannual variations (1977-1989)*. Deep Sea Research Part I. Oceanographic Research Papers. Volume 41, Issue 1. Pages 81-100.
- Divins, D.L.2003. *Total Sediment Thickness of the World's Oceans & Marginal Seas*, NOAA National Geophysical Data Center, Boulder, CO.
- Driscoll N.W & Karner G.D. 1994. *Flexural deformation due to Amazon Fan loading: A feedback mechanism affecting sediment delivery to margins*. Geology 22, pp 1015-1018
- Edgar, N. T., Saunders, J. B., Bolli, H.M., Donnelly, T.W., Hay, W.W., Maurrasse, F., Silva, I.P., Riedel, W. R & Schneidermann, N. (1973a). Site 146/149. In Edgar, et al, *Initial Reports of the Deep Sea Drilling Project*, Vol 15, pp 17-167. doi:10.2973/dsdp.proc.15.102.1973
- Edgar, N. T., Saunders, J. B., Bolli, H. M., Donnelly, T.W., Hay, W.W., Maurrasse, F., Pérez-Nieto, H., Premoli-Silva, I., Riedel, W.R. & Schneidermann, N. (1973b). Site 148. In Edgar, et al, *Initial Reports of the Deep Sea Drilling Project*, Vol 15, pp 217-275. doi:10.2973/dsdp.proc.15.104.1973
- Edgar, N. T., Saunders, J. B., Bolli, H. M., Donnelly, T.W., Hay, W.W., Maurrasse, F., Pérez-Nieto, H., Premoli-Silva, I., Riedel, W.R. & Schneidermann, N. (1973c). Site 150. In Edgar, et al, *Initial Reports of the Deep Sea Drilling Project: Washington (U.S. Govt. Printing Office)*, Vol 15, pp 277-299. doi:10.2973/dsdp.proc.15.105.1973

- Edgar, N. T., Saunders, J. B., Bolli, H. M., Boyce, R.E., Donnelly, T. W., Hay, W. W., Maurrasse, F., Prell W., Premoli-Silva, I., Riedel, W.R. & Schneidermann (1973d). Site 153. In Edgar, et al, *Initial Reports of the Deep Sea Drilling Project*: Washington (U.S. Govt. Printing Office), Vol 15, pp 367-406. doi:10.2973/dsdp.proc.15.108.1973
- Edgar, N. T., Saunders, J. B., Bolli, H. M., Boyce, R.E., Donnelly, T. W., Hay, W. W., Maurrasse, F., Prell W., Premoli-Silva, I., Riedel, W.R. & Schneidermann (1973e). Site 154. In Edgar, et al, *Initial Reports of the Deep Sea Drilling Project*: Washington (U.S. Govt. Printing Office), Vol 15, pp 407-471. doi:10.2973/dsdp.proc.15.109.1973
- Espinoza J.C., Ronchail J, Lavado W., Carranza J., Cochonneau G., De Oliveira E., Pombosa P. V. & Loup G. J. 2010. *Variabilidad espacio-temporal de las lluvias en la cuenca amazónica y su relación con la variabilidad hidrológica regional. Un enfoque particular sobre la región andina. Revista Peruana Geo-Atmosferica RPGA 2*, 99-130.
- Exxon Production Research Company, W.M.P.A.A.o.P.G.F., 1985. *Tectonic map of the world*: [Houston, Tex.]; Tulsa, Okla., Exxon Production Research Co.: AAPG Foundation. In Laske G & Masters G. 1997. *A Global Digital Map of Sediment Thickness*, EOS Trans. AGU, 78, F483.
- Field, A., 2005. *North Brazil current rings viewed by TRMM Microwave Imager SST and the influence of the Amazon Plume*. Deep-Sea Research I 52, 137-160.
- Figueiredo J., Hoorn C., Van der Ven, P & Soares E., 2009. *Late Miocene onset of the Amazon River and the Amazon deep-sea fan: Evidence from the Foz do Amazonas Basin*. Geology 37, pp 619-622
- Forte, A.M., W.R. Peltier, A.M. Dziewonski, and R.L. Woodward., 1993. *Dynamic surface topography: A new interpretation based upon mantle ow models derived from seismic tomography*, Geophys. Res. Lett., 20, 225-228
- Forte Alessandro. *Lecture Notes*. University of Québec at Montreal,
- Furquim Werbeck Lima J.E., Araujo, W.T., De Olivera N., Vieira M.R & Medrano E. 2005. *Suspended sediment fluxes in the large river basins of Brazil*. In *Sediment Budgets 1* (Proceedings of symposium S1 held during the Seventh IAHS Scientific

- Assembly at Foz do Iguaçu, Brazil, April 2005). IAHS Publ. 291, 2005.
- Flagg C. N., R. L. Gordon and S. McDowell. 1986. *Hydrographic and current observations on the continental slope and shelf in the Western Equatorial Atlantic*. Journal of Physical Oceanography, 16, 1412-1429.
- Fratantoni D. M. and Richardson P., 2006. *The evolution and Demise of North Brazil Current Rings*. Journal of Physical Oceanography. Vol 36.
- Framiñan M.B., and Brown O.b., 1996. *Study of the Rio de la Plata turbidity front, Part I: spatial and temporal distribution*. Continental Shelf Research, Vol 16, No.10. Pp 1259-1282
- Garcia J. A., 2003. *3D Numerical model of the flexural isostatic Response to extension induce by crustal scale listric normal faulting*. Geofisica Internacional, Vol 42, N0 001, pp 41-51.
- Garcia N.O & Vargas W. M. 1996. *The spatial variability of runoff and precipitation in the Rio de la Plata basin*. Hydrological Sciences Journal des Sciences Hydrologiques, 41(3).
- Gardel A., Gratiot N., 2006. *Monitoring of coastal dynamics in French Guiana from 16 years SPOT satellite images*. Journal of Coastal Research, Special Issue 39.
- Gordon, Arnold L., 1967. *Circulation of the Caribbean Sea*. Journal of geophysical Research. Vol 72. No.24
- Gratiot Nicolas, Gardel Antoine, Anthony Edward J. 2007. *Trade wind waves and dynamics on the Frech Guiana Coast, South America: input from ERA-40 wave data and field investigations*. Marine Geology, volume 236, Issues 1-2. Pages 15-26
- Gupta H. K. 2011. *Encyclopedia of Solid Earth Geophysics*. National Geophysical Research Institute. © Springer Science
- Glišović, P. and Forte, A.M., 2014. *Reconstructing the Cenozoic evolution of the mantle: Implications for mantle plume dynamics under the Pacific and Indian plates*, Earth Planet. Sci. Lett., 390, 146-156.
- Hayes, D. E., Pimm, A.C., Benson, W.E., Berger, W. H., Rad, U. V., Supko, P.R., Beckmann, J.P. & Roth, P. H. (1972). Shipboard site reports, Site 142. (1972). In

Initial Reports of the Deep Sea Drilling Project: Washington (U.S. Govt. Printing Office), Vol XIV, pp 249-282. doi:10.2973/dsdp.proc.14.109.1972

Hill, P.S., Fox J.M., Crockett, J.S., Curren, K. J., Friedrichs C.t., Geyers, W.r., Milligan, T.g., Ogston, A.s., Puig, P., Scully, M.E., Traykovskis, P.A & Weatcroft, R.A. 2009. *Sediment delivery to the seabed on continental margin. In Continental Margin Sedimentation: From Sediment Transport to Sequence Stratigraphy* (eds C. A. Nittrouer, J. A. Austin, M. E. Field, J. H. Kravitz, J. P. M. Syvitski and P. L. Wiberg), Blackwell Publishing Ltd., Oxford, UK. Doi: 10.1002/9781444304398.ch2

Hoorn, C., 1993. *Marine incursions and the influence of Andean tectonics on the Miocene depositional history of northwestern Amazonia: results of a palynostratigraphic study.* *Palaeogeography, Palaeoclimatol, Palaeoecol.* 105, 267-309.

Hu, C., Montgomery E T., and Schmitt W., 2004. *The dispersal of the Amazon and Orinoco River water in the tropical Atlantic and Caribbean Sea: Observation from space and S-PaLACE floats.* *Deep-Sea Research II*, 51. 1151-1171.

Huppertz, T. J., Henrich, R & Chiessi, C. M., 2011. *Shelf to slope sedimentary regimes on the northern Argentine and Uruguay continental margin a critical review. In: Huppertz, T. J. 2011. Styles of continental margin sedimentation: comparing glaciated and non-glaciated slope systems using case studies on the southeast Canadian and northern Argentine and Uruguay continental Slope.* Dissertation. Universitat Bremen.

Iriondo M. 2004. *The Litoral complex at the Paraná mouth.* *Quaternary International* 114. 143-154

Iriondo, M., 1988. A comparison between the Amazon and Paraná River systems. *Mitt. Geol-Palaont. Inst. Univ. Hamburg.* H. 66:77-92

Jackson, J. D. 1962. *Classical Electrodynamics.* John Wiley & Sons, Inc.

Karner G.D., Watts A.B., 1983. *Gravity Anomalies and Flexure of the Lithosphere at Mountain Ranges.* *Journal of Geophysical Research.* Vol 88, No, B12, PP 10449-10447.

Karner G.D., Watts A.B. 1982. *On Isostasy at Atlantic-Type Continental Margins.* *Journal of Geophysical Research,* Vol 87, No B4, pp 2923-2948

- Kettner A.J., Restrepo J.D & Syvitski J. P. M. 2010. *A spatial Simulation Experiment to Replicate Fluvial Sediment fluxes within Magdalena River Basin, Colombia.* The Journal of Geology, Vol 118. No 4. pp 363-379
- Kineke G.C., Sternberg R.W., Trowbridge J.h & Geyer W.R. 1996. *Fluid-mud processes on the Amazon continental shelf.* Continental Shelf Research. Vol 16 No. 5/6 pp. 667-696
- Kuehl, S.A., Nittrouer, C.A. & De Master, D.J. 1986. *Distribution of sedimentary structures in the Amazon subaqueous delta.* Cont. Shelf Res., 6: 31 1-336
- Kraus, H., 1967. *Thin Elastic Shells* (John Wiley, New York).
- Krepper C.M., Garcia N. O & Jones P.D. 2003. *Interannual variability in the Uruguay River basin.* International Journal of climatology 23: 103-115
- Laske G & Masters G. 1997. *A Global Digital Map of Sediment Thickness*, EOS Trans. AGU, 78, F483.
- Lentz, S. J. 1995a. *Seasonal variations in the horizontal structure of the Amazon Plume inferred from historical hydrographic data.* Journal of Geophysical Research, Vol 100, No C2, pp 2391-2400
- Lentz, S.J. 1995b. *The Amazon River plume during AMASSEDS: subtidal current variability and the importance of wind forcing.* J. Geophys. Res., 100: 2377-2390.
- Lenters, J. D. & Cook K. H., 1995. *Simulation and diagnosis of the regional summertime precipitation climatology of South America.* J. Climate 8, 2988 – 3005.
- Ludwig, W. J., Krasheninnikov, V. A., Basov, I.A., Bayer, U., Bloemendal, J., Bornhold, B., Ciesielski, P.F., Goldstein, E. H., Robert, C., Salloway, J., Usher, J., Von der Dick, H., Weaver, F. & Wise Sherwood W J. (1983). *Site 511.* In Ludwig W. J. et al, Init. Repts. DSDP, Pt. 1: Washington (U.S. Govt. Printing Office), Vol 71, pp 21-109. doi:10.2973/dsdp.proc.71.102.1983
- Ludwig, W.F., J.E. Nafe & C.L. Drake, *Seismic Refraction*, in The Sea, Vol. 4, Ideas and Observations on Progress in the Study of the Seas, A.E. Maxwell, 53-84 (ed.), Wiley-Interscience, New York, 1970

- Mahiques, M.M., Tassinardi, C.C, G., Marcolini, S., Violante, R. A., Figueira, R. C. L., Da Silveira, I.C., Burone, L & Mello e Sous, S. H. 2008. *Nd and Pb isotope signatures on ghe southeastern South American upper margin: Implications for sediment transport and source rocks*. Marine Geology, 250 /1-2) pp 51-63
- Matano, R.P., Palma, E.D. & Piola, A. R. 2010. *The influence of the Brazil and Malvinas Currents on the Southwestern Atlantic Shelf circulation*. Ocean Science, 6, pp 983-995
- Maxwell, AE., Von Herzen, R. P., Andrews, J. E.; Boyce, R. E., Milow, E. D., Hsu, K. J., Percival, S. F. & Saito, T. (1970). *Site 22*. In Maxwell, A.E. et al, *Initial Reports of the Deep Sea Drilling Project*: Washington ((U.S. Government Printing Office) Vol III, pp.413-439. doi:10.2973/dsdp.proc.3.112.1970
- Meade, R. H. 1994. *Suspended sediments of modern Amazon and Orinoco Rivers*. Quaternary International, Vol 21, pp 29-39.
- Meade, R.H., Weibezahn, F.H., Lewis, W.M. & Perez-Hernandez, D. 1990. *Suspended-sediment budget for the Orinoco River*. In: Weibezahn, F.H., Alvarez, H., Lewis, Jr., W.M. (Eds.), *El Río Orinoco Como Ecosistema*. Impresos Rubel, Caracas, Venezuela, pp. 55 – 79.
- Meade, R.H., Dunne, T., Richey, J.E., Santos, U. De M. & Salati, E., 1985. *Storage and remobilization of suspended sediment in the lower Amazon River of Brazil*. Science, 228: 488-490.
- Milliman, J. D. and K. M. Farnsworth. 2011. *River Discharge to the Coastal Ocean: A Global Synthesis*, Cambridge University Press, 392 p.
- Milliman, J.D. & Syvitski, P.M., 1992. *Geomorphic/tectonic control of sediment transport to the ocean: the importance of small mountainous rivers*. J. Geol. 100, 525-544
- Milliman J. D. & R. H. Meade (1983). *World-wide delivery of river sediment to the oceans*. Journal of Geology 91. 1-21
- Modica C.J., Brush E.R. 2004. *Postrift sequence stratigraphy, paleogeography, and fill history of the deep-water Santos Basin, offshore southeast Brazil*.AAPG Bulletin, V.88, No 7. Pp 923.945

- Molinari, R. L., M. Spillane, I. Brooks, D. Atwood, and C. Duckett (1981). *Surface currents in the Caribbean Sea as deduced from Lagrangian observations*, J. Geophys. Res., 86, 6537-6542, 1981.
- Morrison J M., Smith O. P., 1990. *Geostrophic transport variability along the Aves Ridge in the eastern Caribbean Sea during 1985-1986*. Journal of Geophysical Research 95, 699-710
- Moucha, R., A.M. Forte, J.X. Mitrovica, D.B., Rowley, S., Quéré, N.A. Simmons, S.P. Grand. 2008. *Dynamic topography and long-term sea-level variations: There is no such thing as a stable continental platform*, Earth Planet. Sci. Lett., 271, 101-108.
- Muller-Karger, F.E., McClain, C.R., Fisher, T.R., Esaias, W.E., Varela, R., 1989. *Pigment distribution in the Caribbean Sea: observations from space*. Progress in Oceanography 23, 23-64.
- Muller-Karger, F.E., McClain, C.R., Richardson, P.L., 1988. *The dispersal of the Amazon's water*. Nature 333, 56-58.
- McCave, I.N. 1985. *Sedimentology and stratigraphy of box cores from the HEBBLE site on the Nova Scotian continental rise*. Marine Geology, 66(14).pp 59-89
- McNutt M., Menard H. W. 1978. *Lithospheric flexure and uplifted atolls*. Journal of Geophysical research. Vol 83, No B3.
- Nafe, J. E., Drake, C. L., 1957. *Variation with depth in shallow and deep water marine sediments of porosity, density and the velocities of compressional and shear waves*. Geophysics 22(3), 523-552.
- Nikiema, O., Devenon J.L., & Baklouti, M. 2007. *Numerical modeling of the Amazon River Plume*. Continental Shelf Research 27. Pp 873-899
- Nishimura, C. E. & Forsyth, D.W. 1989. *The anisotropic structure of the upper mantle in the Pacific*. Geophys. J. 96, pp 203-229
- Nittrouer, C.A., Kuehl S. A., Sternberg R. W., Figueiredo A. G & Faria L. E.C. 1995. *An introduction to the geological significance of sediment transport and accumulation on the Amazon continental shelf*. Marine Geology 125. 177-192

- Nittrouer, C. A. & Brunskill G. J. 1995. *Importance of tropical coastal environments*. Geo-Marine Letters 15 pages 121-126.
- Nittrouer, C. A & Demaster D. J. 1995. *The Amazon shelf setting: tropical, energetic, and influenced by a large river*. Continental Shelf Research. Vol 16. No 5/6. Pp 553-573. Septiembre
- Nittrouer, C.A. & DeMaster, D.J. 1986. *Sedimentary processes on the Amazon continental shelf: past, present and future research*. Continental Shelf Research, Vol 6, (1-2), pp 5-30.
- Olson, D.D., Podesta, G.P., Evans, R.H. and Brown, O.B. 1988. *Temporal variations in the separation of Brazil and Malvinas Currents*. Deep-Sea Research 35(12): 1971-1990.
- Organización de los Estados Americanos (OEA). 1971. *Cuenca del Rio de la Plata. Estudio para su planificación y Desarrollo: inventario de Datos hidrológicos y Climatológicos*. Organización de los Estados Americanos, Unidad Recursos Naturales, Washington, 272pp.
- Orfeo O & Stevaux J. 2002. *Hydraulic and morphological characteristics of middle and upper reaches of the Paraná River (Argentina and Brazil)*. Geomorphology 44. 309-322.
- Palma Elbio D., Matana Ricardo P., Piola Albergo R. 2008. *A numerical study of the Southwestern Atlantic Shelf circulation: Stratified ocean response to local and offshore forcing*. Journal of geophysical research, Vol 113, C11010, doi: 10.1029/2007JC004720
- Pazzaglia F. & Gardner T. 1994. *Late Cenozoic flexural deformation of the middle U.S. Atlantic passive margin*. Journal of geophysical research, Vol 99, No B6, pages 12,143-12,157.
- Pearson, D. M., Kapp, P., DeCelles, P. G., Reiners, P. W., Gehrels, G. E., Ducea, M. N., & Pullen, A. (2013). *Influence of pre-Andean crustal structure on Cenozoic thrust belt kinematics and shortening magnitude: Northwestern Argentina*. Geosphere, 9(6), 1766-1782.
- Perch-Nielsen, K., Supko, P. R., Boersma, A., Bonatti, E., Carlson, R. L., McCoy, F., Neprochnov, Y. P. & Zimmerman, H. B. (1977a). *Site 354: Ceara Rise*. In Supko, P. R. et al, *Initial Reports of the Deep Sea Drilling Project*, Vol 39: Washington

(U.S. Government Printing Office), pp. 45-99.
doi:10.2973/dsdp.proc.39.103.1977

Perch-Nielsen, K., Supko, P. R., Boersma, A., Carlson, R. L., Dinkelman, M. G., Fodor, R. V., Kumar, N., F., McCoy, F., Thiede, J. & Zimmerman, H. B. (1977b). *Site 355 Brazil Basin*. In Supko, P. R. et al, *Initial Reports of the Deep Sea Drilling Project*, Vol 39: Washington (U.S. Government Printing Office), pp. 101-140. doi:10.2973/dsdp.proc.39.104.1977

Perch-Nielsen, K., Supko, P. R., Boersma, A., Carlson, R. L., Dinkelman, M. G., Fodor, R. V., Kumar, N., F., McCoy, F., Thiede, J. & Zimmerman, H. B. (1977c). *Site 356: São Paulo Plateau*. In Supko, P. R. et al, *Initial Reports of the Deep Sea Drilling Project*, Vol 39: Washington (U.S. Government Printing Office) pp. 141-230. doi:10.2973/dsdp.proc.39.105.1977

Perch-Nielsen, K., Supko, P. R., Boersma, A., Carlson, R. L., Dinkelman, M. G., Fodor, R. V., Kumar, N., F., McCoy, F., Thiede, J. & Zimmerman, H. B. (1977d). *Site 357: Rio Grande Rise*. In Supko, P. R. et al, *Initial Reports of the Deep Sea Drilling Project*, Vol 39: Washington (U.S. Government Printing Office) pp. 231-327. doi:10.2973/dsdp.proc.39.106.1977

Perch-Nielsen, K., Supko, P. R., Boersma, A., Carlson, R. L., Dinkelman, M. G., Fodor, R. V., Kumar, N., F., McCoy, F., Thiede, J. & Zimmerman, H. B. (1977e). *Site 358: Argentina Basin*. In Supko, P. R. et al, *Initial Reports of the Deep Sea Drilling Project*, Vol 39: Washington (U.S. Government Printing Office) pp. 329-371. doi:10.2973/dsdp.proc.39.107.1977

Pérez-Gussinyé, M., Lowry, A. R., Watts, A. B., 2007. Effective elastic thickness of South America and its implications for intracontinental deformation. *Geochemistry, Geophysics, Geosystems*, Vol 8, Number 5. An electronic Journal of The Earth Science. Q05009, doi:10.1029/2006GC001511

Piola A.R. & Falabella v.2009. *The Patagonian Sea*. Atlas del Mar Patagónico.

Piola, A. R., Matano, R.P., Palma, E.D., Möller, O.O. & Campos, E. J.D.2005. *The influence of the Plata River discharge on the western South Atlantic Shelf*. *Geophysical Research Letters*, 32

Piola A. R and Matano R.P., 2001. *Brazil and Falklands currents*. In: *Ocean currents: A Derivative of Encyclopedia of Ocean Sciences*, 2nd Edition. Edited by: Steele J., Steve T and Turekian K.

- Pimienta Felipe M, campos Dias Edmo José, Miller Jerry L, Piola Alberto R. 2005. *A numerical study of the plata river plume along the southeastern south american continental shelf*. Brazilian Journal of oceanography, 53 (3/4): 129-146.
- Philander S. G. 2001. *Atlantic Ocean Equatorial Currents*. Princeton University. doi:10.1006/rwoa.2001.0361
- Pochat V. 2010. *The La Plata river basin*. 7th Biennial Rosenberg International Forum on water Policy water for the Americas: challenges and opportunities.
- Potter, P.E. 1997. *The Mesozoic and Cenozoic paleodrainage of South America: a natural history*. J. S.Am.Earth Sci. 10, 331–344.
- Pratt, J. H. 1855. *On the Attraction of the Himalaya Mountains, and of the elevated Regions beyond them, upon the Plumb-Line in India*. Philosophical Transactions of the Royal Society of London, Vol 145, pp 53-100
- Restrepo, J. D., Zapata, P., Díaz, M. J., Garzón-Ferreira, J. & García, C. B. 2006. *Fluvial fluxes into the Caribbean Sea and their impact on coastal ecosystems: the Magdalena River, Colombia*. Glob. Planet. Change 50:33–49.
- Restrepo J.D. & Kjerfve B. 2000. *Magdalena river: interannual variability (1975-1995) and revised water discharge and sediment load estimates*. Journal of Hydrology. pp 137-149
- Richardson, P. L., G Hufford, r. Limeburner and W.S. Brown. 1994. *North Brazil Current retroflection eddies*. Journal geophys. Res 99, C3 pages 5081-5093
- Sallun, Alethea E.M. & Suguio, Kenitiro. 2010. *Quaternary colluvial episodes (Upper Paraná River Hydrographic Basin, Brazil)*. An. Acad. Bras. Ciênc. [Online]. vol.82, n.3, pp. 701-715. ISSN 0001-3765.
- Souza, Wber Friederchs Landim de., Marone Eduardo., Knoppers Bastiaan A., Silveira Ilson C. da., Godoi Sueli S. de., 2011. *The Brazil current: typology and physical biogeochemical domains*. <http://hdl.handle.net/123456789/354>
- Schmitz, W. J., Jr., and P. L. Richardson, *On the sources of the Florida Current*, Deep Sea Res., Part B, B38, suppl. 1, S379–S409, 1991

- Shipboard Scientific Party, 2004. *Site 1257*. In Erbacher, J., Mosher, D.C., Malone, M.J., et al., *Proc. ODP, Init. Repts.*, 207: College Station, TX (Ocean Drilling Program), 1–111. doi:10.2973/odp.proc.ir.207.104.2004
- Shipboard Scientific Party, 2004. *Site 1258*. In Erbacher, J., Mosher, D.C., Malone, M.J., et al., *Proc. ODP, Init. Repts.*, 207: College Station, TX (Ocean Drilling Program), 1–117. doi:10.2973/odp.proc.ir.207.105.2004
- Shipboard Scientific Party, 2004. *Site 1259*. In Erbacher, J., Mosher, D.C., Malone, M.J., et al., *Proc. ODP, Init. Repts.*, 207: College Station, TX (Ocean Drilling Program), 1–110. doi:10.2973/odp.proc.ir.207.106.2004
- Shipboard Scientific Party, 2004. *Site 1260*. In Erbacher, J., Mosher, D.C., Malone, M.J., et al., *Proc. ODP, Init. Repts.*, 207: College Station, TX (Ocean Drilling Program), 1–113. doi:10.2973/odp.proc.ir.207.107.2004
- Shipboard Scientific Party, 1998. *Site 1044*. In Moore, J.C., Klaus, A., et al., *Proc. ODP, Init. Repts.*, 171A: College Station, TX (Ocean Drilling Program), 19–37. doi:10.2973/odp.proc.ir.171a.103.1998
- Shipboard Scientific Party, 1998. *Site 1047*. In Moore, J.C., Klaus, A., et al., *Proc. ODP, Init. Repts.*, 171A: College Station, TX (Ocean Drilling Program), 77–91. doi:10.2973/odp.proc.ir.171a.106.1998
- Shipboard Scientific Party, 1998. *Site 1048*. In Moore, J.C., Klaus, A., et al., *Proc. ODP, Init. Repts.*, 171A: College Station, TX (Ocean Drilling Program), 93–106. doi:10.2973/odp.proc.ir.171a.107.1998
- Shipboard Scientific Party, 1995. *Site 948*. In Shipley, T.H., Ogawa, Y., Blum, P., et al., *Proc. ODP, Init. Repts.*, 156: College Station, TX (Ocean Drilling Program), 87–192. doi:10.2973/odp.proc.ir.156.106.1995
- Shipboard Scientific Party, 1995. *Site 925*. In Curry, W.B., Shackleton, N.J., Richter, C., et al., *Proc. ODP, Init. Repts.*, 154: College Station, TX (Ocean Drilling Program), 55–152. doi:10.2973/odp.proc.ir.154.104.1995
- Shipboard Scientific Party, 1995. *Site 926*. In Curry, W.B., Shackleton, N.J., Richter, C., et al., *Proc. ODP, Init. Repts.*, 154: College Station, TX (Ocean Drilling Program), 153–232. doi:10.2973/odp.proc.ir.154.105.1995

- Shipboard Scientific Party, 1995. *Site 927*. In Curry, W.B., Shackleton, N.J., Richter, C., et al., *Proc. ODP, Init. Repts.*, 154: College Station, TX (Ocean Drilling Program), 233–279. doi:10.2973/odp.proc.ir.154.106.1995
- Shipboard Scientific Party, 1995. *Site 928*. In Curry, W.B., Shackleton, N.J., Richter, C., et al., *Proc. ODP, Init. Repts.*, 154: College Station, TX (Ocean Drilling Program), 281–336. doi:10.2973/odp.proc.ir.154.107.1995
- Shipboard Scientific Party, 1995. *Site 929*. In Curry, W.B., Shackleton, N.J., Richter, C., et al., *Proc. ODP, Init. Repts.*, 154: College Station, TX (Ocean Drilling Program), 337–417. doi:10.2973/odp.proc.ir.154.108.1995
- Shipboard Scientific Party, 1988. *Site 698*. In Ciesielski, P.F., Kristoffersen, Y., et al., *Proc. ODP, Init. Repts.*, 114: College Station, TX (Ocean Drilling Program), 87–150. doi:10.2973/odp.proc.ir.114.105.1988
- Shipboard Scientific Party, 1988. *Site 699*. In Ciesielski, P.F., Kristoffersen, Y., et al., *Proc. ODP, Init. Repts.*, 114: College Station, TX (Ocean Drilling Program), 151–254. doi:10.2973/odp.proc.ir.114.106.1988
- Shipboard Scientific Party, 1988. *Site 700*. In Ciesielski, P.F., Kristoffersen, Y., et al., *Proc. ODP, Init. Repts.*, 114: College Station, TX (Ocean Drilling Program), 255–362. doi:10.2973/odp.proc.ir.114.107.1988
- Stevaux J. C. 1994. *The Upper Paraná River (Brazil): Geomorphology, sedimentology and Paleoclimatology*. Quaternary International, Vol 21, pp 143-161.
- Syvitski, J.P.M. & Milliman, J.D. 2007: *Geology, geography, and humans battle for dominance over the delivery of fluvial sediment to the coastal ocean*. Journal of Geology, 115, No1, pp 1-19
- Syvitski, J.P.M., Vörösmarty, C.J.; Kettner, A.J. & Green, P. 2005a. *Impacts of humans on the flux of terrestrial sediment to the global coastal ocean*. Science (308): 376-380.
- Syvitski J.P.M., Kettner A.J., Correggiari A. & Nelson B.W. 2005b. *Distributary channels and their impact on sediment dispersal*. Marine Geology 222-223. PP 75-94
- Syvitski, J.P.M., 2003. *Sediment fluxes and rates of sedimentation*. In: Middleton, G.V. (Ed.), *Encyclopedia of Sediments and Sedimentary Rocks*. Kluwer Academic Publishers, Dordrecht, Netherlands, pp. 600 – 606.

- Stow, D.A.V., Faugères, J-C., Howe, J.A., Pudsey, C.J & Viana, A.R., 2002. *Bottom currents, contourites and deep-sea sediment drifts: current state of the art*. In: Stow, D.A.V., Pudsey, C.J., Howe, J.A., Faugères, J-C & Viana, A.R.(Editors), *Deep-water contourite systems:modern drifts and ancient series, seismic and sedimentary characteristics*.The Geological Society, Memoir 22, London, pp 7-20
- Swift, D.J.P., Thorne, J.A., 1991. *Sedimentation on continental margins: I. A general model for shelf sedimentation*. In: Swift, D.J.P., Tillman, R.W., Oertel, G.F., Thorne, J.A. (Eds.), *Shelf Sand and Sandstone Bodies, Geometry, Facies and Sequence Stratigraphy: International Association of Sedimentologists Special Publication, vol. 14*, pp. 3-31
- Turcotte Donald., Schubert Gerald. 2002. *Geodynamics*. Second Edition. Cambridge University Press
- Turcotte, D. L., 1979. *Flexure*. *Advances in Geophysics* 21, 51-86.
- UNEP/GEF/Kalmar Högskola, Invemar. 2006. *Global International Water Assessment (GIWA), Caribbean Sea/Colombia & Venezuela, Central America & Mexico* GIWA Regional Assessment 3b, 3c, Kalmar Sweden
- Vening-Meinesz, F.A., 1939. Tables fondamentales pour la réduction isostatique régionale. *Bull. Geod.* 33, pp 711-776
- Violante, R.A., Paterlini C.M., Costa P. I et al. 2010. *Sismoestratigrafia y Evolucion Geomorfológica del Talud Continental Adyacente al Litoral del Este Bonaerense, Argentina*. *Latin American Journal of Sedimentology and Basin Analysis*. Vol 17 (1) pp, 33.62
- Violante, R.A & Parker, G. 2004. *Calcium carbonate corrosiveness in the South Atlantic during the Last Glacial Maximum as inferred from changes in the preservation of Globigerina bulloides: A proxy to determine deep-water circulation patterns*. *Marine Geology*, 2004 (1-2) pp 43-57
- Walcott R. I. 1969. *Isostatic response to loading of the crust in Canada*. *Canadian Journal of Earth Sciences* 7, pp 716-727.
- Walcott R.I. 1970. *Flexure of the lithosphere at Hawaii*. *Tectonophysics* 9, pp 435-46.
- Warne, A. G., Meade, R. H., White, W. A., Guevara, E. H., Gibeaut, J., Smyth, R. C. Aslan A. & Trambly, T. 2002. *Regional controls on geomorphology, hydrology,*

- and ecosystem integrity in the Orinoco Delta, Venezuela. Geomorphology 44. Pag 273-307.*
- Watts, A. B. & Zhong S. 2000. *Observations of flexure and the rheology of oceanic lithosphere. Geophys. J. Int, 142, pp 855-875*
- Watts A.B. 2001. *Isostasy and Flexure of the lithosphere. Cambridge University Press*
- Watts A. B., Bodine J. H & Steckler M.S. 1980. *Observations of flexure and the state of stress in the oceanic lithosphere. Journal of Geophysical Research, Vol 85, pp 6369-6376.*
- Watts A.B., 1978. *An Analysis of Isostasy in the World's Oceans 1. Hawaiian-Emperor Seamount Chain. Journal of Geophysical Research. Vol 83. No B12.*
- Watts A.B., Cochran J.R. & Selzer G. 1975. *Gravity Anomalies and Flexure of the lithosphere: A three-Dimensional study of the Great Meteor Seamount, Northeast Atlantic. Journal of Geophysical research, Vol 80 No. 11*
- Watts A.B. & Cochran J.R. 1974. *Gravity Anomalies and Flexure of the lithosphere along the Hawaiian-Emperor Seamount Chain. Geophys. J.R. ast.Soc. 38, 119-141*
- Wells J. T. & J. M. Coleman., 1981. *Physical processes and fine-grained sediment Dynamics, coast of Surinam, South America. Journal of Sedimentary Petrology, 51, 1053-1068.*
- Wessel, P. & Smith, W. H. F. 1995. *New version of the Generic Mapping Tools released. EOS Trans AGU, 79, 579*
- www.hidroweb.ana.gov.br: *Sistema de informacoes hidrologicas. Agencia Nacional de Aguas ANA.*